EVALUATING SURFACE AND DEEP-WATER CHANGES OVER EIRIK DRIFT DURING THE LATE PLEISTOCENE: IMPLICATIONS FROM GEOCHEMICAL AND SEDIMENTOLOGICAL PROXIES

by

LAUREN NEITZKE ADAMO

A Dissertation submitted to the

Graduate School-New Brunswick

Rutgers, The State University of New Jersey

in partial fulfillment of the requirements

for the degree of

Doctor of Philosophy

Graduate Program in Geological Sciences

written under the direction of

Dr. James D. Wright

and approved by

____

____

____

____

New Brunswick, New Jersey

January, 2016

ABSTRACT OF THE DISSERATATION

Evaluating Surface and Deep-Water Changes Over Eirik Drift During the Late Pleistocene: Implications from Geochemical and Sedimentological Proxies

by LAUREN NEITZKE ADAMO

Dissertation Director:

Dr. James D. Wright

This dissertation attempts to characterize the sedimentological and isotopic characteristics of the various end-member states of oceanic circulation within the North Atlantic Ocean during the Pleistocene. This ocean is a critical area of deep-water formation, and surface water perturbations alter deep-water production and affect global climate. Understanding the possible mechanisms behind these changes is critical. The Eirik Drift is the ideal location to evaluate these changes because it lies directly in the path of an important bottom water current and sedimentation rates are high, allowing for the reconstruction of high-resolution records on Milankovitch and millennial time scales.

Analysis of a swath of cores from Eirik Drift confirms that the deep-water current fluctuates between a deeply penetrating current during the extreme interglacials and a shallow, less buoyant current during the glacial extremes. A third intermediate mode is inferred that dominates the record. Depositional centers shift up and down the drift in tandem with the shifts in circulation modes.

The last deglaciation was marked by a series of abrupt climate changes and disruptions in the production of deep-water. These events are attributed to variations in

freshwater fluxes to the surface ocean in response to rapid melting of ice sheets. Reconstructed $\delta^{13}C$ values show reduced production during the cold events and vigorous production during warmer intervals. Resumption of deep-water production is coincident with peak meltwater discharge, questioning the validity of the meltwater hypothesis. Results suggest substantial sea-ice cover and we propose, along with perturbations in atmospheric circulation, are the cause of these climatic changes.

To understand the cause and effect of climatic changes, the leads and lags in the proxy records need to be defined with extreme precision and requires the construction of robust age models. Past studies rely on techniques that have inherent errors within the methodology. By combining these methods with additional techniques such as Paleo-intensity Assisted Chronology, the age control on deep-sea sediment records can be greatly improved.

ACKNOWLEDGEMENTS

There are so many people who have helped support me over the years and without which, none of this would have been possible. First of all thank you to my committee members, Dr. Jerry McManus, Dr. Kenneth Miller, Dr. Gregory Mountain and Dr. James Wright. Your comments and insights were invaluable and I am a better scientist because of all your input and support. Ken, Greg, and Jim, I cannot thank you enough for taking a chance on me as an undergraduate and writing letters of support when you hardly knew me. Your wonderful words all those year ago helped launch me on my career path and I would not be where I am today without that support. And special thanks to Jim Wright for being my advisor throughout my undergraduate and graduate career. I have learned so much from you and will forever be indebted to all you have done for me.

I would also like to thank the many graduate students that helped in countless ways over the years. There are way too many to name but in no particular order, a huge thank you to Rhonda Quinn, Nicole Abdul, Linda Godfrey, Rick Mortlock, and Max Needle. You all kept me sane by listening to me complain and helping out with technical and moral support along the way.

Thank you to Dr. Kathy Scott, Dr. Patricia Irizarry and Sue Coletta. You are the dream team to work with and it has been a joy working with all of you over the last few years. You have always been some of my biggest supporters and I will never forget it.

A huge thank you to my wonderful friends Kelly Mannherz and Brianna Muhlenkamp. You two have been such amazing friends to me over the years and I am honored to call you the godmothers of my children. Thank you for always being by my side when I needed you most, I love both of you guys so much.

I would not be where I am today without the love and support of my family. My Mom, Dad and brother Justin have never missed an important event and were always there to help me out when I needed it most. I have you to thank for the women, mother, and scientist I have become and I hope I have made you proud.

And finally, thank you to my wonderful husband Chris Adamo. I know this would not have happened without you. Thank you for allowing me to pursue my goal of becoming a doctor and for working so hard to grant me this opportunity. But most of all, thank you for giving me the metaphorical kick in the backside to keep going. Thank you for not letting me give up when I lost my way and was too scared to move forward. I love the life we have built together and I am so happy to be your partner in this crazy adventure.

I dedicate this dissertation to my children, Cassandra McKinley and Lincoln Walter. You are the reason for everything I do and I love you both so much. This work is written in honor of my grandparents, Grandma Ruth, Grandma Natalie, Mama Pat, Papa Jack, and Papa Eddie John. Even though they did not live to see this day, I know all of them would be very proud.

TABLE OF CONTENTS

LIST OF FIGURES

LIST OF TABLES

1.0 Dissertation Introduction

The North Atlantic Ocean has been intensively studied with respect to present and past circulation patterns, but its role in climate change as either an initiator or responder has yet to be determined. In the North Atlantic, cold, relatively salty water sinks in the Norwegian-Greenland Sea, forming NADW (Figure 1.1). Deep-water production in the northern North Atlantic Ocean forms one of the major limbs in global ocean circulation that helps redistribute heat and salt, impacting global climate (Figure 1.2; Broecker and Denton, 1989; Gordon, 1986; Stommel, 1961). Studies show that variations in this deep-water circulation pattern are associated with dramatic and abrupt climate changes (e.g., Broecker et al., 1985). However, understanding the mechanisms and underlying causes of these abrupt climate changes is one of the major challenges in global climate change research today. Therefore, the reconstruction of past oceanic conditions in the North Atlantic Ocean could help constrain the possible mechanisms responsible for these rapid climate changes.

Our current understanding of the relationship between climate and ocean circulation is based primarily on geochemical reconstructions of late Pleistocene climate. Traditionally, NCW production has been described as a bi-modal system that varies in water mass flux and buoyancy state over glacial and interglacial intervals (Figure 1.3; Boyle and Keigwin, 1987; Broecker and Denton, 1990; Broecker, 1991; Broecker and Denton, 1989; Duplessy et al., 1988a; Hillaire-Marcel et al., 1994; Oppo et al., 1995; Oppo and Fairbanks, 1987; Oppo and Lehman, 1995; Raymo et al., 2004). The end-members of this bi-modal system during the later Pleistocene and Holocene (~0 to 300 ka) are the interglacial and glacial extremes, represented in the climate record as Marine

Isotope Chrons[1] (MIC) 1, 5e, and 7.5 and MIC 2, 6, and 8, respectively (Figure 1.4). Deep-water circulation in the North Atlantic changed accordingly with a dense deeply penetrating current during the warm climate end members (Hillaire-Marcel et al., 1994) and less dense shallower water mass during the cold glacial intervals (Figure 1.3; Berggren and Hollister, 1974; Boyle and Keigwin, 1987; Broecker and Denton, 1990; Broecker, 1991; Broecker et al., 1989; Oppo et al., 1995; Oppo and Fairbanks, 1987; Oppo and Lehman, 1995; Raymo et al., 2004). The goal of this multi-site and proxy study is to characterize the orbital and millennial scale changes in these well-known end-member modes of deep-water circulation on Eirik Drift off the southern tip of Greenland as well as the intervals between these extremes that dominated the majority of the late Pleistocene record.

1.1 Oceanographic Background

The large-scale overturning of oceanic waters has been dubbed the "Great Ocean Conveyor", and thought to be controlled by thermohaline, or density driven differences in water masses (Broecker, 1991; Broecker and Denton, 1989; Gordon, 1986). Thermohaline production of deep-water in the Norwegian, Greenland, Ross and Weddell Seas is coupled with an equator-to-pole transport of cold bottom waters away from high latitude regions and a poleward flow of water surface and intermediate waters (Broecker, 1991 and others). However, there are several inconsistencies in the idea of a dominantly density-driven circulation mode (Toggweiler and Samuels, 1993). The North Atlantic basin produces approximately 15 to 20 Sverdrups (Sv; 10^6 m^3/second) of deep-water (i.e.,

[1] We follow Wright et al. (2009) in using the term Marine Isotope Chron, though these events are typically called stages in paleoceanography. The term stage is a stratigraphic term reserved for characterizing time-rock units (Hedberg, 1976). The proper term for isotopic variations is zones in depth and chron in time.

Broecker, 1991), whereas the rate of deep-water production around Antarctica is around 2 to 5 Sv (Carmack and Foster, 1975; Weiss et al., 1979). One would expect a higher Antarctic production rate in a density driven model since the Antarctic bottom waters are much more dense than those of the Atlantic (Toggweiler and Samuels, 1993). Furthermore, a pure density driven model does not take into account the effects of the Earth's rotation (Warren, 1981) and it is only the presence of boundaries along the eastern and western ocean margins that allows for the geostrophically balanced meridional flows necessary for thermohaline circulation (Toggweiler and Samuels, 1993).

The circumpolar westerlies blowing over the latitudinal band of the Drake Passage produce a northward Ekman drift in the near surface layers. This northward transport of surface waters must be balanced by a geostrophically balanced poleward flow (Toggweiler and Samuels, 1993; Toggweiler and Samuels, 1995). A difference in the shear of wind-stress around Antarctica produces upwelling, and it is the combination of the geostrophic constraints, the northward Ekman drift and upwelling that causes deep-water to be pulled poleward into the latitudinal band of the Drake Passage (Toggweiler and Samuels, 1993). Modeling results link the upwelling and removal of deep water in the circumpolar region to the formation of deep-water in the northern North Atlantic and show that changes in the strength of the Antarctic westerlies affect the rate of production (Toggweiler et al., 2006; Toggweiler and Samuels, 1995).

The subpolar North Atlantic is a key region in understanding the relationship between climate and variations in ocean circulation because it is one of the primary localities of deep-water production (Figure 1.1; i.e. Broecker, 1991). Deep-water production originates in the Norwegian-Greenland Sea after warm saline waters from the

North Atlantic Current flow north and cool due to contact with cold air masses. Evaporation and cooling increase the density of the surface waters to the point where it convects and flows southward, mixing with ambient North Atlantic water and Labrador Sea Water (LSW) south of the Greenland-Scotland Ridge forming one of the major limbs of ocean circulation (Broecker, 1991; Broecker and Denton, 1989; Rossby, 1996; Worthington, 1976). This cold, dense water mass, known as North Atlantic Deep Water (NADW), then flows south, filling most of the deep western Atlantic Ocean basin (Figure 1.2). It mixes in the western Atlantic basin with northward flowing Antarctic Bottom Water (AABW) and southward flowing Mediterranean Outflow Water (MOW), forming the Western Boundary Undercurrent (WBUC). Eventually, the WBUC enters the Southern Ocean from the western Atlantic and joins the rapidly moving deep current that encircles the Antarctic continent, termed circumpolar water (CPW). CPW mixes NADW with new deep water formed by the sinking of dense surface waters produced from sea-ice formation and brine rejection around Antarctica, and old deep water recirculated from the Pacific and Indian Oceans. This mixed water returns to the surface in the northern Indian and Pacific Oceans before flowing west and south through the Indonesian archipelago, west across the central Indian Ocean and around the southern tip of Africa before returning to the North Atlantic (Broecker, 1991; Broecker and Denton, 1989; Schmitz and McCartney, 1993).

NADW is part of a complex circulation system in the North Atlantic Ocean (Schmitz and McCartney, 1993) and is comprised of five different sources (Figure 1.5; Table 1.1; Worthington, 1976). The principle sources of NADW are from the overflow of Norwegian and Greenland Sea water through the Denmark Straits (Denmark Straights

Overflow Water; DSOW) and Iceland-Scotland Ridge (Iceland Scotland Overflow Water; ISOW), respectively. AABW and MOW flow northward in the eastern Atlantic basin and become incorporated as NADW flows through the North Atlantic basin and lower thermocline Atlantic water becomes entrained, respectively (Figure 1.5; Reid, 1979; Worthington, 1976). Much of this entrainment occurs at the Vema, Romanche, and other similar fracture zones as NADW is geostrophically steered west through the East-West trending features before turning and flowing to the north on the western side of the mid-ocean ridge (McCave and Tucholke, 1986; Worthington, 1976). The two other components of NADW are Labrador Sea Water (LSW), produced by the sinking of water cooled in the Labrador Sea, and the saline outflow from the Mediterranean Sea (Mediterranean Outflow Water; MOW) through the Straits of Gibraltar (McCave and Tucholke, 1986; Reid, 1979; Worthington, 1976).

Each of the five water mass components of modern NADW has a unique and identifiable temperature, salinity, and potential density signal (Figure 1.6; Table 1.1), and the combination of these water properties enables deep-water production. The most important property contributing to deep-water production in the North Atlantic is salinity. On average, the thermocline waters of the Atlantic Ocean are 1 psu (practical salinity unit) more saline than the upper waters of the Pacific Ocean (Broecker and Denton, 1989). This creates a critical density where water is dense enough to sink to the bottom of the North Atlantic Ocean at temperatures as warm as 2 °C. Whereas, the less saline waters of the Pacific Ocean can approach temperatures as low as - 2 °C, and only sink several hundreds of meters before reaching their buoyancy limit (Broecker and Denton, 1989; Warren, 1983). A previous study cited the importance of the delivery of saline subtropical waters to the Norwegian-Greenland Sea in the North Atlantic Current system as the major contributor of salinity to the North Atlantic (Reid and Lynn, 1971). However, the importance of the addition of the warm, saline Mediterranean Outflow Waters to the North Atlantic has also been stressed (Reid, 1979). It is clear that without a source of high-salinity water, the North Atlantic would not provide the dense waters that contribute to NADW.

The flow of NADW through the western North Atlantic is governed by geostrophy, which results in flow that follows regional bathymetric contours (Figure 1.3; Worthington, 1976). A deep gyre originates in the Norwegian-Greenland Sea when ISOW flows south between Iceland and the British Isles, and entrains water from the thermocline (between 4° and 17°C) and overflow water from the Iceland-Faroes Ridge (Worthington, 1976). This combined water mass is then steered southward around Iceland and along the Mid-Atlantic Ridge before flowing westward through the Charlie-Gibbs Fracture Zone (McCave and Tucholke, 1986; Worthington, 1976). It continues northward along the western side of the Reykjanes Ridge before mixing with the northernmost component, DSOW. DSOW forms by overflow of the shallow sill between Greenland and Iceland, entraining intermediate Atlantic Water (Worthington, 1976). The combined water mass then travels south along the eastern margin of Greenland before wrapping around Cape Farewell, where it flows over Eirik Drift and mixes with LSW. The current turns back to the north into the Labrador Sea where it flows cyclonically around the Labrador Basin before continuing south along the western edges of the North and South Atlantic Basins as the WBUC (McCave and Tucholke, 1986; Worthington, 1976).

1.2 Changes in North Atlantic Deep Water Circulation

There is strong evidence that the pattern of deep-water circulation during glacial times differed from the modern day (e.g. Boyle and Keigwin, 1987; Broecker and Denton, 1989; Duplessy et al., 1988a; Marchal and Curry, 2008; McManus et al., 2004; Oppo et al., 1995; Oppo and Lehman, 1995). Geochemical records from benthic foraminiferal $\delta^{13}C$ (Boyle and Keigwin, 1987; Oppo and Fairbanks, 1987), Cd/Ca (Boyle and Keigwin, 1987), Zn/Ca (Marchitto et al., 2002), $^{231}Pa/^{230}Th$ (McManus et al., 2004), ^{14}C ventilation ages (Thornalley et al., 2011), and bulk sediment εNd (Piotrowski et al., 2005) all show that large changes in the deep water masses in the Atlantic occurred between the Last Glacial Maximum (LGM) and the present. A system of two flow regimes is inferred (Figure 1.3), with one similar to modern NADW flow where the conveyor is very strong (Hillaire-Marcel et al., 1994). This regime is associated with a deep penetrating, fast moving WBUC, and prevails during the current interglacial, Isotopic Subchron 5e, and possibly during earlier interglacial periods (Figure 1.4; Hillaire-Marcel, 1994). The second flow regime corresponds to glacial periods when the conveyor has weakened considerably (e.g., Boyle and Keigwin, 1987; Broecker and Denton, 1990; Broecker, 1991; Broecker and Denton, 1989; Hillaire-Marcel et al., 1994; Oppo et al., 1995; Oppo and Fairbanks, 1987; Oppo and Lehman, 1995; Raymo et al., 2004). In this regime the WBUC shoals (i.e. Berggren and Hollister, 1974), resulting in a decrease in the production of lower NADW, an increase in the production of intermediate water or upper NADW (Marchitto et al., 1998), and the north ward advance of AABW (i.e., McManus et al., 2004). These patterns hold true on orbital time-scales (Oppo et al., 1995), as well as on the millennial-scales (Piotrowski et al., 2005).

Many studies have shown that glacial-interglacial cycles are paced by variations in the seasonal distribution of insolation, induced by orbital cycles (i.e., Hays et al., 1976; Imbrie and Imbrie, 1980; Imbrie et al., 1993). During the Pleistocene, insolation variability was driven by changes in eccentricity, obliquity and precession with periods of approximately 100, 41, and 19/23 kyr, respectively (Laskar et al., 1993). Variations in the shape of the Earth's orbit and in the tilt and orientation of its axis of spin lead to periods of intensified or reduced summer insolation, and ultimately determine whether glaciers will retreat or advance (Broecker and Denton, 1990; Broecker and Denton, 1989; Raymo and Nisancioglu, 2003). Reorganizations of the ocean-atmosphere system are associated with these orbital changes and are most pronounced at the terminations when the flow regime of the deep-ocean switched abruptly between modes (Broecker et al., 1985; Imbrie et al., 1993; Lisiecki et al., 2008). Over the past 3 million years, variations in deep-water circulation in the North Atlantic occurred in lock step with these orbitally induced climate changes (Raymo et al., 1989).

Over the past ~80,000 years, Earth's climate system has undergone a series of abrupt millennial scale oscillations and reorganizations, commonly referred to as Dansgaard-Oeschger cycles (Figures 1.7 and 1.8; Table 1.2; Bond et al., 1997; Bond et al., 1999; Dansgaard et al., 1984). These climate variations were first recognized in Greenland Ice core temperature records (Alley, 2000; Alley et al., 2003), but have now been identified in other climate proxies around the globe (Voelker, 2002). Deep-water production and circulation changes occur concomitant with these millennial scale cycles (Piotrowski et al., 2005), although the exact mechanisms controlling these changes remains unknown. Some hypotheses suggest that these circulation changes were triggered by variations in the salinity of the surfaces waters (i.e. the salt oscillator hypothesis; Birchfield and Broecker, 1990; Broecker et al., 1990; Zaucker and Broecker, 1992), whereas others argue changes in ocean/atmosphere system and jet stream path were the cause (i.e. the wind field oscillation hypothesis; Romanova et al., 2006; Seager, 2006; Seager and Battisti, 2007; Seager et al., 2002; Wunsch, 2006).

1.3 Geologic and Oceanographic Setting of Eirik Drift

Since the North Atlantic Ocean has undergone massive fluctuations in ice sheet dynamics over the last 15 Myr and especially over the last 2.5 Myrs (e.g., Jansen and Sjøholm, 1991; Wolf and Thiede, 1991), it is one of the most extensively studied locations when trying to understand the mechanisms controlling climate change (e.g., Alley et al., 1997; Barber et al., 1999; Broecker et al., 1989). These climate fluctuations manifest as distinct modes of deep-water circulation (e.g., Boyle and Keigwin, 1987; Oppo and Fairbanks, 1987) and this dissertation attempts to characterize and understand the various end-member and intermediate modes of circulation by examining multiple sediment cores collected from the northern North Atlantic Ocean (Figure 1.9).

As NADW flows through the North Atlantic Ocean, the interaction of the deep-water with sediments and bathymetry results in the creation of current-controlled sediment drifts (Figure 1.4; Berggren and Hollister, 1974; Faugères et al., 1999; Hollister et al., 1978; McCave and Tucholke, 1986). These drifts are ideal locations to study deep-water circulation changes because they generally record very high sedimentation rates (~5 to > 50 cm/kyr) when compared to the average open ocean sedimentation rate (~1 to 2 cm/kyr). Furthermore, in drift systems, sediments are often deposited, reworked and redeposited (Faugères et al., 1999; McCave and Tucholke, 1986), causing large changes in the various sediment proxies that often reflect changes in the strength and position of the deep current (Channell et al., 2014; Hall and Chan, 2004; Hillaire-Marcel et al., 2011; Hunter et al., 2007).

The Eirik Drift, located just south of Greenland, off the tip of Cape Farewell, was chosen as the study site for this dissertation for several reasons (Figure 1.9). First, this subpolar site (Figure 1.10) lies directly in the path of NCW, and by the time this water mass reaches this site, all of the major components except LSW have been added (Worthington, 1976). Previous studies have shown that deposition rates on Eirik Drift vary between 5 to over 100 cm/kyr (Channell et al., 2014; Hillaire-Marcel et al., 2011; Neitzke, 2007); therefore, this site allows for the reconstruction of extremely high-resolution records. Furthermore, the morphology of Eirik Drift is such that it allows the depositional center to shift up and down the drift crest as the buoyancy of the deep current changes (Channell et al., 2014; Hillaire-Marcel et al., 2011).

Sediment is transported to the deep-sea by vertical rain of pelagic sediment through the water column or gravity-driven downslope transport by turbidity currents or debris flows and then redistributed to sediment drifts by the action of deep-water currents (McCave, 2008). The mass movement of sediments by turbidity currents or debris flows can mix the deposits of several glacial/interglacial cycles (Weaver and Thomson, 1993), and therefore do not carry a pure signal of the conditions of the source area (McCave, 2008). Consequently, continental margins can contain records and sediments from varying origins raising concerns about the validity of the sedimentological and geochemical records in drift sediments. Winnowing of the fine-grained material and foraminiferal sands are commonly observed in areas with a mean current velocity above

20 cm s^{-1}. Velocities above 35 cm s^{-1} are required to move coarse-grained (> 200 μm) sand, but do not occur often enough to consistently produce well sorted sand deposits (McCave, 2008). Therefore, deposits of the laterally transported sediments driven by deep-sea currents are in the silt to clay size range (less than 63 μm), whereas the sediments derived from the vertical flux component are comprised of both fine and coarse-grained material. Only the sand and gravel sized particles may be unequivocally attributed to the properties of the overlying water column (McCave, 2008). Unless additional erosional evidence is observed, records obtained from the > 200 μm size fraction can be interpreted as accurately reflecting the ambient water conditions.

The sediment focusing that occurs on deep-sea drifts suggests that accumulation rates must first increase as current speeds increase, and then decrease as occasional erosional events occur (McCave and Hall, 2006). Once flow speeds reach a high velocity (~ 20 to 25 cm/s), winnowing of the fine grain material will occur (Miller and Komar, 1977), resulting in varying depositional patterns related to the spatial variability of deep-water flow (McCave, 2008). Deposition on mud waves and drifts can be described as an anti-dune where maximum accumulation occurs on the upstream or lee-side of the drift and lower accumulation occurs on the downstream or current side of the drift. This would result in slower accumulation or even erosion and coarser grains on the current side of the drift (Flood, 1988). Grain size analysis on the Gardar Drift corroborates this hypothesis and clearly shows reduced sedimentation and increased grain size on the current side of the drift compared to the lee-side of the drift (Bianchi and McCave, 2000). Therefore, areas directly under the core of bottom water currents will be dominated by coarser grained sediments and experience low accumulation, winnowing or erosion, whereas the areas on the outer edges of the current will be finer grained and experience increased deposition.

1.4 Sea Ice

Sea ice, or ice formed from the freezing of seawater, is a defining characteristic of the Arctic Ocean and covers about 7% of the Earth's surface (Weeks, 2010). Ice cover waxes and wanes with the seasons with maximum coverage in March and a minimum extent in September (Polyak et al., 2010). The thickness of sea ice varies by location and over time but is typically cited at 3 m as described by a probability distribution (Wadhams, 1980; Williams et al., 1975), although there is substantial evidence that the recent shrinking of the sea ice coverage has been accompanied by considerable thinning (Polyak et al., 2010). Changes in extent and thickness have been documented on inter-annual and longer time scales, and while driven by climate change, can affect hydrographic and atmospheric conditions in the high latitudes on various time scales (e.g., Miller et al., 2010; Polyak et al., 2010; Smith et al., 2003).

Sea ice can be classified into two basic categories; fast ice or drift ice. If the ice is attached or frozen to the shoreline, between shoals, or grounded icebergs, it is called fast ice, whereas drift ice is free to move with the currents and wind directions and occurs farther offshore (Weeks, 2010). Sea ice can be further classified into new ice, first year ice, and old ice based on whether it is newly formed, has not had more than one year of growth, and has survived at least one melting season, respectively (Weeks, 2010).

The past distribution of sea-ice is preserved in the sedimentological and geochemical records of deep-sea sediment cores, of which the most direct proxy for the presence of floating ice is derived from sediment that melts out of the transported ice

(Polyak et al., 2010). Ice-rafted debris (IRD), usually defined as the greater than 63 μm size fraction, is commonly used to infer deposition from ice. This can include deposition from sea ice and icebergs (i.e. derived from the calving of ice shelves or glaciers; Lisitzin, 2002), and distinguishing between the two modes of delivery is an important, albeit difficult part in interpreting the paleoenvironment (Polyak et al., 2010). Icebergs are capable of carrying clay to boulder-sized sediment, and although some sediment can be fine grained, typically iceberg-rafted sediment has 10-20% or higher content of IRD (Andrews, 2000 and others). Sediments become entrained in sea ice during periods of new ice formation and is mostly composed of the fine-grained silt and clay sediments in suspension in the water column, although the content varies by location (e.g., Lisitzin, 2002). However, coarser grains can be incorporated into sea ice by the transport of coarse sediment shed from coastal cliffs by fast ice and through the entrainment of sediments along shallow shelves by anchor ice (Reimnitz et al., 1987). Examination of modern sea ice shows that the proportion of greater than 63 μm grains is approximately 10 % (e.g., Darby et al., 2009; Darby, 2003). In general, deposits with higher percentages of IRD are indicative of iceberg deposition, whereas lower numbers can be attributed to either iceberg or sea ice processes (Polyak et al., 2010), however, some subarctic deposits may have a higher IRD content than the Arctic due to different sedimentary environments (Lisitzin, 2002).

A significant link between sea ice extent, atmospheric circulation, and ocean circulation exists in the presence of large northern hemisphere ice sheets (e.g., Ruddiman and Wright, 1987). Modeling results show that a large northern hemisphere ice sheet would alter the path of the jet stream forcing cold polar winds to the south (Manabe and

Broccoli, 1985 and others). Geologic and modeling data indicate that the presence of the ice sheet would both cool and seasonally freeze the North Atlantic Ocean north of 45° to 50°N and force a southern shift of the polar front (Ruddiman and Wright, 1987). Although the seasonal limits of sea ice coverage during glacial times is not well defined, foraminiferal evidence supports a southward shift in winter sea ice cover to 50°N and the general trends would track the southward migration of the polar front (Ruddiman and McIntyre, 1981). As the ice sheets gradually melted during Termination 1 (transition from MIC 2 to 1), the polar front would retreat (Figure 1.11) and the southern extent of seasonal sea ice coverage would follow (Ruddiman and McIntyre, 1981; Ruddiman and Wright, 1987). Sea ice formation is particularly important in the polar oceans because it would create a "cap" on the ocean that would prevent the transfer of heat and gases across this interface affecting climate and ocean circulation (e.g., Ruddiman, 2001).

1.5 Objectives and Overview of Chapters

1.5.1 Chapter 2: Shifting Depositional Centers as a Proxy of Variations in North Atlantic Deep Water Flow

Chapter 2 examines the sedimentation patterns during MIC 1 to 4 and the subchrons of MIC 5 (e.g. 5a, 5b, 5c, 5d, and 5e) from a network of piston and gravity cores collected on the Eirik Drift. The location of the depositional center, or area of highest sedimentation, on the drift corresponds to the position of the current axis, that is controlled by changes in the relative density between the northern and southern sourced deep-water (Channell et al., 2014; Evans et al., 2007; Hillaire-Marcel et al., 1994; Stoner et al., 1995; Stoner et al., 1998). These buoyancy changes that were the result of water masses changing over time occurred in response to climate and operated on orbital and millennial time scales (Oppo et al., 1995; Piotrowski et al., 2005).

Sediment accumulation patterns on the Eirik Drift were reconstructed from cores 15JPC (2230 m), 19JPC (3204 m), 18JPC (3435 m) and MD2664 (3450 m; Figure 1.4). Research for this project was initiated as part of the requirements for my M.S. degree (Neitzke, 2006), but has been extended to further evaluate the shifting depositional centers. Additional downcore sedimentological and stable isotopic records were generated for Core 15JPC and MD2664 and the age chronologies for all 4 cores were refined by comparing the downcore stable isotopic data to the published records of Channell et al. (2014) and Lisiecki and Raymo (2005). Fifteen new AMS dates were also obtained to further constrain the upper portion of the age model for core 15JPC.

High-resolution stable isotopic (oxygen and carbon) and sediment proxy records (percent calcium carbonate, percent coarse fraction, sedimentation rates, and number of ice-rafted detritus grains per gram) were produced to reconstruct the fluctuations in deep-water flow in this region. Specifically, sedimentary signatures of the different modes of circulation and variations in the axis of deep-water flow over Eirik Drift were identified and placed into context with the glacial to interglacial timescale climate changes. Results indicate that the axis of deep-water flow constantly shifts up and down the drift in response to changes in climate. Furthermore, the data indicate the presence of two end members and a transitional mode of deep-water circulation corresponding to the glacial, extreme interglacial and interstadial periods, respectively.

This paper will be submitted to Paleoceanography and is authored by Lauren Neitzke Adamo, James D. Wright, Gregory Mountain and Kenneth G. Miller of Rutgers University and Patricia L. Manley of Middlebury College.

1.5.2 Chapter 3: Sedimentological and Stable Isotopic Evidence of Surface Water Forcing During Heinrich Event 1 on Deep-Water Variability in the North Atlantic

Previous studies have cited the importance of surface water variability (i.e. cooling or freshening of surface waters by meltwater/freshwater input) in modulating the millennial-scale climate variability seen during the past 20 kyr, and have proposed that these variations are the forcing mechanisms behind the subsequent changes in deep-water circulation (i.e., Bond et al., 1993; Bond et al., 1992; Boyle and Keigwin, 1987; Broecker, 1994). Chapter 3 reexamines this fundamental relationship between surface water variability and climate/deep-water production changes by creating high-resolution sedimentological and multi-species stable isotopic records from a shallow site on Eirik Drift. Sedimentary and isotopic signatures were characterized for the millennial scale climate changes of the last 20 kyr (i.e. the Last Glacial Maximum, Heinrich 1 event, the Younger Dryas, and the Bolling-Allerod) and the accompanying changes in deep-water production were analyzed.

Core 15JPC, recovered from a depth of 2230 m on Eirik Drift, is ideal for both surface and deep-water paleoceanographic study (Figure 1.4). The Holocene to Last Glacial Maximum (LGM) section in Core 15JPC is very expanded (>2 m) and that sedimentation rates may exceed 60 cm/kyr during certain intervals, allowing for high resolution records to be generated and the millennial scale changes in climate to be assessed. Furthermore, the East Greenland Current and the Labrador Sea directly influence the surface waters of this site. Therefore, the sedimentary signatures on Eirik Drift should reflect any ice sheet variability and freshwater fluxes that may have affected circulation (Hillaire-Marcel and Bilodeau, 2000; Hillaire-Marcel et al., 1994).

Previous investigations have used only a single species of foraminifera to document the circulation changes in the North Atlantic Ocean, therefore providing a one-dimensional view of the surface and deep-water hydrography. Combining $\delta^{18}O$ records from multiple species of planktonic foraminifera provides a more detailed assessment on the upper water column (i.e., the mixed-layer and thermocline waters; Rashid and Boyle, 2007) while certain species of benthic foraminifera accurately reflect changes in bottom water chemistry (Duplessy et al., 1988b; Sarnthein et al., 1994). Therefore, stable isotopic analysis was performed on two planktonic species (*Neogloboquadrina pachyderma,* sinistral; and *Globigerina bulliodes*) and one benthic species (*Planulina wuellerstorfi*) to characterize the surface and deep-water hydrography. Further sedimentological analyses (percent coarse fraction and number of ice rafted detritus grains per gram) were also conducted on the downcore samples. Results were then compared with other deep-sea sediment and ice cores to place the record from 15JPC into a regional context.

Results show a consistent trend in circulation patterns between various deep-water sites and confirm intervals of reduced NCW production. However, no evidence of glacial meltwater perturbations were observed during these periods, questioning the validity of the deep-water circulation and freshwater flux hypothesis. Planktonic foraminiferal $\delta^{18}O$ patterns indicate the presence of extensive sea-ice coverage and the production of brines during the cold intervals (i.e. Heinrich 1). The low glacial meltwater discharge values and independent evidence of increased sea-ice suggest that the sea ice coverage was responsible for the shutdown in deep-water production during H1 or that the North Atlantic deep-water convection sites are highly sensitive to small amounts of meltwater input.

This chapter will be prepared for submission likely to *Paleoceanography* and will be authored by Lauren Neitzke Adamo and James D. Wright.

1.5.3 Chapter 4: Evaluating the errors and uncertainties in $\delta^{18}O$ based chronologies of deep-sea sediment cores

At the completion of cruise KN166-14 onboard the R/V KNORR, a collaborative effort to analyze the sedimentological and geochemical signatures of the numerous piston and gravity cores collected began between Rutgers and several other Universities. This cruise was funded as the site survey for a future Integrated Ocean Drilling Program (IODP) expedition, and the preliminary proxy records and seismic results from cruise KN166-14 were used in the selection of IODP Sites 1305 and 1306.

Evans et al. (2007) published a study from the results of some of these cores titled "Paleointensity-assisted chronostratigraphy of detrital layers on the Eirik Drift (North Atlantic) since marine isotope stage 11." Four long jumbo piston cores (20 to 24 m) were analyzed for %$CaCO_3$, $\delta^{18}O$ stratigraphy, relative paleointensity proxies and magnetic susceptibility (i.e. volume susceptibility) to characterize the detrital layers on Eirik Drift and correlate them to other North Atlantic sites. Downcore $\delta^{18}O$ and %$CaCO_3$ records were generated for 3 of 4 cores examined in this study (i.e., Cores 15JPC, 18JPC, and

19JPC) as part of the requirements for this dissertation and encompasses a data set of nearly 3000 data points. The goal of this study was to identify and examine the orbital and millennial scale changes in the detrital carbonate events recorded in the sediments on Eirik Drift. Consequently, it would not have been possible to identify the carbonate events or place them into a general chronologic framework without the %$CaCO_3$ and $\delta^{18}O$ stratigraphy that was generate for this research, respectively.

Chapter 4 also focuses on reviewing the traditional methods used in creating age models for downcore $\delta^{18}O$ stratigraphies. Since $\delta^{18}O$ chronologies have become the gold standard for correlating between deep-water sites, it is essential to create robust age models. Stacked $\delta^{18}O$ records, like the 5.6 Myr Lisiecki and Raymo (2005) benthic record, are used by comparing peaks, troughs, and transitions between $\delta^{18}O$ records and assigning ages. This method provides very good age control on the orbital time scales, but lacks the resolution to resolve the timing in abrupt climatic events (Martinson et al., 1987) in addition to other environmental factors that can affect the $\delta^{18}O$ ratios (Hillaire-Marcel and de Vernal, 2008; Lisiecki and Raymo, 2009; Skinner and Shackleton, 2005). Radiocarbon dating is the most widely used dating technique today but is subject to several inherent flaws (Fairbanks et al., 2005). Uncertainties in the application of a calendar age correction curve (Fairbanks et al., 2005 and others) and calculation of a reservoir age correction (i.e., Butzin et al., 2005) introduce errors into the age models that can make precise correlation of rapid climatic events difficult. Channell et al. (2009) and others have demonstrated the usefulness of combining traditional $\delta^{18}O$ dating techniques with relative paleointensity data to improve the stratigraphic correlation in deep-sea sediment core proxy records.

Evans et al. (2007) used this tandem correlation method to evaluate the detrital carbonate layers in four Eirik Drift cores. Due to the rapid nature of these events and prolific occurrence of these deposits in the North Atlantic Ocean, this method provides a much higher confidence level in the accuracy of the downcore age models. The methods, results, and conclusions of Evans et al. (2007) are summarized in Chapter 4 and a full copy of the text can be reviewed online at doi:10.1029/2007GC001720.

1.6 References

Alley, R.B., 2000. Ice-core evidence of abrupt climate changes. Proceedings of the National Academy of Sciences, 97(4): 1331-1334.

Alley, R.B. et al., 2003. Abrupt climate change. science, 299(5615): 2005-2010.

Alley, R.B. et al., 1997. Holocene climatic instability: A prominent, widespread event 8200 yr ago. Geology, 25(6): 483-486.

Andrews, J.T., 2000. Icebergs and iceberg rafted detritus (IRD) in the North Atlantic: facts and assumptions. OCEANOGRAPHY-WASHINGTON DC-OCEANOGRAPHY SOCIETY-, 13(3): 100-108.

Barber, D. et al., 1999. Forcing of the cold event of 8,200 years ago by catastrophic drainage of Laurentide lakes. Nature, 400(6742): 344-348.

Berggren, W.A., Hollister, C.D., 1974. Paleogeography, paleobiogeography and the history of circulation in the Atlantic Ocean, Studies in Paleo-oceanography. Special Publication- Society of Economic Mineralogists, 20: 126-186.

Bianchi, G., McCave, I., 2000. Hydrography and sedimentation under the deep western boundary current on Björn and Gardar Drifts, Iceland Basin. Marine Geology, 165(1): 137-169.

Birchfield, G.E., Broecker, W.S., 1990. A salt oscillator in the glacial Atlantic? 2. A "scale analysis" model. Paleoceanography, 5(6): 835-843.

Bond, G. et al., 1993. Correlations between climate records from North Atlantic sediments and Greenland ice. Nature(365): 143-147.

Bond, G. et al., 1992. Evidence for massive discharges of icebergs into the North Atlantic ocean during the last glacial period.

Bond, G. et al., 1997. A pervasive millennial-scale cycle in North Atlantic Holocene and glacial climates. science, 278(5341): 1257-1266.

Bond, G.C., Lotti, R., 1995. Iceberg discharges into the North Atlantic on millennial time scales during the last glaciation. Science, 267(5200): 1005-1010.

Bond, G.C. et al., 1999. The North Atlantic's 1‐2 Kyr Climate Rhythm: Relation to Heinrich Events, Dansgaard/Oeschger Cycles and the Little Ice Age. Mechanisms of global climate change at millennial time scales: 35-58.

Boyle, E.A., Keigwin, L., 1987. North Atlantic thermohaline circulation during the past 20,000 years linked to high-latitude surface temperature. Nature, 330: 5.

Broecker, W., Denton, G.H., 1990. What drives glacial cycles? Scientific American, 262(1): 42-50.

Broecker, W.S., 1991. The great ocean conveyor. Oceanography, 4(2): 79-89.

Broecker, W.S., 1994. Massive iceberg discharges as triggers for global climate change. Nature, 372: 421-424.

Broecker, W.S., Bond, G., Klas, M., Bonani, G., Wolfli, W., 1990. A salt oscillator in the glacial Atlantic? 1. The concept. Paleoceanography, 5(4): 469-477.

Broecker, W.S., Denton, G.H., 1989. The role of ocean-atmosphere reorganizations in glacial cycles. Geochimica et Cosmochimica Acta, 53(10): 2465-2501.

Broecker, W.S. et al., 1989. Routing of meltwater from the Laurentide Ice Sheet during the Younger Dryas cold episode.

Broecker, W.S., Peteet, D.M., Rind, D., 1985. Does the ocean-atmosphere system have more than one stable mode of operation? Nature, 315(6014): 21-26.

Butzin, M., Prange, M., Lohmann, G., 2005. Radiocarbon simulations for the glacial ocean: the effects of wind stress, Southern Ocean sea ice and Heinrich events. Earth and Planetary Science Letters, 235(1): 45-61.

Carmack, E.C., Foster, T.D., 1975. On the flow of water out of the Weddell Sea, Deep Sea Research and Oceanographic Abstracts. Elsevier, pp. 711-724.

Channell, J., Wright, J., Mazaud, A., Stoner, J., 2014. Age through tandem correlation of Quaternary relative paleointensity (RPI) and oxygen isotope data at IODP Site U1306 (Eirik Drift, SW Greenland). Quaternary Science Reviews, 88: 135-146.

Channell, J., Xuan, C., Hodell, D., 2009. Stacking paleointensity and oxygen isotope data for the last 1.5 Myr (PISO-1500). Earth and Planetary Science Letters, 283(1): 14-23.

Charles, C.D., Fairbanks, R.G., 1992. Evidence from Southern Ocean sediments for the effect of North Atlantic deep-water flux on climate.

Classification, I.S.o.S., Hedberg, H.D., 1976. International Stratigraphic Guide: A Guide to Stratigraphic Classification, Terminology, and Procedure. Hollis D. Hedberg, Editor. Wiley.

Conkright, M.E., Levitus, S., Boyer, T.P., 1994. World Ocean Atlas: 1994 Nutrients, 1. DIANE Publishing.

Dansgaard, W. et al., 1984. North Atlantic climatic oscillations revealed by deep Greenland ice cores. Climate processes and climate sensitivity: 288-298.

Darby, D. et al., 2009. The role of currents and sea ice in both slowly deposited central Arctic and rapidly deposited Chukchi–Alaskan margin sediments. Global and Planetary Change, 68(1): 58-72.

Darby, D.A., 2003. Sources of sediment found in sea ice from the western Arctic Ocean, new insights into processes of entrainment and drift patterns. Journal of Geophysical Research: Oceans (1978–2012), 108(C8).

Duplessy, J. et al., 1988a. Deep-water source variation during the last climate variation: Palaeoceanography, v. 3.

Duplessy, J.C., Labeyrie, L., Blanc, P., 1988b. Norwegian Sea deep water variations over the last climatic cycle: paleo-oceanographical implications, Long and short term variability of climate. Springer, pp. 83-116.

Evans, H.F. et al., 2007. Paleointensity ‐ assisted chronostratigraphy of detrital layers on the Eirik Drift (North Atlantic) since marine isotope stage 11. Geochemistry, Geophysics, Geosystems, 8(11).

Fairbanks, R.G. et al., 2005. Radiocarbon calibration curve spanning 0 to 50,000 years BP based on paired 230 Th/234 U/238 U and 14 C dates on pristine corals. Quaternary Science Reviews, 24(16): 1781-1796.

Faugères, J.-C., Stow, D.A., Imbert, P., Viana, A., 1999. Seismic features diagnostic of contourite drifts. Marine Geology, 162(1): 1-38.

Flood, R.D., 1988. A lee wave model for deep-sea mudwave activity. Deep Sea Research Part A. Oceanographic Research Papers, 35(6): 973-983.

Gordon, A.L., 1986. Interocean exchange of thermocline water. Journal of Geophysical Research, 91: 5037-5046.

Grootes, P., Stuiver, M., 1997. Oxygen 18/16 variability in Greenland snow and ice with 10– 3 ‐ to 105 ‐ year time resolution. Journal of Geophysical Research: Oceans (1978–2012), 102(C12): 26455-26470.

Grootes, P., Stuiver, M., White, J., Johnsen, S., Jouzel, J., 1993. Comparison of oxygen isotope records from the GISP2 and GRIP Greenland ice cores.

Hall, J.M., Chan, L.H., 2004. Ba/Ca in Neogloboquadrina pachyderma as an indicator of deglacial meltwater discharge into the western Arctic Ocean. Paleoceanography, 19(1).

Hays, J.D., Imbrie, J., Shackleton, N.J., 1976. Variations in the Earth's orbit: pacemaker of the ice ages. American Association for the Advancement of Science.

Hillaire-Marcel, C., Bilodeau, G., 2000. Instabilities in the Labrador Sea water mass structure during the last climatic cycle. Canadian Journal of Earth Sciences, 37(5): 795-809.

Hillaire-Marcel, C., de Vernal, A., 2008. Stable isotope clue to episodic sea ice formation in the glacial North Atlantic. Earth and Planetary Science Letters, 268(1): 143-150.

Hillaire-Marcel, C., de Vernal, A., McKay, J., 2011. Foraminifer isotope study of the Pleistocene Labrador Sea, northwest North Atlantic (IODP Sites 1302/03 and 1305), with emphasis on paleoceanographical differences between its "inner" and "outer" basins. Marine Geology, 279(1): 188-198.

Hillaire-Marcel, C., Vernal, A.d., Bilodeau, G., Wu, G., 1994. Isotope stratigraphy, sedimentation rates, deep circulation, and carbonate events in the Labrador Sea during the last~ 200 ka. Canadian Journal of Earth Sciences, 31(1): 63-89.

Hollister, C.D., Flood, R., McCave, I.N., 1978. Plastering and Decorating in the North Atlantic. Oceanus.

Hunter, S. et al., 2007. Deep western boundary current dynamics and associated sedimentation on the Eirik Drift, Southern Greenland Margin. Deep Sea Research Part I: Oceanographic Research Papers, 54(12): 2036-2066.

Imbrie, J., Imbrie, J.Z., 1980. Modeling the climatic response to orbital variations. Science, 207(4434): 943-953.

Imbrie, J., Mix, A., Martinson, D., 1993. Milankovitch theory viewed from Devils Hole. Nature, 363(6429): 531-533.

Jansen, E., Sjøholm, J., 1991. Reconstruction of glaciation over the past 6 Myr from ice-borne deposits in the Norwegian Sea. Nature, 349(6310): 600-603.

Laskar, J., Joutel, F., Boudin, F., 1993. Orbital, precessional, and insolation quantities for the Earth from-20 Myr to+ 10 Myr. Astronomy and Astrophysics, 270: 522-533.

Levitus, S., Boyer, T.P., 1994. World Ocean Atlas 1994. Volume 4. Temperature, National Environmental Satellite, Data, and Information Service, Washington, DC (United States).

Lisiecki, L.E., Raymo, M.E., 2005. A Pliocene ‐ Pleistocene stack of 57 globally distributed benthic δ 18O records. Paleoceanography, 20(1).

Lisiecki, L.E., Raymo, M.E., 2009. Diachronous benthic δ18O responses during late Pleistocene terminations. Paleoceanography, 24(3).

Lisiecki, L.E., Raymo, M.E., Curry, W.B., 2008. Atlantic overturning responses to Late Pleistocene climate forcings. Nature, 456(7218): 85-88.

Lisitzin, A.P., 2002. Sea-ice and Iceberg Sedimentation in the Ocean, Recent and Past. . Springer-Verlag, Berlin: 563 pp.

Manabe, S., Broccoli, A., 1985. The influence of continental ice sheets on the climate of an ice age. Journal of Geophysical Research: Atmospheres (1984–2012), 90(D1): 2167-2190.

Marchal, O., Curry, W.B., 2008. On the abyssal circulation in the glacial Atlantic. Journal of Physical Oceanography, 38(9): 2014-2037.

Marchitto, T.M., Curry, W.B., Oppo, D.W., 1998. Millennial-scale changes in North Atlantic circulation since the last glaciation. Nature, 393(6685): 557-561.

Marchitto, T.M., Oppo, D.W., Curry, W.B., 2002. Paired benthic foraminiferal Cd/Ca and Zn/Ca evidence for a greatly increased presence of Southern Ocean Water in the glacial North Atlantic. Paleoceanography, 17(3): 10-1-10-18.

Martinson, D.G. et al., 1987. Age dating and the orbital theory of the ice ages: development of a high-resolution 0 to 300,000-year chronostratigraphy. Quaternary research, 27(1): 1-29.

McCave, I., 2008. Size sorting during transport and deposition of fine sediments: sortable silt and flow speed.

McCave, I., Hall, I.R., 2006. Size sorting in marine muds: Processes, pitfalls, and prospects for paleoflow ‐ speed proxies. Geochemistry, Geophysics, Geosystems, 7(10).

McCave, I., Tucholke, B., 1986. Deep current-controlled sedimentation in the western North Atlantic. The Geology of North America, 1000: 451-468.

McManus, J., Francois, R., Gherardi, J.-M., Keigwin, L., Brown-Leger, S., 2004. Collapse and rapid resumption of Atlantic meridional circulation linked to deglacial climate changes. Nature, 428(6985): 834-837.

Meese, D., 1994. Preliminary depth-age scale of the GISP2 ice core. US Army Corps of Engineers, Cold Regions Research & Engineering Laboratory.

Miller, G.H. et al., 2010. Arctic amplification: can the past constrain the future? Quaternary Science Reviews, 29(15): 1779-1790.

Miller, M., Komar, P., 1977. The development of sediment threshold curves for unusual environments (Mars) and for inadequately studied materials (foram sands). Sedimentology, 24(5): 709-721.

Neitzke, L.C., 2006. Late Pleistocene Sedimentation on Eirik Drift: Implications for North Atlantic Deep Water Variability, Rutgers University.

Neitzke, L.C., 2007. Variations in Deep-Water Circulation on Eirik Drift from the Last Glacial Maximum to early Holocene, 2007 GSA Denver Annual Meeting.

Oppo, D. et al., 1995. A 13C record of Upper North Atlantic Deep Water during the past 2.6 million years. Paleoceanography, 10(3): 373-394.

Oppo, D.W., Fairbanks, R.G., 1987. Variability in the deep and intermediate water circulation of the Atlantic Ocean during the past 25,000 years: Northern Hemisphere modulation of the Southern Ocean. Earth and Planetary Science Letters, 86(1): 1-15.

Oppo, D.W., Lehman, S.J., 1995. Suborbital timescale variability of North Atlantic Deep Water during the past 200,000 years. Paleoceanography, 10(5): 901-910.

Piotrowski, A.M., Goldstein, S.L., Hemming, S.R., Fairbanks, R.G., 2005. Temporal relationships of carbon cycling and ocean circulation at glacial boundaries. Science, 307(5717): 1933-1938.

Polyak, L. et al., 2010. History of sea ice in the Arctic. Quaternary Science Reviews, 29(15): 1757-1778.

Rashid, H., Boyle, E.A., 2007. Mixed-layer deepening during heinrich events: a multi-planktonic foraminiferal δ18O approach. Science, 318(5849): 439-441.

Raymo, M., Ruddiman, W., Backman, J., Clement, B., Martinson, D., 1989. Late Pliocene variation in Northern Hemisphere ice sheets and North Atlantic deep water circulation. Paleoceanography, 4(4): 413-446.

Raymo, M.E., Nisancioglu, K.H., 2003. The 41 kyr world: Milankovitch's other unsolved mystery. Paleoceanography, 18(1).

Raymo, M.E. et al., 2004. Stability of North Atlantic water masses in face of pronounced climate variability during the Pleistocene. Paleoceanography, 19(2).

Reid, J.L., 1979. On the contribution of the Mediterranean Sea outflow to the Norwegian-Greenland Sea. Deep Sea Research Part A. Oceanographic Research Papers, 26(11): 1199-1223.

Reid, J.L., Lynn, R.J., 1971. On the influence of the Norwegian-Greenland and Weddell seas upon the bottom waters of the Indian and Pacific oceans, Deep Sea Research and Oceanographic Abstracts. Elsevier, pp. 1063-1088.

Reimnitz, E., Kempema, E., Barnes, P., 1987. Anchor ice, seabed freezing, and sediment dynamics in shallow Arctic seas. Journal of Geophysical Research: Oceans (1978–2012), 92(C13): 14671-14678.

Romanova, V., Lohmann, G., Grosfeld, K., Butzin, M., 2006. The relative role of oceanic heat transport and orography on glacial climate. Quaternary science reviews, 25(7): 832-845.

Rossby, T., 1996. The North Atlantic Current and surrounding waters: At the crossroads. REVIEWS OF GEOPHYSICS-RICHMOND VIRGINIA THEN WASHINGTON-, 34: 463-482.

Ruddiman, W.F., 2001. Earth's Climate: past and future. Macmillan.

Ruddiman, W.F., McIntyre, A., 1981. The North Atlantic Ocean during the last deglaciation. Palaeogeography, Palaeoclimatology, Palaeoecology, 35: 145-214.

Ruddiman, W.F., Wright, H.E., 1987. North America and adjacent oceans during the last deglaciation. Geological Society of America Boulder.

Sarnthein, M. et al., 1994. Changes in east Atlantic deepwater circulation over the last 30,000 years: Eight time slice reconstructions. Paleoceanography, 9(2): 209-267.

Schmitz, Jr., William J., 1996 On the World Ocean Circulation: Volume II The Pacific and Indian Oceans / A Global Update, Woods Hole Oceanographic Institution, Technical Report, WHOI-96-0B.

Schmitz, W.J., McCartney, M.S., 1993. On the north Atlantic circulation. Reviews of Geophysics, 31(1): 29-49.

Seager, R., 2006. The source of Europe's mild climate. American Scientist, 94(4): 334.

Seager, R., Battisti, D.S., 2007. Challenges to our understanding of the general circulation: abrupt climate change. Global Circulation of the Atmosphere: 331-371.

Seager, R. et al., 2002. Is the Gulf Stream responsible for Europe's mild winters? Quarterly Journal of the Royal Meteorological Society, 128(586): 2563-2586.

Skinner, L., Shackleton, N., 2005. An Atlantic lead over Pacific deep-water change across Termination I: implications for the application of the marine isotope stage stratigraphy. Quaternary Science Reviews, 24(5): 571-580.

Smith, L.M., Miller, G.H., Otto-Bliesner, B., Shin, S.-I., 2003. Sensitivity of the Northern Hemisphere climate system to extreme changes in Holocene Arctic sea ice. Quaternary Science Reviews, 22(5): 645-658.

Smith, W.H., Sandwell, D.T., 1994. Bathymetric prediction from dense satellite altimetry and sparse shipboard bathymetry. JOURNAL OF GEOPHYSICAL RESEARCH-ALL SERIES-, 99: 21,803-21,803.

Steig, E.J., Grootes, P.M., Stuiver, M., 1994. Seasonal precipitation timing and ice core records. Science (Washington, DC);(United States), 266(5192).

Stommel, H., 1961. Thermohaline convection with two stable regimes of flow. Tellus A, 13(2).

Stoner, J., Channell, J., Hillaire-Marcel, C., 1995. Late Pleistocene relative geomagnetic paleointensity from the deep Labrador Sea: Regional and global correlations. Earth and Planetary Science Letters, 134(3): 237-252.

Stoner, J., Channell, J., Hillaire-Marcel, C., 1998. A 200 ka geomagnetic chronostratigraphy for the Labrador Sea: Indirect correlation of the sediment record to SPECMAP. Earth and Planetary Science Letters, 159(3): 165-181.

Stuiver, M., Grootes, P.M., Braziunas, T.F., 1995. The GISP2 δ18O climate record of the past 16,500 years and the role of the sun, ocean, and volcanoes. Quaternary Research, 44(3): 341-354.

Thornalley, D.J., Barker, S., Broecker, W.S., Elderfield, H., McCave, I.N., 2011. The deglacial evolution of North Atlantic deep convection. science, 331(6014): 202-205.

Toggweiler, J., Russell, J.L., Carson, S., 2006. Midlatitude westerlies, atmospheric CO2, and climate change during the ice ages. Paleoceanography, 21(2).

Toggweiler, J., Samuels, B., 1993. Is the magnitude of the deep outflow from the Atlantic Ocean actually governed by Southern Hemisphere winds?, The Global Carbon Cycle. Springer, pp. 303-331.

Toggweiler, J., Samuels, B., 1995. Effect of Drake Passage on the global thermohaline circulation. Deep Sea Research Part I: Oceanographic Research Papers, 42(4): 477-500.

Vidal, L. et al., 1999. Link between the North and South Atlantic during the Heinrich events of the last glacial period. Climate Dynamics, 15(12): 909-919.

Voelker, A.H., 2002. Global distribution of centennial-scale records for Marine Isotope Stage (MIS) 3: a database. Quaternary Science Reviews, 21(10): 1185-1212.

Wadhams, P., 1980. A comparison of sonar and laser profiles along corresponding tracks in the Arctic Ocean. Sea ice processes and models: 283-299.

Warren, B.A., 1981. Deep circulation of the world ocean. Evolution of physical oceanography: 6-41.

Warren, B.A., 1983. Why is no deep water formed in the North Pacific? Journal of Marine Research, 41(2): 327-347.

Weaver, P., Thomson, J., 1993. Calculating erosion by deep-sea turbidity currents during initiation and flow. Nature, 364(6433): 136-138.

Weeks, W., 2010. On sea ice. University of Alaska Press.

Weiss, R., Östlund, H., Craig, H., 1979. Geochemical studies of the Weddell Sea. Deep Sea Research Part A. Oceanographic Research Papers, 26(10): 1093-1120.

Williams, E., Swithinbank, C., Robin, G., 1975. A submarine sonar study of Arctic pack ice. Journal of Claci% gy, 5(73).

Wolf, T.C., Thiede, J., 1991. History of terrigenous sedimentation during the past 10 my in the North Atlantic (ODP Legs 104 and 105 and DSDP Leg 81). Marine Geology, 101(1): 83-102.

Worthington, L., 1970. The Norwegian Sea as a mediterranean basin, Deep Sea Research and Oceanographic Abstracts. Elsevier, pp. 77-84.

Worthington, L.V., 1976. On the north Atlantic circulation. Johns Hopkins University Press.

Wright, J.D. et al., 2009. Late Pleistocene sea level on the New Jersey Margin: Implications to eustasy and deep-sea temperature. Global and Planetary Change, 66(1): 93-99.

Wunsch, C., 2006. Abrupt climate change: An alternative view. Quaternary Research, 65(2): 191-203.

Zaucker, F., Broecker, W.S., 1992. The influence of atmospheric moisture transport on the fresh water balance of the Atlantic drainage basin: general circulation model simulations and observations. Journal of Geophysical Research: Atmospheres (1984–2012), 97(D3): 2765-2773.

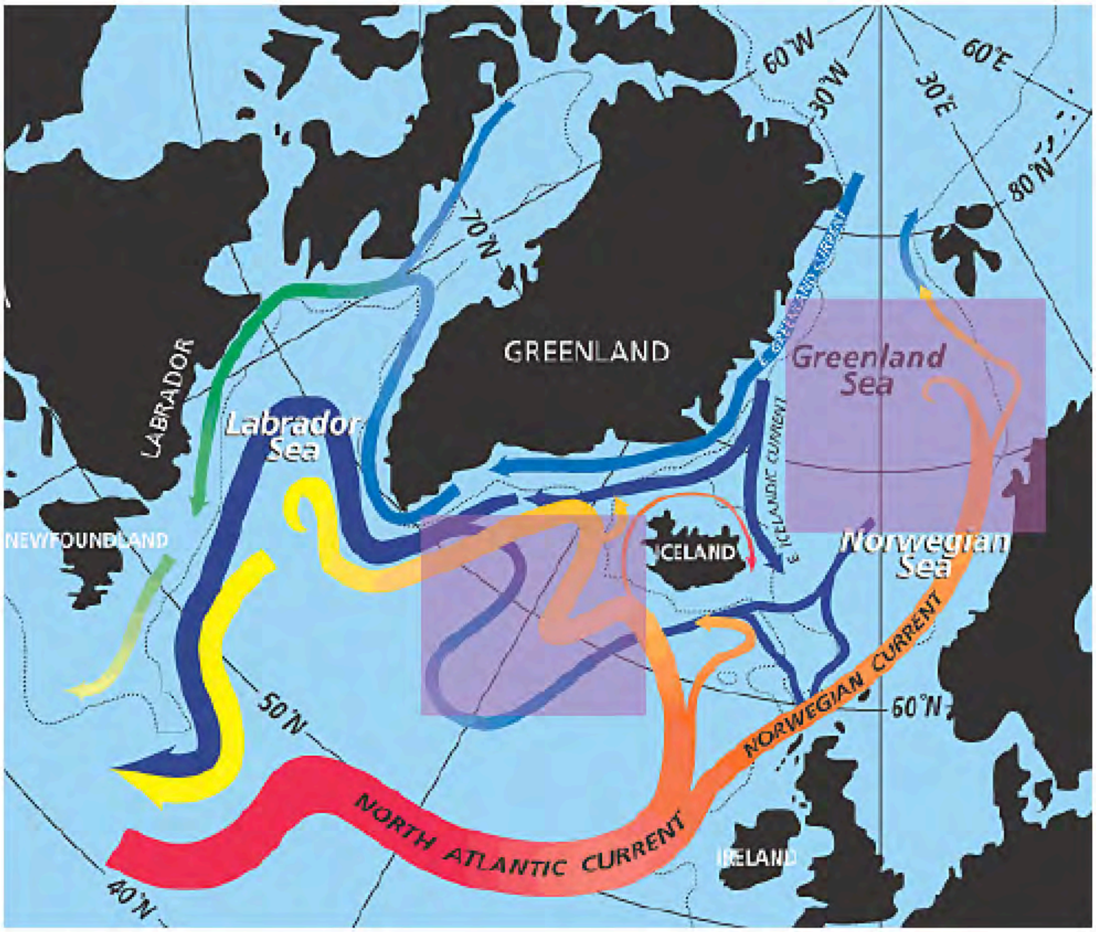

Figure 1.1

Figure 1.1: Schematic portrayal of the surface (red, yellow, orange, light blue and green colored arrows) and deep-water (dark blue) currents in the North Atlantic Ocean. The purple boxes indicate deep-water formation sites.

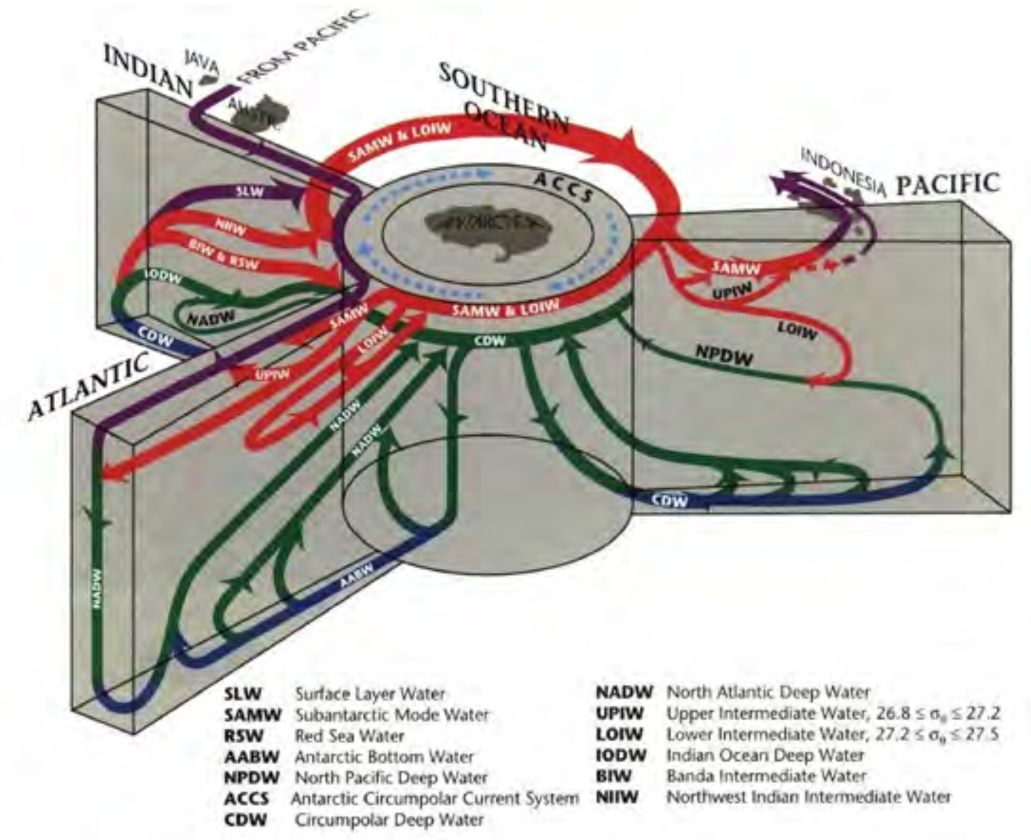

Figure 1.2: Global ocean circulation patterns for the major ocean basins and around Antarctica. Surface currents are shown in red, intermediate flow paths in green, and deep currents in blue. Modified from Charles and Fairbanks (1992).

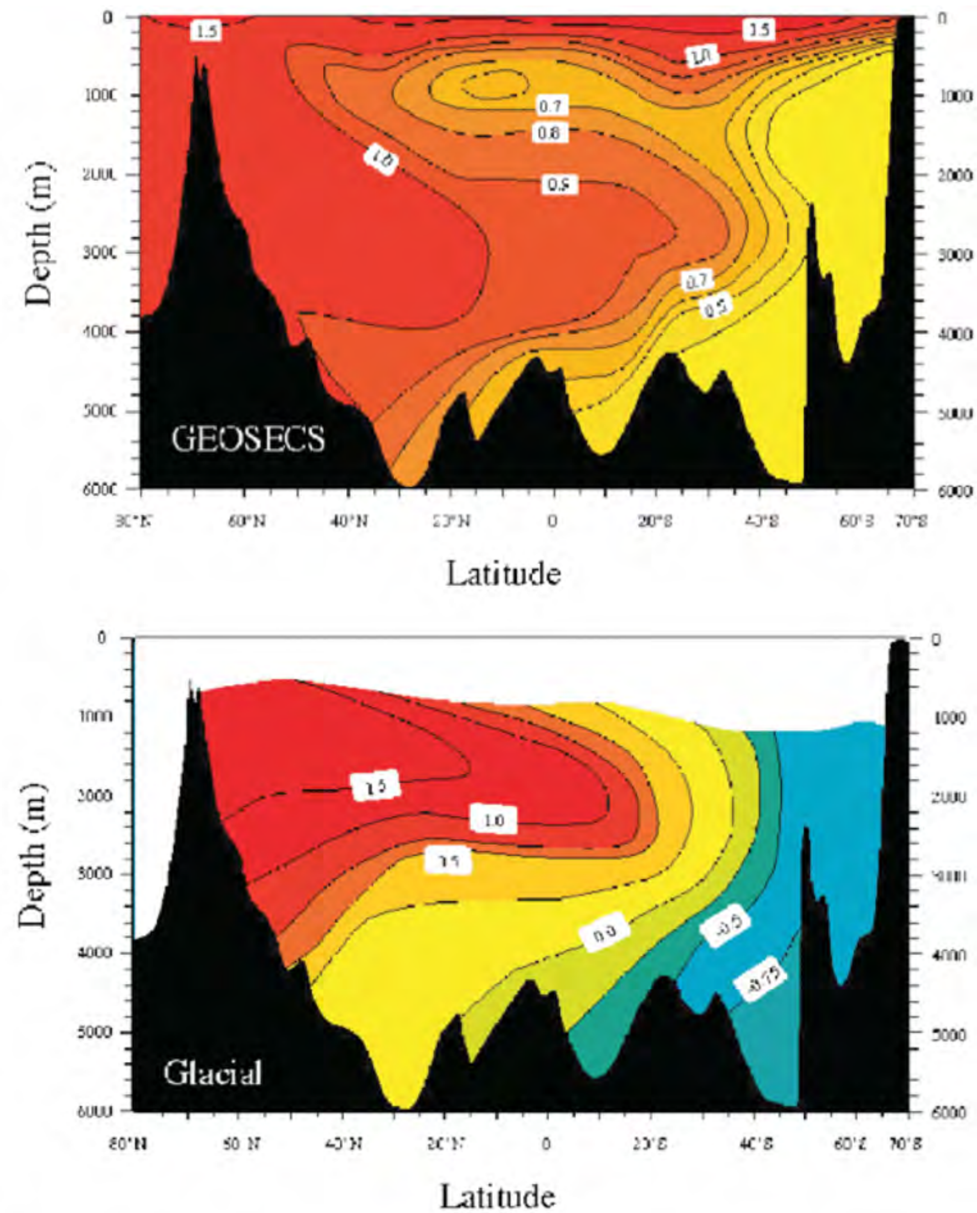

Figure 1.3

Figure 1.3: Modern (GEOSECS, above) and Last Glacial Maximum (LGM; below) $\delta^{13}C$ values from the Atlantic Ocean showing two modes of NCW circulation (Wright, unpublished).

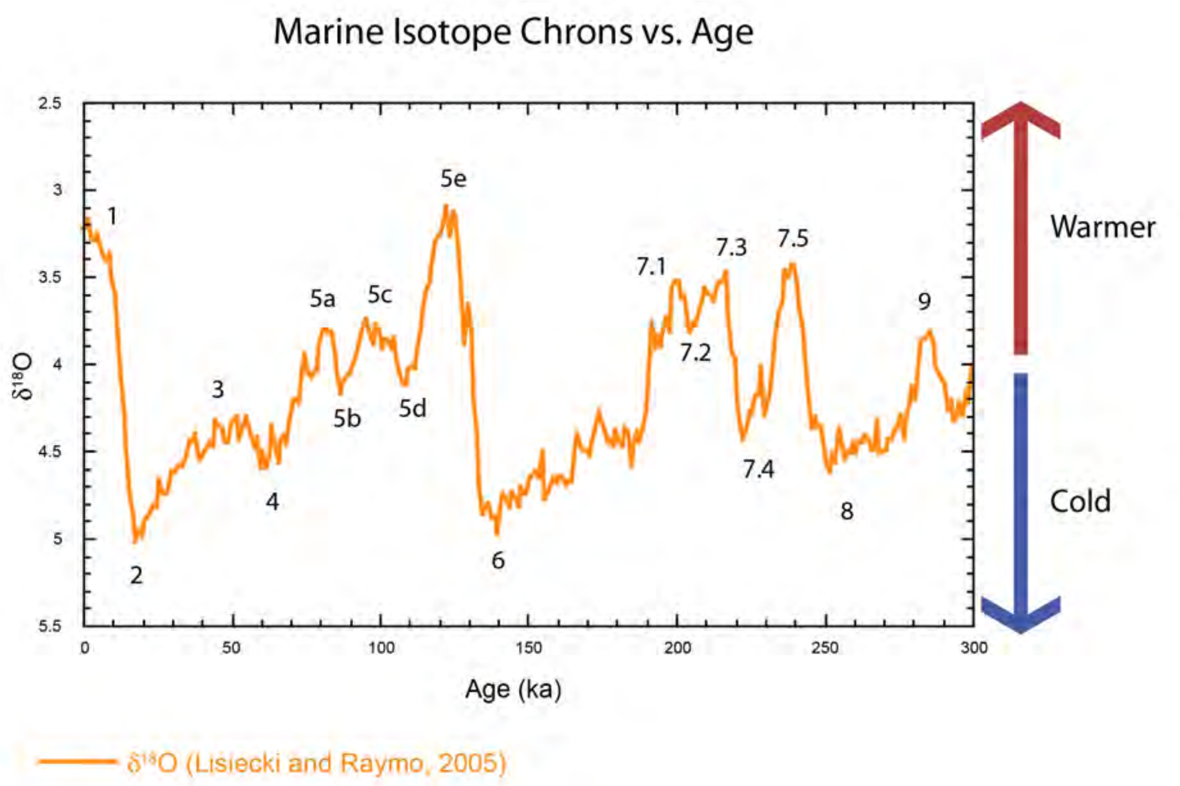

Figure 1.4

Figure 1.4: Stacked benthic foraminiferal $\delta^{18}O$ curve of Lisiecki and Raymo (2005) shown versus age in kyr. Lower values indicate warmer or interglacial times and higher values represent colder or glacial intervals. Marine Isotope Chrons 1 to 9 and the subchrons of 5 and 7 are labeled and identified by maxima and minima in the $\delta^{18}O$ curve. Odd and even numbers are used to label the interglacial and glacial intervals respectively.

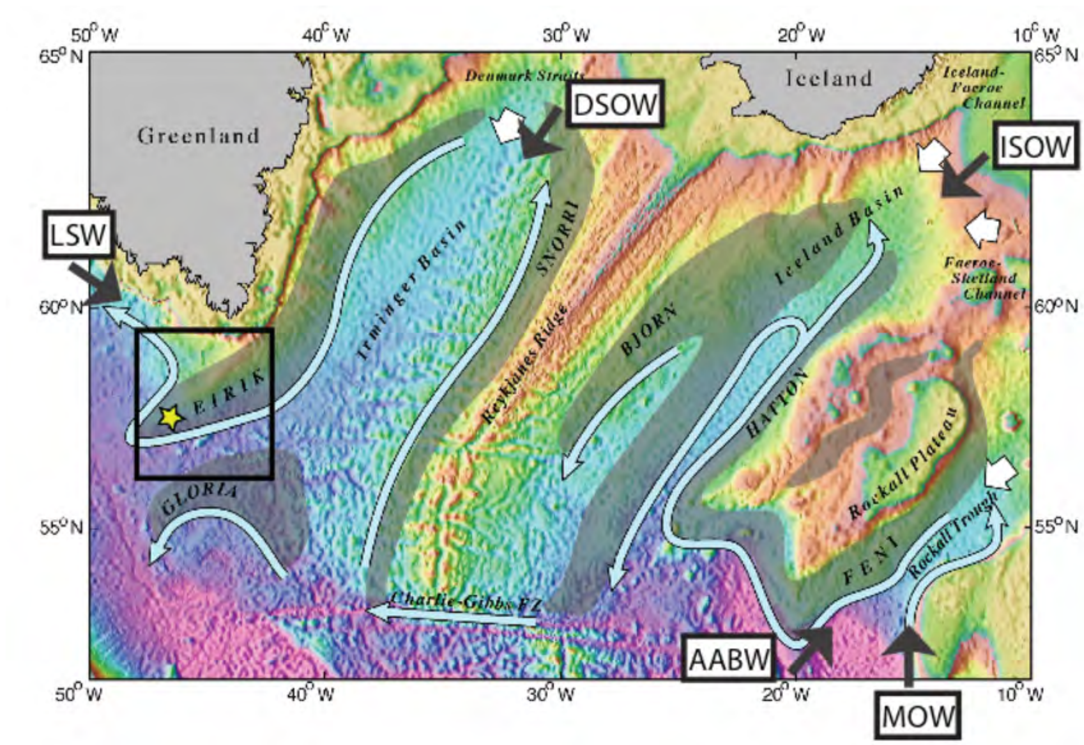

Figure 1.5

Figure 1.5: Shaded bathymetry, modified after Smith and Sandwell (1994), of the North Atlantic showing major drifts (uppercase lettering), generalized bottom currents (blue arrows), the NCW components (black arrows), the study area (black box), and the approximate location of the core sites (yellow star).

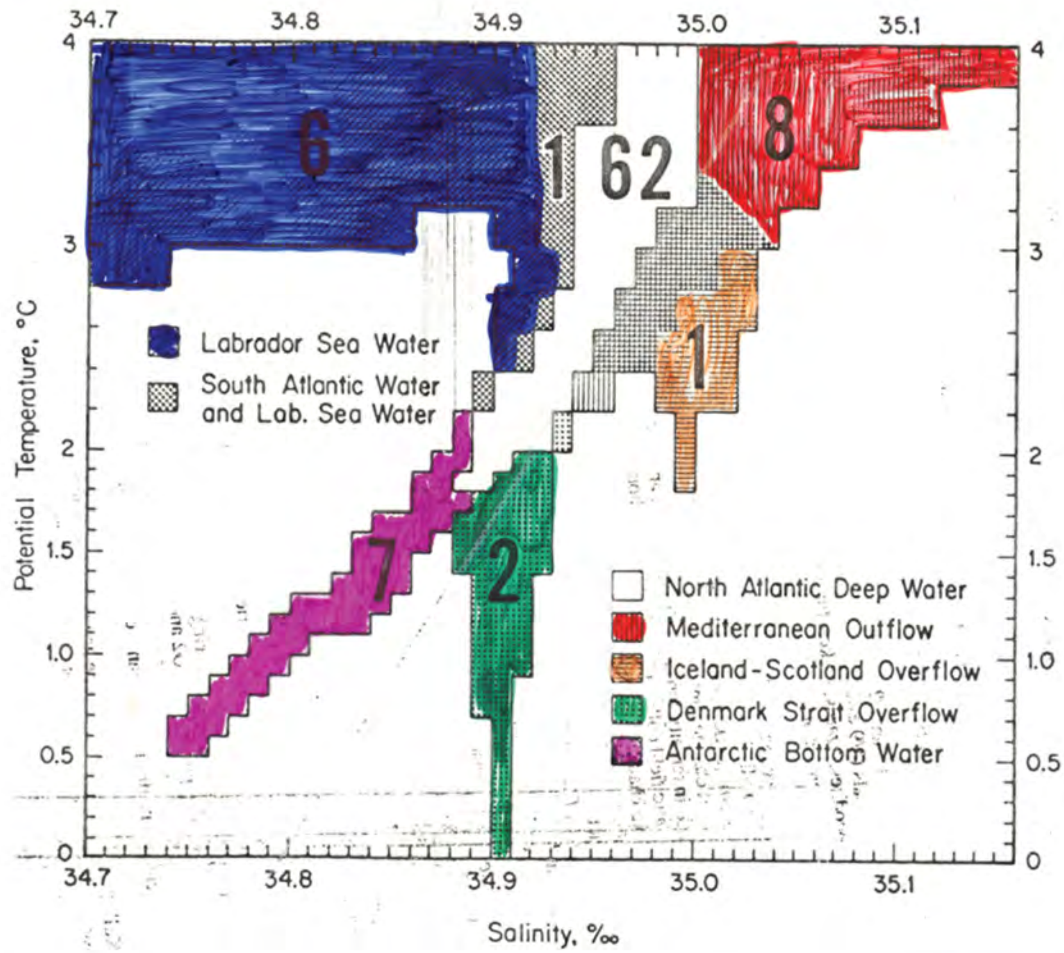

Figure 1.6

Figure 1.6: The density of seawater is a function of temperature, salinity and pressure. The density increases as salinity and pressure increase and temperature decreases. This term is called potential density or σ_Θ (sigma-theta) and is expressed in kg/m^3. Figure modified from Worthington (1976) showing the potential density for the major water masses of NCW.

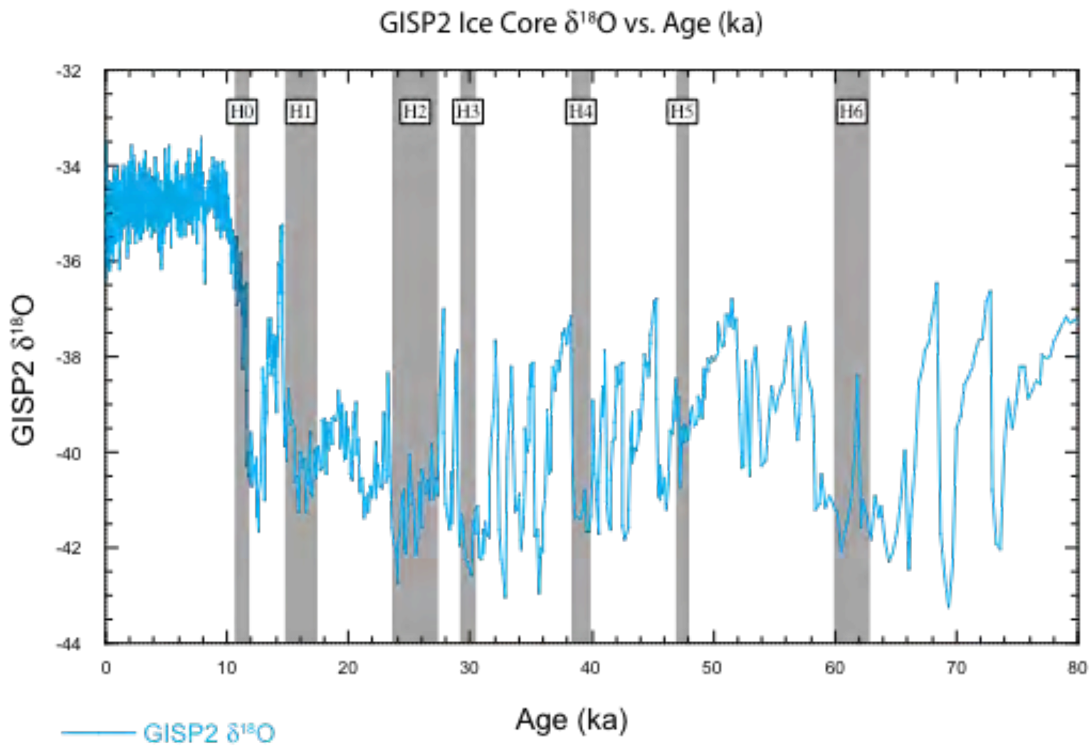

Figure 1.7

Figure 1.7: δ^{18}O curve from the Greenland Ice Sheet Project 2 (GISP2) ice core record versus age (Grootes and Stuiver, 1997; Grootes et al., 1993; Meese, 1994; Steig et al., 1994; Stuiver et al., 1995). The gray bars highlight Heinrich events H0 to H6.

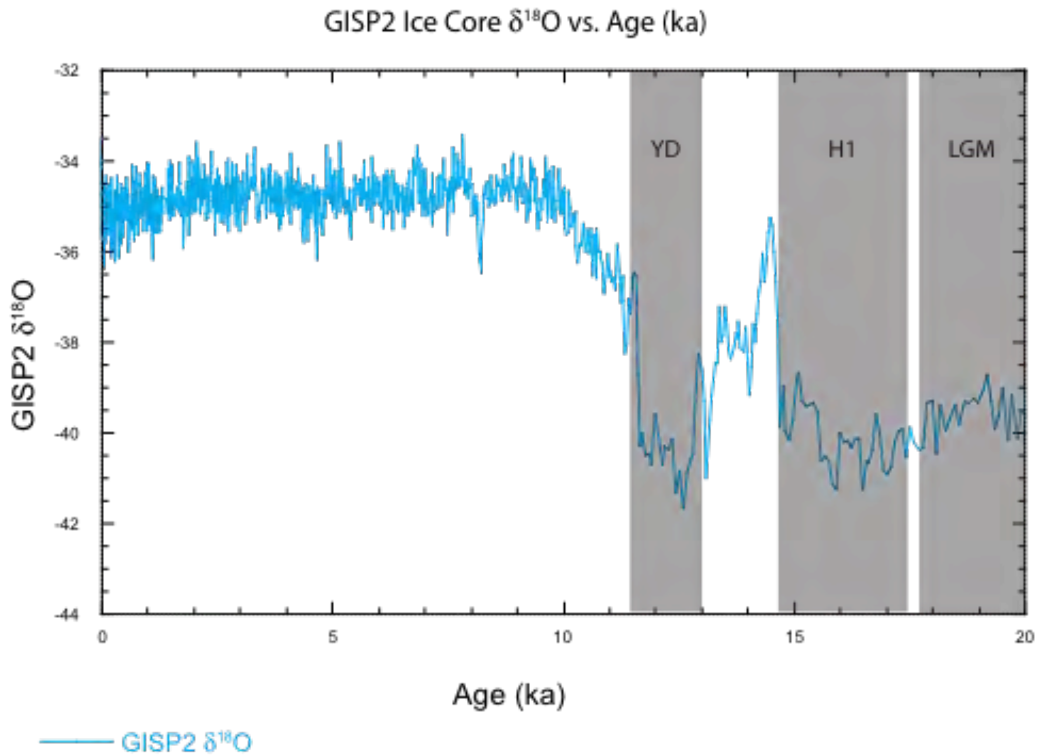

Figure 1.8

Figure 1.8: $\delta^{18}O$ curve from the Greenland Ice Sheet Project 2 (GISP2) ice core record versus age (Grootes and Stuiver, 1997; Grootes et al., 1993; Meese, 1994; Steig et al., 1994; Stuiver et al., 1995). The gray bars highlight the Younger Dryas (YD), Heinrich Event 1 (H1) and the Last Glacial Maximum (LGM).

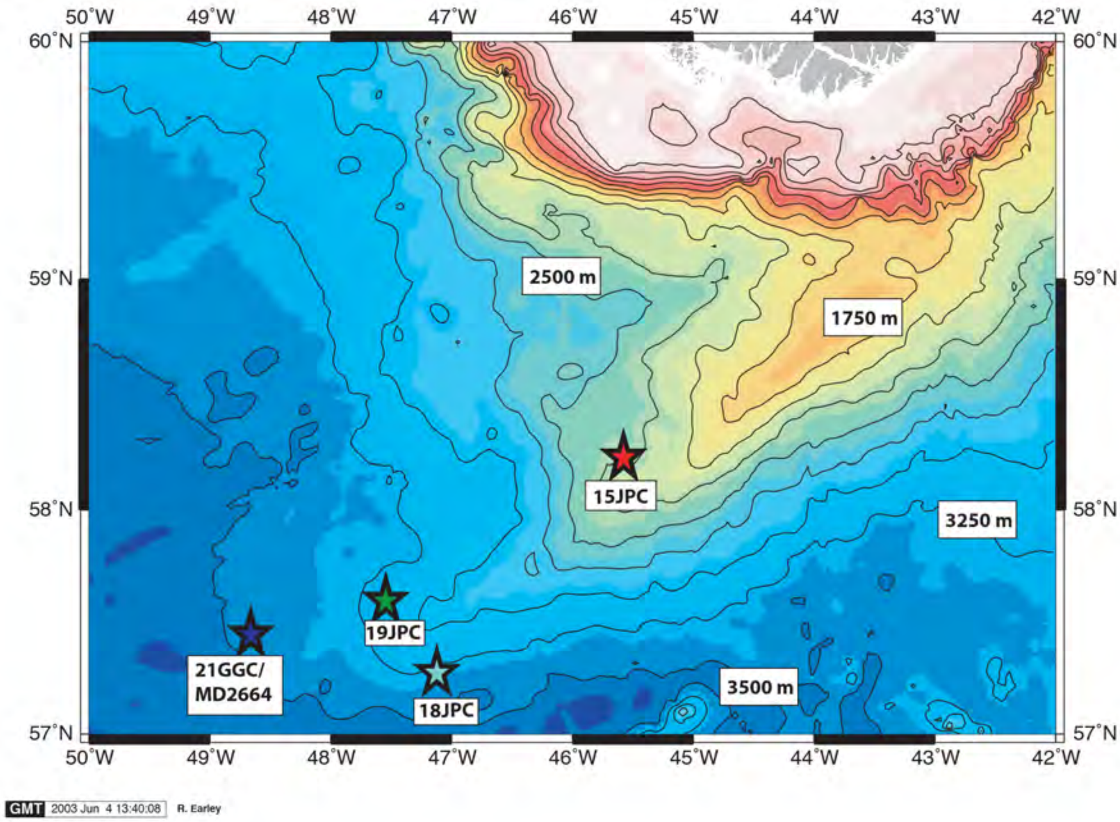

Figure 1.9

Figure 1.9: Map showing the locations of the 4 cores analyzed in Chapter 2 and 4 from the Eirik Drift. Core 15JPC (red) was also used for analysis in Chapter 3. The contour interval is 250 m and the stars indicate the approximate location of cores 15JPC (red; 2230 m), 19JPC (green; 3204 m), 18JPC (light blue; 3435 m), and MD2664 (dark blue; 3450 m).

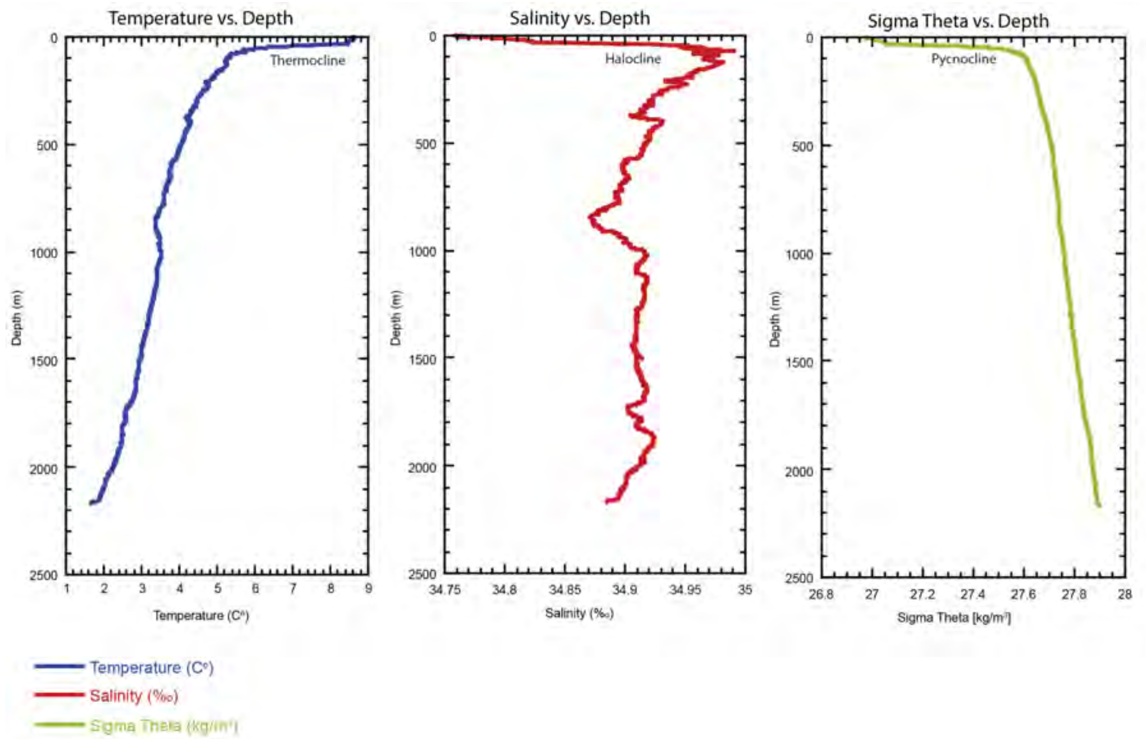

Figure 1.10

Figure 1.10: Hydrocast data retrieved from the British Oceanographic Data Centre collected on 09-SEP-05 for the RAPID-Bacon;Rapid Climate Change Programme at 58°N and 45°W. This site is proximal to site 15JPC. The water column changes in temperature, salinity and potential density (sigma theta) are shown in blue, red, and green respectively.

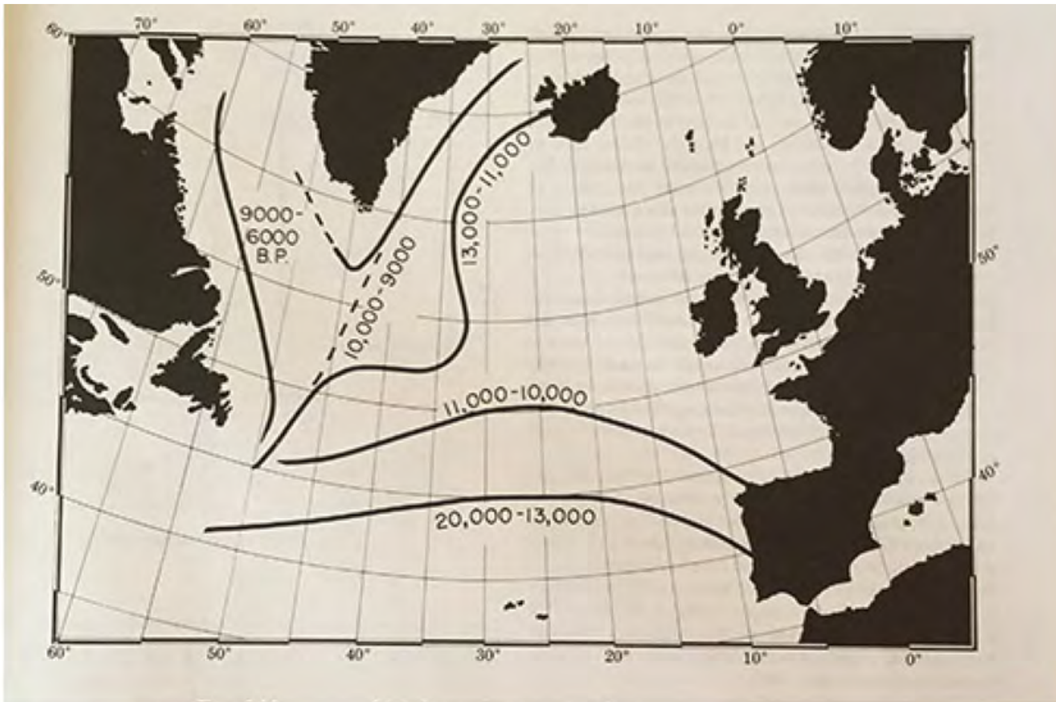

Figure 1.11

Figure 1.11: Summary map of the deglacial retreat of the polar front as first described in Ruddiman and McIntyre (1981) and presented in Ruddiman and Wright (1987).

	Water Properties			
Water Mass	**Temperature**	**Salinity**	**δ θ**	**Sverdrups**
Iceland-Scotland Overflow Water	1.9 to 3 °C [2]	35.0 ‰ [2]	27.66 [4]	4 Sv [2]
Denmark Strait Overflow Water	0 to 2.2 °C [2]	34.9 ‰ [3]	27.98 [3]	5 Sv [2]
Antarctic Bottom Water	0.5 to 2 °C [2]	34.7 to 34.8 ‰ [2]	27.87 [4]	1 Sv [2]
Labrador Sea Water	2.8 to 4 °C [2]	34.7 to 34.9 ‰ [2]	27.86 [4]	2 Sv [2]
Mediterranean Outflow Water	3 to 4 °C [2]	35.5 ‰ [3]	29.1 [1]	1 Sv [2]

Table 1.1: Temperature, Salinity, Potential Density (δ θ), and amount of contributing Sverdrups (1 x 10^6 m^3/sec) for the five sources of North Atlantic Deep Water; Iceland-Scotland Overflow Water, Denmark Strait Overflow Water, Antarctic Bottom Water, Labrador Sea Water, and Mediterranean Outflow Water. The data was complied from Worthington (1970)[1]; Worthington (1976)[2]; Reid (1979)[3], Conkright et al. (1994)[4] and Levitus and Boyer (1994)[4].

Event	Age (ka)		
	Hemming (2004)	**Bond and Lotti (1995)**	**Vidal et al. (1999)**
H0*	~12		
H1	16.8		14
H2	24	23	22
H3	~31	29	
H4	38	37	35
H5	45		45
H6	~60		

* The Younger Dryas is designated as the H0 event
** H1 and H2 ages are estimated from radiocarbon and H3-H6 ages are estimated by correlation to the GISP2 ice core record.

Table 1.2: Approximate ages of the Heinrich ice rafting events in kyr.

2.0 Deposition on Eirik Drift: Tracking North Atlantic Deep Water Variations

2.1 Abstract

The Eirik Drift, located off the southern tip of Greenland, is where south-flowing Northern Component Water (NCW; analogous to North Atlantic Deep Water) turns to the north into the Labrador Sea, slowing and depositing suspended sediment. Planktonic foraminiferal stable isotopes, % $CaCO_3$, and % coarse fraction were analyzed from a network of piston cores collected on the Eirik Drift to evaluate late Pleistocene changes in the flow of NCW and climate. During Marine Isotope Chron (MIC) 1 and Subchron 5e, the fastest sedimentation occurred on the southwestern toe of the drift at rates > 30 cm/kyr. Sedimentation rates slowed to 10 to 12 cm/kyr on the lee (NW) side of the drift with non-depositional to erosional conditions on the SE side of the drift where the seabed was exposed to the fastest SW flow of NCW. Minimum coarse fraction values (< 5%) coincide with the depositional centers, or areas of highest sedimentation, indicating high sedimentation rates and dilution by fine-grained (silt sized) current controlled deposits. Only during interglacial MIC 1 and Subchron 5e did the NCW depo-center shift to depths > 3400 m on the Eirik drift. During Subchrons 5a to 5d, high sedimentation rates and low coarse fraction values (~10 to 42 cm/kyr and ~ 1 to 8 %, respectively) are recorded on the toe and the northeastern crest of the drift, indicating that the outer edges of the current were in close proximity to the sites and yielded increased deposition, but that NCW did not reach as deep as 3400 m. Low sedimentation rates (~ 2 to 10 cm/kyr) are seen on the distal end of Eirik Drift, while high sedimentation rates and low coarse fraction values (~ 10 to 24 cm/kyr and ~ 2-4 %, respectively) are found on the northeastern crest of the drift during the glacial Chrons 2 to 4, and 6, and imply shoaling

of NCW during these intervals. Thus, at least three regimes existed in the thermohaline system in the recent past: (1) a strong, deep penetrating current that eroded the SE flank during interglacial Chrons 1 and 5e; (2) an intermediate regime during Subchrons 5a to 5d that resulted in enhanced current controlled deposition at the toe and northeastern crest of the drift; and (3) a glacial regime in which the deep North Atlantic current shoaled approximately 1 km**,** significantly increasing deposition on the NE portion of the drift. Sedimentation patterns of the Subchrons of MIC 5 indicate that the position of the deep current axis changes in response to orbital, as well as to suborbital variability. Further evidence suggests Subchrons 5a, 5c, and 5e each exhibit distinct circulation patterns indicating significant variability in the southern penetration of NCW on Eirik Drift on the suborbital timescale.

2.2 Introduction

Changes in deep ocean circulation are often causally linked to changes in climate because of the role that deep circulation plays in redistributing heat, salt and nutrients/carbon (i.e., Broecker, 1991). Though patterns of deep circulation in the North Atlantic were starkly different between the Last Glacial Maximum (LGM) and present, much of the late Pleistocene climate operated in modes that were intermediate between these end-members (e.g., Broecker et al., 1985; Curry et al. 1987; Duplessy et al., 1987; Imbrie et al., 1993). Deep-water production in the North Atlantic is described as a bimodal system that varies in water mass flux and buoyancy state over glacial and interglacial intervals (e.g., Broecker et al., 1985; Imbrie et al., 1993; Oppo and Lehman, 1993; Hillarie-Marcel et al., 1994; Liseicki et al., 2008). This study examines the intermediate states of deepwater production as it switched between the glacial and interglacial end members. We present records of various sedimentary and geochemical proxies from a suite of piston cores from the Eirik Drift spanning a water depth range of 2200 to 3500 m. Evaluating the changes in these proxies allows us to estimate the position of the deep current axis, and hence, the relative buoyancy changes in NCW associated with the varying climate states.

2.3 Regional Setting

Eirik Drift extends 800 km SSW from the southern tip of Greenland. It is made largely of sediments dropped from suspension as the NCW flows SW along the eastern margin of Greenland and with reduced velocity spreads westward into the Labrador Basin (Figure 1). Seismic profiles tied to ODP Leg 105 drill cores indicate that most of the drift has been constructed since the late Miocene (Arthur et al., 1989; Wold, 1994). Although sedimentation has been more or less continuous on many parts of the drift, sedimentation rates varied significantly depending on the climatic conditions and position on the drift (Hillaire-Marcel et al., 1994). In drift systems, sediments are often deposited, reworked, and redeposited, modifying the percent coarse fraction and sedimentation rates, both laterally and vertically. These patterns reflect changes in the strength and position of the deep current as it winnows and/or redeposits sediments and they provide insight into the history of deep-water flow and the factors that control it.

Eirik Drift provides an ideal location to study the variations in deep-water flow because it is the first repository of sediment down current from where the major components join to form NCW (Denmark Straits and Iceland-Scotland overflow water). High sedimentation rates (5 to ≥ 100 cm/kyr) on the drift result from high sediment load and decreased current velocities as NCW turns west and enters the Labrador Sea (Hunter et al., 2007; Stanford et al., 2011). Furthermore, the morphology of Eirik Drift is such that the depositional center shifts up and down the drift crest as the buoyancy of the deep current changes (Hillaire-Marcel et al. 1994; Stoner et al., 1995, 1996; Evans et al., 2007; Channel et al., 2014). Thus, the sedimentary record at Eirik Drift has the potential to provide a first-order reconstruction of the changes in the vertical position of the deep current axis over time.

2.4 Materials and Methods

Samples used for this study were taken from a suite of cores collected in the summer of 2002 on cruise KN166-14 of the *R/V Knorr*. Five Jumbo Piston Cores (JPC) were selected and analyzed for this study (Figure 1; Table 1). Cores 19JPC and 18JPC were taken from the northwestern (3204 m) and southeastern (3435 m) flanks of the ridge crest of Eirik Drift, respectively. Core 15JPC was collected to the north and east of the other cores in 2230 m water depth. Cores are archived at Rutgers University where they were split, photographed, sampled, and stored at 5 °C. Approximately 6 to 10 cm^3 samples were taken every 5 cm for the entire length of 15JPC, 18JPC, and 19JPC to obtain roughly 500-year resolution for the past 150 kyr. Core MD03-2664 (Marion Dufresne 132 Leg 2) was collected from the deepest portion of Eirik Drift at 3442 m water depth.

Weight percent coarse fraction, hereafter known as coarse fraction, was determined for each sample. All samples were initially dried overnight and the coarse fraction was determined using the following equation:

Wt. % CF = (Dry wt. washed/Dry wt. initial) * 100 where Dry wt. washed and Dry wt. initial refer to the weights before and after being washed through a 63 μm sieve.

The number of Ice Rafted Detritus (IRD) grains per gram were calculated every 10 cm on samples from core 15PC. The washed samples (> 63 μm) were sieved at 150 μm and split 1 to 4 times (Hemming et al., 1998; McManus et al., 1998; and Stanford et al., 2006). All remaining lithic grains were counted and then converted to the number of IRD grains per gram (#IRD grains per gram) according to the following formula:

$$\#\text{IRD grains per gram} = \#\text{IRD} * (2^{(\#\text{Splits}/\ \text{Dry Wt.})})$$

where #IRD, #Splits, and Dry Wt. refer to the number of lithic grains counted, the number of times the samples were split, and the dry weight of the sample after being washed through a 63 μm sieve, respectively.

Planktonic foraminiferal $\delta^{18}O$ and $\delta^{13}C$ downcore records were generated for all of the cores to provide stratigraphic control. Approximately 10 to 15 *Neogloboquadrina pachyderma (sinistral*) tests were handpicked under a binocular microscope from the > 212 μm size fraction, and selected for stable isotope analysis. All samples were analyzed in the Stable Isotope Laboratory at Rutgers University on a Micromass Optima Mass Spectrometer with an attached Multiprep peripheral for the automated analysis of carbonate material. Samples were loaded into a multi-prep device and reacted with 100 % phosphoric acid at 90 °C for 15 minutes. All measured values are reported relative to V-PDB (Vienna PeeDee Belemnite) using an internal lab standard. This standard is routinely checked against NBS-19, which has values of 1.95 ‰ and - 2.20 ‰ for $\delta^{13}C$ and $\delta^{18}O$, respectively (Coplen et al., 1983). The offsets between the lab standard and NBS-19 are 0.04 ‰ for $\delta^{18}O$ and 0.10 ‰ for $\delta^{13}C$. Typical lab precision for

1-σ of the standards reported versus V-PDB is 0.05 ‰ for $\delta^{13}C$ and 0.08 ‰ for $\delta^{18}O$. The downcore isotopic and percent coarse fraction data can be found in Appendix 1.

Fifteen depths intervals within the upper 200 cm of Core 15JPC were selected for Accelerator mass spectrometry (AMS) dating. For each interval, 4 to 6 mg of planktonic foraminifera *Neogloboquadrina pachyderma,* sinistral were selected using a binocular microscope and sonified in deionized water. The crushed samples were then sent to the National Ocean Sciences Accelerator Mass Spectrometry (NOSAMS) facility for ^{14}C dating. The resulting radiocarbon ages were converted to calendar ages according the Fairbanks0805 calibration after a 600-year reservoir correction was applied (Fairbanks et al., 2005; Thornalley et al., 2011; Bondevik et al., 2006; Appendix 1 and 2). Three ages were discarded due to age reversals and inspection of the core showed foram sands indicating winnowing and sediment reworking at these depths.

Age models for these cores were constructed by comparing the measured $\delta^{18}O$ records of the cores to a published stacked benthic $\delta^{18}O$ curve of Liseicki and Raymo (2006) and to the published $\delta^{18}O$, $\delta^{13}C$, and relative paleointensity (RPI) records from IODP Site 1306 (equivalent to the site of core 15JPC; Channell et al., 2014). Ages were assigned to the major isotopic minimum, maximum, and transitions by comparing the $\delta^{18}O$ and $\delta^{13}C$ records of Cores 15JPC, 18JPC, 19JPC, and MD2664 to the Liseicki and Raymo (2005) and Channell et al. (2014) curves. Further age control was provided by correlating regional magnetic events through the use of RPI (Evans et al., 2007) and shipboard magnetic susceptibility measurements. The 13 selected AMS ^{14}C corrected dates were used to constrain the ages within the upper 200 cm of core 15JPC. Ages between these tie points were linearly interpolated for all 4 downcore records (Appendix 1).

2.5 Results

Site to site correlation of planktonic foraminiferal $\delta^{18}O$ records is difficult in this region due to the large areal and temporal variability in the sedimentation rates (2 to >60 cm/kyr). The downcore $\delta^{18}O$ results for Cores 15JPC, 18JPC, 19JPC, and MD2664 record expanded and condensed intervals among the different localities on the drift (Figure 2). Two end-member depo-centers have previously been identified for this region. One occurs on the deeper, more distal portions of Eirik Drift during warm climates, the other occurs in shallower parts of the Drift during cold climates (Hillaire-Marcel et al. 1994; Stoner et al., 1996; Hall and Becker, 2007; Hillaire-Marcel et al., 2001; Channell et al., 2014).

Our results reveal this same bi-modal pattern with higher accumulation rates in the deeper cores during the warmer intervals and lower accumulation rates in the shallower cores during the colder intervals (Figure 2). For example, the Holocene (MIC 1) is represented by ~ 1200 cm of sediments in core MD2664 (3450 m) and ~ 200 cm in core 19JPC (3204 m), while at the shallower site, there are < 7 cm of highly winnowed sediment in core 15JPC (2230 m; Figure 2). The sediments from this interval are missing in core 18JPC (3435 m), and visual inspection of this core reveals an erosional surface at the top of the core. In contrast, the Last Glacial Maximum (LGM; MIC 2) interval in core 15JPC (2230 m) is represented by > 250 cm, while this same interval in cores 18JPC (3435 m), 19JPC (3204 m), and MD2664 (3450 m; southern toe of drift) contains 60 to 100 cm (Figure 2).

To further illustrate these variations in sediment accumulation among the sites through time, we plotted the average sedimentation rates (Figure 3) at each of the chrons (MIC 1 to 4, and 6) and the subchrons of MIC 5 (MIC 5a to 5e) for cores 15JPC, 18JPC, 19JPC, and MD2664. MIC 1 and subchron 5e are characterized by high sedimentation (~ 12 to > 60 cm/kyr) at the deep sites (MD2664 and 19JPC) and relatively low sedimentation (~ 10 cm/kyr) at the shallow sites (15JPC). In contrast, during the glacial intervals, MIC 2 and 6, accumulation at the shallow site (15JPC) was high (~ 14 to 25 cm/kyr), and lower (< 10 cm/kyr) at the deeper sites (MD2664 and 19JPC).

We also identify accumulation patterns for MIC 3 to 5d that are between the end-members described above. The subchrons of MIC 5 exhibit more complex patterns. In general, higher sedimentation rates occurred at the deeper site, although there was significant accumulation at the shallow site 15JPC (> 8 cm/kyr), especially during MIC 5c (Figure 3). The highest overall sediment accumulation on Eirik Drift occurred during MIC 5c, with all of the sites accumulating sediments at rates > 20 cm/kyr. During MIC 5e, the only significant accumulation occurred at the deepest site, MD2664**,** while sites 15JPC, 18JPC, and 19JPC were highly winnowed or almost completely eroded, as in the case at 18JPC during MIC 5e (Figure 3). We also note that MD2664 displays a bimodal pattern with higher sedimentation rates (~26 to 45 cm/kyr) during interglacial Subchrons 5a, 5c and 5e and low sedimentation rates (~8 to 12 cm/kyr) during glacial Subchrons 5b and 5d. Alternatively, lower sedimentation rates (~0 to 12 cm/kyr) are seen on the distal end of the drift during Subchrons 5a and 5e and higher sedimentation rates are seen in all cores during Subchron 5c (~22 to 45 cm/kyr).

Variations in the coarse fraction indicate: 1) changes in the supply of sand sized particles from either increased productivity of planktonic foraminifera or the presence of icebergs delivering more ice rafted detritus (IRD); or 2) the strength and position of the axis of the deep current, either winnowing or focusing clay and silt sized particles. The general pattern yields high coarse fraction values (>20%) during interglacial MIC 1 and Subchron 5e (Figure 4) and low values (< 5%) during the glacial intervals (MIC 2, 4 and 6; Figure 4). The deeper sites show more variability in the coarse fraction values, particularly during the warmer intervals that indicate deposition in this area is controlled by the position of the deep current axis. For example, the deep core MD2664 appears to show a bi-modal pattern, with low coarse fraction (~3 to 5%) during MIC 1 and subchrons 5a to 5e, and higher values during MIC 2 to 4 (~8%; Figure 4). Coarse fraction values in 19JPC are more variable, with high values (~8 to 16%) during MIC 2, 4, and 6, but the highest coarse fraction values are recorded during MIC 1 and 5e (>25%; Figure 4). The lowest coarse fraction values at 19JPC are recorded during MIC 5a-5d (~3 to 7%). Core 18JPC generally follows 19JPC but has little to no sediments during MIC 1 and 5e.

A general trend can also be seen in the Wt. %CF and #IRD grains per gram of Core 15JPC (Figure 5). During the warmer intervals, MIC 1 and Subchron 5e, both the Wt. %CF and #IRD grains per gram exhibit relatively high values (~ 25 to >60 % and ~ 1500 to 4000 grains per gram, respectively). Conversely, during the colder intervals, MIC 2, 3, 4, and 6, the #IRD grains per gram remains high (~ 1000 to 4000 grains per gram), while the Wt. %CF records relatively low values (~ 5 to 10 %). The other intervals show more variability and record intermediate values between the two end members noted above.

The relationship of the shifting accumulation rates and coarse fraction values is summarized in Figure 6, which demonstrates that the depositional center is at its deepest and shallowest position during MIC 1 and Subchron 5e and glacial intervals, respectively (Figure 6a and 6b). During the intermediate climate intervals, the depositional center fluctuates between these two end-member modes (Figure 6c). Furthermore, during these intervals, the location of the lowest coarse fraction values coincides with the depositional centers. During the MIC 1 and Subchron 5e, the coarse fraction low and the depositional center are both centered above the southwestern toe of the drift (Figure 6a). Alternately, during the glacial intervals, the coarse fraction low and depositional center both shifted upslope (Figure 6b), and during the intermediate intervals, the coarse fraction low and depositional center were both positioned upslope from Cores 19JPC and 18JPC (Figure 6c).

2.6 Discussion

Geochemical evidence from numerous studies has indicated that the pattern of deep-water circulation during glacial times differed from the modern day (Streeter and Shackleton, 1979; Boyle and Keigwin, 1987; Oppo and Fairbanks, 1987; Duplessy et al., 1988; Oppo and Lehman, 1995). A cross-section of the compiled Atlantic Ocean $\delta^{13}C$ records shows that the core of NCW shoaled by approximately 2 km during the last glacial interval (Curry et al., 1988; Sarnthein et al., 1988; Oppo and Lehman, 1995). Our analysis has found changes in sedimentation rate and coarse fraction on Eirik Drift as a result of these oceanographic changes. Two end-members and one intermediate flow regime are inferred from these changes in sedimentation (Figure 7).

During the flow regime associated with MIC 1 and 5e, deposition was concentrated at the southernmost and deepest location of the drift (at least 3400 m; Figure 7a). The core of NCW swept directly across 18JPC (3435 m) and 15JPC (2230 m), creating non-depositional or erosive conditions. This corresponds with modern hydrographic and sedimentological studies, which show that the core of NCW flowing across Eirik Drift is centered between 2000 m (Clarke, 1984; Hunter et al., 2007 and Stanford et al., 2011) and 2500 m, respectively (Evans et al., 2007). Core 19JPC, received limited deposition; however, increased coarse fraction values, indicative of erosion and winnowing, were also recorded at 19JPC during this interval. This indicates that the current axis turned into the Labrador Sea in the vicinity of Core 19JPC.

The second regime operated during glacial intervals, when NCW shoaled significantly to its shallowest position (Figure 7b). As a result, the locus of sediment deposition shifted to the vicinity of 15JPC, suggesting that the current axis shoaled by >1500 m (Figure 7). During this mode, this deep contour current was positioned well to the north and east of MD2664 (sedimentation rate of approximately 7 cm/kyr; Figure 6b) . Cores 18JPC and 19JPC, which are located on opposite sides of the drift crest, recorded similar sedimentation, consistent with the interpretation that NCW had little erosional or winnowing effect on the distal parts of the drift during glacial conditions. Rather, the zone of erosion and/or non-deposition would have migrated upslope closer to 15JPC (Figure 6b).

The intermediate regime prevailed throughout the interglacial Subchrons 5a to 5d, and resulted in increased sedimentation at the base and the northeastern crest of the drift (Figure 6c). During these periods, the outer edge of NCW was situated in close proximity to 19JPC and 18JPC, depositing large amounts of transported sediments at these sites (Figure 7c). Sedimentation rates at upslope locations (i.e., 15JPC) were also high during this interval, and indicate that the outer edges of NCW also affected deposition at this site. It is inferred that during the intermediate mode NCW was situated between the two end-member positions of the glacial and MIC 1 and Subchron 5e regimes (Figure 7c).

These three flow regimes are also seen in the average coarse fraction patterns on Eirik Drift (Figure 6). In all three modes, low coarse fraction values are found near the depositional centers, implying dilution by fine-grained transported material. During the MIC 1 and Subchron 5e regime, the coarse fraction low and the depositional center were both centered on the southwestern toe of the drift, indicating a deep penetration of NCW (Figure 6a and 7a). Interglacial periods had fewer icebergs, and hence less ice-rafted detritus (IRD); therefore we would expect the average coarse fraction values to be lower during these intervals. However, the coarse fraction values increase moving away from the depositional center, implying less dilution by the fine-grained material. Core 15JPC, which is situated outside of the depositional center during these intervals, records high coarse fraction and #IRD grains per gram during MIC 1 and 5e (Figure 5). This indicates that the current was directly over this site during this time, winnowing the fine grains and leaving behind the coarser grained material. Inspection of the core also reveled the presence of foraminiferal sands, further supporting the idea of current controlled deposition and winnowing.

During the glacial regime, the coarse fraction low and depositional center both shifted upslope (15JPC) implying a shoaling of NCW (Figure 6b and 7b). Due to the presence of glaciers and icebergs, glacial intervals generally record higher IRD values (Hemming, 2004), and as expected, Core 15JPC records high values of #IRD grains per gram during MIC 2, 3, 4, and 6. However, the low coarse fraction values also recorded during these intervals indicate that this site was diluted with large amounts of fine-grained material, further supporting the current controlled deposition hypothesis. The deeper portion of Eirik Drift shows lower sedimentation rates and higher coarse fraction values indicating that the majority of the deposition resulted from vertical rain with little to no current controlled deposition. Even though the glacial sedimentation rates (5 to 8 cm/kyr) were still relatively high compared to open ocean sedimentation, the vertical rain interpretation is supported by similar glacial sedimentation rates in North Atlantic cores V23-81 and DSDP 609 (8 to 10 cm/kyr during MIC 2 to 4; Bond et al., 1992) which are located on the eastern flank of the Mid-Atlantic Ridge.

During the intermediate regime, low coarse fraction values and sedimentation rates indicate that the depo-center was positioned upslope from 19JPC and 18JPC (Figure 6c). However, the current is not expected to have shoaled above the depth of 15JPC because, in this position, the deeper cores 18JPC and 19JPC would be too distal to receive the high sediment fluxes. The average sedimentation rate of 10 cm/kyr at 15JPC during MIC 5a to 5d suggests that sediments were preferentially deposited in this area by the deep current. A large vertical flux is not expected in this region at this time because the regional and global climate during MIC 5a to 5d was moderately warm.

It is expected that for much of the glacial-interglacial cycle, during the intermediate mode, the current axis fluctuated between the interglacial and glacial end-members on suborbital timescales (e.g., MIC 3 and 4 and Subchrons 5a-5d; Oppo and Lehman, 1993; Hillaire-Marcel et al., 1994). This conclusion is supported by the comparison of the changes in the sedimentation rates in Subchrons 5a to 5d between 19JPC and 15JPC (Figure 3). Glacial Subchrons 5b and 5d are well defined and expanded in the $\delta^{18}O$ record for 15JPC, whereas, these intervals are not well defined in 19JPC. This pattern reflects subtle changes in the current's position as it shoaled and moved up the eastern flank of Eirik Drift and closer to 15JPC. In contrast, the warmer Subchron 5c is expanded in 19JPC, but not well-defined in 15JPC, and shows a down-slope migration of the current axis during this interval. It is also suspected that higher frequency changes in the position of the deep current axis occurred during the glacial intervals (Piotrowski et al., 2005).

Furthermore, we propose that there were differences in the position of the current axis between the interglacial Subchrons 5a, 5c and 5e. As already stated, the current was situated at its southern most position during Subchron 5e. The majority of this interval is highly winnowed or eroded in Cores 19JPC and 18JPC, but the small portion of the record that appears to be undisturbed shows high sedimentation rates (~8 to 10 cm/kyr), indicating increased deposition immediately preceding the establishment of the interglacial MIC 1 and Subchron 5e NCW flow. Cores 19JPC and 18JPC show higher sedimentation rates (~32 to 38 cm/kyr) during Subchron 5c and lower sedimentation rates

(~12 to 18 cm/kyr) during Subchron 5a. This indicates a more southern penetration of NCW during Subchron 5c than 5a allowing for a higher rate of sediment transport to the distal end of the drift. However, the lack of evidence for winnowing or erosion during Subchron 5c indicates that NCW did not penetrate as deep as during Subchron 5e.

An alternative explanation to the variations in the coarse fraction values and shifting depositional centers is that there is no transitional regime but that these cores are recording the movement of the current from one extreme to the next. This hypothesis suggests that the current continuously varies across the crest of the drift and that the position of the current during the MIC 1 and Subchron 5e and glacial regimes mark the extent of the southern and northern boundaries, respectively. However, both hypothesis indicate that dominate mode of deposition is not represented by the interglacial and glacial extremes and that the axis of the deep current is constantly in flux.

2.7 Conclusions

Analysis of the stable isotopic and sediment proxy records for jumbo piston cores recovered from Eirik Drift show two end-members and an intermediate mode of circulation. The interglacial intervals, MIC 1 and Subchron 5e, exhibit similar depositional patterns and are the warmest intervals recorded in the North Atlantic. During these intervals, deposition on the southwestern toe of the drift was dominated by the spill over of sediments carried by NCW flowing across the crest of the drift, while non-depositional or erosive conditions persisted on the crest and southeastern flank of the drift. This conclusion agrees with modern hydrographic data observed over Eirik Drift of the East Greenland and East Greenland Coastal Current flow pathways (Holliday et al., 2007; Holliday et al., 2009 and Stanford et al., 2011).

Low sedimentation rates at the toe of the drift and high sedimentation rates on the northeastern crest of the drift were observed during the glacial intervals MIC 2, 3, 4 and 6. The low sedimentation rates at the toe of the drift indicate that 19JPC and 18JPC were not under the direct influence of NCW, and that the current was distal to the sites during these intervals. The depositional center moved up the ridge crest, indicating a shoaling of the current axis by about 1500 m, to the vicinity of 15JPC. Here, sedimentation rates averaged 30 cm/kyr during MIC 2 to 4.

The third, or intermediate, mode of circulation dominated during interglacial Subchrons 5a to 5d when global and regional surface water temperatures were between the values characteristic of glacial and full interglacial times (e.g., MIC1 or 5e). Since the sedimentation rates at 15JPC, 18JPC, and 19JPC are too high to be accounted for by a vertical flux alone, we propose that current controlled deposition of silts by NCW elevated the sedimentation rates. The low coarse fraction percentages also support this argument, and suggest that no erosion occurred during these intervals. This implies that neither site lay directly along the path of NCW; however, the outer edges of the current were in close proximity to the sites and yielded increased deposition of transported material. Examination of the sedimentation patterns of Subchrons 5a to 5e indicate that the position of the current axis also changes on suborbital timescales, with a more deeply penetrating current during the more interglacial Subchrons 5a, 5c and 5e, and a shoaled current during the more glacial Subchrons 5b and 5d. We further propose that there were variations in the position of NCW between interglacial Subchrons 5a and 5c.

Based on analysis of the stable isotopic and sedimentological records from the Eirik Drift cores, we infer three regimes that operate on orbital and suborbital timescales.

During the interglacial MIC 1 and 5e regime, NCW is situated at its deepest and southernmost position. The glacial regime, which prevailed during MIC 2 to 4 and 6, is associated with a shoaling of NCW to its shallowest and northernmost position. During these periods, the influence of AABW was greater, and consequently the ratio of NCW to AABW was lower. A third, intermediate regime, which is the dominant regime in this area, is inferred during the interglacial Subchrons 5a to 5d. During these intervals, NCW shoaled slightly and is situated between the two end member positions.

2.8 References

Arthur, M.A., Srivastava, S.P., Kaminski, M., Jarrad, R., Osler, J., 1989. Seismic stratigraphy and history of deep circulation and sediment drift development in Baffin Bay and the Labrador Sea. Proceedings of the Ocean Drilling Program. 105, 957-988.

Bond, G.C., Heinrich, H., Broecker, W.S., Labeyrie, L.D., McManus, J., Andrews, J., Huon, S., Jantschik, R., Clasen, S., Simet, C., Tedesco, K., Klas, M., Bonani, G., Ivy, S., 1992. Evidence for massive discharges of icebergs into the North Atlantic ocean during the last glacial period. Nature. 360(6401), 245-249.

Bondevik, S., Mangerud, J., Birks, H.H., Gulliksen, S., Reimer, P., 2006. Changes in North Atlantic radiocarbon reservoir ages during the Allerød and Younger Dryas. Science, 312(5779): 1514-1517.

Boyle, E.A., Keigwin, L., 1987. North Atlantic thermohaline circulation during the past 20,000 years linked to high-latitude surface temperature. Nature. 330, 35-40.

Broecker, W.S., 1991. The great ocean conveyor. Oceanography, 4(2): 79-89.

Broecker, W.S., Peteet, D.M., Rind, D., 1985. Does the ocean–atmosphere system have more than one stable mode of operation? Nature. 315, 21-26.

Chanell, J.E.T., Wright, J.D., Mazaud, A., Stoner, J.S., 2014. Age through tandem correlation of Quaternary relative paleointensity (RPI) and oxygen isotope data at IODP Site U1306 (Eirik Drift, SW Greenland). Quaternary Science Reveiws. 88, 135-146.

Clarke, R. A. (1984). Transport through the cape farewell-flemish cap section. Rapp. PV Reun. Cons. Int. Explor. Mer, 185, 120-130.

Curry, W.B., Duplessy, J.C., Labeyrie, L.D., Shackleton, N.J., 1988. Changes in the distribution of $\delta^{13}C$ of deep water sigma CO_2 between the last glaciation and the Holocene. Paleoceanography. 3(3), 317-341.

Coplen, T.B., Kendall, C., Hopple, J., 1983. Comparison of stable isotope reference samples. Nature. 302, 236-238.

Duplessy, J.C., Shackleton, N.J,. Fairbanks, R.G., Labeyrie, L., Oppo, D.W., Kallel, N., 1988. Deepwater source variations during the last climatic cycle and their impact on the global deep-water circulation. Paleoceanography, 3(3), 342-360.

Evans, H.F., Channell, J.E.T., Stoner, J.S., Hillaire-Marcel, C., Wright, J.D., Neitzke, L.C., Mountain, G.S., 2007. Paleointensity-assisted chronostratigraphy of detrital layers on the Eirik Drift (North Atlantic) since marine isotope stage 11. Geochem. Geophys. Geosyst. 8, Q11007.

Hall, I.R., Becker, J., 2007. Deep Western Boundary Current variability in the subtropical northwest Atlantic Ocean during marine isotope stages 12-10. Geochem. Geophys. Geosyst. 8, Q06013.

Hemming, S.R., Broecker, W.S., Sharp, W.D., Bond, G.C., Gwiazda, R.H., McManus, J.F., Klas, M., Hajdas, I., 1998. Provenance of Heinrich layers in core V28-82, northeastern Atlantic: 40Ar/39Ar ages of ice-rafted hornblende, Pb isotopes in feldspar grains, and Nd–Sr–Pb isotopes in the fine sediment fraction. Earth and Planetary Science Letters. 164, 317–333.

Henderson, S.S., 2006. Stable isotope and lithologic variations on the Eirik Drift during the holocene : implications for climate and deep-water interactions. Rutgers University. 1-77

Hillaire-Marcel, C., De Vernal, A., Bilodeau, G., Wu, G., 1994. Isotope stratigraphy, sedimentation rates, deep circulation, and carbonate events in the Labrador Sea during the last ~ 200 ka. Canadian Journal of Earth Science. 31, 63-89.

Hillaire-Marcel, C., de Vernal, A., McKay, J., 2011. Foraminifer isotope study of the Pleistocene Labrador Sea, northwest North Atlantic (IODP Sites 1302/03 and 1305), with emphasis on paleoceanographical differences between its “inner” and “outer” basins. Marine Geology. 279. 188-198.

Holliday, N.P., Meyer, A., Bacon, S, Alderson, S.G., de Cuevas, B., 2007. Retroflection of part of the East Greenland Current at Cape Farewell, Greenland. Geophysical Research Letters, 34, L07609. Doi:10.1029/2006GL029085.

Holliday, N.P., Bacon, S., Allen, J., McDonagh, E.L., 2009. Circulation and transport in the Western Boundary Currents at Cape Farewell, Greenland. Journal of Physical Oceanography, 39, 1854-1870.

Hunter, S.E., Wilkinson, D., Louarn, E., McCave, I.N., Rohling, E.J., Stow, D.A.V., Bacon, S., 2007. Deep western boundary current dynamics and associated sedimentation on the Eirik Drift, Southern Greenland Margin. Deep-Sea Research, I 54, 2036-2066.

Imbrie, J., Berger, A., Boyle, E. A., Clemens, S. C., Duffy, A., Howard, W. R., Kukla, G., Kutzbach, J., Martinson, D. G., McIntyre, A., Mix, A. C., Molfino, B., Morley, J. J., Peterson, L. C., Pisias, N. G., Prell, W. L., Raymo, M. E., Shackleton, N. J., Toggweiler, J. R., 1993. On the structure and origin of major glaciation cycles 2. The 100000-year cycle. Paleoceanography, 8(6), 699-736.

Lisiecki, L.E., Raymo, M.E., 2005. A Pliocene-Pleistocene stack of 57 globally distributed benthic $\delta^{18}O$ records. Paleoceanography, 20(1003), 1-17.

Lisiecki, L.E., Raymo, M.E., and W.B. Curry. 2008. Atlantic overturning responses to Late Pleistocene climate forcings. Nature. 456 (6); 85-88

McManus, J. F., R. F. Anderson, W. S. Broecker, M. Q. Fleisher, and S. M. Higgins (1998), Radiometrically determined sedimentary fluxes in the sub-polar North Atlantic during the last 140,000 years, Earth Planet. Sci. Lett., 155, 29–43.

Oppo, D.W., Fairbanks, R.G., 1987. Variability in the deep and intermediate water circulation of the Atlantic Ocean during the past 25,000 years; Northern Hemisphere modulation of the Southern Ocean. Earth and Planetary Science Letters. 86(1), 1-15.

Oppo, D.W., Lehman, S.J., 1993. Mid-Depth Circulation of the Subpolar North Atlantic During the Last Glacial Maximum. Science. 259(5098), 1148-1152.

Oppo, D.W., Lehman, S.J., 1995. Suborbital timescale variability of North Atlantic Deep Water during the past 200,000 years. Paleoceanography. 10(5), 901-910.

Piotrowski, A.M., Goldstein, S.L., Hemming, S.R., Fairbanks, R.G., 2005. Temporal relationships of carbon cycling and ocean circulation at glacial boundaries. Science. 307, 1933-1938.

Sarnthein, M., Winn, K., Duplessy, J.C., Fontugne, M.R., 1988. Global variations of surface ocean productivity in low and mid latitudes; influence on CO (sub 2) reservoirs of the deep ocean and atmosphere during the last 21,000 years. Paleoceanography. 3(3), 361-399

Stanford, J.D., Rohling, E.J., Hunter, S.E., Roberts, A.P., Rasmussen, S.O., Bard, E., McManus, J., Fairbanks, R.G., 2006. Timing of meltwater pulse 1a and climate responses to meltwater injections. Paleoceanography. 21, PA4103, doi: 10.1029/2006PA001340.

Stoner, J.S., Channell, J.E.T., Hillaire-Marcel, C., 1995. Late Pleistocene relative geomagnetic paleointensity from the deep Labrador Sea: relationship to North Atlantic Heinrich layers. Paleoceanography. 11, 309-325.

Stoner, J.S., Channell, J.E.T., Hillaire-Marcel, C., 1996. The magnetic signature of rapidly deposited detrital layers from the deep Labrador Sea; relationship to North Atlantic Heinrich layers. Paleoceanography. 11(3), 309-325.

Streeter, S.S., Shackleton, N.J., 1979. Paleocirculation of the Deep North Atlantic: 150,000-Year Record of Benthic Foraminifera and Oxygen-18. Science. 203(4376), 168-171.

Thornalley, D. J., Barker, S., Broecker, W. S., Elderfield, H., & McCave, I. N. (2011). The deglacial evolution of North Atlantic deep convection. science, 331(6014), 202-205.

Wold, C.N., 1994. Cenozoic sediment accumulation on drifts in the northern North Atlantic. Paleoceanography. 9, 917-941.

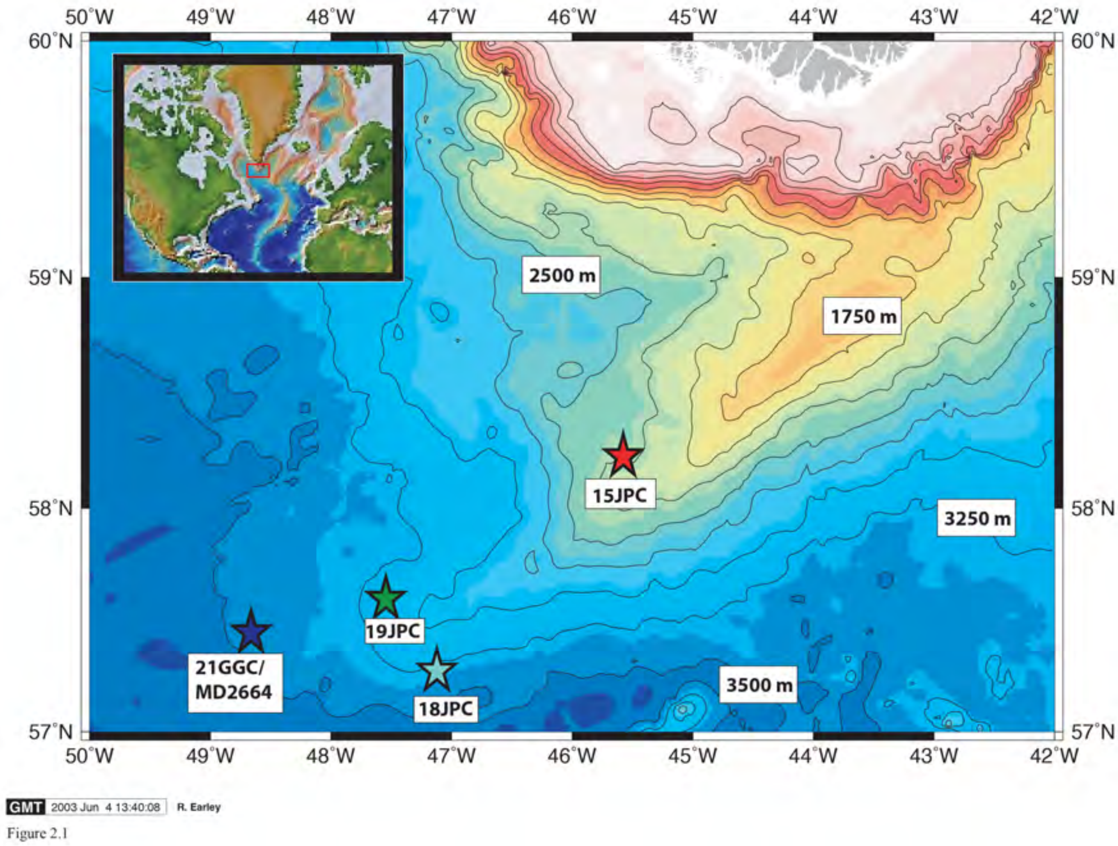

Figure 2.1: Map showing the locations of the 4 cores analyzed in this study on the Eirik Drift. The contour interval is 250 m and the stars indicate the approximate location of cores 15JPC (red; 2230 m), 19JPC (green; 3204 m), 18JPC (light blue; 3435 m), and MD2664 (dark blue; 3450 m).

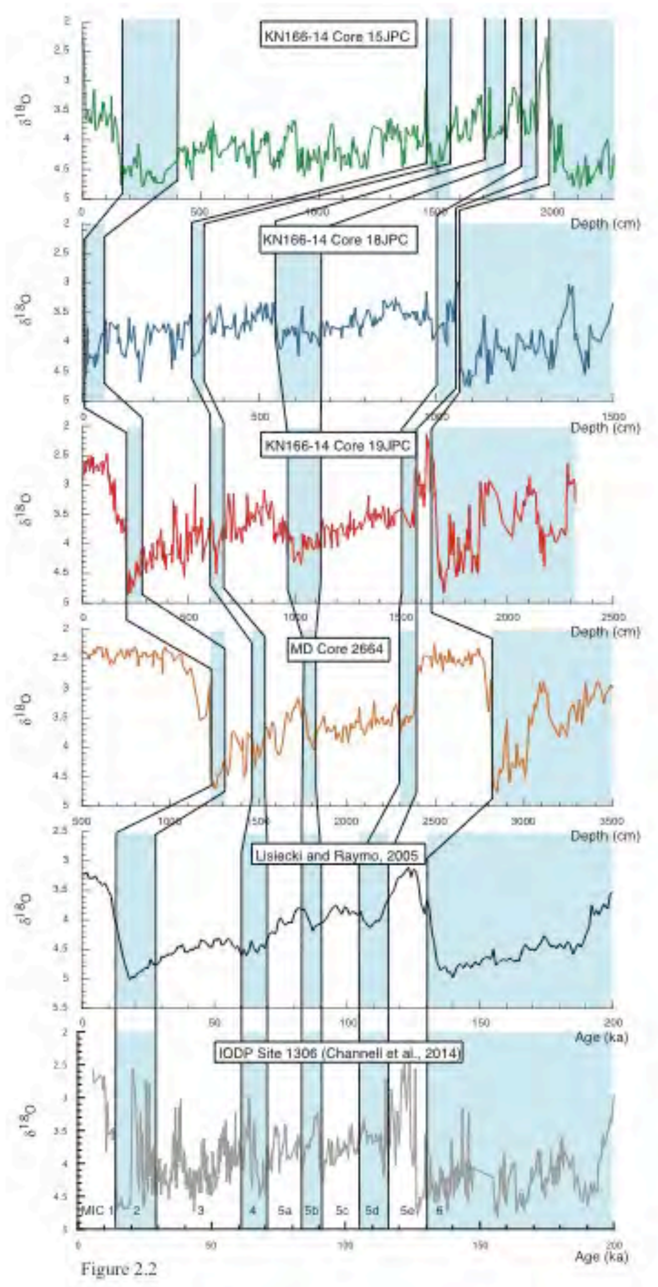

Figure 2.2: Downcore stratigraphies of cores 15JPC, 18JPC, 19JPC, and MD2664. Tie points for the Marine Isotope Chrons are shown versus the Lisiecki and Raymo, 2005 curve.

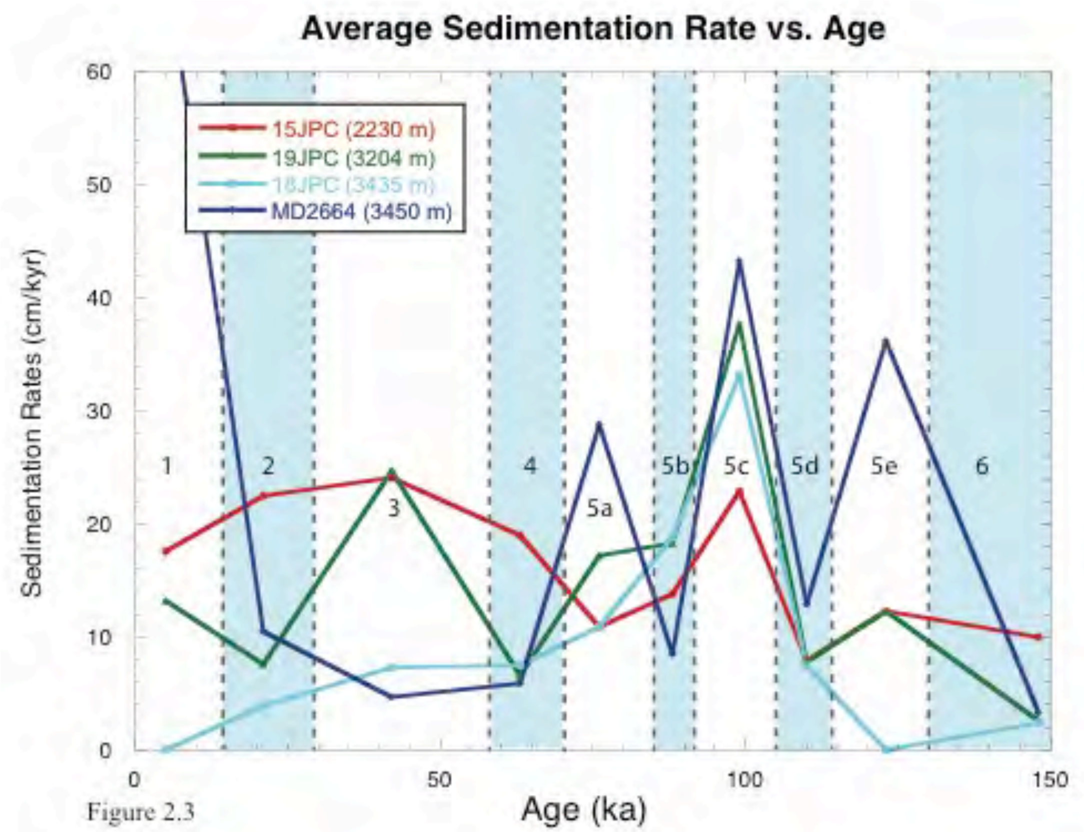

Figure 2.3: Average sedimentation rates plotted using tie points between MIC stage boundaries. The arrows point to the boundaries between the MIC stages.

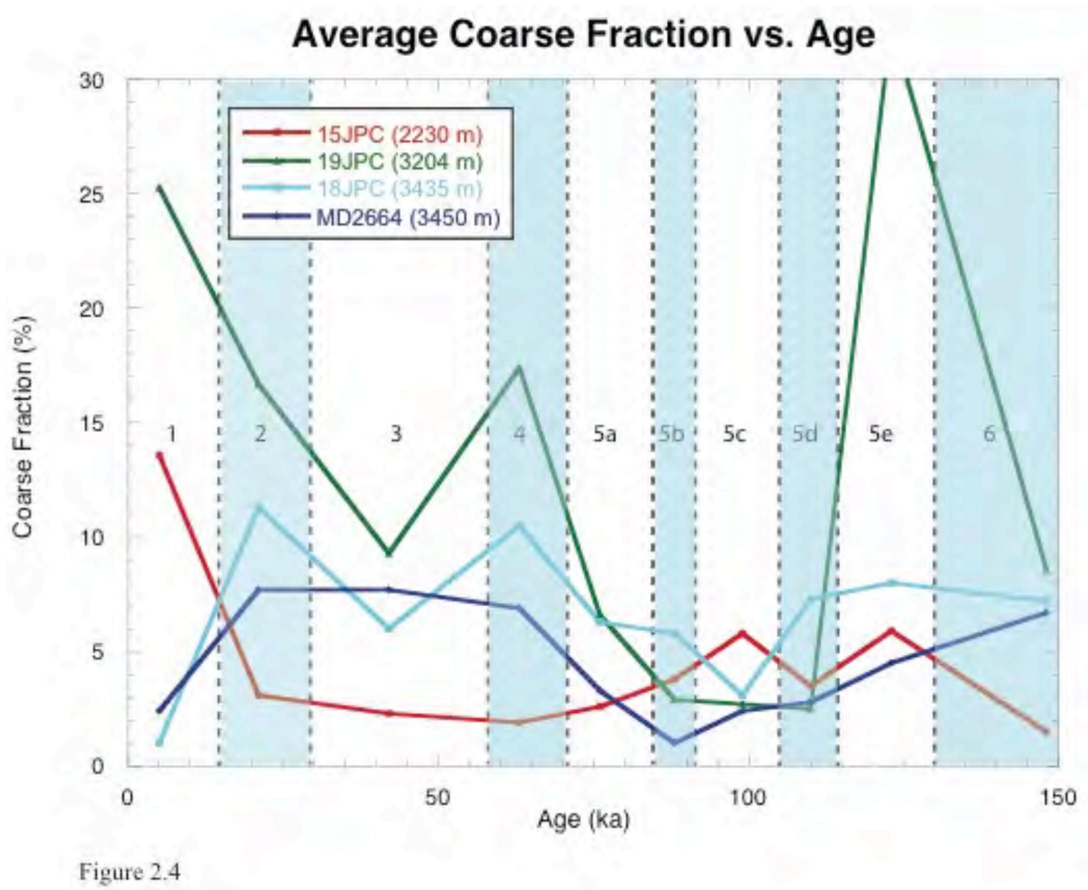

Figure 2.4: Average percent coarse fraction plotted using tie points between MIC stage boundaries. The arrows point to the boundaries between the MIC stages.

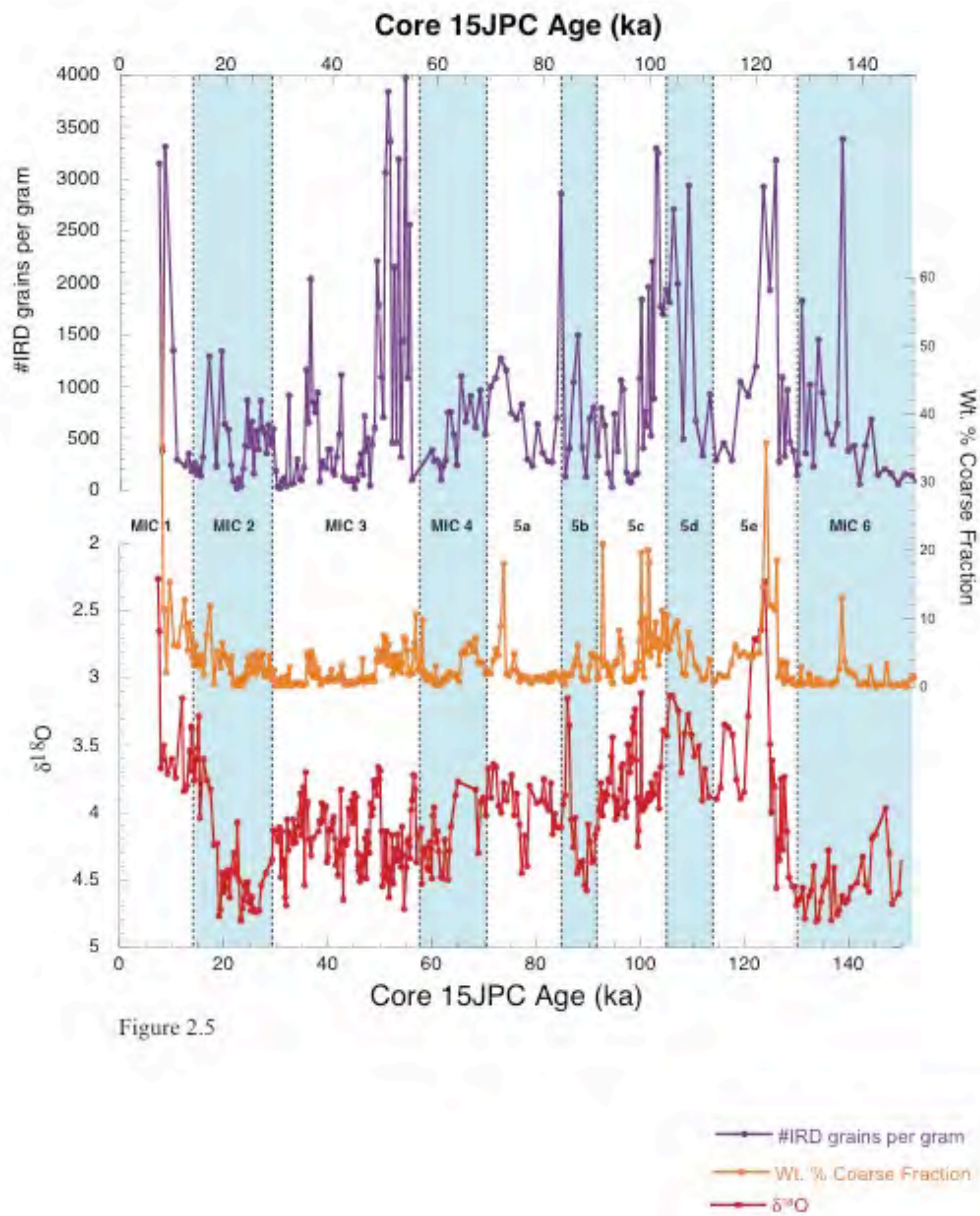

Figure 2.5

Figure 2.5: The number of IRD grains per gram, weight percent coarse fraction, and δ18O values for Core 15JPC plotted versus age (ka). The vertical lines show the division between the different Marine Isotope Chrons (MIC) and Subchrons of MIC 5.

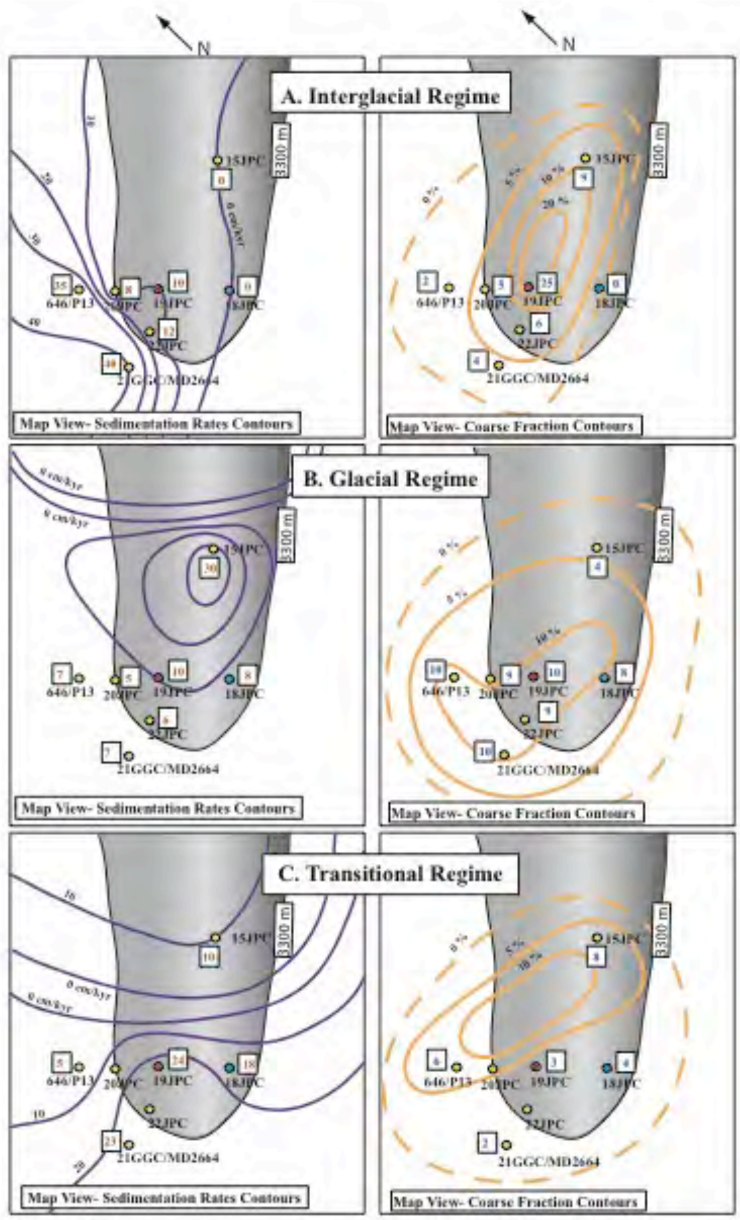

Figure 2.6

Figure 2.6: Contoured map view of average sedimentation rates (cm/kyr) and percent coarse fraction values for the two end-member and the intermediate regime of deep-water circulation on Eirik Drift.

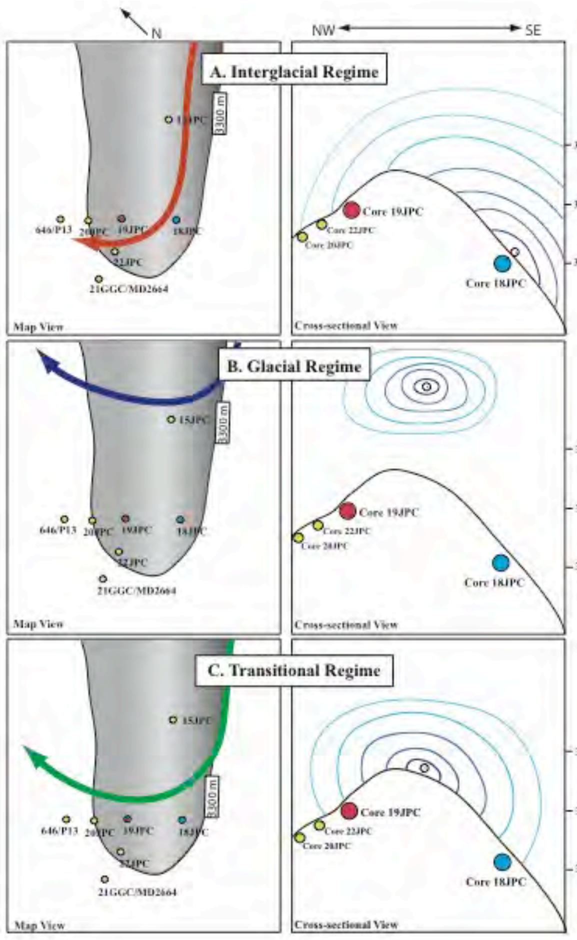

Figure 2.7: Map and cross-sectional view of the two end-member and the intermediate regimes of deep-water circulation over Eirik Drift. A schematic model of each of the regimes of circulation inferred from the sedimentological records. The blue lines on the right side of the figure represent velocity fields, where the center of the circles, or darker blues, indicate the core of the current flow field. Non-depositional or erosive conditions exist when the center of the current is positioned directly above the site. Sedimentation rates steadily increase away from the center of the current, and then decrease as you move to the outer edges of influence of the current

Core #	Latitude	Longitude	Water Depth	Location Description
KN166-14 15JPC	58°11.82 N	45°34.08 W	2230 m	Northeastern Crest of Eirik Drift
KN166-14 18JPC	57°11.09 N	47°07.99 W	3435 m	Southeastern Flank of Eirik Drift
KN166-14 19JPC	57°34.99 N	47°35.99 W	3204 m	Northwestern Flank/Crest of Eirik Drift
KN166-14 21JPC/MD-2664	57°26.32 N	48°36.44 W	3450 m	Toe of Eirik Drift

Table 2.1: Locations of the cores used in this study.

3.0 Sedimentological and Stable Isotopic Evidence of Surface Water Forcing on Deep Water Variability in the North Atlantic During Heinrich Event 1

3.1 Abstract

Abrupt climate changes and disruptions in the production of deep-water in the North Atlantic Ocean during the last glacial termination are typically attributed to the influx of glacially-derived freshwater in response to melting of the Laurentide Ice Sheet and discharge of large armadas of icebergs (i.e., Clarke et al., 2001). Benthic foraminiferal $\delta^{13}C$ values from an intermediate water depth on the Eirik Drift are compared with regional proxy records for Atlantic Meridional overturning circulation (AMOC) and show a well-established pattern whereby Northern Component Water (NCW; analogous to North Atlantic Deep Water) was confined to upper deep water depths during the Last Glacial Maximum (LGM) in contrast to a deeply penetrating NCW during the warm (BA) and Holocene. The Heinrich-1 Event (H1; 17.5 to 14.5 kyr) recorded an extreme NCW shoaling, although the $\delta^{13}C$ gradients are still maintained in the North Atlantic. Global sea level rose only 5 m during the 3-kyr long H1 interval, while a vigorous NCW resumed at the end of H1 at 14.25 kyr and persisted throughout Melt Water Pulse 1A (MWP-1A). These relationships raise questions about the role of glacial meltwater as the mechanism responsible for the observed deep-water circulation changes. Combined with other regional proxies, we follow Hillaire-Marcel and de Vernal (2008) in interpreting the anomalously low planktonic foraminiferal $\delta^{18}O$ values during the colder intervals as reflecting extensive sea-ice cover. We conclude that the abrupt climate changes in the circum-North Atlantic responded to changes in the long-wave atmospheric circulation forced by ice sheet advances and retreats. During H1, a

southward shift in the Jet Stream responding to changes along the southern margin of the Laurentide Ice Sheet caused the polar front, iceberg tracks, and sea ice extent to all migrate southwards, producing changes in the temperature fields and salinities of the subpolar to polar North Atlantic.

3.2 Introduction

The last glacial termination (Termination 1), or transition from Marine Isotope Chron (MIC) 2 to 1, was marked by a series of abrupt, millennial-scale climate changes that are associated with the return of colder temperatures and ice sheet growth (Blunier and Brook, 2001). These changes are well-documented throughout the North Atlantic Ocean in a variety of proxies in marine sediments (Bond et al., 1993; Broecker et al., 1992; Heinrich, 1988; Piotrowski et al., 2005) and in Greenland ice cores (Bond et al., 1993; Dansgaard et al., 1982; Grootes et al., 1993) and are associated with the slowing or complete shut down of NCW production (i.e., Boyle and Keigwin, 1987; Duplessy et al., 1988a; McManus et al., 2004; Oppo and Fairbanks, 1987). Paleoceanographic research has focused on understanding the roles of surface water forcing and deep-water circulation on millennial timescales, with particular emphasis on the role of heat transfer associated with deep-water circulation changes (Broecker and Denton, 1990). Many of these studies invoke surface water changes in the northern North Atlantic as a possible mechanism of climate change (Barber et al., 1999; Boyle and Keigwin, 1987; Broecker, 1994; Curry et al., 1999; Keigwin and Boyle, 1999; Manabe and Stouffer, 1988; Manabe and Stouffer, 2000; Oppo and Lehman, 1995); therefore, determining the role and/or response of the changes in North Atlantic surface waters is crucial in understanding the millennial-scale climate changes during the past 20 kyr. However, uncertainties in dating and the timing of water mass changes make it difficult to determine the cause and effect of this relationship. Working with an expanded deglacial section in a North Atlantic sediment core that records both the surface and deep-water responses, one can potentially work out the leads and lags without the uncertainties of core-to-core correlation.

Northern Component Water (NCW; analogous to North Atlantic Deep Water) production varied over Milankovitch (Raymo et al., 1989) and millennial (Clarke et al., 1999) time scales by altering the density driven thermohaline circulation. Termination 1 produced a series of abrupt climatic events, i.e. Heinrich 1 (H1), the (BA) and the Younger Dryas (YD). Many hypotheses ascribe the cold events (H1 and YD) to increased meltwater input that altered North Atlantic deep-water circulation (e.g., Clarke et al., 2001). This is a natural consequence of adding glacial meltwater to a region of the ocean where deep-water production is marked by the relatively high salinity. It follows that abrupt changes in Atlantic Meridional Ocean Circulation (AMOC) should be related to sudden density changes in source regions, leading to catastrophe hypotheses such as rerouting of the primary meltwater pathways (i.e., Broecker, 1994; Broecker et al., 1989; Tarasov and Peltier, 2005). However, it is important to consider that the millennial-scale events during the deglaciation were part of a long history of abrupt changes that occurred during the “glacial” part of the “glacial-interglacial’ cycle.

Six well-defined Heinrich Events (H1-H6) have been identified in a wide range of North Atlantic (north of 40°N) deep-sea sediments with H6 occurring around 60 ka and H1 during Termination 1 between 17.5 to 14.5 kyr (Figure 3.1; Bond et al., 1992; Heinrich, 1988; Hemming, 2004). Heinrich Events appear as anomalous sedimentation intervals characterized by increased ice-rafted detritus (IRD) interpreted as the byproduct of the melting of large armadas of icebergs (e.g., Bond et al., 1992; Heinrich, 1988). The melting would potentially reduce the salinity of the surface North Atlantic Ocean, thus disrupting thermohaline circulation and creating abrupt climatic changes (e.g., Bond et al., 1993). The exact mechanisms and sources of these meltwater and ice rafting events are still highly debated (Bond et al., 1999 and others).

Millennial-scale climate changes are found in the southern hemisphere as well (Bond et al., 1999; Charles et al., 1996; Kanfoush et al., 2000). However, these abrupt climate changes are not synchronous between the hemispheres and in fact show opposing climate trends throughout the last deglaciation (Grootes et al., 2001; Johnsen et al., 1972; Jouzel et al., 1987). In the southern hemisphere, Antarctica first warmed when glacial conditions existed during the Greenland Stadial 2/H1 event and then cooled when the North Atlantic experienced the BA warmth. This opposing trend continued through the YD where Antarctica warmed while Greenland climate returned to near-glacial conditions (e.g., Blunier and Brook, 2001; Blunier et al., 1998; Broecker, 1998; Kaplan et al., 2010; Pedro et al., 2011; Shakun and Carlson, 2010; Sowers and Bender, 1995). The contrasting behavior of temperature variations in the North Atlantic as compared to the Southern Ocean has been termed the bipolar seesaw (e.g., Barker et al., 2009; Broecker et al., 1992; Pedro et al., 2011; Rind et al., 2001).

The anti-phase relationship between the north and south is explained via coupled oscillations in the heat transport in the Atlantic Ocean due to changes in the AMOC (Broecker, 1998; Broecker, 2006). A shutdown or reduction in thermohaline circulation would trigger cooling in the north and warming in the south by creating a density vacuum in the Southern Ocean (Broecker, 1998). This would allow the downward mixing of the warm water and heat from the Southern Ocean thermocline, warming the surrounding ocean (Broecker, 1998; Pedro et al., 2011; Stocker, 1998; Stocker and Johnsen, 2003). Broecker (1998) proposed that this bipolar seesaw could generate the frequent oscillations observed in the climate record.

Geochemical records from benthic foraminiferal $\delta^{13}C$ (e.g., Boyle and Keigwin, 1987; Oppo and Fairbanks, 1987) , Cd/Ca (Boyle and Keigwin, 1987), Zn/Ca (Marchitto et al., 2002), $^{231}Pa/^{230}Th$ (McManus et al., 2004), ^{14}C ventilation ages (Thornalley et al., 2011), and bulk sediment εNd (Piotrowski et al., 2005) have all been used to elucidate changes in Atlantic deep-water circulation patterns. Benthic foraminiferal $\delta^{13}C$ values are most often used to track variability in deep-water production (i.e., Charles and Fairbanks, 1992; Oppo and Curry, 1997; Oppo and Fairbanks, 1987). This study presents high-resolution multi-species stable isotopic and sediment proxy records from KN166-14 Core 15JPC (Figure 3.2), to evaluate the surface and deep-water response to rapid climate events that occurred during the most recent deglaciation. These results were compared to other regional results to place this core into the context of global climate change. From these observations, the leading hypotheses on the origin and timing of rapid climate changes, i.e. glacial meltwater addition, will be reevaluated.

3.3 Materials and Methods

The R/V KNORR collected jumbo piston core 15JPC in 2002 on cruise 166, leg 14, from 2230 m water depth from the northeastern upslope region of Eirik Drift (3.2, Table 3.1). Shipboard magnetic susceptibility measurements and correlation to nearby cores with radiocarbon dating indicated 15JPC contained an expanded (>2 m) deglacial record and that sedimentation rates exceeded 60 cm/kyr during certain intervals. Eirik

Drift provides an ideal location to monitor the surface and intermediate depth variations in deep-water because the Western Boundary Undercurrent (WBUC) that bathes this site contains two of the major components of NADW, Denmark Strait Overflow Water (DSOW) and Iceland-Scotland Overflow Water (ISOW). Core 15JPC was selected for this study to generate a high-resolution, multiple species, stable isotopic record to characterize the surface and upper deep-water hydrology of the last ~20 kyr. 10-to 20 cm^3 samples were taken every 1 cm for the upper 200 cm of core 15JPC. Each sample was then weighed, dried and then washed through a 63 μm sieve.

The number of Ice Rafted Detritus (IRD) grains per gram were calculated every 10 cm on samples from core 15PC. The washed samples (> 63 μm) were sieved at 150 μm and split 1 to 4 times with a splitter (Hemming et al., 1998; McManus et al., 1998; Stanford et al., 2006). All remaining lithic grains were counted, and then converted to the number of IRD grains per gram (#IRD grains per gram) according to the following formula:

$$\#\text{IRD grains per gram} = \#\text{IRD} * (2^{(\#\text{Splits}/\ \text{Dry Wt.})})$$

where #IRD, #Splits, and Dry Wt. refer to the number of lithic grains counted, the number of times the samples were split, and the dry weight of the sample after being washed through a 63 μm sieve, respectively.

Planktonic foraminifera have preferred depth habitats based on temperature, nutrient availability, and salinity patterns (Bé and Tolderlund, 1971). Because these parameters can vary greatly from season to season, different species of planktonic foraminifera often calcify in different water conditions at the same location. Earlier studies have used a single species of planktonic foraminifera to document the changes of the surface waters in the North Atlantic, and as a result, a detailed assessment of the impact of these freshwaters on upper water column (i.e., the mixed-layer and thermocline waters) could not be made. However, some studies have shown that the generation of $\delta^{18}O$ records from multiple species of planktonic foraminifera provide more information about the overlying water conditions than if only one species was analyzed (e.g., Lagerklint and Wright, 1999; Rashid and Boyle, 2007).

Two species of planktonic foraminifera (*Neogloboquadrina pachyderma,* sinistral; and *Globigerina bulliodes*) and one species of benthic foraminifera (*Planulina wuellerstorfi*) were used in this study to characterize the surface and deep-water hydrography. In glacial environments, the cold water species, *N. pachyderma* (s), usually lives at or below the pycnocline, (Bé and Tolderlund, 1971; Hillaire-Marcel et al., 2011; Kuroyanagi and Kawahata, 2004; Simstich et al., 2003), while *G. bulloides* typically inhabits the water above the pycnocline only during the summer bloom (e.g., Ganssen and Kroon, 2000; Hillaire-Marcel et al., 2011; Schiebel et al., 1997). Ecological studies of *N. pachyderma* (s) suggest that its stable isotope composition reflects conditions around 50 m depth in the water column (Jonkers et al., 2010), but that the majority of its test is secreted at depth between 50 and 200 m (Be, 1960; Kohfeld et al., 1996). The benthic species, *P. wuellerstorfi*, has been shown to accurately reflect changes in bottom water chemistry (Duplessy et al., 1988b; Sarnthein et al., 1994). Combination of the $\delta^{13}C$ and $\delta^{18}O$ stable isotopic records from these three species reflects the surface to deep-water hydrography with some seasonal discrepancies (Hillaire-Marcel et al., 2001; Hillaire-Marcel et al., 2011; Jonkers et al., 2010).

Ten to 15 planktonic foraminiferal and 2 to 5 benthic foraminiferal pristinely preserved tests were handpicked under a binocular microscope from the > 212 μm size fraction, and selected for stable isotope analysis (Figure 3.4). All samples were analyzed in the Stable Isotope Laboratory at Rutgers University using the Micromass Optima Mass Spectrometer. Samples were loaded into a multi-prep device and reacted with 100% phosphoric acid at 90 °C for 15 minutes. All measured values are reported relative to V-PDB (Vienna PeeDee Belemnite) using an internal lab standard. This standard is routinely checked against NBS-19, which has values of 1.95 ‰ and - 2.20 ‰ for $\delta^{13}C$ and $\delta^{18}O$, respectively (Coplen et al., 1983). The offsets between the lab standard and NBS-19 are 0.04 ‰ for $\delta^{18}O$ and 0.10 ‰ for $\delta^{13}C$. Typical lab precision for 1-σ of the standards reported versus V-PDB is 0.05 ‰ for $\delta^{13}C$ and 0.08 ‰ for $\delta^{18}O$.

Fifteen depths intervals were selected and sent to the National Ocean Sciences Accelerator Mass Spectrometry (NOSAMS) facility for Accelerator mass spectrometry (AMS) dating (Figure 3.4). For each interval, 4 to 6 mg of planktonic foraminifera *N. pachyderma* (s) were selected using a binocular microscope, sonicated in deionized water and crushed. The resulting radiocarbon ages were converted to calendar ages according to the Fairbanks0805 calibration after a 600-year reservoir correction was applied (Bondevik et al., 2006; Fairbanks et al., 2005; Appendix 1 and 2). Three ages were discarded due to age reversals; inspection of the core showed foraminiferal sands indicating winnowing and sediment reworking at these depths. Additional age control was provided by correlating regional magnetic events through the use of relative paleointensity (Evans et al., 2007) and shipboard magnetic susceptibility measurements. Linearly interpolating between the tie points produces sedimentation rates from 7.5 to

>100 cm/kyr (Figure 3.4). The final age model was determined by generating linear regressions through two or of the age-depth pairs. The resulting linear equations were then solved to determine the intersection of the lines. It is interesting and perhaps not surprising that three lines correspond to the LGM, H1, and Bølling-Allerod. The lowest rate observed of these three is the H1 interval, which is defined by an increase in coarse fraction percentages between 131 and 164 cm. The intersection of the H1 line with those of the Bølling-Allerod and LGM intersect at these depths and have age estimates of 14.5 kyr and 17.5 kyr, respectively, providing some confidence that this approach of using linear segments to assign ages is justified. Data for this chapter are provided in Appendix 3 and 4.

Cores SU 90-24 (Elliot et al., 2002), OCE326-GGC5 (Boyle and Keigwin, 1987; McManus et al., 2004), 11JPC (Elmore and Wright, 2011), and RC 11-83 (Charles and Fairbanks, 1992) were selected for comparison in this study. Core 11JPC, collected from the Gardar Drift (2707 m; Figure 3.2 and 3.5; Table 3.1), is situated directly in the path of Iceland Scotland Overflow Water, one of the major components of NCW. Core SU 90-24 (2100 m; Figure 3.2 and 3.5; Table 3.1) was collected off the east coast of Greenland and is located along the modern path of the western branch of NCW. Core OCE326-GGC5 (4550 m; Figure 3.2 and 3.5; Table 3.1) was retrieved from the Bermuda Rise in the deep western subtropical Atlantic. This site lies far south of the main study area and at a much greater depth and isopycnal surface, however, all components of modern NCW have been entrained and incorporated by the time the deep-water flows over this site. RC 11-83 (4718 m; Figure 3.2 and 3.5; Table 3.1), recovered from the north flank of Cape Rise, is important because it provides a record from the Southern Ocean. All of these sites have high sedimentation rates (>16 cm/ka) and good age control from multiple AMS 14C dates, allowing direct site-to-site comparison leading to analysis of changes in NCW flow over the last 20 kyr in a north to south transect.

3.4 Results

3.4.1 Benthic foraminiferal $\delta^{13}C$ comparisons

Benthic foraminiferal $\delta^{13}C$ values are used herein to track bottom-water mass changes with high values (~1‰) reflecting sites bathed in NCW (Praetorius et al., 2008), and low values (≤0‰) indicating an Antarctic Bottom Water (AABW) source (e.g., Piotrowski et al., 2005). The benthic foraminiferal $\delta^{13}C$ record from core 15JPC is consistent with the reconstructions shown in Oppo and Curry (2012). We note that our record shows variability in the $\delta^{13}C$ within each interval; however, we focus on the site-to-site differences within the LGM, H1, and BA interval.

The LGM in this paper is defined as the interval from 20 kyr to the start of H1 at 17.5 kyr during which, benthic foraminiferal $\delta^{13}C$ values averaged 0.5±0.24‰ (Figure 3.4). These values are roughly 0.5‰ lower than those found in SU90-24 (Figure 3.4; Elliot et al., 2002), that is 200 m shallower and closer to the Denmark Straits overflow and may reflect a strong $\delta^{13}C$ gradient between these sites. This 0.5‰ difference is consistent with the Curry and Oppo (2005) reconstruction, that shows a $\delta^{13}C$ gradient between 2000 and 2500 m in the northern North Atlantic during the LGM. Another explanation may be that the ~0.5‰ difference is an artifact of higher resolution in core 15JPC that shows $\delta^{13}C$ values increasing between 20 and 18 kyr. $\delta^{13}C$ values in the LGM from core OCE326-GGC5 average 0‰, albeit with only 5 values within the LGM (Boyle and Keigwin, 1987) but suggest that a 0.5‰ difference existed between this location and our Eirik Drift core.

The H1 event has been defined as the interval between 17.5 and 14.5 kyr (Bond et al., 1992; Heinrich, 1988; Hemming, 2004). In core 15JPC, benthic foraminiferal $\delta^{13}C$ values decrease by 0.7‰ to -0.2‰ at the beginning of H1 but average 0.0±0.3‰ throughout this interval. These values are similar to those on the east Greenland margin (Elliot et al., 2002) and about 0.5‰ higher than those on the Bermuda Rise (Boyle and Keigwin, 1987), that average -0.5‰.

Benthic foraminiferal $\delta^{13}C$ values increase to 1.0±0.5‰ during the BA and remain fairly constant until the start of the YD event. Due to a coring gap and possible hiatus in Core 15JPC, the YD record at site 15JPC is not fully resolved but core 11JPC shows a ~0.8‰ decrease in benthic foraminiferal $\delta^{13}C$ values during the YD. Values increase to 1.5‰ during the early Holocene and show some variability (0.5 to 1‰) for the remainder of the record.

3.4.2 Oxygen Isotopes

Planktonic foraminiferal $\delta^{18}O$ values (Figures 3.3, 3.5, and 3.6) are used to reconstruct the surface water conditions over site 15JPC. Trends generally mimic the Greenland $\delta^{18}O$ ice core record, with the exception of the H1 event (Figure 3.6). While the ice core recorded decreased $\delta^{18}O$ values interpreted as cold temperatures, we observe a decrease in the planktonic $\delta^{18}O$ values which reflects either warmer SSTs or lower $\delta^{18}O$ water. When corrected for ice volume effects by subtracting the global ice volume record of Peltier and Fairbanks (2006) from the *N. pachyderma* (s) $\delta^{18}O$ record, extremely low $\delta^{18}O$ values are result (~2.4‰; Figure 3.6). We would expect even lower corrected $\delta^{18}O$

values during the BA because this is a documented warm interval; however, higher $\delta^{18}O$ values are recorded during this time (~3‰). Given that the sedimentological proxies record high percent coarse fraction and IRD counts (Figure 3.3), suggestive of harsh conditions, these isotopic excursions cannot be associated with higher sea surface temperatures and are most likely explained by changes in salinity. This excursion also corresponds with maximum sea ice coverage, as reconstructed from dinocyst assemblages (de Vernal et al., 2005a; Figure 3.6).

3.5 Discussion

A clear picture has emerged from previous work and this study concerning variations in NCW fluxes during the most recent deglaciation. Benthic foraminiferal $\delta^{13}C$ from intermediate and deep North Atlantic sites (Boyle and Keigwin, 1987; Elliot et al., 2002; Elmore and Wright, 2011) and $^{231}Pa/^{230}Th$ ratios (McManus et al., 2004) from the deep North Atlantic all show low to moderate NCW fluxes during the transition from the LGM from 21 to ~18 kyr with values of approximately 0.5‰ and 0.07 respectively (Figure 3.5). During the H1 event (17.5 to 14.5 ka), NCW production decreased although it is difficult to determine if it was a full collapse because the $\delta^{13}C$ values on the Eirik Drift are still higher than those in the subtropical North Atlantic and Southern Ocean (Boyle and Keigwin, 1987; Elliot et al., 2002). Following H1, all NCW proxies indicate vigorous NCW production (14.5 to 12.8 kyr). We are unable to resolve the changes in NCW production during the YD in core 15JPC, but other sites (11JPC; Elmore and Wright, 2011) indicate there was an initial decrease at this time. By the end of the YD, NCW was restored and continued through the Holocene.

Reductions in or a full shutdown of NCW are most often ascribed to massive influxes of freshwater to the North Atlantic Ocean (i.e., Clarke et al., 2001). Ocean circulation models have suggested that meltwater pulses could reduce or shutdown NCW production (Manabe and Stouffer, 1995; Rahmstorf, 1994; Rind et al., 2001; Schiller et al., 1997; Stocker and Wright, 1991). The source of glacial meltwater has been attributed to North American sources including the draining of the glacial Lake Agassiz through the St. Lawrence Seaway (Teller et al., 1983), the Beaufort Sea (Carlson et al., 2007), and the Fram Strait via the Artic Ocean (Tarasov and Peltier, 2005; Tarasov and Peltier, 2006) for the YD event. In contrast, the Heinrich events are most often associated with the launching of large armadas of icebergs through the Hudson Strait (e.g., Bond et al., 1993; Broecker et al., 1992).

Global meltwater flux as recorded by the Barbados sea level record (Fairbanks, 1989) and portrayed in the discharge curve provides one measure of evaluating the role of glacial meltwater on NCW production. Focusing on the initiation and end of H1, there is little similarity between NCW and global delivery of glacial meltwater (Figure 3.6). At the start of H1, NCW production decreased significantly at a time when the addition of glacial meltwater to the ocean decreased. In the discharge curve, the sea level rise was 7 to 8 mm/year and decreased to 3 mm/year at the start of H1 (Fairbanks, 1990). In contrast, the abrupt resumption of NCW at the end of H1 occurred during the apex of MWP1A, which recorded the highest rates of deglacial sea level rise (>25 mm/year; Figure 3.6; Fairbanks, 1990). Therefore, the most parsimonious interpretation is that there is no relationship. Alternatively, glacial meltwater arguments must therefore rely on sites for NCW formation being highly sensitive to small freshwater inputs.

Planktonic foraminiferal $\delta^{18}O$ values from northern North Atlantic sites record values that are far lower than the expected range (Bauch et al., 1997; Hillaire-Marcel and de Vernal, 2008; Hillaire-Marcel et al., 2004; this study). They argued that these lower than expected values would be recorded in the foraminiferal tests as isotopically light brines form and sink to the subsurface during sea ice formation (e.g., Bédard et al., 1981; Tan and Strain, 1980). Whereas, they would expect relatively high values to be incorporated into the foraminifera tests through the addition of low-salinity meltwater. All the Heinrich events observed in these studies record $\delta^{18}O$ decreases of up to 2.5‰ (Clarke et al., 1999; Hillaire-Marcel and Bilodeau, 2000), and contrary to modern interpretations, cannot be fully explained by the addition of glacial meltwater (Hillaire-Marcel and de Vernal, 2008). Calculated paleosalinities and sea surface temperatures do not explain these excursions as they yield salinities too low for the planktonic species present (e.g., de Vernal et al., 2002) and temperatures too warm as suggested by the paleo-sea surface temperature proxies (Bond et al., 1992; de Vernal et al., 2000). Consequently, we interpret the $\delta^{18}O$ excursions associated with H1 as evidence for increased sea-ice (Figure 3.6).

Further evidence for the presence of sea ice during these events comes from dinocyst data from Orphan Knoll located in the Labrador Sea (de Vernal et al., 2005a; de Vernal et al., 2005b). Maximum sea ice coverage (~10 months/year), as reconstructed from dinocyst assemblages, is concomitant with large planktonic isotopic excursions at the H1 event at the Orphan Knoll (Hillaire-Marcel and de Vernal, 2008) and Core 15JPC location (Figure 3.6). Hillaire-Marcel and de Vernal (2008) argued that this is consistent with the interpretation that Heinrich events are associated with ice sheet advances and subsequent iceberg discharge (i.e., Bond et al., 1992), but that they were also accompanied by the formation of substantial seasonal winter sea ice coverage. Thornalley et al. (2011) also noted an anomalously low ^{14}C ventilation age during H1 (Figure 3.5) in a Nordic Sea core at the same interval as the low $\delta^{18}O$ excursion and suggest resulted from brine production.

Alternatively, we propose that the reduction and shoaling of NCW during H1 was the result of sea ice production associated with a southern shift in the airmasses and the polar front with attendant sea-ice coverage resulting and not a massive discharge and subsequent melting of large ice armadas (Alley and MacAyeal, 1994; Bond et al., 1992; Bond and Lotti, 1995; Broecker, 1994; Broecker, 2002; Heinrich, 1988; Hemming, 2004). The extensive coverage of sea ice with summer melting would inhibit a dense deep-watermass, as seen in the $\delta^{13}C$ and $^{231}Pa/^{230}Th$ values (Figure 3.5) and could have maintained a greatly reduced NCW circulation (Hillaire-Marcel and de Vernal, 2008). The idea of sluggish deep-water production during the H1 event is supported by the rapid resumption of deep-water circulation immediately following it (Figure 3.5 and 3.6).

The resumption of NCW at the termination of H1 corresponded to a decrease in sea ice and an increase in ice volume corrected $\delta^{18}O$ values indicating the retreat of sea ice and opening of the surface waters in the North Atlantic. The greater salinities would then promote a deeper NCW water mass as seen in the OCE326-GGC5 proxies (Boyle and Keigwin, 1987; McManus et al., 2004) and ventilation ages (Thornalley et al., 2011).

Many coupled ocean-atmosphere computer models have been generated in which thermohaline circulation is forced to shut down through the addition of a massive amount of freshwater (Manabe and Stouffer, 1997; Rind et al., 2001; Vellinga and Wood, 2002;

Vellinga et al., 2002; Zhang and Delworth, 2005). These models do show that thermohaline circulation can be reduced or shut-down through the addition of freshwater and that North Atlantic cooling would occur; however, the models would require the addition of unrealistic freshwater influxes and they fail to explain the magnitude of cooling observed in the paleoclimate records (Seager and Battisti, 2007). Moreover, the GRIP ice core and other proxy records (Figure 3.5 and 3.6) indicate that the climate warmings, for example the Bølling-Allerød, were much more abrupt than the climate coolings. Simple climate models have reproduced some of these rapid resumptions in thermohaline circulation (Ganopolski and Rahmstorf, 2001), but they are lacking in several key physical parameters (Seager and Battisti, 2007). Therefore, the addition of freshwater fluxes and changes in thermohaline circulation alone are insufficient to account for the global abrupt climate changes (Seager and Battisti, 2007).

It is clear that the abrupt climate changes must be caused by more than just changes in the NCW circulation and production. Seager and Battisti (2007) argue that the degree of winter cooling observed in the proxy records around the North Atlantic necessitate a significant change in atmospheric circulation and a reduction in atmospheric heat transport to the region. Later studies have cited the importance of the atmosphere's role in the timing of deep-water circulation changes and sea-ice production (Hillaire-Marcel et al., 2013; Thornalley et al., 2011) and invoke changes in wind regimes and tropical convection as possible mechanisms for these abrupt climate changes (Seager and Battisti, 2007). Although no current model exists to explain these mechanisms, atmospheric and surface ocean changes could presumably influence the strength and location of deep-water formation and promote the growth of sea ice (Seager and Battisti, 2007).

Variations in the southern margin of the Laurentide Ice Sheet would have produced topographic control on the jet stream masses and hence the polar front. Several reconstructions of the Laurentide, Fennoscandian, and other major circum-North Atlantic Ice Sheets document readvances during the H1 event (Kleiber et al., 2000; Knies et al., 2001; Knies et al., 2007; McCabe and Clark, 1998; Nygård et al., 2004; Polyak et al., 1997; Scourse et al., 2009). As such, the position of the jet stream would have migrated to the south, steering the polar front, sea ice extent and iceberg tracks to the south as well. It is therefore likely that the armadas of icebergs are just a consequence of climate change and not the instigator (Seager and Battisti, 2007).

3.6 Conclusions

The deglacial history of NCW shows a pattern that indicates it is resilient during the warm climate phases, when rapid ice sheet melting occurs. Reductions in NCW and minor Northern Hemisphere ice sheet advances occurred during the H1 stadial. Large benthic foraminiferal $\delta^{13}C$ gradients among North Atlantic sites (e.g., cores 15JPC than in OCE326-GGC5) indicates a strong and variable presence of AABW throughout the deglaical interval.

Large meltwater events (MWP1A and MWP1B) appear to have little to no effect on circulation and coincide with periods of rapid resumption of deep-water production. Several studies of meltwater discharge records show little evidence for increased discharge during H1 (Abdul et al., Submitted; Peltier and Fairbanks, 2006); therefore, the traditional theory of shutdown of NCW due to freshwater flux from melting armadas of icebergs needs to be reevaluated. Anomalously low planktonic foraminiferal $\delta^{18}O$ values during the cold intervals point to the presence of extensive sea ice and brine production and is supported by independent ocean proxies (de Vernal et al., 2005a) and evidence of glacial readvance (Kleiber et al., 2000; Knies et al., 2001; Knies et al., 2007; McCabe and Clark, 1998; Nygård et al., 2004; Polyak et al., 1997; Scourse et al., 2009). We propose that the climate impact on NCW is through the production of sea ice that follows the atmospheric circulation as a result of the southern advance of the polar front in response to re-advance of ice sheets (Seager and Battisti, 2007).

3.7 References

Abdul, N., Wright, J.D., Mortlock, R.A., Fairbanks, R.G., Submitted. Younger Dryas Sea-Level and Meltwater Pulse 1B Recorded in Barbados Reef Crest Coral Acropora palmata.

Alley, R., MacAyeal, D., 1994. Ice-rafted debris associated with binge/purge oscillations of the Laurentide Ice Sheet. Paleoceanography, 9(4): 503-511.

Barber, D. et al., 1999. Forcing of the cold event of 8,200 years ago by catastrophic drainage of Laurentide lakes. Nature, 400(6742): 344-348.

Barker, S. et al., 2009. Interhemispheric Atlantic seesaw response during the last deglaciation. Nature, 457(7233): 1097-1102.

Bauch, D., Carstens, J., Wefer, G., 1997. Oxygen isotope composition of living Neogloboquadrina pachyderma (sin.) in the Arctic Ocean. Earth and Planetary Science Letters, 146(1): 47-58.

Bé, A., Tolderlund, D., 1971. Distribution and ecology of living planktonic foraminifera in surface waters of the Atlantic and Indian Oceans. The micropaleontology of oceans: 105-149.

Be, A.W., 1960. Some observations on Arctic planktonic foraminifera. Contributions from the Cushman Foundation for Foraminiferal Research, 11(2): 64-68.

Bédard, P., Hillaire-Marcel, C., Page, P., 1981. 18O-modeling of freshwater inputs in Baffin Bay and Canadian Arctic coastal waters. Nature, 293: 287-289.

Blunier, T., Brook, E.J., 2001. Timing of millennial-scale climate change in Antarctica and Greenland during the last glacial period. Science, 291(5501): 109-112.

Blunier, T. et al., 1998. Asynchrony of Antarctic and Greenland climate change during the last glacial period. Nature, 394(6695): 739-743.

Bond, G. et al., 1993. Correlations between climate records from North Atlantic sediments and Greenland ice. Nature(365): 143-147.

Bond, G. et al., 1992. Evidence for massive discharges of icebergs into the North Atlantic ocean during the last glacial period.

Bond, G.C., Lotti, R., 1995. Iceberg discharges into the North Atlantic on millennial time scales during the last glaciation. Science, 267(5200): 1005-1010.

Bond, G.C. et al., 1999. The North Atlantic's 1-2 Kyr Climate Rhythm: Relation to Heinrich Events, Dansgaard/Oeschger Cycles and the Little Ice Age. Mechanisms of global climate change at millennial time scales: 35-58.

Bondevik, S., Mangerud, J., Birks, H.H., Gulliksen, S., Reimer, P., 2006. Changes in North Atlantic radiocarbon reservoir ages during the Allerød and Younger Dryas. Science, 312(5779): 1514-1517.

Boyle, E.A., Keigwin, L., 1987. North Atlantic thermohaline circulation during the past 20,000 years linked to high-latitude surface temperature. Nature, 330: 5.

Broecker, W., Bond, G., Klas, M., Clark, E., McManus, J., 1992. Origin of the northern Atlantic's Heinrich events. Climate Dynamics, 6(3-4): 265-273.

Broecker, W., Denton, G.H., 1990. What drives glacial cycles? Scientific American, 262(1): 42-50.

Broecker, W.S., 1994. Massive iceberg discharges as triggers for global climate change. Nature, 372: 421-424.

Broecker, W.S., 1998. Paleocean circulation during the last deglaciation: a bipolar seesaw? Paleoceanography, 13(2): 119-121.

Broecker, W.S., 2002. Constraints on the glacial operation of the Atlantic Ocean's conveyor circulation. Israel journal of chemistry, 42(1): 1-14.

Broecker, W.S., 2006. Was the Younger Dryas triggered by a flood? Science, 312(5777): 1146-1148.

Broecker, W.S. et al., 1989. Routing of meltwater from the Laurentide Ice Sheet during the Younger Dryas cold episode.

Carlson, A.E. et al., 2007. Geochemical proxies of North American freshwater routing during the Younger Dryas cold event. Proceedings of the National Academy of Sciences, 104(16): 6556-6561.

Charles, C.D., Fairbanks, R.G., 1992. Evidence from Southern Ocean sediments for the effect of North Atlantic deep-water flux on climate.

Charles, C.D., Lynch-Stieglitz, J., Ninnemann, U.S., Fairbanks, R.G., 1996. Climate connections between the hemisphere revealed by deep sea sediment core/ice core correlations. Earth and Planetary Science Letters, 142(1): 19-27.

Clarke, A., Church, J., Gould, J., 2001. Ocean processes and climate phenomena.

Clarke, G., Marshall, S.J., Hillaire-Marcel, C., Bilodeau, G., Veiga-Pires, C., 1999. A glaciological perspective on Heinrich events. GEOPHYSICAL MONOGRAPH-AMERICAN GEOPHYSICAL UNION, 112: 243-262.

Coplen, T.B., Kendall, C., Hopple, J., 1983. Comparison of stable isotope reference samples.

Curry, W., Marchitto, T., McManus, J., Oppo, D., Laarkamp, K., 1999. Millennial-scale changes in ventilation of the thermocline, intermediate, and deep waters of the glacial North Atlantic. GEOPHYSICAL MONOGRAPH-AMERICAN GEOPHYSICAL UNION, 112: 59-76.

Curry, W.B., Oppo, D.W., 2005. Glacial water mass geometry and the distribution of $\delta 13C$ of $\Sigma CO2$ in the western Atlantic Ocean. Paleoceanography, 20(1).

Dansgaard, W. et al., 1982. A new Greenland deep ice core. Science, 218(4579): 1273-1277.

de Vernal, A. et al., 2005a. Reconstruction of sea-surface conditions at middle to high latitudes of the Northern Hemisphere during the Last Glacial Maximum (LGM) based on dinoflagellate cyst assemblages. Quaternary Science Reviews, 24(7): 897-924.

de Vernal, A., Hillaire-Marcel, C., Turon, J.-L., Matthiessen, J., 2000. Reconstruction of sea-surface temperature, salinity, and sea-ice cover in the northern North Atlantic during the last glacial maximum based on dinocyst assemblages. Canadian Journal of Earth Sciences, 37(5): 725-750.

de Vernal, A., Hillaire-Marcel, C., Darby, D.A., 2005b. Variability of sea ice cover in the Chukchi Sea (western Arctic Ocean) during the Holocene. Paleoceanography, 20(4).

de Vernal, A., Hillaire-Marcel, C., Peltier, W.R., Weaver, A.J., 2002. Structure of the upper water column in the northwest North Atlantic: Modern versus Last Glacial Maximum conditions. Paleoceanography, 17(4): 2-1-2-15.

Duplessy, J. et al., 1988a. Deep-water source variation during the last climate variation: Palaeoceanography, v. 3.

Duplessy, J.C., Labeyrie, L., Blanc, P., 1988b. Norwegian Sea deep water variations over the last climatic cycle: paleo-oceanographical implications, Long and short term variability of climate. Springer, pp. 83-116.

Elliot, M., Labeyrie, L., Duplessy, J.-C., 2002. Changes in North Atlantic deep-water formation associated with the Dansgaard–Oeschger temperature oscillations (60–10ka). Quaternary Science Reviews, 21(10): 1153-1165.

Elmore, A.C., Wright, J.D., 2011. North Atlantic Deep Water and climate variability during the Younger Dryas cold period. Geology, 39(2): 107-110.

Evans, H.F. et al., 2007. Paleointensity‐assisted chronostratigraphy of detrital layers on the Eirik Drift (North Atlantic) since marine isotope stage 11. Geochemistry, Geophysics, Geosystems, 8(11).

Fairbanks, R.G., 1989. A 17, 000-year glacio-eustatic sea level record: influence of glacial melting rates on the Younger Dryas event and deep-ocean circulation. Nature, 342(6250): 637-642.

Fairbanks, R.G., 1990. The age and origin of the "Younger Dryas climate event" in Greenland ice cores. Paleoceanography, 5(6): 937-948.

Fairbanks, R.G. et al., 2005. Radiocarbon calibration curve spanning 0 to 50,000 years BP based on paired 230 Th/234 U/238 U and 14 C dates on pristine corals. Quaternary Science Reviews, 24(16): 1781-1796.

Ganopolski, A., Rahmstorf, S., 2001. Rapid changes of glacial climate simulated in a coupled climate model. Nature, 409(6817): 153-158.

Ganssen, G., Kroon, D., 2000. The isotopic signature of planktonic foraminifera from NE Atlantic surface sediments: implications for the reconstruction of past oceanic conditions. Journal of the Geological Society, 157(3): 693-699.

Grootes, P., Stuiver, M., White, J., Johnsen, S., Jouzel, J., 1993. Comparison of oxygen isotope records from the GISP2 and GRIP Greenland ice cores.

Grootes, P.M. et al., 2001. The Taylor Dome Antarctic 18 O record and globally synchronous changes in climate. Quaternary Research, 56(3): 289-298.

Heinrich, H., 1988. Origin and consequences of cyclic ice rafting in the northeast Atlantic Ocean during the past 130,000 years. Quaternary research, 29(2): 142-152.

Hemming, S. et al., 1998. Provenance of Heinrich layers in core V28-82, northeastern Atlantic: 40 Ar/39 Ar ages of ice-rafted hornblende, Pb isotopes in feldspar grains, and Nd–Sr–Pb isotopes in the fine sediment fraction. Earth and Planetary Science Letters, 164(1): 317-333.

Hemming, S.R., 2004. Heinrich events: Massive late Pleistocene detritus layers of the North Atlantic and their global climate imprint. Reviews of Geophysics, 42(1).

Hillaire-Marcel, C., Bilodeau, G., 2000. Instabilities in the Labrador Sea water mass structure during the last climatic cycle. Canadian Journal of Earth Sciences, 37(5): 795-809.

Hillaire-Marcel, C., de Vernal, A., 2008. Stable isotope clue to episodic sea ice formation in the glacial North Atlantic. Earth and Planetary Science Letters, 268(1): 143-150.

Hillaire-Marcel, C., De Vernal, A., Bilodeau, G., Weaver, A., 2001. Absence of deep-water formation in the Labrador Sea during the last interglacial period. Nature, 410(6832): 1073-1077.

Hillaire-Marcel, C., de Vernal, A., McKay, J., 2011. Foraminifer isotope study of the Pleistocene Labrador Sea, northwest North Atlantic (IODP Sites 1302/03 and 1305), with emphasis on paleoceanographical differences between its “inner” and “outer” basins. Marine Geology, 279(1): 188-198.

Hillaire-Marcel, C., De Vernal, A., Polyak, L., Darby, D., 2004. Size-dependent isotopic composition of planktic foraminifers from Chukchi Sea vs. NW Atlantic sediments—implications for the Holocene paleoceanography of the western Arctic. Quaternary Science Reviews, 23(3): 245-260.

Hillaire-Marcel, C., Maccali, J., Not, C., Poirier, A., 2013. Geochemical and isotopic tracers of Arctic sea ice sources and export with special attention to the Younger Dryas interval. Quaternary Science Reviews, 79: 184-190.

Johnsen, S., Dansgaard, W., Clausen, H., Langway, C., 1972. Oxygen isotope profiles through the Antarctic and Greenland ice sheets. Nature, 235(5339): 429-434.

Jonkers, L. et al., 2010. A reconstruction of sea surface warming in the northern North Atlantic during MIS 3 ice-rafting events. Quaternary Science Reviews, 29(15): 1791-1800.

Jouzel, J., Genthon, C., Lorius, C., Petit, J., Barkov, N., 1987. Vostok ice core-A continuous isotope temperature record over the last climatic cycle (160,000 years). Nature, 329: 403-408.

Kanfoush, S.L. et al., 2000. Millennial-scale instability of the Antarctic ice sheet during the last glaciation. Science, 288(5472): 1815-1819.

Kaplan, M.R. et al., 2010. Glacier retreat in New Zealand during the Younger Dryas stadial. Nature, 467(7312): 194-197.

Keigwin, L.D., Boyle, E.A., 1999. Surface and deep ocean variability in the northern Sargasso Sea during marine isotope stage 3. Paleoceanography, 14(2): 164-170.

Kleiber, H., Knies, J., Niessen, F., 2000. The Late Weichselian glaciation of the Franz Victoria Trough, northern Barents Sea: ice sheet extent and timing. Marine Geology, 168(1): 25-44.

Knies, J., Kleiber, H.-P., Matthiessen, J., Müller, C., Nowaczyk, N., 2001. Marine ice-rafted debris records constrain maximum extent of Saalian and Weichselian ice-sheets along the northern Eurasian margin. Global and Planetary Change, 31(1): 45-64.

Knies, J. et al., 2007. Re-advance of the Fennoscandian ice sheet during Heinrich event 1. Marine Geology, 240(1): 1-18.

Kohfeld, K.E., Fairbanks, R.G., Smith, S.L., Walsh, I.D., 1996. Neogloboquadrina pachyderma (sinistral coiling) as paleoceanographic tracers in polar oceans: Evidence from Northeast Water Polynya plankton tows, sediment traps, and surface sediments. Paleoceanography, 11(6): 679-699.

Kuroyanagi, A., Kawahata, H., 2004. Vertical distribution of living planktonic foraminifera in the seas around Japan. Marine Micropaleontology, 53(1): 173-196.

Lagerklint, I.M., Wright, J.D., 1999. Late glacial warming prior to Heinrich event 1: The influence of ice rafting and large ice sheets on the timing of initial warming. Geology, 27(12): 1099-1102.

Manabe, S., Stouffer, R., 1988. Two stable equilibria of a coupled ocean-atmosphere model. Journal of Climate, 1(9): 841-866.

Manabe, S., Stouffer, R.J., 1995. Simulation of abrupt climate change induced by freshwater input to the North Atlantic Ocean. Nature, 378(6553): 165-167.

Manabe, S., Stouffer, R.J., 1997. Coupled ocean-atmosphere model response to freshwater input: Comparison to Younger Dryas event. Paleoceanography, 12(2): 321-336.

Manabe, S., Stouffer, R.J., 2000. Study of abrupt climate change by a coupled ocean–atmosphere model. Quaternary Science Reviews, 19(1): 285-299.

Marchitto, T.M., Oppo, D.W., Curry, W.B., 2002. Paired benthic foraminiferal Cd/Ca and Zn/Ca evidence for a greatly increased presence of Southern Ocean Water in the glacial North Atlantic. Paleoceanography, 17(3): 10-1-10-18.

McCabe, A.M., Clark, P.U., 1998. Ice-sheet variability around the North Atlantic Ocean during the last deglaciation. Nature, 392(6674): 373-377.

McManus, J., Francois, R., Gherardi, J.-M., Keigwin, L., Brown-Leger, S., 2004. Collapse and rapid resumption of Atlantic meridional circulation linked to deglacial climate changes. Nature, 428(6985): 834-837.

McManus, J.F., Anderson, R.F., Broecker, W.S., Fleisher, M.Q., Higgins, S.M., 1998. Radiometrically determined sedimentary fluxes in the sub-polar North Atlantic during the last 140,000 years. Earth and Planetary Science Letters, 155(1): 29-43.

Nygård, A., Sejrup, H.P., Haflidason, H., Cecchi, M., Ottesen, D., 2004. Deglaciation history of the southwestern Fennoscandian Ice Sheet between 15 and 13 14C ka BP. Boreas, 33(1): 1-17.

Oppo, D., Curry, W., 1997. The mid-Pleistocene climate transition: A deep sea carbon isotopic perspective.

Oppo, D., Curry, W., 2012. Deep Atlantic circulation during the Last Glacial Maximum and deglaciation. Nature Education Knowledge, 3(10): 1.

Oppo, D.W., Fairbanks, R.G., 1987. Variability in the deep and intermediate water circulation of the Atlantic Ocean during the past 25,000 years: Northern Hemisphere modulation of the Southern Ocean. Earth and Planetary Science Letters, 86(1): 1-15.

Oppo, D.W., Lehman, S.J., 1995. Suborbital timescale variability of North Atlantic Deep Water during the past 200,000 years. Paleoceanography, 10(5): 901-910.

Pedro, J.B. et al., 2011. The last deglaciation: timing the bipolar seesaw. Climate of the Past, 7.

Peltier, W., Fairbanks, R.G., 2006. Global glacial ice volume and Last Glacial Maximum duration from an extended Barbados sea level record. Quaternary Science Reviews, 25(23): 3322-3337.

Piotrowski, A.M., Goldstein, S.L., Hemming, S.R., Fairbanks, R.G., 2005. Temporal relationships of carbon cycling and ocean circulation at glacial boundaries. Science, 307(5717): 1933-1938.

Polyak, L., Forman, S.L., Herlihy, F.A., Ivanov, G., Krinitsky, P., 1997. Late Weichselian deglacial history of the Svyataya (Saint) Anna Trough, northern Kara Sea, Arctic Russia. Marine geology, 143(1): 169-188.

Praetorius, S.K., McManus, J.F., Oppo, D.W., Curry, W.B., 2008. Episodic reductions in bottom-water currents since the last ice age. Nature Geoscience, 1(7): 449-452.

Rahmstorf, S., 1994. Rapid climate transitions in a coupled ocean-atmosphere model. Nature, 372(6501): 82-85.

Rashid, H., Boyle, E.A., 2007. Mixed-layer deepening during heinrich events: a multi-planktonic foraminiferal δ18O approach. Science, 318(5849): 439-441.

Raymo, M., Ruddiman, W., Backman, J., Clement, B., Martinson, D., 1989. Late Pliocene variation in Northern Hemisphere ice sheets and North Atlantic deep water circulation. Paleoceanography, 4(4): 413-446.

Rind, D. et al., 2001. Effects of glacial meltwater in the GISS coupled atmosphereocean model: 1. North Atlantic Deep Water response. Journal of Geophysical Research: Atmospheres (1984–2012), 106(D21): 27335-27353.

Sarnthein, M. et al., 1994. Changes in east Atlantic deepwater circulation over the last 30,000 years: Eight time slice reconstructions. Paleoceanography, 9(2): 209-267.

Schiebel, R., Bijma, J., Hemleben, C., 1997. Population dynamics of the planktic foraminifer Globigerina bulloides from the eastern North Atlantic. Deep Sea Research Part I: Oceanographic Research Papers, 44(9): 1701-1713.

Schiller, A., Mikolajewicz, U., Voss, R., 1997. The stability of the North Atlantic thermohaline circulation in a coupled ocean-atmosphere general circulation model. Climate Dynamics, 13(5): 325-347.

Scourse, J.D. et al., 2009. Growth, dynamics and deglaciation of the last British–Irish ice sheet: the deep-sea ice-rafted detritus record. Quaternary Science Reviews, 28(27): 3066-3084.

Seager, R., Battisti, D.S., 2007. Challenges to our understanding of the general circulation: abrupt climate change. Global Circulation of the Atmosphere: 331-371.

Shakun, J.D., Carlson, A.E., 2010. A global perspective on Last Glacial Maximum to Holocene climate change. Quaternary Science Reviews, 29(15): 1801-1816.

Simstich, J., Sarnthein, M., Erlenkeuser, H., 2003. Paired δ 18 O signals of Neogloboquadrina pachyderma (s) and Turborotalita quinqueloba show thermal stratification structure in Nordic Seas. Marine Micropaleontology, 48(1): 107-125.

Sowers, T., Bender, M., 1995. Climate records covering the last deglaciation. Science, 269(5221): 210-214.

Stanford, J.D. et al., 2006. Timing of meltwater pulse 1a and climate responses to meltwater injections. Paleoceanography, 21(4).

Stocker, T.F., 1998. The seesaw effect. Science, 282(5386): 61.

Stocker, T.F., Johnsen, S.J., 2003. A minimum thermodynamic model for the bipolar seesaw. Paleoceanography, 18(4).

Stocker, T.F., Wright, D.G., 1991. Rapid transitions of the ocean's deep circulation induced by changes in surface water fluxes. Nature, 351(6329): 729-732.

Tan, F., Strain, P., 1980. The distribution of sea ice meltwater in the eastern Canadian Arctic. Journal of Geophysical Research: Oceans (1978–2012), 85(C4): 1925-1932.

Tarasov, L., Peltier, W., 2005. Arctic freshwater forcing of the Younger Dryas cold reversal. Nature, 435(7042): 662-665.

Tarasov, L., Peltier, W., 2006. A calibrated deglacial drainage chronology for the North American continent: evidence of an Arctic trigger for the Younger Dryas. Quaternary Science Reviews, 25(7): 659-688.

Teller, J.T., Thorleifson, L.H., Dredge, L., Hobbs, H.C., Schreiner, B., 1983. Maximum extent and major features of Lake Agassiz. Geological Association of Canada.

Thornalley, D.J., Barker, S., Broecker, W.S., Elderfield, H., McCave, I.N., 2011. The deglacial evolution of North Atlantic deep convection. science, 331(6014): 202-205.

Vellinga, M., Wood, R.A., 2002. Global climatic impacts of a collapse of the Atlantic thermohaline circulation. Climatic change, 54(3): 251-267.

Vellinga, M., Wood, R.A., Gregory, J.M., 2002. Processes governing the recovery of a perturbed thermohaline circulation in HadCM3. Journal of Climate, 15(7): 764-780.

Zhang, R., Delworth, T.L., 2005. Simulated tropical response to a substantial weakening of the Atlantic thermohaline circulation. Journal of Climate, 18(12): 1853-1860.

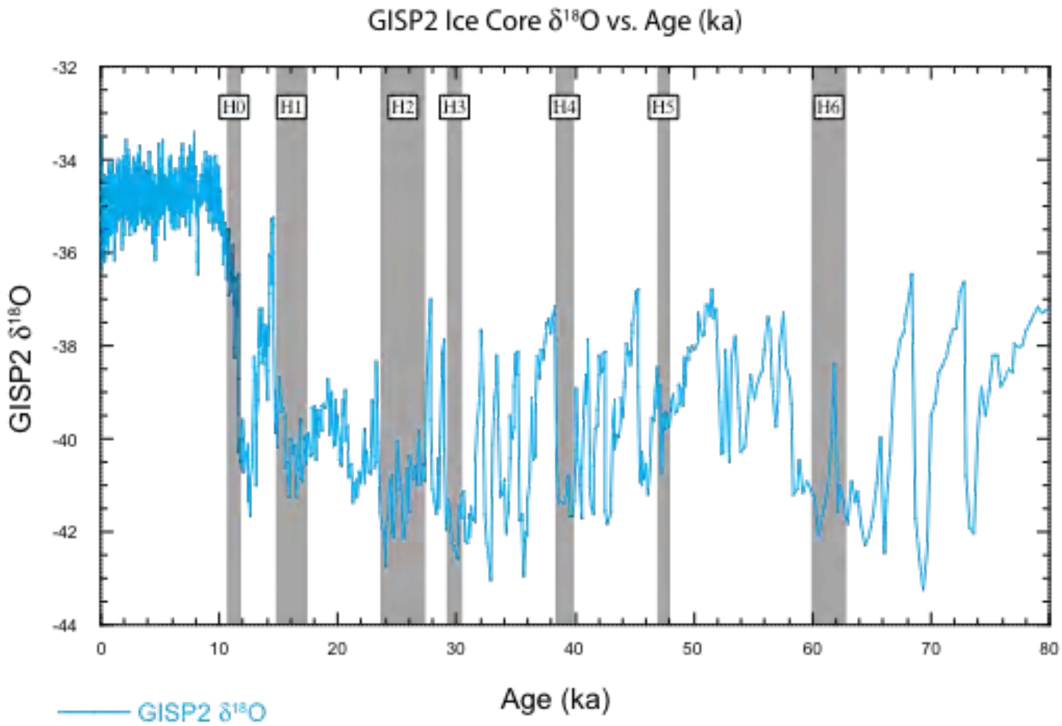

Figure 3.1

Figure 3.1: $\delta^{18}O$ curve from the Greenland Ice Sheet Project 2 (GISP2) ice core record versus age (Grootes and Stuiver, 1997; Grootes et al., 1993; Meese, 1994; Steig et al., 1994; Stuiver et al., 1995). The gray bars highlight Heinrich events H0 to H6.

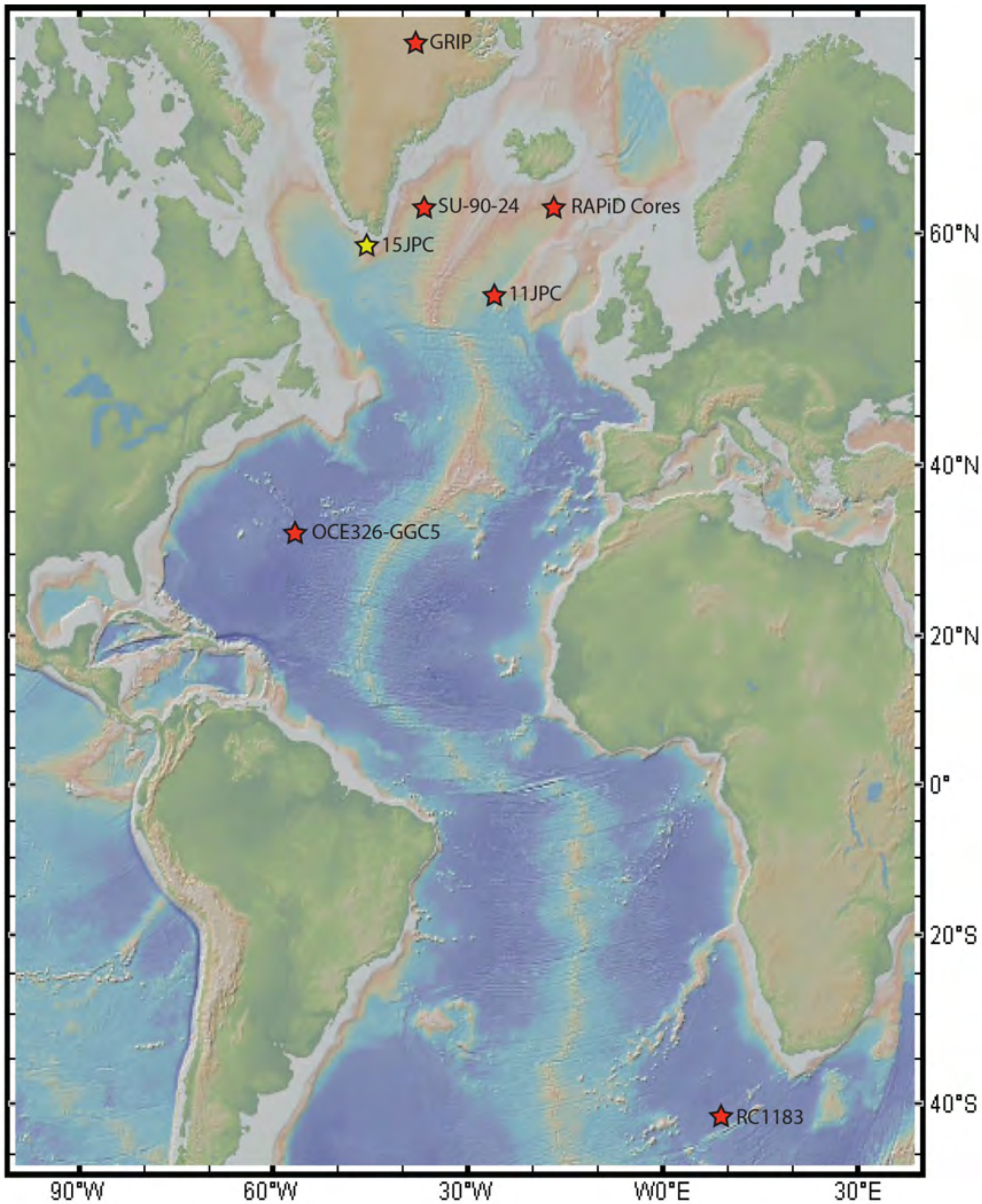

Figure 3.2

Figure 3.2: Base map showing the locations of the cores analyzed in the study (red star) and used for comparison (yellow stars). Refer to Table 3.1 for latitudes, longitudes, core depths and original references.

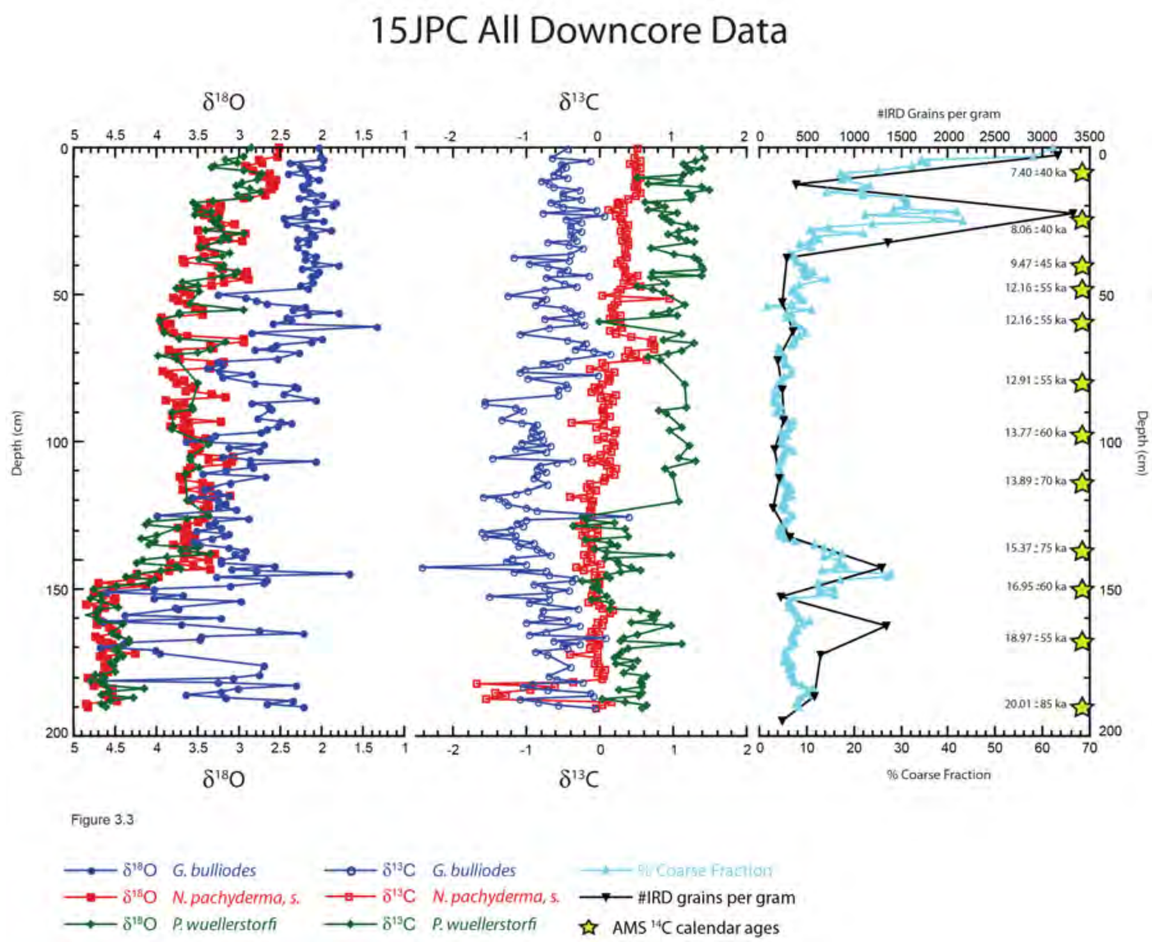

Figure 3.3: Age and depth picks from core 15JPC that were used to generate the downcore age model. Ages between tie points were originally linearly interpolated and then a linear regression was applied to the Bolling-Allerod, Heinrich 1 and Last Glacial Maximum sections of the age model (red line). Refer to Appendix 1 for list of ^{14}C ages used for this age model.

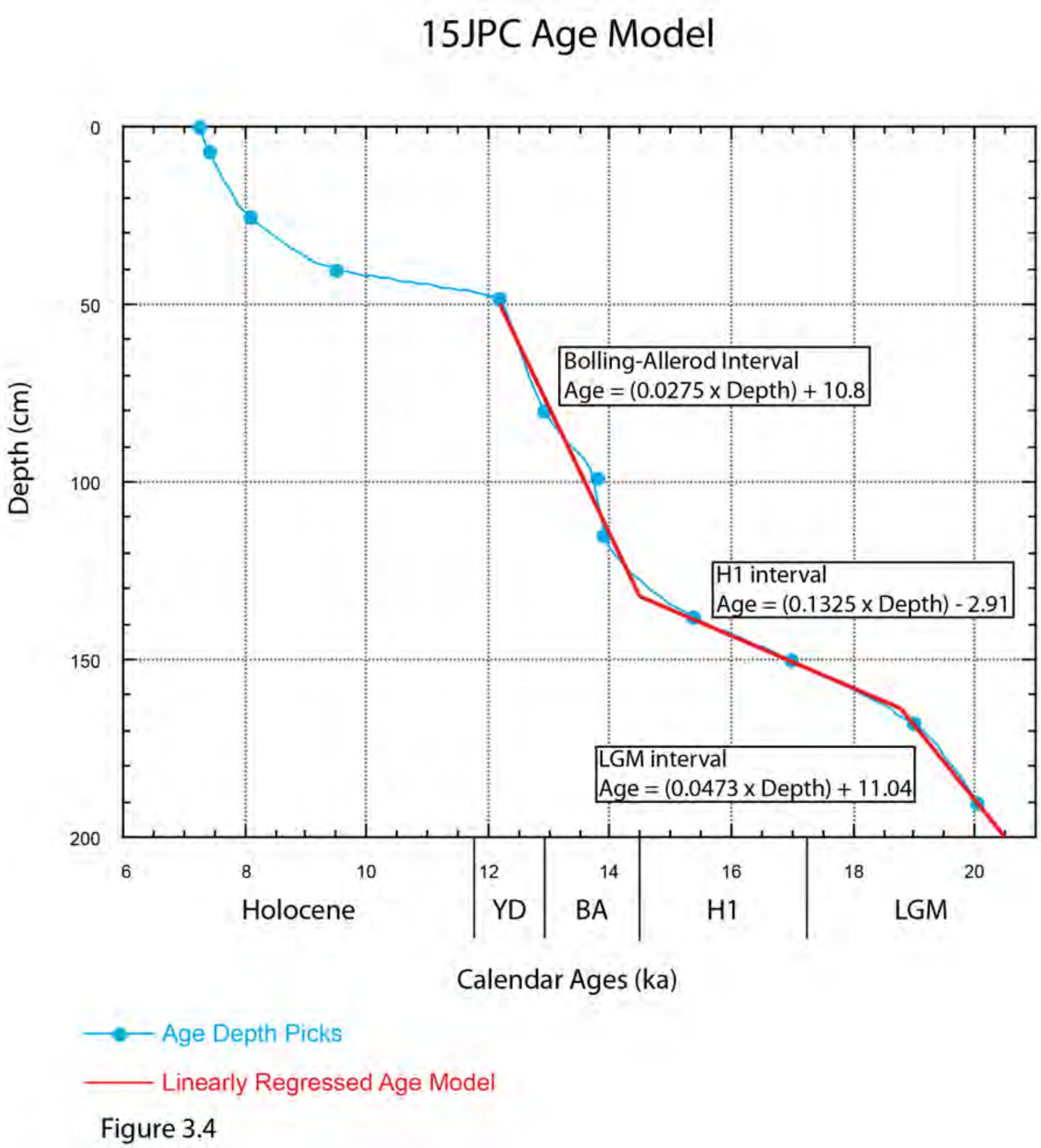

Figure 3.4: Downcore data versus depth for core 15JPC. The δ18O (closed circles) for and δ13C (open circles) values for P. wuellerstorfi (green), G. bulliodes (blue) and N. pachyderma, s. (red), percent coarse fraction (light blue triangles), number of IRD grains per gram (black triangles), and AMS 14C calendar ages (yellow stars) are displayed.

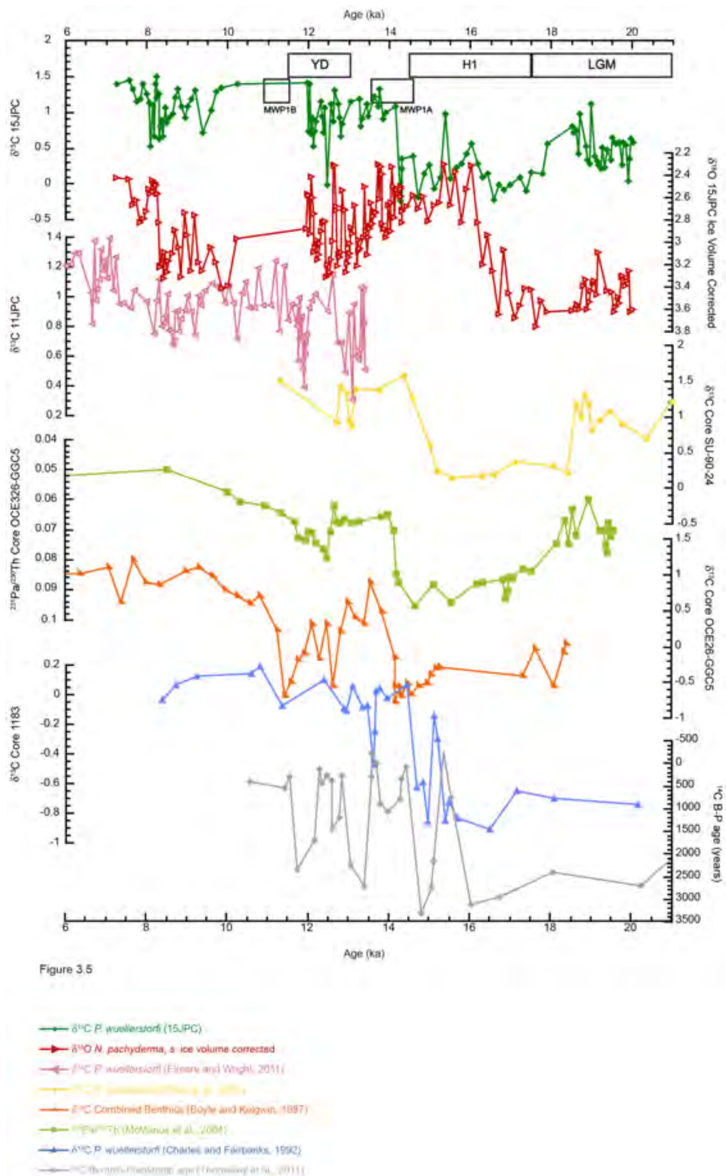

Figure 3.5: Comparison figure showing δ13C values for core 15JPC (orange diamonds; this study), 11JPC (pink triangle; Elmore and Wright, 2011), ice volume corrected $\delta^{18}O$ for core 15JPC (red triangles), SU-90-24 (gold circles, Elliot et al., 2002), OCE26-GGC5 (dark green triangles; Boyle and Keigwin, 1987), and 1183 (blue triangles, Charles and Fairbanks, 1992), the 231Pa/230Th values for core OCE26-GGC5 (Boyle and Keigwin, 1987; McManus et al., 2004), and the 14C ventilation ages (grey diamonds; Thornalley et al., 2011) versus age (ka).

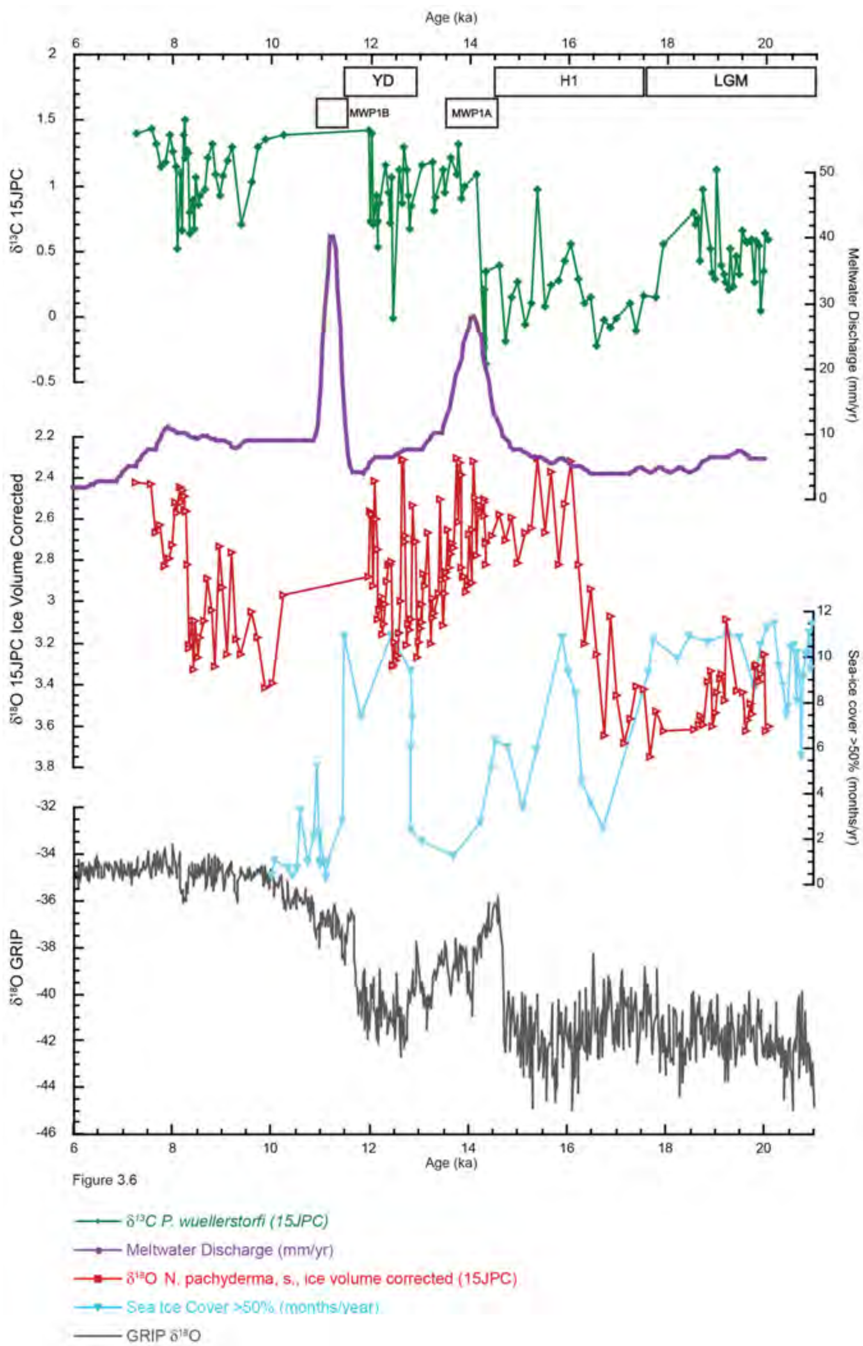

Figure 3.6: Comparison figure showing the $\delta^{13}C$ (orange diamonds) ice volume corrected $\delta^{18}O$ for core 15JPC (red triangles), the Bermuda meltwater discharge rates (purple circles; Abdul et al., submitted; Fairbanks et al., in prep; Peltier and Fairbanks, 2006), sea ice coverage (light blue triangles; de Vernal et al., 2005a), and the GRIP δ18O ice core record (Rasmussen et al., 2006).

Core Name	Latitude	Longitude	Depth	Reference
15JPC	58° 11.82' N	45° 34.08' W	2230 m	This Study
GRIP	72° 58' N	37° 64' W	Greenland Ice Core	Rasmussen et al., 2006
SU-90-24	62° 04' N	37° 02' W	2085 m	Elliot et al., 2002
RAPiD-10-1P	62° 58.53' N	17° 35.37' W	1237 m	Thornalley et al., 2011 (data from all 3 cores combined)
RAPiD-12-1K	62° 05.43' N	17° 49.18' W	1938 m	
RAPiD-15-4P	62° 17.58' N	17° 08.04' W	2133 m	
11JPC	56° 14' N	27° 38' W	2707 m	Elmore and Wright, 2011
HU-91-045-094	50° 20' N	45° 68' W	3448 m	de Vernal et al., 2005; Hillaire-Marcel et al., 2008
OCE326-GGC5	33° 42' N	57° 35' W	4550 m	McManus et al., 2004 Boyle and Keigwin, 1987
RC1183	41° 36' S	9° 48' E	4718 m	Charles and Fairbanks, 1992

Table 3.1: List of latitudes, longitudes and depths of the cores analyzed and used for comparison in this study.

4.0 Evaluating the errors and uncertainties in $\delta^{18}O$-based chronologies of deep-sea sediment cores

4.1 Abstract

Paleoceanographic research relies on the construction of robust age models. Site-to-site correlation is limited by the uncertainties associated with different methodologies. Stacked $\delta^{18}O$ records proved an excellent tool for correlating sites on orbital timescales (Raymo et al., 1989), but often lack the resolution to correlate millennial scale deep-water events. For sites in polar regions, the paucity of benthic foraminifera often requires $\delta^{18}O$ records based on planktonic foraminifera, which are susceptible to local surface-water variability in temperature and fresh-water runoff. Highly variable sedimentation rates can also introduce uncertainties in the $\delta^{18}O$ records. Radiocarbon dating is widely used to constrain the chronologies of deep-sea records of the Late Pleistocene, but is subject to uncertainties in calibration (Fairbanks et al., 2005) and variable reservoir age corrections (Butzin et al., 2005). Combining $\delta^{18}O$ stratigraphies with an independent age control unaffected by environmental factors can increase the confidence in the timing of deep-water events. Paleointensity assisted chronologies provide another tool to further refine site-to-site correlation based on $\delta^{18}O$ age models (Channell et al., 2014; Channell et al., 2009; Evans et al., 2007). Relative paleointensity records and $\delta^{18}O$ stratigraphies generated from 4 cores collected on the Eirik Drift provide further constraints on the age control and highlight changes in detrital layers in the sediments (Evans et al., 2007).

4.2 Introduction

The construction of high-resolution $\delta^{18}O$ records with improved stratigraphic age control remains one of the major goals of paleoceanographic research today. The oxygen isotope changes in seawater appear to be globally synchronous on orbital timescales (Raymo et al., 1989), but due to the associated mixing times of the ocean, are not on millennial timescales (Skinner and Shackleton, 2005). In order to fully understand the cause and effect of the millennial scale changes in Northern Component Water (NCW; analogous to North Atlantic Deep Water) the leads and lags between bottom water production and circulation need to be known with better than a century precision.

Evaluating a cause-effect relationship between the resumption of NCW production and the start of the Bolling-Allerod warm interval illustrates the need for highly accurate age control of these deep-water events. The sharp transition in the proxy records during this event indicates of the switch between modes of deep-water circulation recorded in several northern North Atlantic and one subtropical Atlantic deep-sea sediment cores (Table 4.1 and Figure 4.1). Ages for the initiation of this deep-water event vary from 15.2 ka (Figure 4. 2; Core SU-90-24; Elliot et al., 2002), to 14.7 ka (RAPID Cores; Thornalley et al., 2011), and 14.2 ka (Core 15JPC and OCE26-GGC5; Chapter 2 of this study; Boyle and Keigwin, 1987; McManus et al., 2004). This offset is a function of the radiocarbon uncertainties in the age model (i.e., Butzin et al., 2005; Stuiver et al., 1991) and the amount of time it takes (~100 years) for this event to propagate throughout the Atlantic Basin (Broecker, 1979).

Traditional approaches of constructing age models for marine $\delta^{18}O$ records allows for the correlation of deep-water events between sites within the error constraints of the various methodologies. The use of an independent age control method that is unaffected by environmental inputs could help resolve a more precise chronology of the observed deep-water events. This chapter reviews the current techniques used to constrain age for the $\delta^{18}O$ records of deep-sea sediment cores as well as explore the inherent errors within. The published results of Evans et al. (2007) that used paleo-intensity assisted chronologies in tandem with traditional $\delta^{18}O$ stratigraphic methods is reviewed and presented as a promising method to further constrain deep-sea sediment core age models.

4.2.1 $\delta^{18}O$ Stacks

Sediment core records of $\delta^{18}O$ from foraminiferal calcite tests provide some of the best data on past climate change. The recorded foraminiferal $\delta^{18}O$ values are controlled by the temperature and $\delta^{18}O$ the water during calcification. The $\delta^{18}O_{water}$ term is a function of global ice volume and evaporation/precipitation and riverine runoff (Craig and Gordon, 1965). In general, changes in temperature and global ice volume affect marine $\delta^{18}O$ records the same way; warm, low ice volume are associated with low values of $\delta^{18}O_{water}$ while colder, higher ice volume climates are the reverse. Furthermore, the $\delta^{18}O_{water}$ term dominates Late Pleistocene changes and $\delta^{18}O$ correlations have relied on benthic foraminiferal records that are less susceptible to local temperature and $\delta^{18}O_{water}$ changes. Even so, local variations in temperature and $\delta^{18}O_{water}$ can make direct site-to-site correlation difficult, therefore "stacking" is used to decrease the background noise and increase the signal strength in the records (Bassinot et al., 1994; Hays et al., 1976; Imbrie et al., 1984; Lisiecki and Raymo, 2005; Martinson et al., 1987). In this process, records from multiple locations are combined so that the global signal is resolved while local signals are minimized (i.e., Hays et al., 1976). These stacks can then be used as type sections to which other paleoceanographic records can be compared to create age models on a common timescale (i.e., Lisiecki and Raymo, 2005).

A number of these stacks have been created since their inception using a variety of methods, proxies, locations, and tuning techniques. Early iterations utilized multiple planktonic foraminifera $\delta^{18}O$ records (i.e., SPECMAP Imbrie et al., 1984) or multiple proxies from a single location (Martinson et al., 1987) to create these global climate records. Subsequent studies applied benthic $\delta^{18}O$ records to the stacks to reduce the local signal variations due to surface water variability recorded in planktonic foraminifera and added multiple sites due to the availability of better and longer $\delta^{18}O$ records (Bassinot et al., 1994; Karner et al., 2002; Pisias et al., 1984; Prell et al., 1986; Raymo et al., 1990; Shackleton et al., 1995). The most recent $\delta^{18}O$ stack is the LR04 curve (Lisiecki and Raymo, 2005) constructed from the benthic foraminifera $\delta^{18}O$ records from 57 globally distributed sites. This stack spans the entire Pliocene and Pleistocene, has a resolution comparable to that of the GISP2 $\delta^{18}O$ record, with 10 to 20 samples for each 20 kyr (Grootes et al., 1993), and an average error of 0.1‰ (Lisiecki and Raymo, 2005).

It is important to take into consideration the factors that can introduce errors into these records. This stacking method calls upon the orbital tuning concept proposed by Milankovitch (1941), that requires the records be “tuned” to the various orbitally based parameters (Lisiecki and Raymo, 2005 and others). Each of these methods requires different assumptions to be made and makes the results susceptible and more sensitive to errors (i.e., Martinson et al., 1987). Furthermore, variations in sedimentation rates can distort the climate signal and need to be accounted for and normalized when applying a tuning mechanism (i.e., Lisiecki and Raymo, 2005; Martinson et al., 1987). This would prevent sites with extreme high or low sedimentation rates from being overly or under weighted in the records, respectively (Lisiecki and Raymo, 2005). Planktonic foraminifera $\delta^{18}O$ records can be significantly influenced by local variations in ocean water temperature, salinity, and chemistry (Hillaire-Marcel and de Vernal, 2008), and further studies suggest the benthic foraminifera $\delta^{18}O$ record can be heavily influenced as well (Lisiecki and Raymo, 2009; Skinner and Shackleton, 2005). Bioturbation introduces additional errors by moving core material up and/or down within the sediment colum. The magnitude of the errors within these records is depends on the degree of errors in the initial chronology and can average up ±5000 years (Martinson et al., 1987).

4.2.2 Radiocarbon Dating Calibration

Creating stacked $\delta^{18}O$ records requires the use of an initial age model and the most common method radiocarbon dating. Accelerator Mass Spectrometry (AMS) ^{14}C dating is the most widely used dating technique (Fairbanks et al., 2005) and radiocarbon dating allows the correlation of a wide range of Late Pleistocene to Holocene terrestrial and marine records. However, a radiocarbon age is not a true calendar age and must be corrected due to the fluctuations in the amount of atmospheric ^{14}C by using a calibration curve (Bard et al., 1993; Bard et al., 1990; Beck et al., 2001; Burr et al., 1998; Damon, 1988; Edwards et al., 1993; Fairbanks et al., 2005; Goslar et al., 2000a; Hughen et al., 2000; Schramm et al., 2000; Stuiver et al., 1986; Stuiver et al., 1998; Stuvier, 1982; Voelker et al., 2000). Radiocarbon ages from the last 11.9 kyr are calibrated by comparing the radiocarbon measurements in wood and applying the widely accepted tree ring calibration curve (Damon, 1988; Reimer et al., 2004; Reimer et al., 2002; Stuiver et al., 1986; Stuiver et al., 1998). For samples between 12 and 50 kyr BP, radiocarbon ages are calibrated by comparing the measurements to either varved sediments (Goslar et al., 2000a; Hughen et al., 1998; Hughen et al., 2004b; Hughen et al., 2000; Kitagawa and van der Plicht, 2000; Schramm et al., 2000; van der Plicht et al., 2004), the Greenland ice cores (Hughen et al., 2004a; Hughen et al., 2000; Voelker et al., 2000), speleothems (Beck et al., 2001; Goslar et al., 2000b; Vogel and Kronfeld, 1997), or corals (Bard et al., 1998; Bard et al., 1990; Burr et al., 1998; Cutler et al., 2004; Edwards et al., 1993; Fairbanks, 1990; Fairbanks et al., 2005; Paterne et al., 2004; van der Plicht et al., 2004; Yokoyama and Esat, 2004). Each of these methods has its own set of errors and disadvantages (Fairbanks et al., 2005) but allow for the reconstruction of useful radiocarbon calendar age chronologies. Calendar ages for this research are calculated using the Fairbanks0107 calibration curve (Fairbanks et al., 2005) constructed from a stand alone coral spanning the last 50 kyr.

4.2.3 Reservoir Age Corrections

Further uncertainties arise due to the need to apply reservoir age corrections to radiocarbon ages and the wide range of cited values (i.e., Bondevik et al., 2006; Butzin et al., 2005; Butzin et al., 2012; Cao et al., 2007). Conventional radiocarbon ages do not take into account the differences in ages between the various carbon reservoirs. One of these reservoir effects is between the ocean and atmosphere, where the average difference in radiocarbon ages between modern terrestrial and marine samples is about 400 years (i.e., Stuiver and Braziunas, 1993). The apparent older age of the marine sample is caused by a delay in the exchange rates between the carbon in the atmosphere and the ocean and by the mixing of surfaces waters with older deep-water (Mangerud, 1972); as well as variations in the production rate of atmospheric ^{14}C (Stuiver et al., 1986) and changes in ventilation between the ocean and atmosphere (Bard et al., 1994; Stocker and Wright, 1996).

The global mean average of this difference between surface and deep-water ages is ~400 years (i.e., Butzin et al., 2005; Stuiver and Braziunas, 1993) but can be as much a 2000 years in the high latitudes (Butzin et al., 2005). These translate to reservoir correction ages between 200 to 300 years in the subtropical gyres to 1200 years in the high latitudes of the Southern and North Pacific Ocean (Bard, 1988; Broecker et al., 1985; Butzin et al., 2005). However, the modern reservoir age in the North Atlantic Ocean between 40°N and 70°N is fairly constant at about 400 years (Bard, 1988; Broecker et al., 1985; Butzin et al., 2005; Cao et al., 2007) due to the transport of partially equilibrated tropical and subtropical waters to the high latitudes and the rapid downward mixing of the surface waters to the deep (Lazier et al., 2002).

Broecker et al. (1990) estimated that the age of deep-water in the North Atlantic during the Last Glacial Maximum (LGM) was significantly older than modern deep-water with an average age of 600 to 700 years. Therefore it is important to consider that reservoir ages have not been constant through time and many studies have been conducted since to calculate these values during the last glacial period (Austin et al., 1995; Bard et al., 1994; Bondevik et al., 1999; Bondevik et al., 2006; Bondevik et al., 2001; Schmittner, 2003; Siani et al., 2001). Bondevik et al. (2006) suggested that during the 3 kyr of Termination 1 the reservoir age increased from 400 to 600 years in the early Younger Dryas before dropping by 300 years at the start of the Holocene. Whereas, Cao et al. (2007) estimated the reservoir age changed from 380±140 years, to 590±130 years, to 270±20 years across the transition from the Bolling-Allerod, during the Younger Dryas, and the end of the Younger Dryas, respectively. Therefore, radiocarbon-based chronologies are unlikely to have the certainty to determine lead-lag relationships on the centennial scale.

4.2.4 Relative Paleointensity Data

The marriage between oxygen isotopes and geomagnetic polarity changes has been a backbone of Cenozoic correlation schemes (e.g., Shackleton, 1977; Shackleton and Opdyke, 1973). The "100 kyr" glacial-interglacial pacing was established for the Brunhes polarity chron (Hays et al., 1976; Martinson et al., 1987; Shackleton and Opdyke, 1973) and confirmed U/Th ages for uplifted corals that had earlier shown that the last interglacial highstand was ~125 kyr BP (Broecker and van Donk, 1970). Subsequently, $\delta^{18}O$ records tuned to astronomical forcing led to a revision of some of the chron boundaries in the geomagnetic polarity timescale (GPTS; e.g., Shackleton et al., 1990; An alternative astronomical calibration of the Lower Pleistocene time scale based on ODP site 677). Obviously, polarity changes combined with $\delta^{18}O$ records cannot provide the sub-millennial-scale certainties now required in Late Pleistocene studies.

Relative paleointensity (RPI) of the Earth's magnetic field is recorded in marine sediments and may reduce the errors and uncertainties described above associated with using $\delta^{18}O$ records alone for global correlation. The theory of using relative paleo-intensity measurements for correlation is based on the observations that the Earth's magnetic field varies in strength, that is, it is not static. In essence, these magnetic intensity variations provide the potential for much finer scale correlation than afforded by the GPTS. For the stratigrapher, it is not essential to understand why the intensity varied, but only that these variations occurred, were global, and can be measured in cores. Global stacked paleointensity templates have been generated for the last 8 Myr (Guyodo and Valet, 1999) and 200 Myrs (Valet et al., 2005). Regionally stacked records for the North Atlantic (Laj et al., 2000), the South Atlantic (Stoner et al., 2002), and the global ocean (Laj et al., 2004) have been developed as well.

The Late Pleistocene North Atlantic and South Atlantic Paleo-intensity stacks (Laj et al., 2000; Stoner et al., 2002) relied on $\delta^{18}O$ records for correlation. One of the aspects for Integrated Ocean Drilling Program (IODP) Expeditions 303 and 306 was to recover long-Plio-Pleistocene sections with high sedimentation rates. The site survey for Expeditions 303/306 recovered a series of Giant Gravity and Jumbo Piston cores from Eirik Drift (see Chapter 2) for which I developed the $\delta^{18}O$ and $CaCO_3$ stratigraphies. These records formed the backbone for the first RPI records published from cores collected on the Eirik Drift (Evans et al., 2007). The integration of the $\delta^{18}O$ and RPI records is described in Evans et al. (2007).

4.3 Review of Evans et al., 2007

The published study by Evans et al. (2007) titled "Paleointensity-assisted chronostratigraphy of detrital layers on the Eirik Drift (North Atlantic) since marine isotope stage 11" was initiated as a joint project between Rutgers University and the University of Florida. Four 20 to 24 m long jumbo piston cores were analyzed for percent carbonate ($CaCO_3$), $\delta^{18}O$ stratigraphy, relative paleointensity proxies, and magnetic susceptibility (i.e. volume susceptibility) to characterize the detrital layers on Eirik Drift and correlate them to other North Atlantic sites. Significant portions of the data cited in this publication were produced for this dissertation (i.e. downcore $\delta^{18}O$ and percent carbonate records for 3 of the 4 cores). Approximately 3000 data points (Appendix 3) for $\delta^{18}O$ and percent carbonate for cores 15JPC, 18JPC and 19JPC were contributed to Evans et al. (2007). The following is a synopsis of the methods and the major results and conclusions of Evans et al. (2007) as well as an overview of my contribution to the study.

One of the key observations in the interpretation of abrupt climate change is the recognition of detrital sediment layers in North Atlantic sediment cores (e.g., Bond et al., 1992; Broecker et al., 1992; Heinrich, 1988; Ruddiman, 1977). A detrital layer is defined as a rapidly deposited centimeter-scale layer composed of coarse-grained material and little to no biogenic input. These layers can be derived from multiple modes of deposition in addition to ice rafting events (Evans et al., 2007). Six Heinrich layers (H1 to H6; Bond et al., 1992) were originally identified by their high lithic to foraminiferal percentage and increased abundance in the cold water planktonic foraminiferal species, *Neogloboquadrina pachyderma, sinistral* (Heinrich, 1988). In the North Atlantic, four of these layers (H1, H2, H4 and H5) contain high amounts of detrital carbonate (Bond et al., 1992; Broecker et al., 1992), sourced from the Paleozoic carbonate rocks below the Laurentide Ice Sheet via the Hudson Strait (MacAyeal, 1993). H3 and H6 are characterized by a lower flux of lithic grains and the detrital input is thought to be sourced from European sources (Hemming, 2004).

Previous studies have utilized radiocarbon ages, $\delta^{18}O$ stacks, and correlation to Greenland Ice Core stratigraphies to construct age chronologies of the detrital events (i.e., Bond et al., 1999). Determining the sources of these layers and correlating them across the North Atlantic is very important in unraveling the forcings on the climate system. Due to the increasing number of identified layers and locations where they have been found, the precise correlation of these events from site-to-site is beyond the limits of traditional chronostratigraphic correlation techniques. Therefore, combining an independent proxy for age control with traditional chronostratigraphic methods would greatly enhance our ability to correlate these fine scale events between sites.

Evans et al. (2007) documented the detrital layer stratigraphy from 4 Eirik Drift cores by combining oxygen isotope data and RPI proxies to assist in correlation to other regional deep-sea detrital records. Due to the highly variable geomagnetic field intensity (variations of ~5% per century for the last few centuries), RPI has the potential for high-resolution millennial scale correlation (Evans et al., 2007).

4.3.1 Material and Methods

Four jumbo piston cores from the Eirik Drift, collected in 1999 onboard the *Marion Dufresne* and in 2002 onboard the *R/V KNORR,* were selected and analyzed for this study (Table 4.1, Figure 4.3). The Eirik Drift provides an ideal location to conduct paleoceanographic investigations because it lays directly in the path of the Western Boundary Undercurrent (WBUC), and results in high sedimentation rates (5 to ≥ 100 cm/kyr) as the deep current slows around the tip of the drift and turns west into the Labrador Sea (Hunter et al., 2007; Stanford et al., 2011). Furthermore, the morphology of Eirik Drift is such that it allows the deep current to shift up and down the drift crest as the buoyancy state of the deep current changes (Channell et al., 2014; Evans et al., 2007; Hillaire-Marcel et al., 1994; Stoner et al., 1995; Stoner et al., 1996). Sedimentation has been more or less continuous during the Late Pliocene and Pleistocene, but sedimentation rates have varied significantly depending on the climatic conditions and position on the drift (Hillaire-Marcel et al., 1994).

Magnetic susceptibility and velocity measurements were taken on cores 15JPC, 18JPC, and 19JPC onboard the R/V KNORR before they were brought to the core repository at Rutgers University where they were split, photographed, sampled, and stored at 5 °C in a refrigerated container. Approximately 6 to 10 cm^3 samples were taken every 5 cm for the entire length of all three cores. One half of the raw sample was weighed, placed into a 50 ml centrifuge vial, and reacted with ~ 40 ml of 1.0 N acetic acid for approximately 24 hours to remove all carbonate from the sample. Each sample was shaken once during this time to ensure a complete reaction. The vials were then centrifuged for approximately 1 minute and the acid was decanted. This process was repeated once more before washing the samples with approximately 40 ml of deionized water (DIW). The sediments were allowed to settle, and the vials were placed back in the centrifuge for 1 minute before the DIW was decanted. This process was repeated two more times, and the vials were then dried overnight at 50 °C and reweighed. Once the final weight was determined, the following equation was used to determine the weight percent of carbonate (Wt. % CaCO3).

Wt. % CaCO3 = (1- (Wt. minus CaCO3/ Dry wt. initial.)) *100

where the Wt. minus CaCO3 and Dry wt. initial refer to the weights before and after adding acetic acid to the sample. The standard error was not calculated; however, errors in the data may exist if the samples were not completely dried before they were weighed, or if some sample was lost during the decanting process.

The other half of the sample was washed through a 63 µm sieve, dried, weighed and processed for percent coarse fraction (not shown in this study). Approximately 10 to 15 *Neogloboquadrina pachyderma,* sinistral tests were handpicked under a binocular microscope from the > 212 μm size fraction, and selected for stable isotope analysis. All samples were analyzed in the Stable Isotope Laboratory at Rutgers University using the Micromass Optima Mass Spectrometer. Samples were loaded into a multi-prep device and reacted with 100 % phosphoric acid at 90 °C for 15 minutes. All measured values are reported relative to V-PDB (Vienna PeeDee Belemnite) using an internal lab standard. This standard is routinely checked against NBS-19, which has values of 1.95 ‰ and -2.20 ‰ for $\delta^{13}C$ and $\delta^{18}O$, respectively (Coplen et al., 1983). The offsets between the lab standard and NBS-19 are 0.04 ‰ for $\delta^{18}O$ and 0.10 ‰ for $\delta^{13}C$. Typical lab precision for 1-σ of the standards reported versus V-PDB is 0.05 ‰ for $\delta^{13}C$ and 0.08 ‰ for $\delta^{18}O$.

Continuous U-channel samples (2 x 2 cm cross-section and 150 cm in length) were taken down the center of the split cores for RPI analysis. Samples were processed at the University of Florida on a 2G-Enterprises narrow-access pass-through cryogenic magnetometer. For a full review of the methods used for this portion of the study, please refer to the methods section of Evans et al. (2007).

4.3.2 Results and Discussion

The natural remanent magnetization (NRM), anhysteretic remanent magnetization (ARM), isothermal remanent magnetization (IRM), and volume susceptibility for cores 15JPC, 18JPC, and were combined with the individual $\delta^{18}O$ records, the published $\delta^{18}O$ record from ODP Site 983 (Channell et al., 1997), and the stacked $\delta^{18}O$ benthic record of Lisiecki and Raymo (2005) to create the downcore age models and calculate the sedimentation rates (Figures 4.4 to 4.6; core MD99-2227 not shown). The Laschamp (~40 ka) and Iceland Basin (~245 ka) polarity excursions were observed in these cores, further adding to the age control (Table 4.2). Age depth points were used to estimate average sedimentation rates of 15 cm/ka, 9 cm/ka, and 10.5 cm/ka for cores 15JPC, 18JPC, and 19JPC, respectively.

Sedimentation patterns on Eirik Drift indicate that water depth and position on the drift influence the accumulation rates in addition to climatic conditions (Chapter 2 of this study; Hillaire-Marcel et al., 1994). The core of NCW was thought to occupy water depths between 2500 and 3000 m (Hillaire-Marcel et al., 1994), but the erosional events in core 18JPC (~450 m below this depth) imply that the deep current was active at lower depths than previously estimated.

Several centimeter-scale detrital layers were identified in Core MD99-2227 (Appendix 5), that extend the record of these events in the North Atlantic well beyond the last glacial cycle. Detrital layers are observed during both glacial and interglacial intervals, but the interglacial layers occur close to the onset of these warm events. The ages of two of the layers coincide with H2 and H4, whereas no detrital events for Heinrich events H1, H2, H5 and H6 were seen in these cores. Two types of detrital events were identified by the types of grains they deposited, detrital carbonate (DC) and low detrital carbonate (LDC). The former indicated ice rafted sediment delivery, the latter indicated mass movement from the Greenland slope. The LDC layers identified on Eirik Drift during Marine Isotope Chrons 7 and 9 appear to be coeval with layers identified at Orphan Knoll (Hiscott et al., 2001), indicating that the Laurentide Ice Sheet instabilities that triggered these events were synchronous with the events on the Greenland slope that triggered the LDC events on Eirik Drift.

4.3.3 Conclusions

The combination of paleointensity records and oxygen isotope data provide enhanced temporal resolution compared to using either data set independently (i.e. Channell, 1999; Channell et al., 2000; Channell et al., 2014; Evans et al., 2007; Laj et al., 2000). Detrital layers from four Eirik Drift cores were placed into a chronostratigraphic framework by utilizing this tandem $\delta^{18}O$ and RPI data approach and through recognition of two magnetic excursions. Characterization of the small-scale detrital layers reveals two types of carbonate layers, detrital carbonate (DC) and low detrital carbonate (LDC) that represent material derived from the Hudson Strait and turbidites from the Greenland slope, respectively.

4.4 References

Austin, W.E., Bard, E., Hunt, J.B., Kroon, D., Peacock, J.D., 1995. The 14C age of the Icelandic Vedde Ash: implications for Younger Dryas marine reservoir age corrections. Radiocarbon, 37(1): 53-62.

Bard, E., 1988. Correction of accelerator mass spectrometry 14C ages measured in planktonic foraminifera: paleoceanography implications Paleoceanography, 3(6): 635-695.

Bard, E., Arnold, M., Fairbanks, R., Hamelin, B., 1993. 230Th/234U and 14C Ages Obtained by Mass Spectrometry on Corals. Radiocarbon, 35(1): 191-199.

Bard, E., Arnold, M., Hamelin, B., Tisnerat-Laborde, N., Cabioch, G., 1998. Radiocarbon calibration by means of mass spectrometric 230Th/234U and 14C ages of corals: an updated database including samples from Barbados, Mururoa and Tahiti. Radiocarbon, 40(3): 1085-1092.

Bard, E. et al., 1994. The North Atlantic atmosphere-sea surface 14 C gradient during the Younger Dryas climatic event. Earth and Planetary Science Letters, 126(4): 275-287.

Bard, E., Hamelin, B., Fairbanks, R.G., Zindler, A., 1990. Calibration of 14C over the last 30,000 years using U/Th ages obtained by mass spectrometry on Barbados corals. Nature, 345: 405-410.

Bassinot, F.C. et al., 1994. The astronomical theory of climate and the age of the Brunhes-Matuyama magnetic reversal. Earth and Planetary Science Letters, 126(1): 91-108.

Beck, J.W. et al., 2001. Extremely large variations of atmospheric 14C concentration during the last glacial period. Science, 292(5526): 2453-2458.

Bond, G. et al., 1992. Evidence for massive discharges of icebergs into the North Atlantic ocean during the last glacial period.

Bond, G.C. et al., 1999. The North Atlantic's 1‐2 Kyr Climate Rhythm: Relation to Heinrich Events, Dansgaard/Oeschger Cycles and the Little Ice Age. Mechanisms of global climate change at millennial time scales: 35-58.

Bondevik, S., Birks, H.H., Gulliksen, S., Mangerud, J., 1999. Late Weichselian marine 14 C reservoir ages at the western coast of Norway. Quaternary Research, 52(1): 104-114.

Bondevik, S., Mangerud, J., Birks, H.H., Gulliksen, S., Reimer, P., 2006. Changes in North Atlantic radiocarbon reservoir ages during the Allerød and Younger Dryas. Science, 312(5779): 1514-1517.

Bondevik, S., Mangerud, J., Gulliksen, S., 2001. The marine 14C age of the Vedde Ash Bed along the west coast of Norway. Journal of Quaternary Science, 16(1): 3-8.

Boyle, E.A., Keigwin, L., 1987. North Atlantic thermohaline circulation during the past 20,000 years linked to high-latitude surface temperature. Nature, 330: 5.

Broecker, W., Bond, G., Klas, M., Clark, E., McManus, J., 1992. Origin of the northern Atlantic's Heinrich events. Climate Dynamics, 6(3-4): 265-273.

Broecker, W., Peng, T.-H., Ostlund, G., Stuiver, M., 1985. The Distribution of bomb radiocarbon in the ocean. Journal of geophysical Research-Oceans, 90: 6953-6970.

Broecker, W.S., 1979. A revised estimate for the radiocarbon age of North Atlantic Deep Water. Journal of Geophysical Research: Oceans (1978–2012), 84(C6): 3218-3226.

Broecker, W.S., Peng, T.-H., Trumbore, S., Bonani, G., Wolfli, W., 1990. The distribution of radiocarbon in the glacial ocean. Global Biogeochemical Cycles, 4(1).

Broecker, W.S., van Donk, J., 1970. Insolation changes, ice volumes, and the O18 record in deep‐sea cores. Reviews of Geophysics, 8(1): 169-198.

Burr, G. et al., 1998. A high-resolution radiocarbon calibration between 11,700 and 12,400 calendar years BP derived from 230 Th ages of corals from Espiritu Santo Island, Vanuatu. Radiocarbon, 40(3): 1093-1105.

Butzin, M., Prange, M., Lohmann, G., 2005. Radiocarbon simulations for the glacial ocean: the effects of wind stress, Southern Ocean sea ice and Heinrich events. Earth and Planetary Science Letters, 235(1): 45-61.

Butzin, M., Prange, M., Lohmann, G., 2012. Readjustment of glacial radiocarbon chronologies by self-consistent three-dimensional ocean circulation modeling. Earth and Planetary Science Letters, 317: 177-184.

Cao, L., Fairbanks, R.G., Mortlock, R.A., Risk, M.J., 2007. Radiocarbon reservoir age of high latitude North Atlantic surface water during the last deglacial. Quaternary Science Reviews, 26(5): 732-742.

Channell, J., 1999. Geomagnetic paleointensity and directional secular variation at Ocean Drilling Program (ODP) Site 984 (Bjorn Drift) since 500 ka: comparisons with ODP Site 983 (Gardar Drift). Journal of Geophysical Research: Solid Earth (1978–2012), 104(B10): 22937-22951.

Channell, J., Hodell, D., Lehman, B., 1997. Relative geomagnetic paleointensity and δ 18 O at ODP Site 983 (Gardar Drift, North Atlantic) since 350 ka. Earth and Planetary Science Letters, 153(1): 103-118.

Channell, J., Stoner, J., Hodell, D., Charles, C., 2000. Geomagnetic paleointensity for the last 100 kyr from the sub-antarctic South Atlantic: a tool for inter-hemispheric correlation. Earth and Planetary Science Letters, 175(1): 145-160.

Channell, J., Wright, J., Mazaud, A., Stoner, J., 2014. Age through tandem correlation of Quaternary relative paleointensity (RPI) and oxygen isotope data at IODP Site U1306 (Eirik Drift, SW Greenland). Quaternary Science Reviews, 88: 135-146.

Channell, J., Xuan, C., Hodell, D., 2009. Stacking paleointensity and oxygen isotope data for the last 1.5 Myr (PISO-1500). Earth and Planetary Science Letters, 283(1): 14-23.

Coplen, T.B., Kendall, C., Hopple, J., 1983. Comparison of stable isotope reference samples.

Craig, H., Gordon, L.I., 1965. Deuterium and oxygen 18 variations in the ocean and the marine atmosphere.

Cutler, K. et al., 2004. Radiocarbon calibration and comparison to 50 kyr BP with paired 14C and 230Th dating of corals from Vanuatu and Papua New Guinea. Radiocarbon, 46(3): 1127-1160.

Damon, P.E., 1988. Production and decay of radiocarbon and its modulation by geomagnetic field-solar activity changes with possible implications for global environment, Secular Solar and Geomagnetic Variations in the Last 10,000 Years. Springer, pp. 267-285.

Edwards, R.L. et al., 1993. A Large Drop in Atmospheric 14C/12C and Reduced Melting in the Younger Dryas, Documented with 230Th Ages of Corals. SCIENCE-NEW YORK THEN WASHINGTON-, 260: 962-962.

Elliot, M., Labeyrie, L., Duplessy, J.-C., 2002. Changes in North Atlantic deep-water formation associated with the Dansgaard–Oeschger temperature oscillations (60–10ka). Quaternary Science Reviews, 21(10): 1153-1165.

Evans, H.F. et al., 2007. Paleointensity‐assisted chronostratigraphy of detrital layers on the Eirik Drift (North Atlantic) since marine isotope stage 11. Geochemistry, Geophysics, Geosystems, 8(11).

Fairbanks, R.G., 1990. The age and origin of the “Younger Dryas climate event” in Greenland ice cores. Paleoceanography, 5(6): 937-948.

Fairbanks, R.G. et al., 2005. Radiocarbon calibration curve spanning 0 to 50,000 years BP based on paired 230 Th/234 U/238 U and 14 C dates on pristine corals. Quaternary Science Reviews, 24(16): 1781-1796.

Goslar, T. et al., 2000a. Radiocarbon Calibration by Means of Varves Versus 14C Ages of Terrestrial Macrofossils from Lake Gosciaz and Lake Perespilno, Poland. Radiocarbon, 42(3): 335-348.

Goslar, T., Hercman, H., Pazdur, A., 2000b. Comparison of U-series and radiocarbon dates of speleothems. Radiocarbon, 42(3): 403-414.

Grootes, P., Stuiver, M., White, J., Johnsen, S., Jouzel, J., 1993. Comparison of oxygen isotope records from the GISP2 and GRIP Greenland ice cores.

Guyodo, Y., Valet, J.-P., 1999. Global changes in intensity of the Earth's magnetic field during the past 800 kyr. Nature, 399(6733): 249-252.

Hays, J.D., Imbrie, J., Shackleton, N.J., 1976. Variations in the Earth's orbit: pacemaker of the ice ages. American Association for the Advancement of Science.

Heinrich, H., 1988. Origin and consequences of cyclic ice rafting in the northeast Atlantic Ocean during the past 130,000 years. Quaternary research, 29(2): 142-152.

Hemming, S.R., 2004. Heinrich events: Massive late Pleistocene detritus layers of the North Atlantic and their global climate imprint. Reviews of Geophysics, 42(1).

Hillaire-Marcel, C., de Vernal, A., 2008. Stable isotope clue to episodic sea ice formation in the glacial North Atlantic. Earth and Planetary Science Letters, 268(1): 143-150.

Hillaire-Marcel, C., Vernal, A.d., Bilodeau, G., Wu, G., 1994. Isotope stratigraphy, sedimentation rates, deep circulation, and carbonate events in the Labrador Sea during the last~ 200 ka. Canadian Journal of Earth Sciences, 31(1): 63-89.

Hiscott, R.N., Aksu, A.E., Mudie, P.J., Parsons, D.F., 2001. A 340,000 year record of ice rafting, palaeoclimatic fluctuations, and shelf-crossing glacial advances in the southwestern Labrador Sea. Global and Planetary Change, 28(1): 227-240.

Hughen, B.K., McCormac, G., van der Plicht, J., Spurk, M., 1998. INTCAL98 radiocarbon age calibration, 24,000-0 cal BP. Radiocarbon, 40(3): 1041-1083.

Hughen, K. et al., 2004a. 14C activity and global carbon cycle changes over the past 50,000 years. Science, 303(5655): 202-207.

Hughen, K.A. et al., 2004b. Marine04 marine radiocarbon age calibration, 0-26 cal kyr BP.

Hughen, K.A., Southon, J.R., Lehman, S.J., Overpeck, J.T., 2000. Synchronous radiocarbon and climate shifts during the last deglaciation. Science, 290(5498): 1951-1954.

Hunter, S. et al., 2007. Deep western boundary current dynamics and associated sedimentation on the Eirik Drift, Southern Greenland Margin. Deep Sea Research Part I: Oceanographic Research Papers, 54(12): 2036-2066.

Imbrie, J. et al., 1984. The orbital theory of Pleistocene climate: Support from a revised chronology of the marine delta18 O record, Milankovitch and climate: Understanding the response to astronomical forcing, pp. 269.

Karner, D.B., Levine, J., Medeiros, B.P., Muller, R.A., 2002. Constructing a stacked benthic δ18O record. Paleoceanography, 17(3): 2-1-2-16.

Kitagawa, H., van der Plicht, J., 2000. Atmospheric radiocarbon calibration beyond 11, 900 cal BP from Lake Suigetsu laminated sediments. Radiocarbon, 42(3): 369-380.

Laj, C., Kissel, C., Beer, J., 2004. High Resolution Global Paleointensity Stack Since 75 kyr (GLOPIS-75) Calibrated to Absolute Values. Timescales of the Paleomagnetic Field: 255-265.

Laj, C., Kissel, C., Mazaud, A., Channell, J., Beer, J., 2000. High resolution paleointensity stack from the North Atlantic for the 75-10 kyr interval (NAPIS-75) and the duration of the Laschamp event. Phil. Trans. R. Soc. London A, 358: 1009-1025.

Lazier, J., Hendry, R., Clarke, A., Yashayaev, I., Rhines, P., 2002. Convection and restratification in the Labrador Sea, 1990–2000. Deep Sea Research Part I: Oceanographic Research Papers, 49(10): 1819-1835.

Lisiecki, L.E., Raymo, M.E., 2005. A Pliocene-Pleistocene stack of 57 globally distributed benthic δ18O records. Paleoceanography, 20(1).

Lisiecki, L.E., Raymo, M.E., 2009. Diachronous benthic δ18O responses during late Pleistocene terminations. Paleoceanography, 24(3).

MacAyeal, D., 1993. Binge/purge oscillations of the Laurentide ice sheet as a cause of the North Atlantic's Heinrich events. Paleoceanography, 8(6): 775-784.

Mangerud, J., 1972. Radiocarbon dating of marine shells, including a discussion of apparent age of recent shells from Norway. Boreas, 1(2): 143-172.

Martinson, D.G. et al., 1987. Age dating and the orbital theory of the ice ages: development of a high-resolution 0 to 300,000-year chronostratigraphy. Quaternary research, 27(1): 1-29.

McManus, J., Francois, R., Gherardi, J.-M., Keigwin, L., Brown-Leger, S., 2004. Collapse and rapid resumption of Atlantic meridional circulation linked to deglacial climate changes. Nature, 428(6985): 834-837.

Milankovitch, M., 1941. History of radiation on the Earth and its use for the problem of the ice ages. K. Serb. Akad. Beogr.

Paterne, M. et al., 2004. Paired 14C and 230Th/U Dating of Surface Corals from the Marquesas and Vanuatu (Sub-Equatorial Pacific) in the 3000 to 15,000 cal yr Interval. Radiocarbon, 46(2): 551-566.

Pisias, N. et al., 1984. High resolution stratigraphic correlation of benthic oxygen isotopic records spanning the last 300,000 years. Marine Geology, 56(1): 119-136.

Prell, W.L. et al., 1986. Graphic correlation of oxygen isotope stratigraphy application to the late Quaternary. Paleoceanography, 1(2): 137-162.

Raymo, M., Ruddiman, W., Backman, J., Clement, B., Martinson, D., 1989. Late Pliocene variation in Northern Hemisphere ice sheets and North Atlantic deep water circulation. Paleoceanography, 4(4): 413-446.

Raymo, M., Ruddiman, W., Shackleton, N., Oppo, D., 1990. Evolution of Atlantic-Pacific δ 13 C gradients over the last 2.5 my. Earth and Planetary Science Letters, 97(3): 353-368.

Reimer, P.J. et al., 2004. IntCal04 terrestrial radiocarbon age calibration, 0-26 cal kyr BP.

Reimer, P.J. et al., 2002. Preliminary report of the first workshop of the IntCal04 radiocarbon calibration/comparison working group. Radiocarbon, 44(3): 653-662.

Ruddiman, W.F., 1977. Late Quaternary deposition of ice-rafted sand in the subpolar North Atlantic (lat 40 to 65 N). Geological Society of America Bulletin, 88(12): 1813-1827.

Schmittner, A., 2003. Southern Ocean sea ice and radiocarbon ages of glacial bottom waters. Earth and Planetary Science Letters, 213(1): 53-62.

Schramm, A., Stein, M., Goldstein, S.L., 2000. Calibration of the 14 C time scale to> 40 ka by 234 U–230 Th dating of Lake Lisan sediments (last glacial Dead Sea). Earth and Planetary Science Letters, 175(1): 27-40.

Shackleton, N., Berger, A., Peltier, W., 1990. An alternative astronomical calibration of the lower Pleistocene timescale based on ODP Site 677. Transactions of the Royal Society of Edinburgh: Earth Sciences, 81(04): 251-261.

Shackleton, N., Hall, M.A., Pate, D., 1995. Pliocene stable isotope stratigraphy of Site 846, Proc. ODP, Sci. Results. College Station, TX (Ocean Drilling Program), pp. 337-355.

Shackleton, N.J., 1977. Oxygen isotope and palaeomagnetic evidence for early Northern Hemisphere glaciation. Nature, 270: 216-219.

Shackleton, N.J., Opdyke, N.D., 1973. Oxygen isotope and palaeomagnetic stratigraphy of Equatorial Pacific core V28-238: oxygen isotope temperatures and ice volumes on a 10 5 year and 10 6 year scale. Quaternary research, 3(1): 39-55.

Siani, G. et al., 2001. Mediterranean Sea surface radiocarbon reservoir age changes since the last glacial maximum. Science, 294(5548): 1917-1920.

Skinner, L., Shackleton, N., 2005. An Atlantic lead over Pacific deep-water change across Termination I: implications for the application of the marine isotope stage stratigraphy. Quaternary Science Reviews, 24(5): 571-580.

Stanford, J., Rohling, E., Bacon, S., Holliday, N., 2011. A review of the deep and surface currents around Eirik Drift, south of Greenland: Comparison of the past with the present. Global and Planetary Change, 79(3): 244-254.

Stocker, T., Wright, D.G., 1996. Rapid changes in ocean circulation and atmospheric radiocarbon. Paleoceanography, 11(6): 773-795.

Stoner, J., Channell, J., Hillaire-Marcel, C., 1995. Late Pleistocene relative geomagnetic paleointensity from the deep Labrador Sea: Regional and global correlations. Earth and Planetary Science Letters, 134(3): 237-252.

Stoner, J., Laj, C., Channell, J., Kissel, C., 2002. South Atlantic and North Atlantic geomagnetic paleointensity stacks (0–80ka): implications for inter-hemispheric correlation. Quaternary Science Reviews, 21(10): 1141-1151.

Stoner, J.S., Channell, J.E., Hillaire-Marcel, C., 1996. The magnetic signature of rapidly deposited detritai layers from the deep Labrador Sea: Relationship to North Atlantic Heinrich layers. Paleoceanography, 11(3): 309-325.

Stuiver, M., Braziunas, T.F., 1993. Modeling Atmospheric 14C Influences and 14C Ages of Marine Samples to 10,000 BC. Radiocarbon, 35: 137-137.

Stuiver, M., Braziunas, T.F., Becker, B., Kromer, B., 1991. Climatic, solar, oceanic, and geomagnetic influences on late-glacial and holocene atmospheric 14C/12C change. Quaternary research, 35(1): 1-24.

Stuiver, M., Kromer, B., Becker, B., Ferguson, C., 1986. Radiocarbon age calibration back to 13,300 years BP and the 14C age matching of the German oak and US bristlecone pine chronologies. Radiocarbon, 28(2B): 969-979.

Stuiver, M. et al., 1998. INTCAL98 radiocarbon age calibration. 24,000-0 cal BP. Radiocarbon, 40(3): l04l-83.

Stuvier, M., 1982. A high-precision calibration of the AD radiocarbon time scale. Radiocarbon, 24: 1-26.

Thornalley, D.J., Barker, S., Broecker, W.S., Elderfield, H., McCave, I.N., 2011. The deglacial evolution of North Atlantic deep convection. science, 331(6014): 202-205.

Turon, J., Hillaire-Marcel, C., Participants, S., 1999. IMAGES V mission of the Marion Dufresne, Leg 2, 30 June to 24 July 1999. Geol. Surv. Canada.

Valet, J.-P., Meynadier, L., Guyodo, Y., 2005. Geomagnetic dipole strength and reversal rate over the past two million years. Nature, 435(7043): 802-805.

van der Plicht, J. et al., 2004. NotCal04; comparison/calibration 14C records 26-50 cal kyr BP.

Voelker, A.H., Grootes, P.M., Nadeau, M.-J., Sarnthein, M., 2000. Radiocarbon levels in the Iceland Sea from 25-53 kyr and their link to the Earth's magnetic field intensity. Radiocarbon, 42(3): 437-452.

Vogel, J.C., Kronfeld, J., 1997. Calibration of radiocarbon dates for the Late Pleistocene using U/Tho dates on stalagmites SCI: JS, 39(1): 27-32.

Yokoyama, Y., Esat, T., 2004. Long term variations of uranium isotopes and radiocarbon in the surface seawater recorded in corals. Global environmental change in the ocean and on land, 1: 279-309.

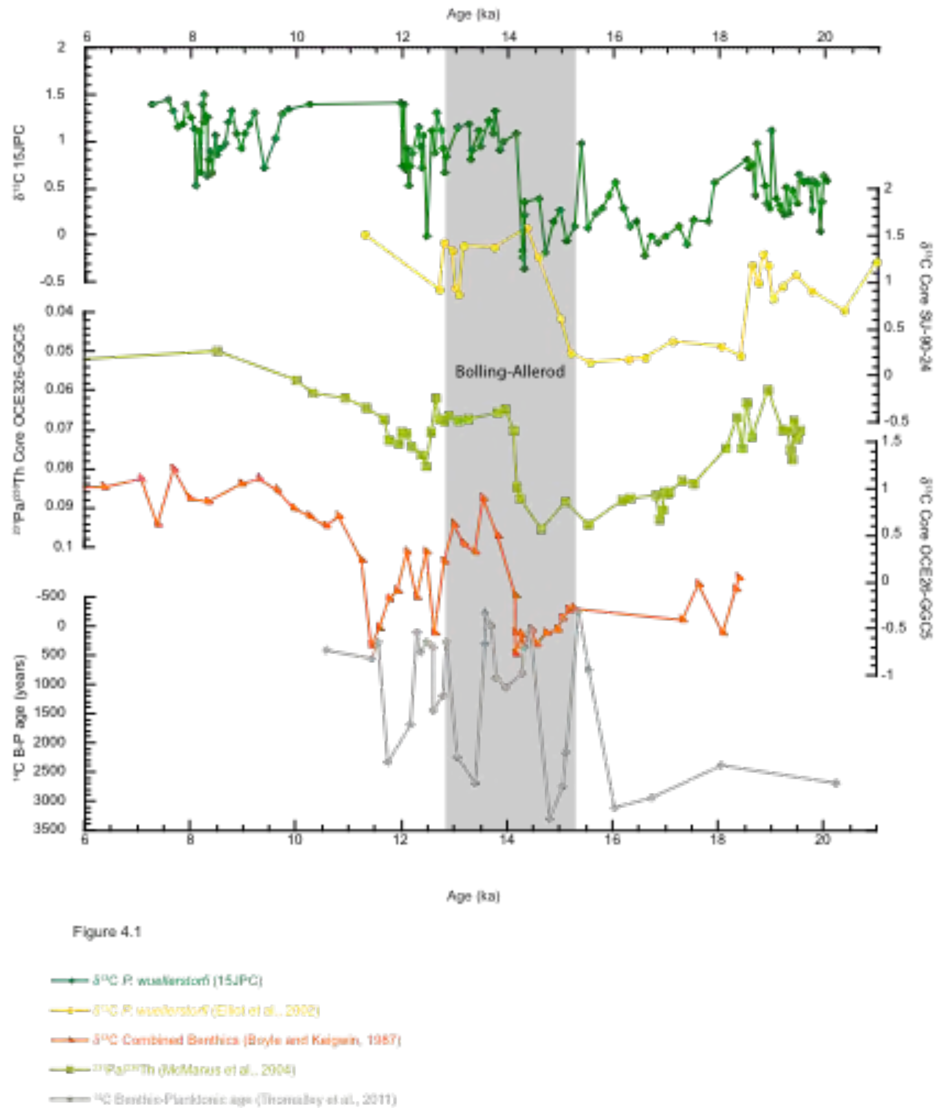

Figure 4.1: Bottom water proxies from several North and subtropical Atlantic cores showing the differences in timing of the initiation of the Bolling-Allerod warm interval (gray box). The $^{231}Pa/^{230}Th$ values of core OCE26-GGC5 (green squares; McManus et al., 2004), ^{14}C ventilation ages (gray diamonds; Thornalley et al., 2011), and $\delta^{13}C$ values of cores 15JPC (green diamonds; this study), SU-90-24 (gold circles; Elliot et al., 2002), and OCE26-GGC5 (orange triangles; Boyle and Keigwin, 1987) are displayed versus age (ka).

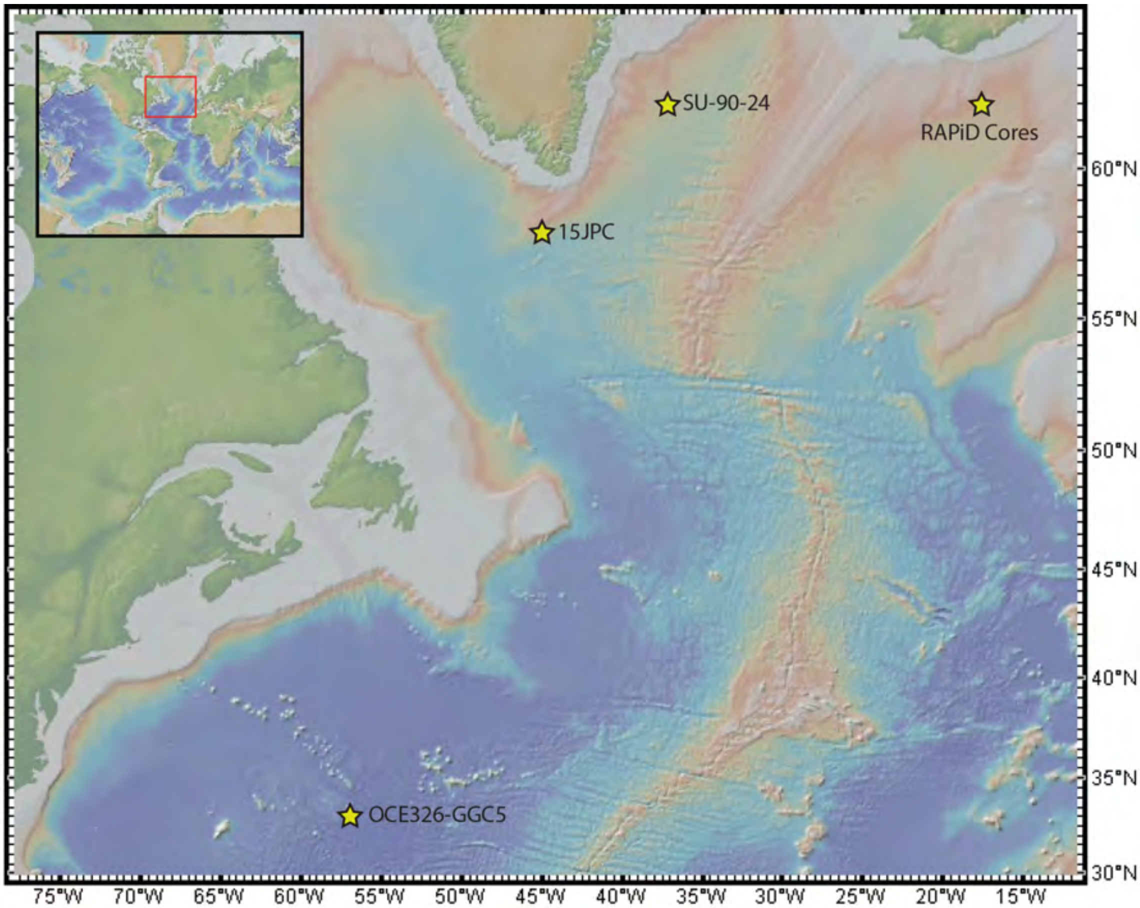

Figure 4.2

Figure 4.2: Base map showing the core locations of the deep-water proxy record shown in Figure 4.1.

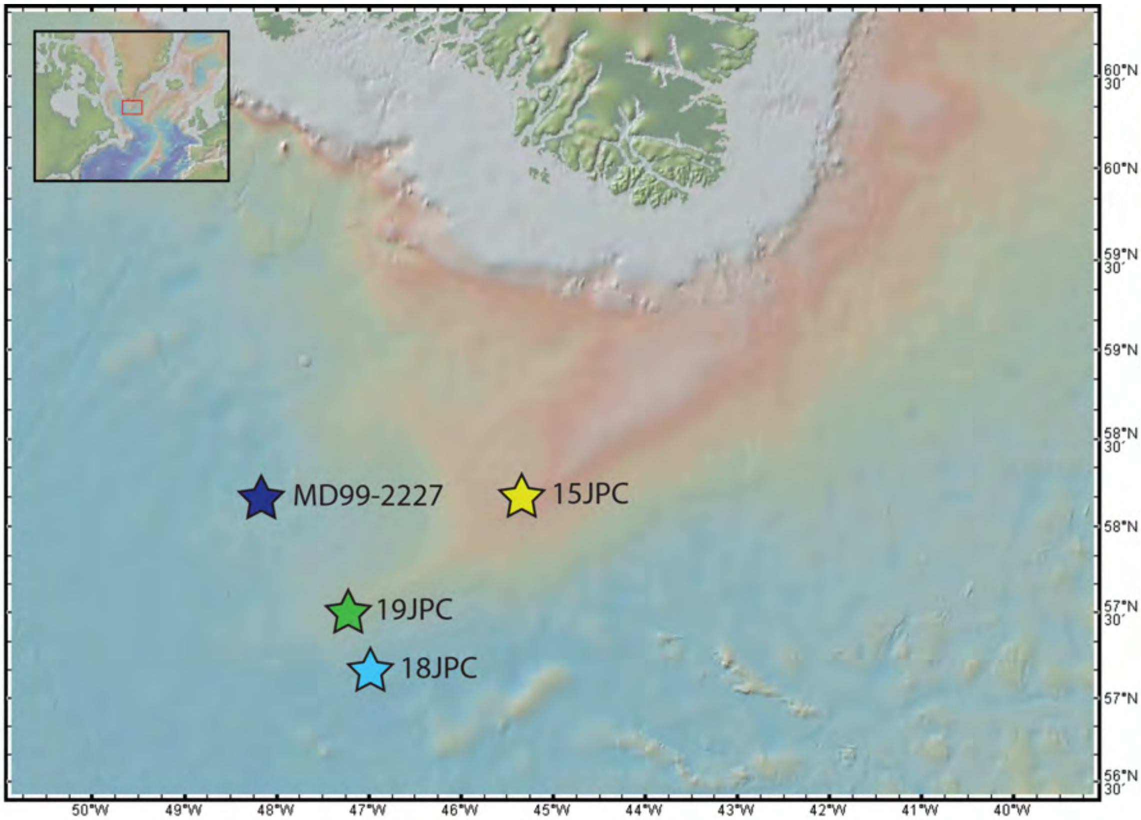

Figure 4.3

Figure 4.3: Location map showing the location of the four piston cores analyzed in Evans et al., 2007.

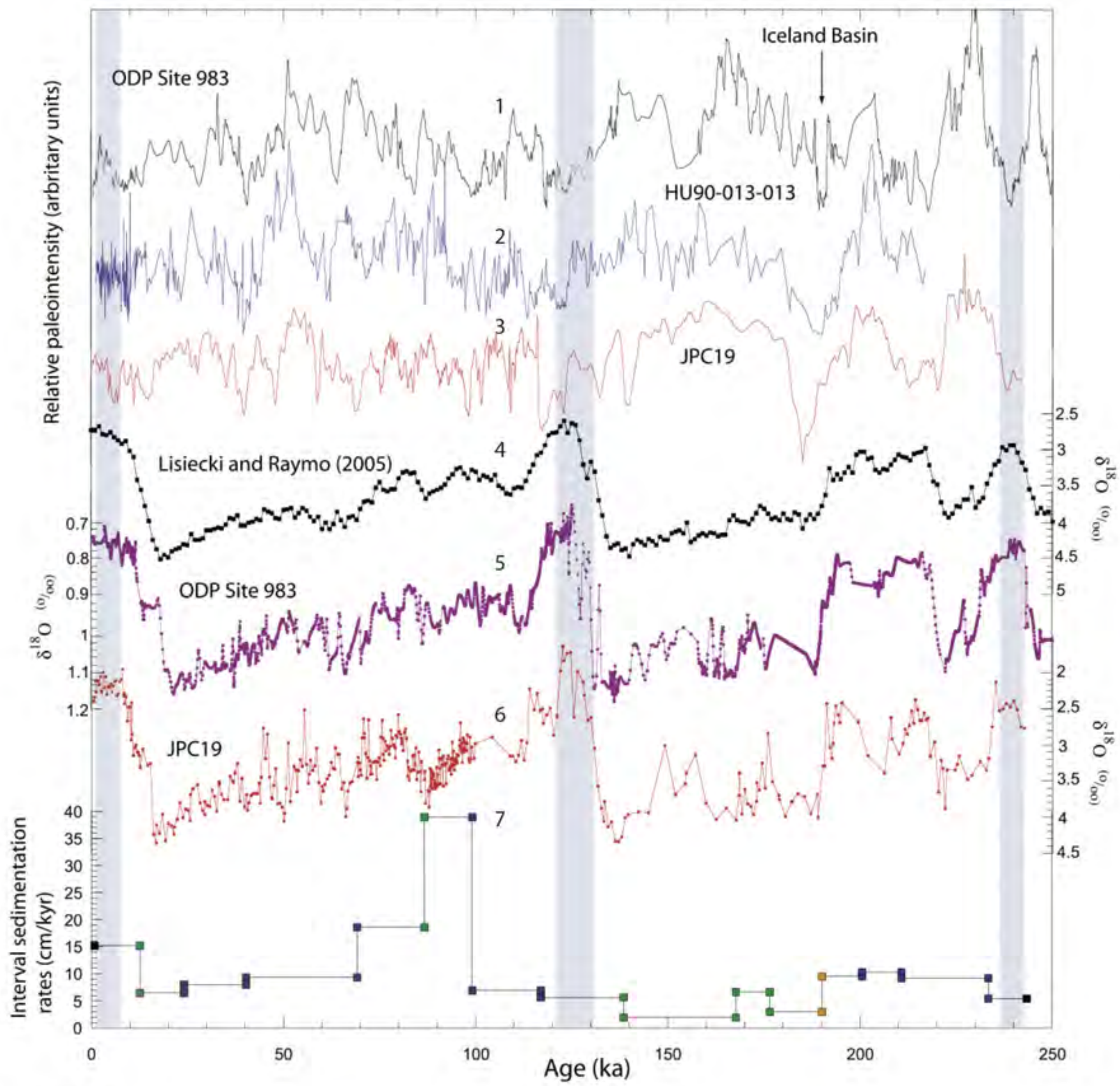

Figure 4.4

Figure 4.4: Original figure published in Evans et al., 2007. Relative paleointensity record (RPI; 3) and $\delta^{18}O$ (6) from 19JPC correlated to the records from ODP Site 983 (1; Channell et al., 1997), Core HU90-013-013 (2; Stoner et al., 1995), the stacked benthic $\delta^{18}O$ record (4) of Lisiecki and Raymo (2005) and sedimentation rates (7).

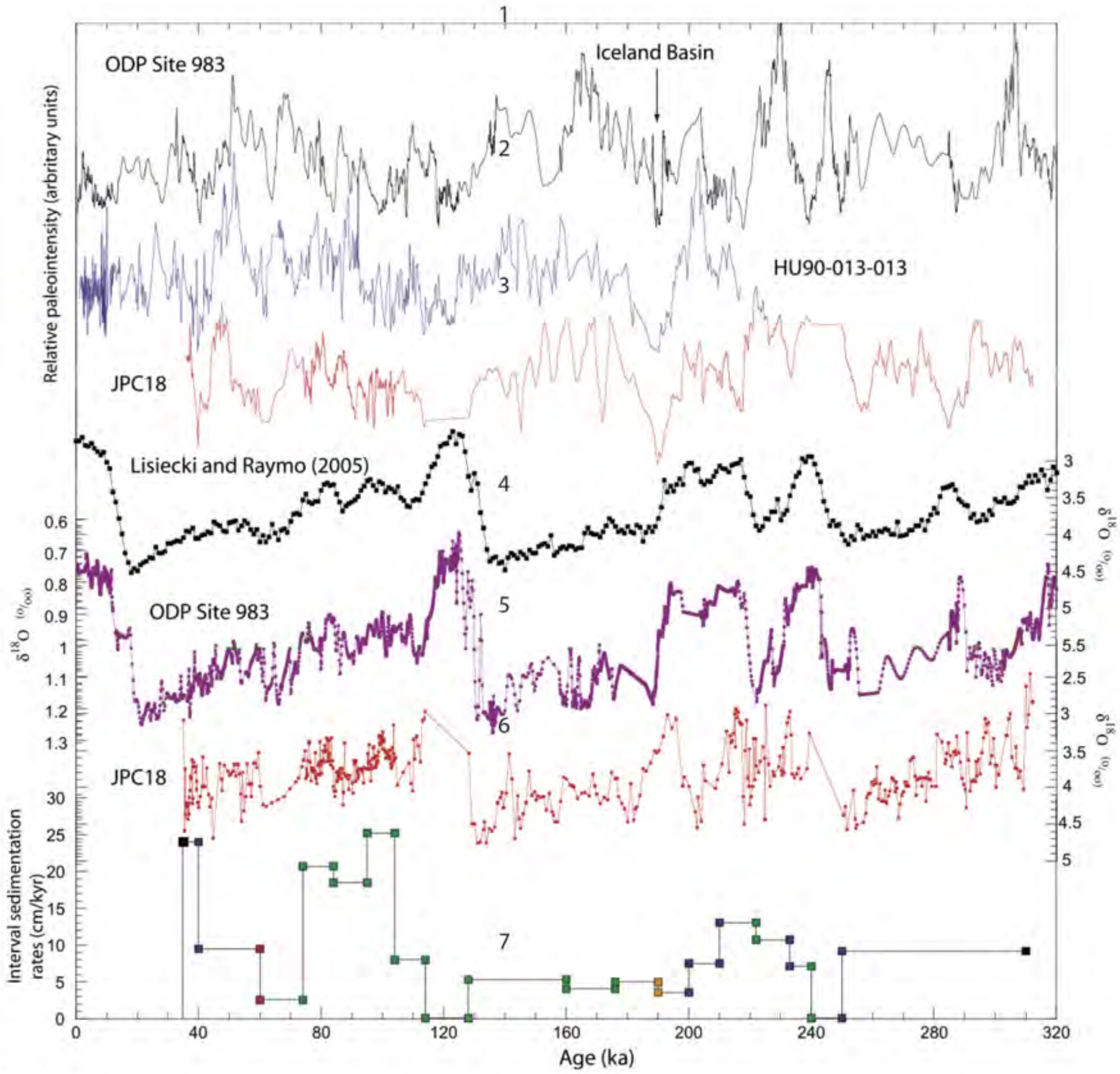

Figure 4.5

Figure 4.5: Original figure published in Evans et al., 2007. Relative paleointensity record (RPI; 3) and δ^{18}O (6) from 18JPC correlated to the records from ODP Site 983 (1; Channell et al., 1997), Core HU90-013-013 (2; Stoner et al., 1995), the stacked benthic δ^{18}O record (4) of Lisiecki and Raymo (2005) and sedimentation rates (7).

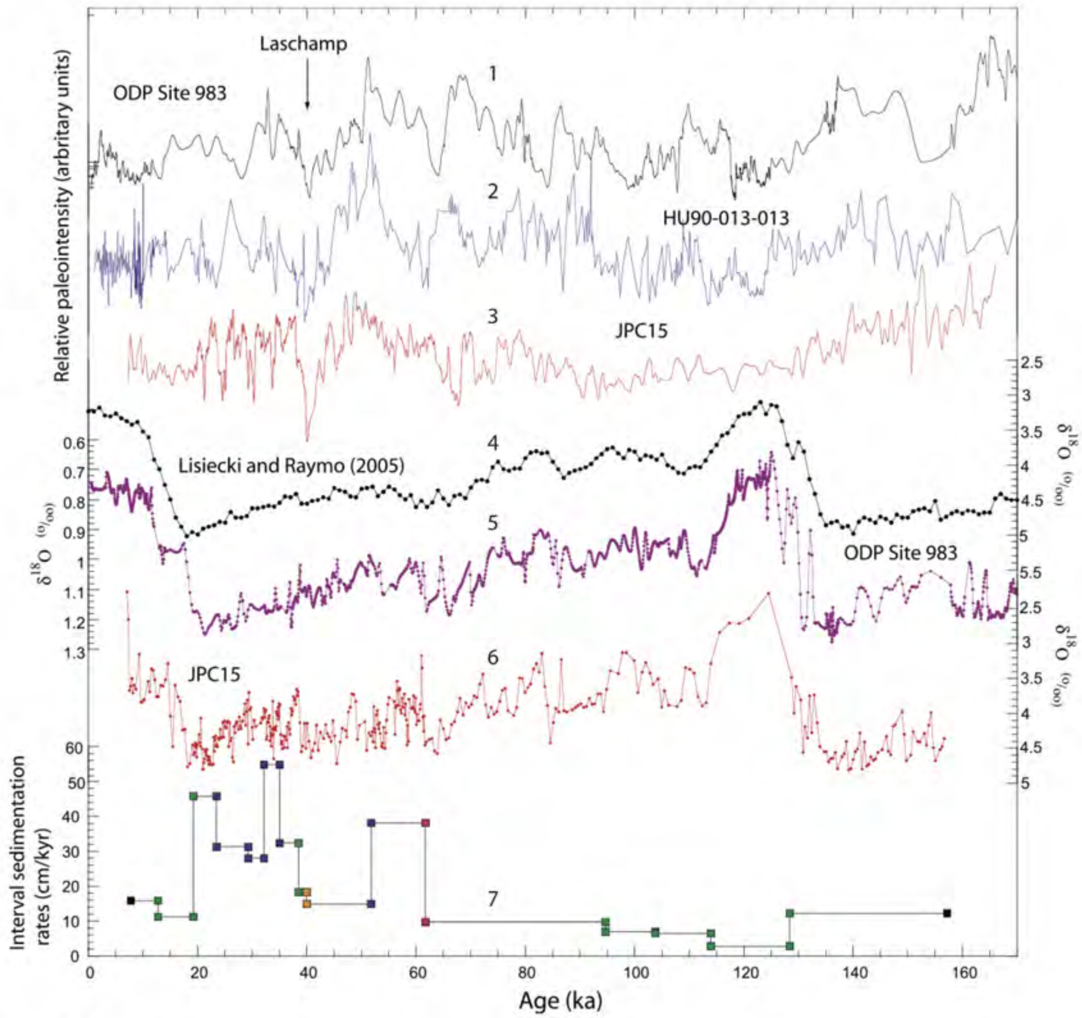

Figure 4.6

Figure 4.6: Original figure published in Evans et al., 2007. Relative paleointensity record (RPI; 3) and $\delta^{18}O$ (6) from 15JPC correlated to the records from ODP Site 983 (1; Channell et al., 1997), Core HU90-013-013 (2; Stoner et al., 1995), the stacked benthic $\delta^{18}O$ record (4) of Lisiecki and Raymo (2005) and sedimentation rates (7).

Core Name	Latitude	Longitude	Depth	Reference
KN166-14 15JPC	58° 11.82 N	45° 34.08 W	2230 m	This study, Chapter 3 Evans et al., 2007
KN166-14 18JPC	57°11.09 N	47°07.99 W	3435 m	This study, Chapter 3 Evans et al., 2007
KN166-14 19JPC	57°34.99 N	47°35.99 W	3204 m	This study, Chapter 3 Evans et al., 2007
MD99-2227	58°12 N	48°22 W	3460 m	Evans et al., 2007 Turon et al., 1999
SU-90-24	62° 04 N	37° 02 W	2085 m	Elliot et al., 2002
RAPiD-10-1P	62° 58.53 N	17° 35.37 W	1237 m	Thornalley et al., 2011 (data from all 3 cores combined)
RAPiD-12-1K	62° 05.43 N	17° 49.18 W	1938 m	
RAPiD-15-4P	62° 17.5' N	17° 08.04 W	2133 m	
OCE326-GGC5	33° 42 N	57° 35 W	4550 m	McManus et al., 2004 Boyle and Keigwin, 1987

Table 4.1: List of the latitudes, longitude and depth of the deep-sea sediment cores analyzed and used for comparison in this study.

Core Name	Core Depth	Event Name	Event Depth	Event Age
15JPC	2230 m	Laschamp Excursion	930 cm	40 ka
18JPC	3435 m	Iceland Basic Excursion	1345 cm	185 ka
19JPC	3184 m	Iceland Basic Excursion	1870 cm	185 ka

Table 4.2: List of the relative ages and depths of the Laschamp and Iceland Basin magnetic excursions identified in core 15JPC, 18JPC, and 19JPC.

5.0 Conclusions of the Dissertation

5.1 Summary of Work

In this dissertation, I used multiple paleoceanographic proxies in several sediment cores collected from the Eirik Drift in an effort to characterize and better understand the timing and mechanisms behind the various modes of deep-water circulation. I have utilized well-established geochemical (planktonic and benthic foraminiferal $\delta^{18}O$ and $\delta^{13}C$) and sedimentological (number of Ice Rafted Detrital grains per gram and percent coarse fraction) proxies and chronologic methods (radiocarbon dating, $\delta^{18}O$ stacks, and relative paleointensity data) to examine the orbital and millennial scale changes in the production of Northern Component Water (NCW). These results were compared with published results from additional North and South Atlantic proxy records to place our results within a regional context. Conventional $\delta^{18}O$ stratigraphic tools were assessed and an additional independent age control was examined to aid in future paleoceanographic correlation.

Numerous studies have extensively documented the glacial and interglacial end-member modes of circulation and the resulting changes in buoyancy states (Boyle and Keigwin, 1987; Broecker and Denton, 1990; Broecker, 1991; Broecker and Denton, 1989; Duplessy et al., 1988; Hillaire-Marcel et al., 1994; Oppo et al., 1995; Oppo and Fairbanks, 1987; Oppo and Lehman, 1995; Raymo et al., 2004). The deep-water circulation/production changes result in a dense deeply penetrating current during the warm extremes (Hillaire-Marcel et al., 1994) and a more buoyant, shallower water mass during the cold extremes (Berggren and Hollister, 1974; Boyle and Keigwin, 1987; Broecker and Denton, 1990; Broecker, 1991; Broecker et al., 1989; Oppo et al., 1995;

Oppo and Fairbanks, 1987; Oppo and Lehman, 1995; Raymo et al., 2004). The goal of Chapter 2 was to characterize the sedimentological and geochemical signatures of these end-member modes on the Eirik Drift. Changes in percent coarse fraction and sedimentation rates from a collection of shallow and deep-water cores were analyzed to assess the deep-water changes on the orbitally forced glacial/interglacial cycle. As expected, these two modes were detected where NCW shoaled to approximately 2000 during glacial extremes (i.e. Marine Isotope Chrons 2, 4 and 6) and deepened to roughly 3000 m during the extreme interglacial intervals (i.e. Marine Isotope Chrons 1 and 5e). Interestingly, a third intermediate mode was discovered, that dominates the record of the last ~125 kyr (Marine Isotope Chron 3 and Subchrons 5a to 5d) where NCW resided in a transitional position centered around ~2500 m.

A series of abrupt millennial scale oscillations and reorganizations in the climate system was first recognized in the Greenland Ice core temperature records (Alley, 2000; Alley et al., 2003; Blunier and Brook, 2001), but have since been identified in other climate proxies around the globe (Voelker, 2002). Although the mechanisms behind these abrupt changes remain elusive, they are associated with major reorganizations in deep-water production and circulation (Piotrowski et al., 2005). Most studies cite either the salt oscillator (Birchfield and Broecker, 1990; Broecker et al., 1990; Zaucker and Broecker, 1992) or the wind field oscillation (Romanova et al., 2006; Seager, 2006; Seager and Battisti, 2007; Seager et al., 2002; Wunsch, 2006) hypotheses as possible triggers. High-resolution multi-species stable isotopic $\delta^{13}C$ and $\delta^{18}O$ records from the Eirik drift are consistent with other North and South Atlantic deep-water reconstructions during the Last Glacial Maximum, Heinrich 1 event, and the Bolling-Allerod (Boyle and

Keigwin, 1987; Charles and Fairbanks, 1992; Elliot et al., 2002; McManus et al., 2004; Thornalley et al., 2011). No change in deep-water circulation is observed during peak times of glacial meltwater discharge (Abdul et al., submitted; Fairbanks et al., in prep.; Peltier and Fairbanks, 2006), suggesting little to no connection between surface freshwater inputs and alterations to deep-water circulation patterns. Dinocyst data (de Vernal et al., 2005) and anomalously high ice $\delta^{18}O$ values corrected for ice volume during Heinrich 1 suggests the presence of extensive sea ice and we propose, sea ice cover coupled with perturbations to atmospheric circulation, were the trigger for the abrupt climate changes during Termination 1.

Detrital layers, or small-scale rapidly deposited coarse-grained layers, have been documented through out the North Atlantic (Bond et al., 1992; Broecker et al., 1992; Heinrich, 1988; Ruddiman, 1977) and are associated with abrupt climate events (Alley and MacAyeal, 1994). Understanding the nature and timing of these detrital layers is critical in unraveling the underlying mechanisms behind these abrupt climatic events, however, site-to-site correlation of these rapid events proves difficult within the confines of traditional dating methods. The tandem use of traditional $\delta^{18}O$ chronostratigraphic techniques with relative paleointensity (RPI) has been shown to increase the precision of age models compared to when these methods are used independently (i.e., Channell, 1999; Channell et al., 2000; Channell et al., 2014; Channell et al., 2009; Evans et al., 2007; Laj et al., 2000; Stoner et al., 1995; Stoner et al., 1998). A collaborative effort between Rutgers University and the University of Florida was conducted to characterize the millennial and orbital scale changes in the detrital layers in four piston cores collected on the Eirik Drift. Downcore $\delta^{18}O$ and percent carbonate records were generated for this dissertation and approximately 3000 data points were contributed to the published study of Evans et al. (2007). Sedimentation patterns are consistent with the results of Hillaire-Marcel et al. (1994) and Chapter 2 of this dissertation and that the core of NCW is approximately 500 m deeper during interglacial periods than previously proposed. Two different types of detrital layers were recognized in these sediments that correspond to intervals of increase ice rafted detritus (IRD) deposition and mass movement along the Greenland slope. Results further support the combination of traditional $\delta^{18}O$ chronostratigraphic methods in combination with RPI data in creating more robust age models.

5.2 Future Work

As with any scientific research, this study raises more questions than it is able to fully answer and there many avenues of investigation that future research could take. The work in Chapter 2 has provided a thorough view of the changes in the positional depth of NCW over glacial/interglacial cycles for the past ~125 kyr, but what is still unknown is if these same changes occur on the millennial timescales and farther back in time. It is well established that NCW production varies on millennial timescales (i.e., Piotrowski et al., 2005), but it would be interesting to see if we can track the millennial scale movement of the current up and down the drift crest during Termination 1 and between the abrupt climatic events (i.e. Heinrich Event 1, the Bolling-Allerod and the Younger Dryas). 15JPC is currently the only core with high enough resolution (samples taken every 1 cm) to begin to address this question, but a series of cores from carefully selected water depths with the same sampling resolution is needed to fully address this question. The deglacial section of several additional Eirik Drift cores would need to be resampled and analyzed employing the same methods as those described in Chapter 2. A high resolution record of Termination 1 from the southern toe of the drift was generated by Henderson (2009) on core 21GGC, but an additional record from an intermediate depth would be ideal. Core 19JPC or another core from that general area (Figure 5.1) could potentially yield the necessary record to evaluate these changes. However, due to the dynamic nature of sedimentation with respect to the climatic conditions and location on the drift (Hillaire-Marcel et al., 1994), it remains unclear if the desired record would even be preserved in the sediments.

Integrated Ocean Drilling Program (IODP) Sites U1306 (58.24°N, 45.64°W; 2272 m) and U1305 (57.48°N, 48.53°W; 3460) were collected from the northern crest and southern toe of Eirik Drift, respectively (Figure 5.1). Published results of the $\delta^{18}O$ and relative paleointensity records from these sites confirm the general trend of increased deposition on the toe of the drift during extreme interglacials and on the northeastern crest of the drift during glacials over the past ~1.5 myr (Channell et al., 2014; Hillaire-Marcel et al., 2011). A corresponding intermediate depth site is still lacking in order to track the positional changes in NCW prior to 120 ka during the intermediate climate states that dominate the majority of the climate record. An additional drill site in the vicinity of Core 19JPC (Figure 5.1) would be ideal to further evaluate this issue, but is not likely to come to fruition prior to 2020.

Another key piece of paleoceanographic evidence missing from this and other research in this area is benthic foraminifera stable isotopic records. Benthic foraminiferal records have been very difficult to generate in this area due to the extremely low abundances; consequently, reconstructions have primarily relied on planktonic foraminiferal isotopic records (Channell et al., 2014; Evans et al., 2007; Henderson, 2009). The high-resolution benthic record of Termination 1 from Core 15JPC is currently one of the only records of its kind in the area. A downcore benthic foraminiferal isotope stratigraphy has largely already been compiled for the downcore record in Core 15JC spanning Marine Isotope Chrons 1 through 6, and preliminary results of this work can be seen in Figure 5.2. To date, this core has been sampled and sub-sampled 5 times to obtain the necessary material for this record. Several foraminiferal barren zones have been observed in this core making it difficult to find enough benthic foraminifera to generate data, although enough planktonic foraminifera can usually be found during these intervals. Preference was given to the benthic foraminifera *P. wuellerstorfi* because Elmore and Wright (unpublished data) have shown that *Cibicidoides robertsoniensis* does not record equilibrium values and may be up to 1‰ lower in $\delta^{13}C$ values. This species of *Cibicidoides* was excluded from analysis, however, due to the scarcity of benthics in this core, it was necessary to analyze both *P. wuellerstorfi* and *Cibicidoides sp*. Despite the exclusion of *C. robertsoniensis*, several outliers were observed in key intervals of deep-water change (i.e. Marine Isotope Subchron 5e) and these intervals are currently being reanalyzed. Possible benthic foraminiferal faunal analysis could also be conducted to evaluate whether there was any downslope transport of material or if the fauna are insitu. Downslope movement of material could potentially be a problem because evidence of mass movement has been identified in these cores by the presence of low carbonate detrital layers, sharp basal contacts, graded bedding, and traction structures (Evans et al., 2007).

Many questions and uncertainties remain to be addressed in Chapter 3 as well. Due to the coring gap and possible hiatus around 48 cm in Core 15JPC, the record of deep-water change during the Younger Dryas remains unresolved. Investigation would need to be conducted to see if an adequate Eirik Drift core site exists within the archives stored at Rutgers University of KN166-14 that contains high-resolution Younger Dryas aged sediments. It would also be interesting to conduct the same multi-species isotopic analyses on core 19JPC, and possibly others, to track the millennial scale surface and deep-water variations to help test the sea-ice hypothesis proposed in Chapter 3. Additional proxy records, like Mg/Ca and dinocyst data, could be generated as well. The incorporation of magnesium into foraminiferal calcite varies with calcification temperature (Chave, 1954; Rosenthal et al., 1997) and by generating Mg/Ca records on the high-resolution record for Core 15JPC we would be able to separate the temperature effect from the $\delta^{18}O$ record and potentially estimate the total salinity effect (i.e., Rosenthal et al., 1997). Dinocyst data would provide an independent estimate of sea ice cover (Hillaire-Marcel and de Vernal, 2008) and allow further evaluation of the sea-ice/atmospheric circulation change hypothesis.

The transect of $\delta^{13}C$, $^{231}Pa/^{230}Th$ ratios, and ventilation ages presented in Chapter 3 (Figure 3.4) shows that Antarctic Bottom Water (AABW) penetrated as far North as 33°N (Core OCE326-GGC5) but not as far as the Eirik Drift site during the Last Glacial Maximum and Heinrich 1 events. Additional studies could be conducted at deep ocean sites between these two end members to further constrain the extent of northward penetration of AABW during glacial intervals. Research would need to be done to evaluate if existing cores could address this issue or if further sites must be obtained. The ideal study site would be located directly in the path of NCW, exhibit high sedimentation rates, and located between Core 15JPC and OCE326-GGC5 (Figure 5.3).

Several studies have demonstrated the usefulness of applying relative paleointensity data in tandem with traditional $\delta^{18}O$ correlation methods in increasing the confidence level of downcore age models (Channell et al., 2014; Channell et al., 2009; Evans et al., 2007). This is a method that will continue to be used to improve the precision in generating future downcore age models.

5.3 References

Abdul, N., Wright, J.D., Mortlock, R.A., Fairbanks, R.G., submitted.

Alley, R., MacAyeal, D., 1994. Ice-rafted debris associated with binge/purge oscillations of the Laurentide Ice Sheet. Paleoceanography, 9(4): 503-511.

Alley, R.B., 2000. Ice-core evidence of abrupt climate changes. Proceedings of the National Academy of Sciences, 97(4): 1331-1334.

Alley, R.B. et al., 2003. Abrupt climate change. science, 299(5615): 2005-2010.

Berggren, W.A., Hollister, C.D., 1974. Paleogeography, paleobiogeography and the history of circulation in the Atlantic Ocean, Studies in Paleo-oceanography. Special Publication- Society of Economic Mineralogists, 20: 126-186.

Birchfield, G.E., Broecker, W.S., 1990. A salt oscillator in the glacial Atlantic? 2. A "scale analysis" model. Paleoceanography, 5(6): 835-843.

Blunier, T., Brook, E.J., 2001. Timing of millennial-scale climate change in Antarctica and Greenland during the last glacial period. Science, 291(5501): 109-112.

Bond, G. et al., 1992. Evidence for massive discharges of icebergs into the North Atlantic ocean during the last glacial period.

Boyle, E.A., Keigwin, L., 1987. North Atlantic thermohaline circulation during the past 20,000 years linked to high-latitude surface temperature. Nature, 330: 5.

Broecker, W., Bond, G., Klas, M., Clark, E., McManus, J., 1992. Origin of the northern Atlantic's Heinrich events. Climate Dynamics, 6(3-4): 265-273.

Broecker, W., Denton, G.H., 1990. What drives glacial cycles? Scientific American, 262(1): 42-50.

Broecker, W.S., 1979. A revised estimate for the radiocarbon age of North Atlantic Deep Water. Journal of Geophysical Research: Oceans (1978–2012), 84(C6): 3218-3226.

Broecker, W.S., 1991. The great ocean conveyor. Oceanography, 4(2): 79-89.

Broecker, W.S., Bond, G., Klas, M., Bonani, G., Wolfli, W., 1990. A salt oscillator in the glacial Atlantic? 1. The concept. Paleoceanography, 5(4): 469-477.

Broecker, W.S., Denton, G.H., 1989. The role of ocean-atmosphere reorganizations in glacial cycles. Geochimica et Cosmochimica Acta, 53(10): 2465-2501.

Broecker, W.S. et al., 1989. Routing of meltwater from the Laurentide Ice Sheet during the Younger Dryas cold episode.

Channell, J., 1999. Geomagnetic paleointensity and directional secular variation at Ocean Drilling Program (ODP) Site 984 (Bjorn Drift) since 500 ka: comparisons with ODP Site 983 (Gardar Drift). Journal of Geophysical Research: Solid Earth (1978–2012), 104(B10): 22937-22951.

Channell, J., Stoner, J., Hodell, D., Charles, C., 2000. Geomagnetic paleointensity for the last 100 kyr from the sub-antarctic South Atlantic: a tool for inter-hemispheric correlation. Earth and Planetary Science Letters, 175(1): 145-160.

Channell, J., Wright, J., Mazaud, A., Stoner, J., 2014. Age through tandem correlation of Quaternary relative paleointensity (RPI) and oxygen isotope data at IODP Site U1306 (Eirik Drift, SW Greenland). Quaternary Science Reviews, 88: 135-146.

Channell, J., Xuan, C., Hodell, D., 2009. Stacking paleointensity and oxygen isotope data for the last 1.5 Myr (PISO-1500). Earth and Planetary Science Letters, 283(1): 14-23.

Charles, C.D., Fairbanks, R.G., 1992. Evidence from Southern Ocean sediments for the effect of North Atlantic deep-water flux on climate.

Chave, K.E., 1954. Aspects of the biogeochemistry of magnesium 1. Calcareous marine organisms. The Journal of Geology: 266-283.

de Vernal, A. et al., 2005. Reconstruction of sea-surface conditions at middle to high latitudes of the Northern Hemisphere during the Last Glacial Maximum (LGM) based on dinoflagellate cyst assemblages. Quaternary Science Reviews, 24(7): 897-924.

Duplessy, J. et al., 1988. Deep-water source variation during the last climate variation: Palaeoceanography, v. 3.

Elliot, M., Labeyrie, L., Duplessy, J.-C., 2002. Changes in North Atlantic deep-water formation associated with the Dansgaard–Oeschger temperature oscillations (60–10ka). Quaternary Science Reviews, 21(10): 1153-1165.

Elmore, A.C., Wright, J.D., unpublished data.

Evans, H.F. et al., 2007. Paleointensity ‐ assisted chronostratigraphy of detrital layers on the Eirik Drift (North Atlantic) since marine isotope stage 11. Geochemistry, Geophysics, Geosystems, 8(11).

Fairbanks, R.G., Wright, J.D., Mortlock, R.A., in prep.

Heinrich, H., 1988. Origin and consequences of cyclic ice rafting in the northeast Atlantic Ocean during the past 130,000 years. Quaternary research, 29(2): 142-152.

Henderson, S.S., 2009. Tracking deep-water flow on Eirik Drift over the past 160 kyr: Linking deep-water changes to freshwater fluxes. ProQuest.

Hillaire-Marcel, C., de Vernal, A., 2008. Stable isotope clue to episodic sea ice formation in the glacial North Atlantic. Earth and Planetary Science Letters, 268(1): 143-150.

Hillaire-Marcel, C., de Vernal, A., McKay, J., 2011. Foraminifer isotope study of the Pleistocene Labrador Sea, northwest North Atlantic (IODP Sites 1302/03 and 1305), with emphasis on paleoceanographical differences between its “inner” and “outer” basins. Marine Geology, 279(1): 188-198.

Hillaire-Marcel, C., Vernal, A.d., Bilodeau, G., Wu, G., 1994. Isotope stratigraphy, sedimentation rates, deep circulation, and carbonate events in the Labrador Sea during the last~ 200 ka. Canadian Journal of Earth Sciences, 31(1): 63-89.

Laj, C., Kissel, C., Mazaud, A., Channell, J., Beer, J., 2000. High resolution paleointensity stack from the North Atlantic for the 75-10 kyr interval (NAPIS-75) and the duration of the Laschamp event. Phil. Trans. R. Soc. London A, 358: 1009-1025.

McManus, J., Francois, R., Gherardi, J.-M., Keigwin, L., Brown-Leger, S., 2004. Collapse and rapid resumption of Atlantic meridional circulation linked to deglacial climate changes. Nature, 428(6985): 834-837.

Oppo, D. et al., 1995. A 13C record of Upper North Atlantic Deep Water during the past 2.6 million years. Paleoceanography, 10(3): 373-394.

Oppo, D.W., Fairbanks, R.G., 1987. Variability in the deep and intermediate water circulation of the Atlantic Ocean during the past 25,000 years: Northern Hemisphere modulation of the Southern Ocean. Earth and Planetary Science Letters, 86(1): 1-15.

Oppo, D.W., Lehman, S.J., 1995. Suborbital timescale variability of North Atlantic Deep Water during the past 200,000 years. Paleoceanography, 10(5): 901-910.

Peltier, W., Fairbanks, R.G., 2006. Global glacial ice volume and Last Glacial Maximum duration from an extended Barbados sea level record. Quaternary Science Reviews, 25(23): 3322-3337.

Piotrowski, A.M., Goldstein, S.L., Hemming, S.R., Fairbanks, R.G., 2005. Temporal relationships of carbon cycling and ocean circulation at glacial boundaries. Science, 307(5717): 1933-1938.

Raymo, M.E. et al., 2004. Stability of North Atlantic water masses in face of pronounced climate variability during the Pleistocene. Paleoceanography, 19(2).

Romanova, V., Lohmann, G., Grosfeld, K., Butzin, M., 2006. The relative role of oceanic heat transport and orography on glacial climate. Quaternary science reviews, 25(7): 832-845.

Rosenthal, Y., Boyle, E.A., Slowey, N., 1997. Temperature control on the incorporation of magnesium, strontium, fluorine, and cadmium into benthic foraminiferal shells from Little Bahama Bank: Prospects for thermocline paleoceanography. Geochimica et Cosmochimica Acta, 61(17): 3633-3643.

Ruddiman, W.F., 1977. Late Quaternary deposition of ice-rafted sand in the subpolar North Atlantic (lat 40 to 65 N). Geological Society of America Bulletin, 88(12): 1813-1827.

Seager, R., 2006. The source of Europe's mild climate. American Scientist, 94(4): 334.

Seager, R., Battisti, D.S., 2007. Challenges to our understanding of the general circulation: abrupt climate change. Global Circulation of the Atmosphere: 331-371.

Seager, R. et al., 2002. Is the Gulf Stream responsible for Europe's mild winters? Quarterly Journal of the Royal Meteorological Society, 128(586): 2563-2586.

Stoner, J., Channell, J., Hillaire-Marcel, C., 1995. Late Pleistocene relative geomagnetic paleointensity from the deep Labrador Sea: Regional and global correlations. Earth and Planetary Science Letters, 134(3): 237-252.

Stoner, J., Channell, J., Hillaire-Marcel, C., 1998. A 200 ka geomagnetic chronostratigraphy for the Labrador Sea: Indirect correlation of the sediment record to SPECMAP. Earth and Planetary Science Letters, 159(3): 165-181.

Thornalley, D.J., Barker, S., Broecker, W.S., Elderfield, H., McCave, I.N., 2011. The deglacial evolution of North Atlantic deep convection. science, 331(6014): 202-205.

Voelker, A.H., 2002. Global distribution of centennial-scale records for Marine Isotope Stage (MIS) 3: a database. Quaternary Science Reviews, 21(10): 1185-1212.

Wunsch, C., 2006. Abrupt climate change: An alternative view. Quaternary Research, 65(2): 191-203.

Zaucker, F., Broecker, W.S., 1992. The influence of atmospheric moisture transport on the fresh water balance of the Atlantic drainage basin: general circulation model simulations and observations. Journal of Geophysical Research: Atmospheres (1984–2012), 97(D3): 2765-2773.

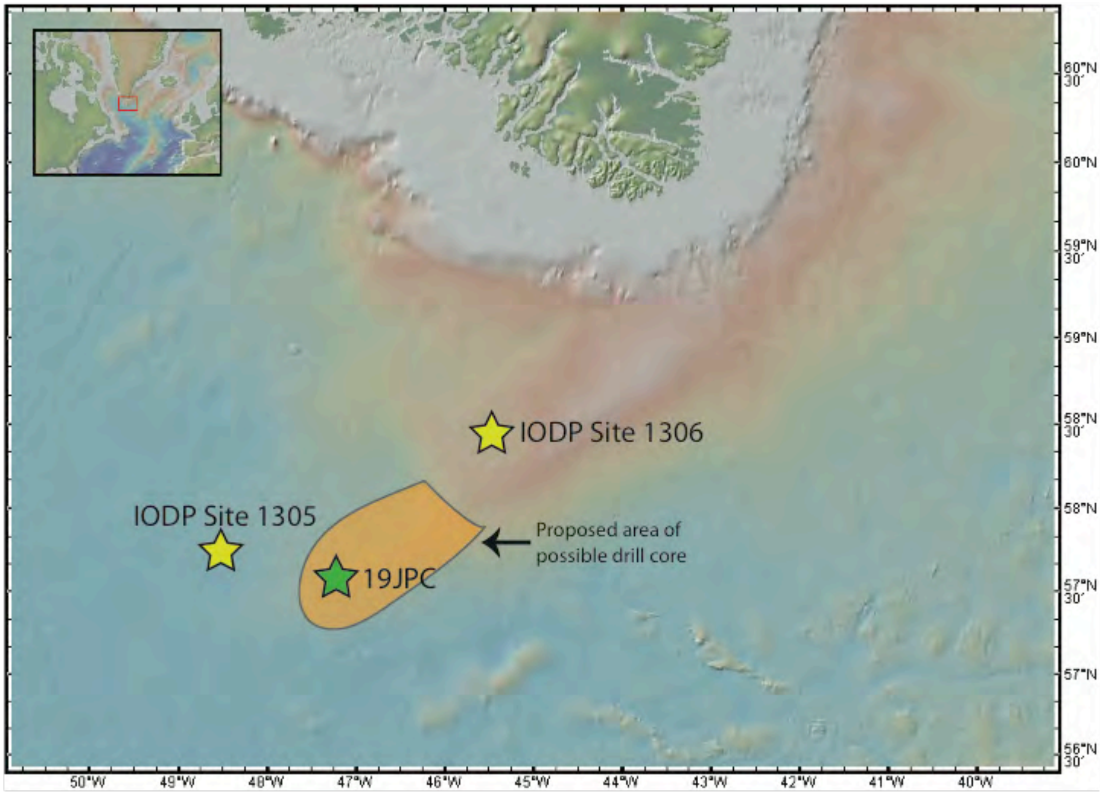

Figure 5.1

Figure 5.1: Map showing the location of IODP site 1306, 1305 (yellow star) and 15JPC (red star) and the study area for possible future/archive cores that could be analyzed for further study.

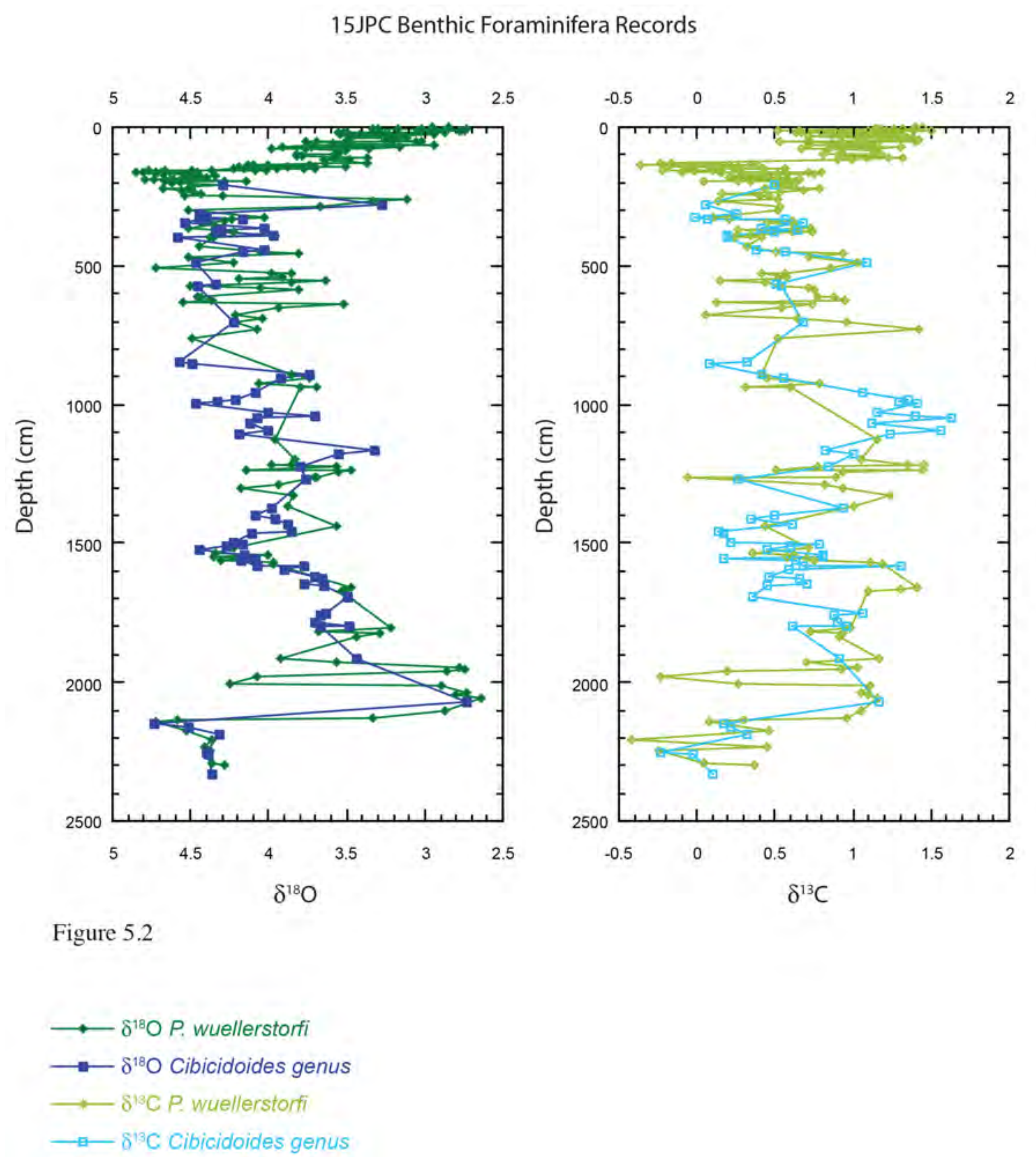

Figure 5.2

Figure 5.2: Downcore stable isotopic benthic foraminiferal records for Core 15JPC versus depth. The benthic species Planulina wuellerstorfi (green) and Cibicidoides species (blue) were both analyzed for $\delta^{18}O$ (closed symbols) and $\delta^{13}C$ (open symbols).

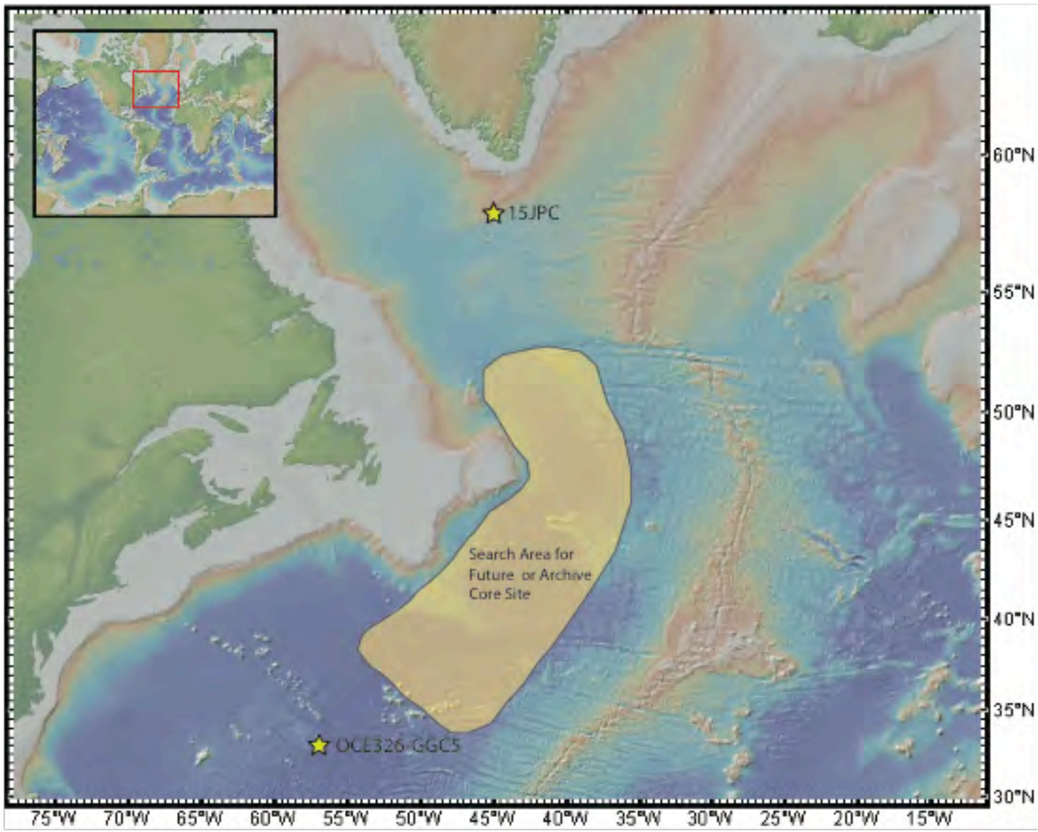

Figure 5.3

Figure 5.3: Map showing the location of cores OCE326-GGC5 and 15JPC (yellow stars) and the study area for possible future/archive cores that could be analyzed for further study.

6.0- Appendices

6.1 Appendix 1

Sampled Depth (cm)	Depth Corrected (cm)	14C Age (ka)	Minus Reservoir Age (ka)	Age Error	Calendar Age (ka)*	1std dev
7	7	7.08	6.48	40	7.406	34
14	14	5.5	4.9	40	**5.624	30
25	25	7.86	7.26	40	8.067	55
40	40	9.06	8.46	45	9.479	28
48	48	10.95	10.35	45	12.163	97
67	60	11.25	10.65	55	12.163	97
87	80	11.65	11.05	55	12.916	54
100	93	12.55	11.95	55	**13.772	58
99	99	12.55	11.95	60	13.772	62
115	115	12.7	12.1	70	13.892	77
127	120	12.35	11.75	50	**13.609	61
145	138	13.8	13.2	75	15.372	134
157	150	15	14.4	60	16.957	144
175	168	16.4	15.8	55	18.97	88
199	190	17.45	16.85	85	20.018	122

*All calendar ages were calculated according to the Fairbanks0107 calibration curve as described in Fairbanks et al., 2005.

**Indicates an age that was discarded due to age reversals and evidence of sediment reworking.

6.2 Appendix 2

15JPC Age Model Depth Picks			
Depth (cm)	**Age (ka)**	**AMS Dates**	**Discarded AMS Dates**
0	7.25		
7	7.41	✔	
14	5.62	✔	✔
25	8.07	✔	
40	9.48	✔	
48	12.16	✔	
60	12.16	✔	✔
80	12.92	✔	
93	13.77	✔	✔
99	13.77	✔	
115	13.89	✔	
120	13.61	✔	✔
138	15.37	✔	
150	16.96	✔	
168	18.97	✔	
190	20.02	✔	
405	29.5		
1212	63.6		
1424	83.5		
1524	91		
1828	106		
1961	124		
2001	126		
2223	147		

19JPC Age Model Depth Picks	
Depth (cm)	**Age (ka)**
0	0
125	11.5
166	13
207	18
272	29.5
619	57.5
653	70
905	85
1040	92.5
1250	98
1525	105
1563	114
1664	124
1690	125
1762	165
1847	191
1872	201
2102	212
2288	215

18JPC Age Model Depth Picks	
Depth (cm)	**Age (ka)**
0	0
2	10.9
5	18
50	29.5
300	64
325	67
372	79
515	89
882.5	101.4
960	107
990	114
1002	117
1003	126
1016	126
1066	127
1130	147

MD2664 Age Model Depth Picks	
Depth	**Age**
0	0
1170	11.5
1220	14.5
1270	16
1335	29.5
1466	57.5
1530	70
1775	85
1815	92.5
2011	99
2290	105
2390	114
2655	120.5
2830	128.1
2900	143
3010	189
3100	215
3200	220
3320	235
3410	243
3490	251

6.3 Appendix 3

15JPC Downcore Data						
Depth (cm)	**Age (ka)**	**d18O Npl**	**d13C Npl**	**Sed Rate (cm/kyr)**	**Coarse Fraction (%)**	**#IRD per gram**
2.5	7.3861	2.26	0	18.38	76.38	3152
7.5	7.6582	2.65	0.07	18.38	35.32	
12.5	7.9303	3.67	0.17	18.38	11.43	383
17.5	8.2024	3.61	0.34	18.08	11.39	
22.5	8.479	3.5	0.3	6.61	2.20	3317
27.5	9.2349	3.71	0.34	6.61	15.47	
32.5	9.9908	3.6	0.21	6.61	6.15	1354
37.5	10.747	3.74	0.23	7.82	5.99	299
47.5	12.026	3.15	0.17	16.23	12.78	
52.5	12.334	3.84	0.36	16.23	8.79	237
57.5	12.642	3.83	0.45	16.29	5.38	
62.5	12.949	3.8	0.25	20.49	9.35	355
72.5	13.437	3.54	0.07	27.32	4.29	191
77.5	13.62	3.69	0.13	27.32	5.08	
82.5	13.803	3.36	0.01	27.32	3.45	238
87.5	13.986	3.38	0.08	30.67	3.33	
92.5	14.149			34.01	6.11	267
97.5	14.296	3.76	-0.08	34.25	3.75	
102.5	14.442	3.76	0.19	34.25	3.96	155
107.5	14.588	3.6	0.18	33.33	3.04	
112.5	14.738	3.61	0.1	22.52	4.48	218
117.5	14.96	3.52	-0.48	22.52	3.98	
122.5	15.182	3.28	-0.03	22.52	4.71	140
127.5	15.404	4.04	0.25	22.52	3.41	
132.5	15.626			10.55	1.82	320
137.5	16.1	3.6	-0.38	7.37	7.54	
142.5	16.778	3.76	-0.03	7.39	12.02	1292
147.5	17.455	3.83	0.05	7.37	0.51	
152.5	18.133	4.24	-0.01	7.66	5.22	231
157.5	18.786	4.23	0.15	16.72	2.86	
162.5	19.085	4.77	-0.01	16.67	6.53	1345
167.5	19.385	4.72	0.06	16.72	5.05	
172.5	19.684	4.45	0.12	16.72	4.36	643
177.5	19.983	4.59	0.07	19.16	3.88	
182.5	20.244	4.56	-0.22	21.39		
186.5	20.431	4.47	0.01	21.55	3.24	587

Depth (cm)	Age (ka)	d18O Npl	d13C Npl	Sed Rate (cm/kyr)	Coarse Fraction (%)	#IRD per gram
191.5	20.663	4.43	-0.21	21.46	2.01	
201.5	21.128	4.63	-0.04	23.92	0.73	
206.5	21.337	4.45	-0.1	24.35	0.32	92
221.5	21.953	4.3	-0.18	24.39	1.17	
226.5	22.158	4.42	-0.06	24.51	0.27	
231.5	22.362	4.47	-0.15	24.39	1.05	117
236.5	22.567	4.07	0.13	24.45	0.76	
246.5	22.976	4.51	0.04	24.51	1.60	
251.5	23.18	4.8	0.15	24.39	1.06	212
256.5	23.385	4.8	0.09	24.39	1.01	
261.5	23.59	4.71	0.16	24.51	1.82	431
266.5	23.794	4.65	0.13	24.39	2.97	
271.5	23.999	4.55	0.01	24.39	4.40	872
276.5	24.204	4.52	-0.08	24.39	1.87	
281.5	24.409	4.6	0.03	24.39	2.20	428
286.5	24.614	4.52	0.07	24.39	3.68	
291.5	24.819	4.67	0.13	24.39	4.64	666
296.5	25.024	4.62	-0.02	24.39	2.57	
301.5	25.229	4.73	-0.04	24.27	2.03	165
306.5	25.435	4.63	-0.14	24.39	1.93	
311.5	25.64	4.73	0.13	24.27	5.07	575
316.5	25.846	4.72	-0.15	24.39	2.52	
321.5	26.051	4.73	-0.05	24.27	3.55	399
326.5	26.257	4.74	-0.02	24.25	4.19	
339.5	26.793	4.73	-0.09	24.27	2.93	603
344.5	26.999			24.27	1.68	
349.5	27.205	4.54	-0.08	24.27	2.04	561
354.5	27.411			24.27	1.66	
359.5	27.617			24.15	2.29	359
364.5	27.824			24.15	2.75	
369.5	28.031	4.45	-0.06	24.27	4.52	630
374.5	28.237			24.15	2.70	
379.5	28.444			24.15	1.24	446
384.5	28.651			24.15	1.45	
389.5	28.858			24.15	2.47	594
394.5	29.065			24.15	0.21	
399.5	29.272	4.35	0.24	24.15	0.50	191
404.5	29.479	4.13	0.37	24.04	0.98	

Depth (cm)	Age (ka)	d18O Npl	d13C Npl	Sed Rate (cm/kyr)	Coarse Fraction (%)	#IRD per gram
409.5	29.687			24.15	0.19	32
414.5	29.894			24.15	0.41	
429.5	30.516	4.13	0.04	24.15	0.44	95
434.5	30.723	4.11	-0.01	24.04	0.43	
439.5	30.931	4.48	0.16	24.15	0.50	119
444.5	31.138	4.14	-0.06	24.15	1.30	
449.5	31.345	4.39	-0.08	24.04	1.63	42
454.5	31.553	4.35	0.39	24.15	0.21	
459.5	31.76	4.63	0.39	24.15	2.94	918
464.5	31.967	4.69	0.04	24.04	0.22	
469.5	32.175	4.05	-0.23	24.15	0.23	67
474.5	32.382	4.28	0.05	24.15	0.53	
479.5	32.589	4.15	-0.07	24.04	0.59	70
484.5	32.797			24.15	0.32	
494.5	33.211	4.23	0.08	24.04		
499.5	33.419	4.05	0	24.15	0.66	301
504.5	33.626	4.18	0.1	24.15	0.56	
509.5	33.833	4.22	0.1	24.04	0.43	121
514.5	34.041	4.11	0.05	24.15	0.52	
519.5	34.248	4.11	0.05	24.04	0.21	99
524.5	34.456	4.01	0.01	24.15	0.42	
529.5	34.663	3.86	-0.12	24.15	0.42	220
534.5	34.87	4.17	-0.09	24.04	0.64	
539.5	35.078	3.97	-0.09	24.15	4.92	1166
544.5	35.285	3.81	-0.12	24.15	4.25	
549.5	35.492	4.54	0.06	24.04	2.10	651
554.5	35.7	3.7	-0.16	24.15	2.13	
559.5	35.907	3.95	-0.02	24.15	5.34	2040
564.5	36.114	3.92	0.18	24.04	4.70	
569.5	36.322	4.2	-0.04	24.15	1.45	854
574.5	36.529			24.04	3.77	
579.5	36.737	4.32	0.03	24.15	2.22	756
589.5	37.151	4.19	0.12	24.11	2.73	947
614.5	38.188	4.14	0.37	24.04	0.99	
619.5	38.396	4.06	0.21	24.15	0.92	239
624.5	38.603	4.08	0.26	24.15	0.93	
629.5	38.81	3.93	0.23	24.04	0.98	216
634.5	39.018	4.05	0.29	24.15	1.12	

Depth (cm)	Age (ka)	d18O Npl	d13C Npl	Sed Rate (cm/kyr)	Coarse Fraction (%)	#IRD per gram
639.5	39.225	3.98	0.36	24.04	1.44	396
644.5	39.433	3.97	0.07	24.10	0.93	
648.5	39.599	3.95	0.18	24.15	1.43	399
653.5	39.806	4.37	0.28	24.15	2.54	
658.5	40.013	4.33	0.34	24.04	1.15	192
673.5	40.636	4.13	0.28	24.15	1.32	
678.5	40.843	4.07	0.28	24.04	0.96	324
683.5	41.051	4.03	0.34	24.15	1.17	
688.5	41.258	4.19	0.38	24.15	1.94	541
693.5	41.465	4.39	0.24	24.04	2.03	
698.5	41.673	4.28	0.25	24.15	3.26	1113
703.5	41.88	4.47	0.29	24.04	1.44	
708.5	42.088	4.32	0.28	24.15	0.51	135
713.5	42.295	4.23	0.31	24.04	0.46	
718.5	42.503	3.83	0.35	24.15	0.69	102
723.5	42.71	4.3	0.29	24.04	0.36	
728.5	42.918	4.65	0.29	24.15	0.72	95
733.5	43.125	4.21	0.28	24.15	0.70	
738.5	43.332	4.21	0.48	24.04	0.82	97
743.5	43.54	4.24	0.4	24.15	0.52	
748.5	43.747	4.19	0.44	24.04	0.60	112
753.5	43.955	3.97	0.25	24.15	0.50	
758.5	44.162	4	0.3	24.04	0.60	24
763.5	44.37	4.03	0.16	24.15	0.79	
768.5	44.577	3.91	0.21	24.04	0.73	99
773.5	44.785	4.08	0.22	24.15	1.21	
778.5	44.992	3.86	0.15	24.04	0.96	235
783.5	45.2	4.04	0.24	24.15	1.22	
788.5	45.407	3.88	0.16	24.04	1.44	356
793.5	45.615	4.3	0.55	24.04	4.11	
798.5	45.823	4.44	0.07	24.19	0.66	154
800	45.885	4.4	0.42	24.15	1.22	
805	46.092	4.51	0.74	24.04	1.07	721
810	46.3	4.32	0.53	24.15	0.95	385
815	46.507	4.49	0.44	24.04	0.93	
820	46.715	4.33	0.3	24.04	1.46	503
825	46.923	4.38	0.24	24.15	1.24	
830	47.13	4.19	0.19	24.04	0.94	47

Depth (cm)	Age (ka)	d18O Npl	d13C Npl	Sed Rate (cm/kyr)	Coarse Fraction (%)	#IRD per gram
835	47.338	4.49	0.18	24.15	1.58	
840	47.545	4.14	0.26	24.04	0.78	448
845	47.753	4.23	0.13	24.04	0.84	
850	47.961	4.3	0.46	24.15	0.97	603
855	48.168	3.93	0.49	24.04	4.01	
860	48.376	4.02	0.3	24.15	5.58	2210
865	48.583	3.97	0.13	24.04	5.02	
870	48.791	3.76	0.13	24.04	3.87	1785
885	49.414	3.87	0	24.04	4.40	
890	49.622	3.66	0.13	24.04	7.57	706
895	49.83	3.75	0.4	24.15	5.23	
900	50.037	3.69	-0.04	24.04	7.15	3066
905	50.245	4.14	0.12	24.04	3.46	
910	50.453	4.549	0.04	24.04	6.29	3846
915	50.661	4.469	0.18	24.15	3.17	
920	50.868	4.144	0.01	24.04	3.73	3365
925	51.076	4.499	0.37	24.04	4.55	
930	51.284	4.141	0.3	24.04	1.83	459
935	51.492	4.405	0.32	24.04	4.74	
940	51.7	4.632	0.43	24.04	2.62	2155
945	51.908	4.529	0.11	24.04	3.24	
950	52.116	4.423	0.31	24.04	2.90	461
955	52.324	4.167	0.15	24.04	4.46	
960	52.532	4.527	0.03	24.04	4.68	3196
965	52.74	4.269	0.1	24.04	2.54	
975	53.156	4.36	0.12	24.04	3.46	
980	53.364	4.16		24.04	7.34	1442
985	53.572	4.287	0.09	24.04	7.05	
990	53.78	4.335		24.04	6.90	3984
995	53.988	4.404	0.05	23.92	5.36	
1000	54.197	4.104		24.04	1.89	1083
1005	54.405	4.321	0.34	24.04	1.83	
1010	54.613	4.716		23.98	2.65	2561
1020	55.03	4.41	0.14	23.92	2.05	104
1025	55.239	4.217	-0.28	23.98	5.33	
1035	55.656	4.245	-0.13	23.81	10.74	
1032	55.53	4.19	-0.11	23.92		
1037	55.739	4.34	-0.07	23.92		

Depth (cm)	Age (ka)	d18O Npl	d13C Npl	Sed Rate (cm/kyr)	Coarse Fraction (%)	#IRD per gram
1042	55.948	3.98	-0.16	23.92	4.16	
1047	56.157	3.91	-0.06	23.92	2.60	
1052	56.366	3.72	-0.04	23.92	2.58	
1057	56.575	3.73	-0.21	23.92	3.59	
1062	56.784	3.83	-0.14	23.92	5.31	
1067	56.993	4.37	-0.14	23.81	9.91	
1072	57.203	4.17	-0.23	23.85	1.78	
1087	57.832	4.12	-0.18	23.81	1.05	
1092	58.042	4.53	-0.32	23.81	1.27	
1097	58.252	4.28	0.02	23.81	1.70	
1102	58.462	4.32	0.3	23.70	1.64	
1112	58.884	4.26	0.03	23.58	0.97	387
1117	59.096	4.41	0.08	23.70	0.49	
1122	59.307	4.43	0.03	23.47	0.67	286
1127	59.52	4.22	-0.29	23.47	3.11	
1132	59.733	4.27	0.06	23.47	1.02	292
1137	59.946	4.49	-0.14	23.36	0.25	
1142	60.16	4.02	-0.06	23.26	0.74	268
1147	60.375	3.96	-0.16	23.04	0.44	
1152	60.592	4.16	0.03	22.94	0.65	107
1157	60.81	4.22	-0.25	22.94	0.63	
1162	61.028	4.14	-0.17	22.94	1.30	236
1167	61.246	4.29	-0.01	21.79	1.53	
1177	61.705	4.48	-0.1	21.74	1.06	
1182	61.935	4.43	0.09	21.65	1.92	752
1187	62.166	4.49	-0.22	19.53	2.20	
1192	62.422	4.2	-0.27	16.81	1.83	757
1202	63.017	4.5	-0.33	16.78	1.77	536
1207	63.315	4.28	-0.42	16.78	1.46	
1212	63.613	4.1	-0.29	11.79	1.75	247
1222	64.461	3.87	-0.3	11.60	4.97	1103
1227	64.892	3.77	-0.15	10.96	5.54	
1265	68.36	3.83	-0.16	10.46	3.53	
1270	68.838	4.3	-0.25	10.46	1.89	543
1275	69.316	3.92	-0.2	10.44	2.39	
1280	69.795	3.89	0.22	10.18	1.95	1001
1285	70.286	4.02	0.34	10.16	3.95	
1290	70.778	3.67	0.34	10.16	5.61	1087

Depth (cm)	Age (ka)	d18O Npl	d13C Npl	Sed Rate (cm/kyr)	Coarse Fraction (%)	#IRD per gram
1295	71.27	3.89	0.19	10.18	4.68	
1300	71.761	3.64	0.41	10.10	9.01	1273
1305	72.256	3.66	0.38	10.04	18.08	
1310	72.754	3.95	0.27	10.04	1.99	1159
1315	73.252	4	0.15	10.04	1.69	
1320	73.75	3.78	0.43	10.04	2.43	747
1325	74.248	3.91	0.33	10.07	4.95	
1335	75.241	3.72	0.4	10.06	0.81	
1340	75.738	4.02	0.5	10.08	1.75	831
1345	76.234	3.86	0.34	10.16	1.23	
1350	76.726	4.09	0.47	10.27	1.48	301
1355	77.213	4.45	0.35	10.27	0.64	
1360	77.7	4.17	0.3	10.29	0.71	239
1365	78.186	4.4	0.37	10.29	1.39	
1370	78.672	3.8	0.38	10.68	1.44	641
1385	80.077	3.93	0.57	10.87	1.22	
1395	80.997	3.91	0.39	11.36	1.89	
1400	81.437	3.75	0.49	11.36	0.92	273
1405	81.877	3.94	0.41	11.36	2.12	
1410	82.317	3.98		11.44	1.57	699
1415	82.754	3.78	0.39	12.30	1.44	
1419.5	83.12	4.16	0.71	12.29	0.90	2861
1424.5	83.527	4.01		12.29	2.15	
1429.5	83.934	4.11	0.37	12.32	0.45	136
1434.5	84.34	4.11	0.37	12.53	1.71	
1439.5	84.739	4.11	0.47	12.79	2.02	407
1444.5	85.13	3.94	0.42	12.79	1.76	
1449.5	85.521	3.87	0.5	12.79	3.05	1048
1454.5	85.912	3.15	0.57	12.79	4.06	
1459.5	86.303	3.35	0.29	13.23	6.18	1498
1464.5	86.681	4.05	0.25	13.26	3.14	
1469.5	87.058	4.26	0.14	13.23	1.44	417
1474.5	87.436	4.04	-0.04	13.26	0.99	
1479.5	87.813	4.45		13.51	0.92	131
1484.5	88.183	4.41	0.45	13.74	1.10	
1489.5	88.547	4.37	0.42	13.77	2.93	692
1494.5	88.91	4.36	0.54	13.77	4.91	
1499.5	89.273	4.54	0.48	13.77	4.22	801

Depth (cm)	Age (ka)	d18O Npl	d13C Npl	Sed Rate (cm/kyr)	Coarse Fraction (%)	#IRD per gram
1504.5	89.636	4.58	0.56	14.33	4.62	
1509.5	89.985	4.09	0.67	14.37	1.33	333
1514.5	90.333	4.22	0.66	14.33	1.28	
1519.5	90.682	4.37	0.22	14.37	4.18	796
1524.5	91.03	4.35	0.34	14.88	21.00	
1529.5	91.366	4.16	0.42	15.53	3.10	628
1534.5	91.688	4.12	0.32	15.48	3.52	
1539.5	92.011	3.98	0.36	15.48	1.64	170
1544.5	92.334	3.78	0.28	15.58	2.87	
1549.5	92.655	4.02	0.32	17.12	0.71	34
1554.5	92.947	3.85	0.28	17.18	0.56	
1559.5	93.238	3.91	0.28	17.18	3.10	741
1564.5	93.529	3.87	0.29	17.12	3.78	
1569.5	93.821	3.75	0.54	18.18	3.55	380
1574.5	94.096	3.77	0.4	19.08	8.26	
1579.5	94.358	3.58	0.39	19.08	7.09	1064
1584.5	94.62	3.44	0.48	19.08	5.75	
1589.5	94.882	3.88	0.35	19.23	4.67	975
1594.5	95.142	4.05	0.63	21.28	1.36	
1599.5	95.377	3.91	0.43	21.28	0.88	173
1604.5	95.612	4.01	0.263	21.28	1.23	
1609.5	95.847	3.97	0.188	21.37	1.00	96
1614.5	96.081	3.83	0.16	22.52	0.83	
1619.5	96.303	3.67	0.04	23.70	1.01	78
1624.5	96.514	3.64	0.214	23.70	1.21	
1629.5	96.725	3.96	0.142	23.81	1.55	148
1639.5	97.145	4.03	0.08	26.18	1.81	152
1644.5	97.336	3.92	0.235	26.32	3.50	
1649.5	97.526	3.49	0.441	26.18	2.58	172
1654.5	97.717	3.5	0.266	26.18	3.69	
1659.5	97.908	3.7	0.205	27.47	6.78	1084
1664.5	98.09	3.63	0.401	28.41	9.47	
1669.5	98.266	3.58	0.295	28.57	19.73	1843
1674.5	98.441	3.37	0.251	28.41	12.79	
1679.5	98.617	3.29	0.167	28.57	2.52	408
1684.5	98.792	3.41	0.079	29.76	1.37	
1689.5	98.96	3.23	0.106	29.94	5.43	757
1694.5	99.127	3.61	0.028	29.76	10.16	

Depth (cm)	Age (ka)	d18O Npl	d13C Npl	Sed Rate (cm/kyr)	Coarse Fraction (%)	#IRD per gram
1699.5	99.295	3.89	0.261	29.76	5.28	622
1704.5	99.463	4.25	0.279	29.76	7.25	
1709.5	99.631	4.13	-0.099	29.59	20.12	1962
1714.5	99.8	3.93	-0.264	29.59	18.23	
1719.5	99.969	3.98	0.206	30.53	7.96	528
1723.5	100.1	3.11	-0.101	29.41	4.54	
1728.5	100.27	3.96	-0.294	27.78	6.00	2204
1733.5	100.45	3.98	-0.528	27.03	6.58	
1743.5	100.82	3.95	-0.02	26.32	7.37	
1748.5	101.01	3.92	0.137	26.32	9.51	3299
1753.5	101.2	3.89	0.087	22.73	5.84	
1758.5	101.42	3.86	-1.117	22.73	7.06	3253
1763.5	101.64	3.91	0.015	23.81	3.26	
1768.5	101.85	3.9	-0.054	22.73	5.47	1774
1773.5	102.07	3.78	-0.08	18.52	6.48	
1778.5	102.34	3.87	-0.25	17.86	11.25	1699
1783.5	102.62	3.86	-0.14	17.86	9.22	
1788.5	102.9	3.72	-0.1	17.86	6.15	1941
1793.5	103.18	3.72	-0.14	15.15	10.59	
1798.5	103.51	3.97	-0.09	13.16	5.42	1818
1803.5	103.89	3.66	0.18	12.82	6.77	
1808.5	104.28	3.387	-0.11	12.99	7.98	2713
1818.5	105.05	3.427	0.01	9.26	9.62	1998
1823.5	105.59	3.129	-0.21	9.26	4.90	
1828.5	106.13	3.133	-0.08	9.17	1.97	497
1838.5	107.22	3.243	0.16	8.33	8.06	
1843.5	107.82	3.702	0.21	7.69	5.72	
1848.5	108.47	3.41	0.06	7.69	3.22	678
1853.5	109.12	3.27	-0.06	7.69	2.43	
1858.5	109.77	3.42	-0.04	7.69	1.09	341
1862.5	110.29	3.582	-0.27	6.98	1.24	
1868.5	111.15	3.506	-0.21	6.82	4.00	928
1873	111.81	3.91	-0.19	6.86	0.66	
1876.5	112.32	3.677	-0.15	6.94	0.92	291
1881.5	113.04	3.881	-0.08	6.62	1.93	
1891.5	114.55	3.899	0.33	6.49	1.55	
1896.5	115.32	3.814	-0.18	6.49	3.48	293
1901.5	116.09	3.343	-0.18	6.49	6.17	

Depth (cm)	Age (ka)	d18O Npl	d13C Npl	Sed Rate (cm/kyr)	Coarse Fraction (%)	#IRD per gram
1906.5	116.86	3.368	0.11	6.49	4.64	1052
1911.5	117.63	3.419	0.02	6.67	5.06	
1916.5	118.38	3.756	0.12	6.67	4.56	913
1921.5	119.13	3.894	0.08	6.58	4.25	
1926.5	119.89	3.847	-0.18	6.76	4.92	1199
1931.5	120.63	3.281	0.01	8.06	4.95	
1936.5	121.25	2.842	-0.23	8.06	14.66	2928
1941.5	121.87	2.707	-0.67	7.94	35.79	
1946.5	122.5	2.713	0.18	8.06	12.12	1933
1951.5	123.12	2.641	-0.12	13.33	11.91	
1961.5	123.87	2.278	-0.13	16.13	18.54	
1976.5	124.8	3.487	-0.23	20.83	3.90	1095
1981.5	125.04	4	-0.33	20.83	3.37	
1986.5	125.28	3.613	-0.34	20.83	0.62	328
1996.5	125.76	3.806	0.05	17.86	3.59	972
2001.5	126.04	4.56	-0.34	16.67	1.29	
2006.5	126.34	4.193	-0.29	16.67	1.05	461
2011.5	126.64	4.354	-0.56	17.24	0.65	
2016.5	126.93	3.75	-0.32	16.13	1.20	381
2021.5	127.24	4.275	-0.23	15.15	0.57	
2026.5	127.57	3.733	-0.14	14.71	0.42	148
2034	128.08	4.14	-0.12	14.71	0.57	
2039	128.42	4.48	-0.09	14.08	2.97	1830
2049	129.13	4.55	0.05	13.16	0.64	359
2054	129.51	4.55	-0.27	13.51	0.64	
2059	129.88	4.69	4.69	13.16	2.00	1020
2064	130.26	4.65	4.65	12.50	1.21	
2069	130.66	4.64	4.64	12.20	0.29	230
2074	131.07	4.56	4.56	11.90	0.33	
2079	131.49	4.79	4.79	12.05	1.22	1451
2089	132.32	4.62	4.62	11.11	0.98	944
2094	132.77	4.58	4.58	11.11	0.52	
2099	133.22	4.4	4.40	11.11	0.58	553
2104	133.67	4.81	4.81	11.11	0.37	
2109	134.12	4.79	4.79	10.42	0.39	447
2114	134.6	4.66	4.66	10.20	0.70	
2119	135.09	4.55	4.55	10.20	0.97	642
2124	135.58	4.51	4.51	10.20	2.73	

Depth (cm)	Age (ka)	d18O Npl	d13C Npl	Sed Rate (cm/kyr)	Coarse Fraction (%)	#IRD per gram
2129	136.07	4.28	4.28	10.00	13.18	3388
2134	136.57	4.8	4.80	9.43	3.76	
2139	137.1	4.41	4.41	9.62	2.57	383
2144	137.62	4.76	4.76	9.43	2.12	
2149	138.15	4.73	4.73	9.43	1.91	435
2154	138.68	4.62	4.62	9.09	1.64	
2159	139.23	4.67	4.67	8.77	0.37	64
2164	139.8	4.65	4.65	8.77	0.37	
2169	140.37	4.56	4.56	8.77	0.75	430
2179	141.51	4.52	4.52	8.26	2.91	685
2188	142.6	4.33	4.33	8.33	0.07	152
2193	143.2	4.54	4.54	8.33	0.40	
2198	143.8	4.59	4.59	7.94	0.39	209
2203	144.43	4.19	4.19	7.81	3.42	
2208	145.07	4.16	4.16	7.77	0.47	167
2223	147	3.97	3.97	7.81	0.24	
2228	147.64	4.3	4.3	7.69	0.71	160
2233	148.29	4.68	4.68	7.81	0.13	
2243	149.57	4.6	4.6	7.81	1.58	
2248	150.21	4.26	4.26	7.75	0.22	38
2258	151.5	4.4	4.4	7.81	0.38	
2263	152.14	4.41	4.41	7.75	0.15	
2273	153.43	4.29	4.29	7.81	0.28	
2278	154.07	4.46	4.46	7.69	0.91	190
2283	154.72	4.55	4.55	7.81	5.64	
2288	155.36	3.99	3.99	7.81	5.98	611
2293	156	4.49	4.49	7.81	0.47	
2298	156.64	4.68	4.68	7.75	0.08	65
2308	157.93	4.52	4.52	7.81	0.16	113
2313	158.57	4.48	4.48	7.69	0.12	
2318	159.22	4.36	4.36	8.97	0.23	65

19JPC Downcore Data					
Depth (cm)	Age (ka)	d18O	d13C	Sed Rate (cm/kyr)	Coarse Fraction (%)
2.5	0.29547	2.89	0.66	8.46	30.99
5	0.59093	2.84	0.65	8.46	37.22
10	1.1819	2.61	0.78	8.46	44
15	1.7728	2.77	0.74	8.46	36.09
20	2.3637	2.61	0.77	8.46	37.37
25	2.9547	2.67	0.59	8.46	38.09
30	3.5456	2.55	0.64	8.46	40.8
32.5	3.841	2.75	0.52	8.46	25.81
35	4.1365	2.78	0.51	8.46	48.2
40	4.7274	2.491	0.489	8.46	22.27
45	5.3184	2.71	0.55	10.25	30.88
50	5.8061	2.55	0.532	11.50	23.32
55	6.2408	2.8	0.5	11.50	25.81
60	6.6756	2.69	0.49	11.50	18.52
62.5	6.893	2.68	0.52	11.50	26.08
65	7.1104	2.7	0.43	11.50	27.42
70	7.5452	2.65	0.48	11.50	29.66
75	7.98	2.77	0.42	11.50	32.07
80	8.4148	2.68	0.48	11.50	29.66
85	8.8495	2.62	0.36	11.50	31.33
90	9.2843	2.61	0.42	11.50	23.75
92.5	9.5017	2.82	0.41	15.23	25.14
95	9.6659	2.82	0.35	18.54	25.12
100	9.9356	2.79	0.48	18.56	21.76
105	10.205	2.62	0.25	18.52	26.08
110	10.475	2.59	0.05	18.52	22.89
115	10.745	2.45	-0.03	18.59	12.83
120	11.014	2.82	0.27	18.52	9.07
122.5	11.149	2.79	0.35	18.52	9.12
125	11.284	2.93	0.31	18.52	13.48
130	11.554	2.83	0.2	18.59	20.69
135	11.823	3.17	0.21	18.52	17.48
140	12.093	2.98	0.16	14.88	19.98
145	12.429	2.97	0.348	14.84	24.44
150	12.766	3.43	0.45	14.79	13.43
152.5	12.935	2.92	0.19	14.88	12.19

Depth (cm)	Age (ka)	d18O	d13C	Sed Rate (cm/kyr)	Coarse Fraction (%)
155	13.103	3.35	0.19	14.84	17.43
160	13.44	3.65	0.31	14.84	21.31
165	13.777	3.54	0.1	14.84	15.93
170	14.114	3.5	0.235	14.84	18.15
175	14.451	3.6	0.11	14.79	32.43
180	14.789	3.609	0.184	14.88	21.52
182.5	14.957	3.65	0.1	14.79	20.01
185	15.126	3.81	-0.03	7.96	10.17
190	15.754	3.562	0.054	6.33	17.35
198	17.017	3.78	0.17	6.33	20.62
203	17.807	3.762	0.22	6.34	15.81
208	18.596	4.74	0.05	6.34	5.4
212.5	19.306	4.86	0.06	6.33	20.64
213	19.385	4.612	0.001	6.34	21.61
218	20.174	4.73	-0.06	6.33	16.75
223	20.964	4.461	0.006	6.34	19.47
228	21.753	4.83	0.08	6.34	19.15
233	22.542	4.586	-0.028	5.77	23.38
238	23.409	4.62	0	5.72	11.88
242.5	24.196	4.74	0.16	5.75	9.7
243	24.283	4.642	0.133	5.71	15.4
248	25.158	4.533	0.01	5.72	20.7
253	26.032	4.301	0.062	5.72	15.63
258	26.906	4.51	0.09	5.71	9.77
263	27.781	4.386	0.128	5.72	11.21
268	28.655	4.408	0.166	5.72	9.13
272.5	29.442	4.55	0.09	5.75	13.36
273	29.529	4.19	0.14	5.71	7.15
278	30.404	4.11	0.245	6.73	11.39
283	31.147			7.78	9.73
288	31.79	4.053	0.228	7.78	10.65
293	32.433	4.3	0.19	7.78	10.81
298	33.076	4.41	0.3	7.77	9.46
302.5	33.655	4.47	0.32	7.81	9
303	33.719	4.29	0.38	7.78	9.03
308	34.362	4.34	0.29	7.78	7.38
313	35.005	4.35	0.48	7.78	11.05

Depth (cm)	Age (ka)	d18O	d13C	Sed Rate (cm/kyr)	Coarse Fraction (%)
323	36.291	4.22	0.5	8.45	9.35
328	36.883	4.42	0.47	11.90	3.36
332.5	37.261	4.01	0.36	11.90	20.97
333	37.303	4.049	0.361	11.93	8.79
338	37.722	4.19	0.36	11.90	9.46
343	38.142	4.26	0.51	11.92	
351	38.813	4.26	0.26	11.93	9.46
356	39.232	3.94	0.5	11.90	6.99
361	39.652	4	0.08	11.90	8.85
362.5	39.778	4.02	0.48	11.90	13.75
366	40.072	3.89	0.34	11.93	20.73
371	40.491	3.76	0.23	15.24	19.78
376	40.819	4.28	0.42	21.55	28.54
381	41.051	3.96	0.23	21.46	14.8
386	41.284	4.36	0.43	21.55	16.51
391	41.516	4.19	0.32	21.43	8.09
392.5	41.586	4.41	0.45	21.60	11.13
396	41.748	4.3	0.45	21.46	10.37
401	41.981	4.2	0.03	21.55	7.98
406	42.213	4.18	0.46	21.55	8.57
411	42.445	4.17	0.31	21.46	8.79
416	42.678	4.18	0.5	23.47	15.81
421	42.891	4.03	0.31	48.39	2.17
422.5	42.922	4.31	0.38	48.61	3.61
426	42.994	3.95	0.36	48.08	1.44
431	43.098	3.27	0.18	48.54	4.56
436	43.201	3.69	0.506	48.08	2.52
441	43.305	3.35	0.21	48.54	1.36
446	43.408	3.946	0.38	48.08	4.37
451	43.512	4.23	0.16	48.39	7.66
452.5	43.543	4.25	0.31	48.61	12.69
456	43.615	4.059	0.14	48.54	16.18
461	43.718	3.83	0.21	48.08	9.34
466	43.822	4.319	0.482	62.50	7.9
471	43.902	4.31	0.19	67.57	4.19
476	43.976	4.363	0.384	67.57	4.76
481	44.05	4.56	0.28	68.18	8.9
482.5	44.072	4.45	0.31	67.31	2.01

Depth (cm)	Age (ka)	d18O	d13C	Sed Rate (cm/kyr)	Coarse Fraction (%)
486	44.124	4.105	0.29	66.67	1.76
491	44.199	3.47	0.14	67.57	1.94
496	44.273	4.291	0.275	67.16	13.43
505	44.407	3.8	0.19	67.57	2.42
510	44.481	3.847	0.225	67.57	13.4
512.5	44.518	4.15	0.12	31.25	2.15
515	44.598	3.86	0.25	21.74	3.83
520	44.828	3.705	0.209	21.65	13.88
525	45.059	3.8	0.12	21.65	13.4
530	45.29	3.01	-0.18	21.65	15.09
535	45.521	3.77	0.08	21.74	6.39
540	45.751	4.027	0.164	21.55	11.81
542.5	45.867	3.91	0.08	21.74	6.7
545	45.982	3.71	0.16	21.65	11.52
550	46.213	3.854	0.151	21.74	4.94
555	46.443	3.79	-0.2	21.65	17.75
560	46.674	3.55	-0.388	6.74	8.17
565	47.416	4.02	-0.1	6.44	9.54
570	48.193	4.303	0.017	6.44	10.16
572.5	48.581	4.07	0.03	6.43	11.43
575	48.97	4.14	0.02	6.44	6.02
580	49.747	4.045	0.091	6.44	10.06
585	50.524	3.97	0.06	6.43	5.59
590	51.302	3.92	-0.017	6.44	7.55
595	52.079	3.74	-0.11	6.44	8.33
600	52.856	3.826	0.133	6.43	7.96
602.5	53.245	3.84	-0.01	6.44	7.21
605	53.633	3.54	-0.17	3.70	11.82
610	54.984	3.629	-0.016	2.88	11.74
615	56.723	3.63	-0.27	2.88	7.32
620	58.462	4.112	-0.076	2.87	16.76
625	60.202	4.02	-0.14	2.88	12.23
630	61.941	4.5	0.24	2.87	19.88
632.5	62.811	4.38	0.04	2.88	9.4
635	63.68	4.14	0.11	2.87	9.91
640	65.42	4.03	0.47	2.88	24
645	67.159	4.01	0.23	3.92	9.91
658	70.478	3.74	0.456	14.85	39.04

Depth (cm)	Age (ka)	d18O	d13C	Sed Rate (cm/kyr)	Coarse Fraction (%)
662.5	70.781	3.94	0.3	15.15	19.96
663	70.814	3.67	0.22	14.84	13.08
668	71.151	3.75	0.47	14.88	17.22
673	71.487	3.85	0.58	14.88	8.62
678	71.823	3.92	0.7	14.88	25.14
683	72.159	3.4	0.47	14.88	20.04
688	72.495	3.137	-0.021	14.85	11.05
692.5	72.798	3.34	0.5	15.15	8.92
693	72.831	3.4	0.47	14.84	6.88
698	73.168	3.618	0.626	16.13	12.87
703	73.478	3.96	0.07	17.48	14.3
708	73.764	3.674	0.501	17.48	11.24
713	74.05	3.15	-0.07	17.42	9.01
718	74.337	3.717	0.547	17.51	15.81
722.5	74.594	3.91	0.46	17.24	8.64
723	74.623	3.79	0.52	17.48	4.39
728	74.909	3.904	0.619	17.48	4.4
733	75.195	3.74	0.57	17.42	2.85
738	75.482			17.48	2.56
743	75.768	3.73	0.52	17.48	1.94
748	76.054			17.51	3.42
752.5	76.311	3.98	0.6	17.86	0.78
753	76.339	3.73	0.52	17.54	2.61
758	76.624	3.74	0.523	17.48	3.85
763	76.91	3.68	0.49	17.54	3.43
768	77.195	3.789	0.606	17.54	3.06
773	77.48	3.39	-0.25	17.54	1.78
778	77.765	3.161	-0.0389	17.51	4.32
782.5	78.022	3.41	0.31	17.86	3.6
783	78.05	3.63	0.35	17.54	2.43
788	78.335	3.716	0.57	17.48	4.47
793	78.621	3.45	0.39	17.61	5.2
798	78.905	3.585	0.617	17.54	4.65
803	79.19	3.51	0.39	17.54	3.45
811	79.646	3.551	0.491	17.44	22.7
812.5	79.732	3.63	0.44	17.59	2.07
816	79.931	3.52	0.47	17.54	4.21
821	80.216	3.297	0.307	17.54	3.98

Depth (cm)	Age (ka)	d18O	d13C	Sed Rate (cm/kyr)	Coarse Fraction (%)
826	80.501	3.41	0.44	17.54	5.18
831	80.786	3.5	0.47	17.61	6.09
836	81.07	3.5	0.29	17.54	3.02
841	81.355	3.54	0.42	17.44	3.91
842.5	81.441	3.68	0.45	17.59	3.25
846	81.64	3.37	0.41	17.54	6.18
851	81.925	3.39	0.51	17.54	3.63
856	82.21	3.08	0.38	17.61	5.71
861	82.494	3.32	0.48	17.54	7.73
866	82.779	3.35	0.33	17.54	3.85
871	83.064	3.41	0.44	17.65	3.65
872.5	83.149	3.48	0.4	17.50	3.66
876	83.349	3.45	0.45	17.61	3.87
881	83.633	3.58	0.5	17.54	2.88
886	83.918	3.33	0.25	17.54	8.64
891	84.203	3.28	0.45	17.61	10.96
896	84.487	3.41	0.43	17.54	5.3
901	84.772	3.73	0.68	17.65	8.47
902.5	84.857	3.94	0.72	17.59	2.44
906	85.056	3.81	0.62	17.54	2.88
911	85.341	3.99	0.79	17.54	2.53
916	85.626	3.86	0.68	17.61	3.94
921	85.91	3.85	0.76	17.54	5.46
926	86.195	3.66	0.77	17.61	1.67
931	86.479	3.64	0.78	17.44	8.92
932.5	86.565	3.85	0.81	17.68	0.7
936	86.763	3.77	0.79	17.61	3.2
941	87.047	3.54	0.67	17.67	2.12
946	87.33	3.98	0.46	17.67	2.71
951	87.613	3.88	0.61	17.61	3.31
956	87.897	3.6	0.38	17.66	1.73
964	88.35	3.87	0.54	17.65	2.07
965.5	88.435	4.15	0.47	17.68	2.4
969	88.633	3.73	0.32	17.61	7
974	88.917			17.67	3.32
979	89.2			17.92	1.91
984	89.479	3.98	0.46	18.12	1.76
989	89.755	3.87	0.5	18.04	4.44

Depth (cm)	Age (ka)	d18O	d13C	Sed Rate (cm/kyr)	Coarse Fraction (%)
992.5	89.949			18.07	1.56
994	90.032	4.31	0.19	18.12	2.09
999	90.308			18.05	2.3
1004	90.585			18.12	3.1
1009	90.861			18.05	3.98
1014	91.138			18.12	2.31
1019	91.414	4.13	0.09	18.04	3.09
1022.5	91.608			18.29	1.56
1024	91.69			20.92	1.35
1029	91.929	4.36	0.01	29.76	1.25
1034	92.097	4.15	0.54	29.59	10.57
1039	92.266	3.83	0.25	29.76	1.39
1044	92.434	4.08	0.4	29.76	2.05
1049	92.602	3.85	0.35	29.91	1.74
1052.5	92.719	4.04	0.42	29.41	0.81
1054	92.77	3.96	0.28	29.76	2.71
1059	92.938	4.11	0.33	29.76	1.99
1064	93.106	3.88	0.42	29.76	3.74
1069	93.274	3.9	0.16	29.76	2.13
1074	93.442	3.93	0.34	38.46	2.94
1079	93.572	3.99	0.41	38.89	2.86
1082.5	93.662	4.07	0.46	38.46	2.78
1084	93.701	4.03	0.42	38.46	4.46
1089	93.831	4.11	0.43	38.46	5.27
1094	93.961			38.46	3.83
1099	94.091	4.04	0.46	38.76	1.94
1104	94.22	3.81	0.45	38.46	0.96
1109	94.35	4.08	0.21	38.46	2.1
1112.5	94.441			38.46	0.75
1118	94.584	3.91	0.37	38.76	3.16
1123	94.713	4.05	0.39	38.46	1.57
1128	94.843	3.57	0.24	38.76	1.22
1133	94.972	3.69	0.42	38.46	0.52
1138	95.102	3.83	0.27	38.79	1.12
1142.5	95.218	4.04	0.26	38.46	1.27
1143	95.231	3.7	0.14	38.76	0.46
1148	95.36			38.46	1.79
1153	95.49	3.69	0.46	38.76	0.71

Depth (cm)	Age (ka)	d18O	d13C	Sed Rate (cm/kyr)	Coarse Fraction (%)
1158	95.619			38.46	1.51
1163	95.749	3.78	0.09	38.76	1.44
1168	95.878			38.46	2.45
1172.5	95.995	4.07	0.21	38.46	1.38
1173	96.008	3.66	0.14	38.76	1.56
1178	96.137			38.76	3.39
1183	96.266	3.77	-0.05	38.46	1.29
1188	96.396			38.76	1.67
1193	96.525	3.78	0.22	38.46	1.38
1198	96.655			38.79	3.02
1202.5	96.771	4.04	0.06	38.46	0.35
1203	96.784	3.75	0.33	38.76	1.95
1208	96.913			38.46	3.26
1213	97.043	3.7	0.25	38.76	1.65
1218	97.172			38.76	5.67
1223	97.301	3.65	0.17	38.46	1.15
1228	97.431			38.79	1.92
1232.5	97.547	3.85	0.36	38.46	1.8
1233	97.56	3.85	0.3	38.76	2.7
1238	97.689	3.85	0.18	38.46	2.84
1243	97.819	3.81	0.36	38.76	1.29
1248	97.948	3.69	0.2	38.76	1.77
1253	98.077	3.91	0.3	38.46	0.96
1258	98.207	3.8	0.4	38.79	1.38
1262.5	98.323	3.46	0.18	38.46	2.54
1263	98.336	3.77	0.31	38.99	0.78
1271.5	98.554	3.7	0.28	39.06	2.35
1276.5	98.682	3.59	0.15	39.06	0.99
1281.5	98.81	3.85	0.51	38.76	2.1
1286.5	98.939	3.77	0.03	39.06	1.04
1291.5	99.067	3.72	0.33	38.46	1.88
1292.5	99.093			39.22	
1296.5	99.195	3.72	0.38	38.76	1.07
1301.5	99.324	3.69	0.21	39.06	1.87
1306.5	99.452	3.63	0.47	39.37	1.48
1311.5	99.579	3.75	0.47	39.37	2.26
1316.5	99.706	3.74	0.34	39.37	1
1321.5	99.833			40.00	2.38

Depth (cm)	Age (ka)	d18O	d13C	Sed Rate (cm/kyr)	Coarse Fraction (%)
1322.5	99.858			39.22	1.68
1326.5	99.96	3.65	0.28	38.46	0.87
1331.5	100.09			41.67	1.19
1336.5	100.21	3.51	0.24	38.46	1.36
1341.5	100.34	3.434	0.122	38.46	3.24
1346.5	100.47	3.19	-0.1	41.67	2.4
1351.5	100.59	3.551	0.297	33.33	1.57
1352.5	100.62			40.00	0.8
1356.5	100.72	3.6	0.41	38.46	2.49
1361.5	100.85	3.483	0.394	41.67	2.18
1366.5	100.97	3.74	0.39	38.46	1.36
1371.5	101.1	3.564	0.428	41.67	1.89
1376.5	101.22	3.4	0.36	38.46	2.33
1381.5	101.35	3.44	0.361	50.00	3.88
1382.5	101.37	3.6	0.19	40.00	3.11
1386.5	101.47	3.55	0.39	38.46	1.63
1391.5	101.6			41.67	1.81
1396.5	101.72	3.47	0.4	38.46	1.13
1401.5	101.85			41.67	2.81
1406.5	101.97	3.58	0.33	38.46	4.17
1411.5	102.1			50.00	7.81
1412.5	102.12	3.48	0.47	40.00	5.98
1416.5	102.22	3.36	0.47	39.13	7.51
1425.5	102.45			41.67	6.9
1430.5	102.57	3.7	0.52	41.67	3.33
1435.5	102.69			38.46	7.82
1440.5	102.82	3.74	0.48	40.00	10.34
1442.5	102.87	3.39	0.31	42.86	5.7
1445.5	102.94			38.46	4.38
1450.5	103.07	3.7	0.45	41.67	10.82
1455.5	103.19			41.67	10.69
1460.5	103.31	3.53	0.38	41.67	5.34
1465.5	103.43	0		38.46	5.39
1470.5	103.56	3.69	0.44	40.00	6.94
1472.5	103.61	3.48	0.39	42.86	5.22
1475.5	103.68			41.67	0.73
1480.5	103.8			41.67	1.29
1485.5	103.92			38.46	1.36

Depth (cm)	Age (ka)	d18O	d13C	Sed Rate (cm/kyr)	Coarse Fraction (%)
1490.5	104.05			22.73	2.76
1495.5	104.27			10.20	0.96
1500.5	104.76			10.53	1.57
1502.5	104.95	3.39	0.03	10.00	1.96
1505.5	105.25			10.20	1.51
1510.5	105.74			10.20	1.61
1515.5	106.23			10.20	1.37
1520.5	106.72			10.20	1.22
1525.5	107.21			10.20	0.52
1530.5	107.7			10.53	1.39
1532.5	107.89			10.00	1.42
1535.5	108.19	3.654	0.182	10.20	2.28
1540.5	108.68	3.66	0.23	5.32	1.56
1545.5	109.62	3.73	0.24	5.05	2.36
1550.5	110.61	3.64	0.33	5.10	2.59
1555.5	111.59	3.436	0.287	5.10	2.57
1560.5	112.57	3.71	0.29	5.00	2.78
1562.5	112.97			5.08	7.66
1565.5	113.56	3.465	0.266	5.10	6.71
1570.5	114.54	2.72	0.1	5.09	13.8
1579	116.21	3.019	0.406	5.10	36.01
1584	117.19	2.79	0.23	5.95	50.33
1589	118.03	3.03	0.076	10.61	92.17
1592.5	118.36	3	0.1	10.71	88.41
1594	118.5	3.2	0.07	10.87	81.57
1599	118.96	3.082	0.085	10.64	6.41
1604	119.43	2.99	-0.05	10.87	74.31
1609	119.89	3.369	-0.001	10.64	70.27
1614	120.36	3.1	-0.25	10.64	44.53
1619	120.83	2.475	0.028	10.94	35.84
1622.5	121.15	2.15	0.02	10.71	31.29
1624	121.29	2.35	0.02	10.64	16.72
1629	121.76	2.242	-0.04	10.87	31.08
1634	122.22	2.23	-0.08	18.52	26.43
1639	122.49	3.119	0.153	20.00	55.46
1644	122.74	2.48	0.09	20.00	27.56
1649	122.99			19.44	12.08
1652.5	123.17	2.63	0.12	21.43	12.23

Depth (cm)	Age (ka)	d18O	d13C	Sed Rate (cm/kyr)	Coarse Fraction (%)
1654	123.24	2.81	0.07	20.00	12.34
1659	123.49	3.16	-0.04	19.23	10.89
1664	123.75	3.12	-0.06	20.00	16.9
1669	124	3.55	-0.12	20.00	11.6
1674	124.25	4.07	0.02	20.00	16.92
1679	124.5	4.376	-0.064	4.38	6.71
1682.5	125.3	4.56	-0.13	2.17	10.49
1684	125.99	4.29	0.14	2.17	7.22
1689	128.29	4.635	0.08	2.17	7.31
1694	130.59	4.57	0.08	2.17	5.81
1699	132.89	4.836	-0.195	2.17	9.07
1704	135.19	4.84	0.02	2.17	7.74
1709	137.49	4.776	0.105	2.17	4.75
1712.5	139.1	4.51	0.02	2.17	6.36
1714	139.79	4.47	0.02	2.17	3.02
1719	142.09	4.426	0.046	2.16	8.88
1724	144.4	4.44	-0.11	2.07	5.13
1732	148.27	3.51	0.01	1.98	5.64
1737	150.79	4.185	-0.132	1.98	6.64
1742	153.31	4.042	-0.152	2.00	8.34
1742.5	153.56	3.89	-0.17	1.98	11.62
1747	155.83	3.634	-0.345	1.98	14.03
1752	158.35	4.308	-0.146	1.98	16.5
1757	160.87	4.534	-0.06	1.98	9.79
1762	163.39	4.379	-0.099	1.98	6.97
1767	165.91	4.544	-0.052	1.98	9.32
1772	168.43	4.2	0.02	2.00	5.55
1772.5	168.68	3.89	-0.17	2.69	6.55
1777	170.35	4.46	-0.03	3.62	16.47
1782	171.73	4.12	0.01	3.65	12.7
1787	173.1	4.32	0.11	3.62	11.39
1792	174.48	4.35	0.1	3.62	10.5
1797	175.86	4.47	0.2	3.62	9.2
1802	177.24	4.28	0.28	3.85	4.58
1802.5	177.37	4.02	0.2	3.63	4.47
1807	178.61	4.13	0.23	3.62	4.11
1812	179.99	3.75	0.02	3.62	6.34
1817	181.37	4.1	0.04	3.42	8.55

Depth (cm)	Age (ka)	d18O	d13C	Sed Rate (cm/kyr)	Coarse Fraction (%)
1822	182.83	3.34	0	2.76	8.9
1827	184.64	4.01	0.13	2.76	4.91
1832	186.45	4.2	0.14	2.78	16.3
1832.5	186.63	4.26	-0.17	2.78	13.44
1837	188.25	4.49	0.11	2.76	11.77
1842	190.06	4.29	-0.02	2.76	4.02
1847	191.87	4.18	0.02	2.76	7.73
1852	193.68	4.22	0.05	2.76	12.96
1857	195.49	4.45	0.17	2.76	20.03
1862	197.3	4.19	-0.03	2.78	11.3
1862.5	197.48	4.51	0.15	2.76	7.6
1867	199.11	3.79	0.12	5.95	4.94
1872	199.95	3.8	0.57	7.35	5.66
1877	200.63	2.93	0	7.48	11.58
1885	201.7	3.53	0.32	7.35	8.09
1890	202.38	3.69	0.39	7.58	13.83
1892.5	202.71	3.48	0.39	7.35	21.27
1895	203.05	3.2	0.41	7.46	9.54
1900	203.72	2.96	0.18	7.35	15.58
1905	204.4	3.08	0.42	7.46	0
1910	205.07	3.19	0.56	8.06	8.84
1915	205.69	2.92	0.41	25.00	0
1920	205.89			25.00	5.37
1922.5	205.99			25.00	4.23
1925	206.09			25.00	2.62
1930	206.29			25.00	1.24
1935	206.49			25.00	1.55
1940	206.69			25.00	9.34
1945	206.89			25.00	4.28
1950	207.09			25.00	1.8
1952.5	207.19			25.00	2.83
1955	207.29	3.18	0.34	25.00	1.77
1960	207.49			29.41	1.83
1965	207.66			29.41	0.98
1970	207.83			31.25	0.8
1975	207.99			29.41	0.97
1980	208.16	3.65	0.41	31.25	1.13
1982.5	208.24			27.78	1.28

Depth (cm)	Age (ka)	d18O	d13C	Sed Rate (cm/kyr)	Coarse Fraction (%)
1985	208.33			31.25	1.11
1990	208.49			29.41	0.6
1995	208.66			29.41	3.27
2000	208.83			31.25	1.66
2005	208.99			31.25	0.98
2010	209.15			31.25	1.49
2012.5	209.23			31.25	1.96
2015	209.31			31.25	0.65
2020	209.47			33.33	1.64
2025	209.62	3.89	0.36	31.25	9.18
2030	209.78			32.14	1.49
2039	210.06			31.82	3.08
2042.5	210.17	3.12	0.23	30.00	2.57
2044	210.22	3.42	0.07	31.25	2.55
2049	210.38			33.33	2.68
2054	210.53			31.25	3.44
2059	210.69			33.33	4.26
2064	210.84	3.63	0.44	33.33	4.78
2069	210.99			31.82	4.53
2072.5	211.1			30.00	5.74
2074	211.15	3.48	0.69	33.33	5.96
2079	211.3	3.28	0.68	33.33	11.68
2084	211.45	3.35	0.55	33.33	15.66
2089	211.6	3.23	0.64	31.25	15.98
2094	211.76	3.03	0.33	33.33	15.94
2099	211.91	3.2	0.64	35.00	25.9
2102.5	212.01			37.50	18.26
2104	212.05	2.87	0.15	41.67	20.27
2109	212.17	3.01	0.35	38.46	30.7
2114	212.3	3.16	0.38	41.67	12.82
2119	212.42	3.16	0.3	38.46	28.65
2124	212.55	3.06	0.23	41.67	27.49
2129	212.67	3.15	0.29	38.89	7.81
2132.5	212.76			37.50	6.54
2134	212.8	3.13	0.26	41.67	15.94
2139	212.92	3.66	0.06	38.46	7.32
2144	213.05			45.45	8.51
2149	213.16	3.46	0.01	55.56	5.16

Depth (cm)	Age (ka)	d18O	d13C	Sed Rate (cm/kyr)	Coarse Fraction (%)
2154	213.25			62.50	2.35
2159	213.33	4.16	0.16	50.00	3.93
2162.5	213.4			75.00	5.97
2164	213.42	3.71	0.23	55.56	4.92
2169	213.51	3.83	0.27	62.50	1.96
2174	213.59	4.38	0.48	55.56	6.71
2179	213.68	3.85	0.3	55.56	0.83
2184	213.77			60.00	0.57
2193	213.92			62.50	1.52
2195.5	213.96			83.33	2.06
2198	213.99	3.85	0.63	71.43	1.26
2203	214.06	3.77	0.62	83.33	1
2208	214.12	3.66	0.02	71.43	1.41
2213	214.19			83.33	1.81
2218	214.25			75.00	0.99
2222.5	214.31				0.89
2223	214.31			71.43	1.49
2228	214.38	3.98	0.45	83.33	0.66
2233	214.44			83.33	1.11
2238	214.5	3.92	0.23	83.33	1.74
2243	214.56			100.00	0.95
2248	214.61			112.50	1.21
2252.5	214.65			50.00	3.24
2253	214.66			100.00	1.35
2258	214.71	3.73	0.47	100.00	2.26
2263	214.76			100.00	1.11
2268	214.81			125.00	2.1
2273	214.85	3.85	0.4	100.00	1.14
2278	214.9	3.69	0.52	90.00	1.1
2282.5	214.95				2.03
2283	214.95	3.25	0.58	100.00	3.32
2288	215	2.63	-0.15	100.00	6.13
2293	215.05	3.03	0.39	100.00	19.7
2298	215.1	3	0.28	100.00	27.31
2303	215.15	2.93	0.29	125.00	35.75
2308	215.19	2.97	0.34	100.00	36.95
2313	215.24	2.89	0.25	83.33	17.28
2315.5	215.27			125.00	21.22

Depth (cm)	Age (ka)	d18O	d13C	Sed Rate (cm/kyr)	Coarse Fraction (%)
2318	215.29	3.01	-0.14	100.00	29.73
2323	215.34	3.25	0.11	100.00	30.63
2328	215.39	3.27	-0.13	36.36	21.82
18JPC Downcore Data					
Depth (cm)	**Age (ka)**	**d18O**	**d13C**	**Sed Rate (cm/kyr)**	**Coarse Fraction (%)**
2	10.9	3.09	0.51	1.16	
10	17.791	4.59	0.1	0.90	9.35
12.5	20.569	3.75	0.4	4.16	
15	21.17	4.383	0.19	4.16	14.84
20	22.372	4.214	0.214	4.18	16.42
25	23.569	4.266	0.136	4.21	11.43
30	24.757	4.259	0.167	4.21	10.26
35	25.944	4.431	0.314	4.22	9.94
40	27.13	4.218	0.244	4.22	7.39
42.5	27.722	4.36	0.34	4.22	
45	28.315	4.138	0.393	4.37	8.67
50	29.46	4.044	0.383	4.39	6.86
55	30.599	3.846	0.298	4.81	8.47
60	31.639	3.89	0.34	5.15	6.53
65	32.609	3.627	0.335	5.34	9.99
70	33.545	4.218	0.446	5.80	6.9
72.5	33.976	4.15	0.54	5.80	
75	34.407	3.721	0.437	5.81	5.42
80	35.267	3.661	0.169	6.44	8.12
98	38.063	3.799	0.247	6.67	19.42
100	38.363	3.718	0.224	6.68	3.56
102.5	38.737	4.03	0.24	6.94	
105	39.097	3.914	0.093	6.97	2.7
110	39.814	4.207	0.31	7.01	5.9
115	40.527	4.206	0.543	7.19	23.73
120	41.222	4.278	0.523	7.20	15.25
125	41.916	4.128	0.464	7.36	14.05
130	42.595	3.994	0.544	7.37	5.98
132.5	42.934	3.589	-0.093	7.40	

Depth (cm)	Age (ka)	d18O	d13C	Sed Rate (cm/kyr)	Coarse Fraction (%)
135	43.272	3.985	0.511	7.47	4.62
140	43.941	3.993	0.395	7.53	1.87
145	44.605	3.732	0.392	7.56	0.71
150	45.266	4.097	0.342	7.65	0.71
155	45.92	4.271	0.445	7.66	4.2
160	46.573	4.152	0.472	7.74	6.74
162.5	46.896			7.76	
165	47.218	4.692	0.736	7.74	5.59
170	47.864			7.81	2.34
175	48.504			7.82	1.96
180	49.143			7.86	3.69
185	49.779	3.68	0.421	7.90	1.35
190	50.412	3.891	0.259	7.89	1.65
192.5	50.729	4.044	0.354	7.91	
195	51.045			7.96	3.15
200	51.673	3.7	0.26	7.95	1.6
205	52.302			8.00	2.62
210	52.927	3.78	0.34	8.00	2.13
215	53.552	3.84	0.31	8.04	3.22
220	54.174	3.82	0.25	8.04	6.41
225	54.796	3.78	0.23	8.06	8.48
230	55.416	3.69	0.11	8.08	7.57
235	56.035	3.85	0.14	8.09	3.21
242	56.9	3.69	-0.06	8.11	3.92
245	57.27	3.82	0.04	8.12	10.97
250	57.886	4.09	0.04	8.14	9.96
252.5	58.193	4.46	-0.002	8.14	
255	58.5	3.8	0.02	8.14	11.72
260	59.114	4.32	0.2	8.14	7.96
265	59.728	4.13	0.13	8.17	6.42
270	60.34	3.68	0.19	8.17	5.97
275	60.952	3.96	0.09	8.20	5.33
280	61.562	3.95	0.09	8.17	4.54
282.5	61.868	4.128	-0.056	8.20	
285	62.173	3.96	0.08	8.21	5.02
290	62.782	3.67	-0.02	8.21	3.45
295	63.391	3.67	-0.01	8.25	6.36
300	63.997	3.73	-0.03	8.26	29.67

Depth (cm)	Age (ka)	d18O	d13C	Sed Rate (cm/kyr)	Coarse Fraction (%)
305	64.602	3.53	-0.29	8.35	10.39
310	65.201	3.99	-0.01	8.45	12.61
312.5	65.497	4.239	0.064	8.47	
315	65.792	4.26	0.18	8.20	11.44
320	66.402	4.21	0.41	6.06	12.52
325	67.227	4.17	0.34	6.05	12.72
330	68.053	4.13	0.49	4.07	13.85
335	69.281	4.02	0.43	3.76	15.09
340	70.611	3.93	0.38	3.75	14.09
342.5	71.278	3.876	0.368	3.51	
345	71.991	3.72	0.4	3.51	6.16
350	73.417	3.63	0.51	3.58	4.2
355	74.814			3.83	2.8
360	76.118	3.51	0.38	3.83	2.05
365	77.423	3.88	0.55	4.94	5.23
370	78.436	3.75	0.58	5.01	12.33
372.5	78.935	3.801	0.568	5.01	
375	79.434	3.85	0.5	7.41	11.64
380	80.109	3.64	0.61	9.73	16.23
385	80.623	3.4	0.55	10.78	8.05
390	81.087	3.38	0.5	12.99	8.2
395	81.472	3.66	0.52	13.12	9.29
400	81.853	3.91	0.56	14.53	9.33
402.5	82.025	3.732	0.433	14.53	
405	82.197	3.77	0.62	14.49	8.27
410	82.542	3.74	0.58	15.20	8.9
415	82.871	3.75	0.64	15.34	4.02
420	83.197	3.8	0.51	15.58	2.25
425	83.518	3.77	0.68	15.82	5.02
430	83.834	3.53	0.5	15.82	3.27
432.5	83.992	3.848	0.529	16.03	
435	84.148	3.89	0.51	16.08	1.97
440	84.459	3.95	0.64	16.13	1.72
445	84.769	3.83	0.51	16.29	2.33
450	85.076	3.7	0.48	16.29	2.4
455	85.383	3.66	0.44	16.39	2.11
460	85.688	3.83	0.52	16.45	3.94
462.5	85.84	3.382	0.135	16.45	

Depth (cm)	Age (ka)	d18O	d13C	Sed Rate (cm/kyr)	Coarse Fraction (%)
465	85.992	3.7	0.48	16.50	3.43
470	86.295	3.64	0.5	16.50	3.24
475	86.598	3.81	0.61	16.56	2.09
480	86.9	3.51	0.48	16.61	3.76
485	87.201	3.63	0.44	16.61	2.67
490	87.502	3.66	0.5	16.67	2.53
492.5	87.652	3.436	0.212	16.67	
495	87.802	3.52	0.39	16.67	2.68
500	88.102	3.49	0.29	16.67	3.14
505	88.402	3.33	0.35	16.72	5.14
510	88.701	3.65	0.56	16.84	6.02
515	88.998	3.37	0.43	17.24	8.46
520	89.288	3.6	0.55	17.24	7.84
522.5	89.433	3.354	0.395	17.24	
525	89.578	3.55	0.54	18.59	10.69
530	89.847	3.64	0.58	18.66	11.94
535	90.115	3.7	0.58	19.69	12.89
540	90.369	3.33	0.41	20.16	4.23
545	90.617	3.64	0.58	20.83	6.35
550	90.857	3.74	0.68	21.93	7.62
552.5	90.971	3.99	0.69	21.93	
555	91.085	4.05	0.72	22.12	8.42
560	91.311	4.13	0.82	23.81	7.85
565	91.521	4.05	0.77	23.81	5.87
570	91.731	3.8	0.76	25.51	6.56
575	91.927	3.92	0.73	25.91	8.11
580	92.12	3.78	0.82	26.32	7.48
582.5	92.215	3.84	0.61	28.09	
585	92.304	3.87	0.75	28.09	4.56
590	92.482	3.8	0.65	28.90	7.76
595	92.655	3.74	0.61	30.67	2.44
600	92.818	3.89	0.9	30.67	3.12
605	92.981	3.75	0.67	33.33	5.86
610	93.131	4.24	0.53	33.33	3.64
612.5	93.206	4.07	0.54	33.33	
615	93.281	3.81	0.39	35.46	3.23
620	93.422	3.4	0.26	35.97	3
625	93.561	3.85	0.29	37.59	3.46

Depth (cm)	Age (ka)	d18O	d13C	Sed Rate (cm/kyr)	Coarse Fraction (%)
630	93.694			39.06	4.5
635	93.822	3.84	0.37	39.68	5.5
640	93.948	3.89	0.21	41.67	7.66
642.5	94.008			42.37	
645	94.067	4.03	0.33	42.02	4.54
650	94.186	3.84	0.21	44.25	3.36
655	94.299			45.05	3.23
660	94.41			46.30	2.17
665	94.518	3.94	0.45	47.17	2.45
670	94.624	4.08	0.47	47.17	2.93
672.5	94.677			49.02	
675	94.728	3.64	0.07	49.50	2.97
680	94.829	3.68	0.4	49.50	2.31
685	94.93	3.92	0.35	50.51	1.65
690	95.029	3.64	0.25	51.28	1.27
698	95.185	3.78	0.25	51.28	1.76
700	95.224	3.88	0.34	51.02	2.67
702.5	95.273	3.83	0.47	52.08	
705	95.321	3.76	0.4	51.55	1.8
710	95.418	3.75	0.26	51.02	1.9
715	95.516			51.02	1.91
720	95.614			50.51	0.86
725	95.713	3.79	0.27	50.00	0.79
730	95.813	3.75	0.36	49.02	1.18
732.5	95.864	3.94	0.33	48.08	
735	95.916	3.73	0.36	48.54	1.56
740	96.019			46.73	3.94
745	96.126			45.87	0.99
750	96.235	3.75	0.38	44.64	2.57
755	96.347	3.75	0.4	43.10	3.7
760	96.463	3.55	0.37	43.10	4.6
762.5	96.521	3.76	0.38	42.37	
765	96.58	3.67	0.37	39.68	4.64
770	96.706	3.42	0.3	39.68	1.73
775	96.832	3.65	0.23	37.31	1.61
780	96.966	3.75	0.32	36.50	1.76
785	97.103	3.91	0.07	34.72	1.45
790	97.247	3.7	0.22	33.33	1.12

Depth (cm)	Age (ka)	d18O	d13C	Sed Rate (cm/kyr)	Coarse Fraction (%)
792.5	97.322	3.75	0.48	33.33	
795	97.397	3.62	0.35	32.68	1.78
800	97.55	3.61	0.28	30.12	1.99
805	97.716	3.46	0.08	30.30	4.43
810	97.881	3.45	0.29	27.47	1.07
815	98.063	3.61	0.37	27.32	1.7
820	98.246	3.73	0.34	26.60	2.1
822.5	98.34	3.73	0.34	24.75	
825	98.441	3.57	0.1	24.75	2.46
830	98.643	3.7	0.31	23.81	2.04
835	98.853	3.67	0.48	22.32	2.91
840	99.077	3.58	0.47	22.22	3.05
845	99.302	3.65	0.3	20.16	2.31
850	99.55	3.52	0.28	20.16	2.56
852.5	99.674	3.31	0.29	20.16	
855	99.798	3.3	0.13	18.38	3.62
860	100.07	3.41	0.39	18.52	3.87
865	100.34	3.42	0.29	17.24	4.69
870	100.63	3.35	0.3	16.67	3.44
875	100.93	3.31	0.33	16.13	2.42
880	101.24	3.38	0.31	15.62	4.18
882.5	101.4	3.48	0.34	14.71	
885	101.57	3.25	0.28	15.62	2.01
890	101.89	3.38	0.27	15.15	0.87
895	102.22	3.35	0.34	15.15	1.63
900	102.55	3.49	0.45	15.15	2.27
905	102.88	3.52	0.48	15.15	2.28
910	103.21	3.61	0.58	15.62	3.69
912.5	103.37	3.61	0.25	14.71	
915	103.54	3.53	0.51	15.15	3.77
920	103.87	3.52	0.54	15.15	6.68
925	104.2	3.58	0.52	14.71	4.86
930	104.54			14.71	7.85
935	104.88	3.49	0.6	14.29	0
940	105.23	3.57	0.55	13.89	3.66
942.5	105.41	3.62	0.37	14.71	
945	105.58	3.49	0.37	12.20	5.02
950	105.99	3.68	0.48	10.87	6.97

Depth (cm)	Age (ka)	d18O	d13C	Sed Rate (cm/kyr)	Coarse Fraction (%)
955	106.45	3.74	0.43	8.20	14.4
960	107.06	3.7	0.48	4.72	11.09
965	108.12	3.46	0.47	4.72	8.97
970	109.18	3.65	0.48	4.24	4.74
972.5	109.77	3.15	-0.03	4.17	
975	110.37	3.55	0.41	4.17	9.96
980	111.57	3.62	0.57	4.13	5.45
985	112.78	3.6	0.46	4.10	2.44
990	114	3.97	0.58	1.86	3.73
995	116.69			1.01	5.06
1000	121.64			1.01	2.13
1002.5	124.11			1.30	
1005	126.03	3.8	0.22	-500.00	3.1
1010	126.02			-250.00	3.53
1015	126			250.00	2.41
1020	126.02	3.67	0.39	250.00	3.59
1025	126.04	3.95	0.39	166.67	2.66
1030	126.07	4.05	0.23	125.00	2.67
1032.5	126.09	3.35	0.21	250.00	
1035	126.1	3.62	0.13	125.00	2.94
1040	126.14	3.31	0.4	83.33	5.38
1045	126.2	3.44	0.23	83.33	5.84
1050	126.26	3.66	0.33	33.33	5.86
1055	126.41	3.1	0.41	35.71	9.4
1060	126.55	3.07	0.32	13.89	12.36
1062.5	126.73	2.97	0.33	7.58	
1065	127.06	3.54	0.35	7.58	36.84
1070	127.72	4.5	0.22	6.10	27.82
1075	128.54	4.5	0.05	4.76	7.07
1080	129.59	4.76	0.08	4.63	9.86
1085	130.67	4.74	0.14	3.70	7.51
1090	132.02	4.57	-0.14	3.68	9.34
1092.5	132.7	4.47	0.02	3.73	
1095	133.37	4.76	0.16	3.11	8.17
1100	134.98	4.56	0.02	3.01	8.69
1105	136.64	4.59	0.12	2.73	6.89
1110	138.47	4.54	0.04	2.55	5.74
1115	140.43	4.21	-0.02	2.45	6.84

Depth (cm)	Age (ka)	d18O	d13C	Sed Rate (cm/kyr)	Coarse Fraction (%)
1120	142.47	4.14	-0.02	2.21	5.09
1122.5	143.6	4.07	-0.14	2.19	
1125	144.74	4.28	-0.12	2.21	3.92
1130	147	4.08	-0.02	2.21	3.2
1135	149.26	3.55	-0.24	2.20	11.22
1140	151.53	3.89	0.01	2.21	9.79
1145	153.79	4.7	-0.06	2.20	11.13
1150	156.06	4.12	-0.28	2.21	10.73
1152.5	157.19	4.43	-0.2	2.21	
1155	158.32	4.56	-0.04	2.20	10.11
1160	160.59	4.36	-0.12	2.21	7.12
1165	162.85	4.21	0.01	2.20	9.44
1170	165.12	3.78	0.02	2.21	3.29
1175	167.38	4.11	0.07	2.21	1.71
1180	169.64	4.06	0.18	2.19	2.71
1182.5	170.78	4.17	-0.23	2.21	
1185	171.91	4.12	0.01	2.21	5.61
1190	174.17	4.14	0.05	2.20	9.44
1195	176.44	4.13	0.06	2.21	6
1200	178.7	4.31	0.03	2.20	4.47
1205	180.97	4.08	0.05	2.21	3.97
1210	183.23	4.33	0.03	2.21	6.68
1212.5	184.36	4.38	-0.04	2.21	
1215	185.49	4.47	0.2	2.20	4.84
1220	187.76	4.47	0.26	2.21	17.78
1225	190.02	4.19	0.03	2.20	6.77
1230	192.29	3.86	0.24	2.21	6.3
1235	194.55	3.89	0.16	2.20	3.49
1240	196.82	3.97	0.17	2.21	5.55
1242.5	197.95	3.98	-0.03	2.21	
1245	199.08	4	-0.02	2.20	2.65
1250	201.35	4.15	0.04	2.21	3.7
1255	203.61	4.08	-0.07	2.21	5.65
1260	205.87	4.07	0.04	2.20	5.79
1265	208.14	4.12	0.08	2.21	9.79
1270	210.4	3.82	-0.38	2.19	7.01
1272.5	211.54	3.98	-0.2	2.21	
1275	212.67	4.09	0.09	2.21	7.78

Depth (cm)	Age (ka)	d18O	d13C	Sed Rate (cm/kyr)	Coarse Fraction (%)
1280	214.93	4.22	0.03	2.20	9.92
1285	217.2	4.14	0.07	2.21	11.84
1290	219.46	4.17	-0.04	2.20	2.52
1295	221.73	3.8	0.5	2.21	1.67
1300	223.99	3.89	0.48	2.21	2.1
1302.5	225.12	3.88	0.09	2.21	
1305	226.25	4.13	0.35	2.20	6.24
1310	228.52	4.22	0.12	2.21	2.05
1315	230.78	4.29	0.13	2.20	3.36
1320	233.05	4.47	0.06	2.21	33.68
1325	235.31	3.95	-0.08	2.20	18.52
1330	237.58	4.45	0.29	2.21	20.67
1332.5	238.71	4.29	0.28	2.21	
1335	239.84	4.27	0.44	2.21	13.44
1340	242.1	4.11	0.66	2.20	8.67
1345	244.37	3.75	0.55	2.21	3.22
1350	246.63	3.78	0.45	2.20	9.05
1355	248.9	3.67	0.53	2.21	13.71
1360	251.16	3.51	0.61	2.21	12.59
1362.5	252.29	3.53	0.52	2.19	
1365	253.43	3.51	0.65	2.21	16.22
1370	255.69	3.31	0.54	2.20	15.13
1375	257.96	3.02	0.64	2.21	14.9
1380	260.22	3.2	0.67	2.21	16.38
1385	262.48	3.07	0.54	2.20	15.61
1390	264.75			2.21	10.11
1392.5	265.88	3.98	0.76	2.21	
1395	267.01	3.86	0.59	2.20	2.55
1400	269.28	3.99	0.99	2.21	4.97
1405	271.54			2.20	3.46
1410	273.81			2.21	5.82
1415	276.07	4.33	0.23	2.20	3.91
1420	278.34	4.55	0.22	2.21	2.96
1422.5	279.47	4.14	0.62	2.21	
1425	280.6			2.21	2.18
1430	282.86	4.46	0.12	2.20	1.6
1435	285.13	3.7	0.26	2.21	1.38
1440	287.39	3.91	0.42	2.20	8.97

Depth (cm)	Age (ka)	d18O	d13C	Sed Rate (cm/kyr)	Coarse Fraction (%)
1445	289.66			2.21	2.58
1450	291.92			2.21	1.78
1452.5	293.05			2.19	
1455	294.19			2.21	1.25
1460	296.45			2.21	1.31
1465	298.71	4.01	0.91	2.20	1.38
1470	300.98	3.9	0.73	2.21	1.48
1475	303.24			2.20	2.08
1480	305.51			2.21	1.83
1482.5	306.64			2.21	
1485	307.77	3.68	0.4	2.20	1.99
1490	310.04			2.21	2.75
1495	312.3			2.20	2.58
1500	314.57			2.21	3.2
1505	316.83	3.24	0.26	2.21	2.88
1510	319.09			2.19	3.28
1512.5	320.23			2.21	
1515	321.36	3.8	0.37	2.21	5.73
1520	323.62	3.3	0.38	2.20	10.18
1525	325.89	3.39	0.57	2.21	3.77
1530	328.15	3.37	0.67	2.20	6.67
1535	330.42	3.27	0.63	2.21	6.91
1540	332.68	3	0.56	2.21	11.22
1542.5	333.81	3.45	0.64	2.19	
1545	334.95	2.94	0.39	2.21	7.57
1550	337.21	3.06	0.42	2.21	13.34
1555	339.47	2.98	0.45	2.20	17.71
1560	341.74	3.11	0.4	2.21	26.3
1565	344	3.14	0.32	2.20	23.73
1570	346.27	3.14	0.15	2.21	11.19
1572.5	347.4			2.21	
1575	348.53	4.13	0.29	2.20	9.98
1580	350.8	4.5	0.36	2.21	8.17
1585	353.06	3.51	0.55	2.21	3.65
1590	355.32	3.09	0.43	2.20	2
1595	357.59	3.87	0.53	2.21	5.76
1600	359.85	3.99	0.49	2.19	3.11
1602.5	360.99	3.48	0.3	2.21	

Depth (cm)	Age (ka)	d18O	d13C	Sed Rate (cm/kyr)	Coarse Fraction (%)
1605	362.12	4.24	0.56	2.21	4.11
1610	364.38	4.13	0.65	2.20	3.44
1615	366.65	3.99	0.66	2.21	2.42
1620	368.91	3.34	0.19	2.20	2.05
1625	371.18	3.9	0.21	2.21	2.08
1630	373.44	3.34	0.3	2.21	1.07
1632.5	374.57	3.71	0.33	2.21	
1635	375.7			2.20	4.55
1640	377.97	3.8	0.47	2.21	0.94
1645	380.23	3.65	0.46	2.20	1.18
1650	382.5			2.21	1.34
1655	384.76	3.45	0.11	2.20	1.02
1660	387.03	3.61	0.37	2.21	1.64
1662.5	388.16	4.44	0.17	2.21	
1665	389.29	2.89	0.42	2.21	0.71
1670	391.55			2.20	3.23
1675	393.82	3.69	0.14	2.21	2.01
1680	396.08	3.99	0.49	2.20	2.12
1685	398.35			2.21	1.52
1690	400.61	3.79	0.36	2.21	1.91
1692.5	401.74			2.19	
1695	402.88	3.85	0.45	2.21	8.73
1700	405.14			2.20	1.42
1705	407.41			2.21	1.27
1710	409.67	3.72	0.26	2.21	0.76
1715	411.93	3.58	0.35	2.20	1.83
1720	414.2	3.77	0.53	2.21	2.17
1722.5	415.33	3.83	0.62	2.21	
1725	416.46	3.46	0.32	2.20	2.11
1730	418.73	3.8	0.21	2.21	1.58
1735	420.99	3.32	0.57	2.20	2.44
1740	423.26	3.13	0.46	2.21	2.01
1745	425.52	3.05	0.45	2.20	8.93
1750	427.79	2.97	0.34	2.21	16.07
1752.5	428.92	3.29	0.41	2.21	
1755	430.05	3.82	0.11	2.21	29.24
1760	432.31	3.87	0.11	2.20	8.41
1765	434.58	3.82	0.07	2.21	7.91

Depth (cm)	Age (ka)	d18O	d13C	Sed Rate (cm/kyr)	Coarse Fraction (%)
1770	436.84	3.74	0.11	2.20	3.7
1775	439.11	3.89	0.31	2.21	3
1780	441.37			2.21	1.5
1782.5	442.5			2.19	
1785	443.64			2.21	1.97
1790	445.9	3.75	0.51	2.21	3.04
1795	448.16	3.27	0.64	2.20	3.02
1800	450.43			2.21	2.79
1805	452.69	4.38	0.14	2.20	5.76
1810	454.96	4.26	-0.07	2.21	8.79
1812.5	456.09			2.21	
1815	457.22	4.57	0.08	2.20	4.22
1820	459.49			2.21	4.05
1825	461.75			2.20	2.52
1830	464.02			2.21	2.68
1835	466.28	4.04	0.14	2.21	4.31
1840	468.54	4.43	0.02	2.19	4.22
1842.5	469.68	4.56		2.21	
1845	470.81	4.51	-0.16	2.21	4.31
1850	473.07			2.20	4.41
1855	475.34			2.21	2.34
1860	477.6			2.20	3.29
1865	479.87	4.48	0.11	2.21	1.96
1870	482.13			2.21	3.2
1872.5	483.26	4.35		2.19	
1875	484.4	4.14	0.18	2.21	2.87
1880	486.66	4.09	0	2.21	2.29
1885	488.92	4.08	-0.12	2.20	1.95
1890	491.19	3.93	-0.07	2.21	5.04
1895	493.45	3.97	-0.05	2.20	3.67
1900	495.72	3.9	-0.18	2.21	8.32
1902.5	496.85	3.95		2.21	
1905	497.98	3.72	-0.33	2.20	5.41
1910	500.25	4.16	-0.26	2.21	15.12
1915	502.51	3.95	-0.24	2.21	18.36
1920	504.77	4.19	-0.21	2.20	3.27
1925	507.04	4.19	-0.21	2.21	4.76
1930	509.3	4.04	-0.36	2.19	3.55

Depth (cm)	Age (ka)	d18O	d13C	Sed Rate (cm/kyr)	Coarse Fraction (%)
1932.5	510.44	4.2	-0.42	2.21	
1935	511.57	4.22	-0.12	2.21	3.92
1940	513.83	4.12	-0.29	2.20	3.4
1945	516.1	4.05	-0.29	2.21	5.61
1950	518.36	3.87	-0.4	2.20	4.1
1955	520.63	3.9	-0.42	2.21	3.86
1960	522.89	4.06	-0.31	2.21	7.86
1962.5	524.02	3.93		2.21	
1965	525.15	4.01	-0.32	2.20	11.72
1970	527.42	4.42	-0.02	2.21	8.85
1975	529.68	4.23	0.22	2.20	13.27
1980	531.95	4.11	0.43	2.21	6.95
1985	534.21	4.06	0.44	2.20	4.26
1990	536.48	3.93	0.42	2.21	3.71
1992.5	537.61	3.93		2.21	
1995	538.74	3.98	0.4	2.20	6.65
2000	541.01	3.98	0.43	2.21	6.25
2005	543.27	3.64	0.24	2.21	2.37
2010	545.53	3.61	0.41	2.20	5.23
2015	547.8	3.59	0.43	2.21	2.83
2020	550.06	3.85	0.03	2.19	4.08
2022.5	551.2	4.11	0.37	2.21	
2025	552.33	3.9	0.1	2.21	0.64
2030	554.59	3.89	0.06	2.20	1.11
2035	556.86	3.87	0.14	2.21	0.4
2040	559.12	3.99	0.21	2.21	0.58
2045	561.38	3.87	0.3	2.20	0.56
2050	563.65	3.87	0.11	2.21	0.49
2052.5	564.78	4.19	0.44	2.21	
2055	565.91	3.88	0.16	2.20	0.61
2060	568.18	3.8	0.14	2.21	0.92
2065	570.44	3.892	0.101	2.20	0.93
2070	572.71	3.99	0.14	2.21	0.71
2075	574.97			2.20	0.94
2080	577.24			2.21	0.99
2082.5	578.37	3.99	0.01	2.21	
2085	579.5	3.28	0.42	2.21	1.13
2090	581.76			2.20	2.3

Depth (cm)	Age (ka)	d18O	d13C	Sed Rate (cm/kyr)	Coarse Fraction (%)
2095	584.03			2.21	1.34
2100	586.29	3.38	0.21	2.20	0.7
2105	588.56			2.21	1.13
2110	590.82	3.68	0.13	2.21	1.83
2112.5	591.95	3.63	0.18	2.19	
2115	593.09	3.54	0.29	2.21	1.84
2120	595.35	3.4	0.24	2.20	0.95
2125	597.62	3.57	0.34	2.21	4.79
2130	599.88	3.72	0.04	2.21	2.33
2135	602.14	3.52	0.07	2.20	2.04
2140	604.41	3.51	0.16	2.21	2.15
2142.5	605.54	3.56	0.24	2.21	
2145	606.67	3.31	-0.01	2.20	3.01
2150	608.94	3.53	0.11	2.21	3.27
2155	611.2	3.66	0.3	2.20	3.06
2160	613.47	3.88	0.38	2.21	8.42
2165	615.73	3.96	0.39	2.21	9.05
2170	617.99	4.03	0.53	2.19	16.75
2172.5	619.13	4.28	0.21	2.21	
2175	620.26	3.26	0.09	2.21	5.46
2180	622.52	3.63	0.24	2.20	3.72
2185	624.79	4.05	0.45	2.21	1.28
2190	627.05	3.92	0.35	2.20	0.58
2195	629.32	3.9	0.47	2.21	0.93
2200	631.58	3.92	0.51	2.21	1.78
2202.5	632.71	3.65	0.4	2.19	
2205	633.85	3.85	0.46	2.21	1.68
2210	636.11	3.62	0.25	2.21	0.32
2215	638.37	3.82	0.49	2.20	0.51
2220	640.64	3.53	0.26	2.21	1.02
2225	642.9	3.33	0.19	2.20	3.2
2230	645.17	3.07	0.02	2.21	3.59
2232.5	646.3	3.26	0.11	2.21	
2235	647.43	3.14	0.12	2.20	6
2240	649.7	3.12	-0.16	2.21	5.95
2245	651.96	3.68	0.23	2.20	8.51
2250	654.23	3.57	0.34	2.21	5.24
2255	656.49	3.34	0.14	2.21	6.29

Depth (cm)	Age (ka)	d18O	d13C	Sed Rate (cm/kyr)	Coarse Fraction (%)
2260	658.75	3.7	0.34	2.19	7.74
2262.5	659.89	4	0.35	2.21	
2265	661.02	3.7	0.18	2.21	3.2
2270	663.28	3.83	0.32	2.20	2.43
2275	665.55			2.21	2.43
2280	667.81			2.20	1.47
2285	670.08			2.21	2.15
2290	672.34			2.21	4.19
2292.5	673.47	3.3	0	2.21	
2295	674.6	3.3	0.16	2.20	3.39
2300	676.87	3.07	0.24	2.21	4.39
2305	679.13	3	0.26	2.20	11.27
2310	681.4	3.59	0.02	2.21	21.58
2315	683.66			2.20	3.79
2320	685.93	3.74	0.34	2.21	1.72
2322.5	687.06	3.45	0.37	2.21	
2325	688.19	3.75	0.13	2.20	1.42
2330	690.46	3.87	0.23	2.21	2.34
2335	692.72	3.78	0.05	2.21	2.25
2340	694.98			2.20	3.26
2345	697.25	4.03	0.3	2.21	1.57
2350	699.51			2.19	1.32
2352.5	700.65	2.63	0.19	2.21	
2355	701.78	3.192	0.558	2.21	1.55
2360	704.04	3.014	0.438	2.20	1.88
2365	706.31	2.462	0.244	2.21	9.28
2370	708.57	2.848	0.482	2.21	20.44
2373	709.93	2.833	0.09	71.43	5.3
MD2664 Downcore Data					
Depth (cm)	Age (ka)	d18O	d13C	Sed Rate (cm/kyr)	Coarse Fraction (%)
0	0	2.66	0.49	569.38	2.38
10	0.017563	2.50	0.47	569.38	3.14
20	0.035126	2.62	0.53	569.38	5.20
30	0.052689	2.45	0.52	569.38	5.03

Depth (cm)	Age (ka)	d18O	d13C	Sed Rate (cm/kyr)	Coarse Fraction (%)
40	0.070252	2.50	0.52	569.41	5.91
50	0.087814	2.67	0.59	569.28	3.28
60	0.10538	2.55	0.52	569.48	2.41
70	0.12294	2.63	0.63	518.13	4.76
80	0.14224	2.62	0.58	512.03	4.98
90	0.16177	2.60	0.63	511.77	4.73
100	0.18131	2.46	0.39	511.77	4.01
110	0.20085	2.58	0.50	511.77	4.85
120	0.22039	2.51	0.49	511.77	5.66
130	0.23993	2.56	0.47	512.03	5.17
140	0.25946	2.68	0.52	463.28	2.94
160	0.30263	2.64	0.61	457.46	3.06
170	0.32449	2.73	0.54	457.25	4.57
180	0.34636	2.69	0.52	457.25	4.49
190	0.36823	2.68	0.55	457.46	4.67
200	0.39009	2.63	0.59	457.25	1.97
210	0.41196	2.65	0.62	423.37	2.67
220	0.43558	2.61	0.65	405.84	2.28
230	0.46022	2.69	0.49	406.01	2.68
240	0.48485	2.77	0.63	405.84	4.04
250	0.50949	2.39	0.54	405.84	3.07
260	0.53413	2.32	0.45	405.84	3.39
270	0.55877	2.43	0.47	406.01	3.07
280	0.5834	2.65	0.68	379.65	4.02
290	0.60974	2.69	0.70	357.53	2.84
300	0.63771	2.72	0.69	357.53	2.14
310	0.66568	2.69	0.76	357.53	3.38
320	0.69365	2.64	0.46	357.53	6.80
330	0.72162	2.59	0.51	357.53	2.81
340	0.74959	2.63	0.57	357.53	3.04
350	0.77756	2.52	0.52	338.41	3.39
360	0.80711	2.59	0.60	312.21	2.95
370	0.83914	2.45	0.23	312.30	3.64
380	0.87116	2.48	0.44	312.21	3.66
390	0.90319	2.60	0.55	312.21	2.18
400	0.93522	2.75	0.48	312.21	3.79
410	0.96725	2.55	0.55	312.21	2.32
420	0.99928	2.61	0.55	300.12	2.44

Depth (cm)	Age (ka)	d18O	d13C	Sed Rate (cm/kyr)	Coarse Fraction (%)
430	1.0326	2.51	0.52	269.54	2.46
440	1.0697	2.61	0.57	270.27	1.68
450	1.1067	2.57	0.35	269.54	0.64
460	1.1438	2.59	0.57	270.27	1.47
470	1.1808	2.56	0.45	270.27	2.72
480	1.2178	2.66	0.53	269.54	1.30
490	1.2549	2.21	0.17	263.85	2.98
500	1.2928	2.34	0.08	230.95	3.04
510	1.3361	2.40	0.38	230.41	1.74
520	1.3795	2.37	0.43	230.95	2.61
530	1.4228	2.42	0.40	230.95	2.06
540	1.4661	2.50	0.28	230.41	1.11
550	1.5095	2.41	0.31	230.95	1.66
560	1.5528	2.43	0.42	229.89	1.03
570	1.5963	2.34	0.20	194.93	1.70
580	1.6476	2.43	0.35	194.55	1.55
590	1.699	2.30	0.17	194.55	1.33
600	1.7504	2.34	0.19	194.93	1.24
610	1.8017	2.29	0.23	194.55	1.48
620	1.8531	2.48	0.24	194.55	1.89
630	1.9045	2.46	0.34	194.93	1.63
640	1.9558	2.32	0.18	164.47	1.67
650	2.0166	2.51	0.32	161.55	1.08
660	2.0785	2.61	0.27	161.81	1.09
670	2.1403	2.51	0.32	161.55	0.21
680	2.2022	2.58	0.35	161.55	0.87
690	2.2641			161.81	0.60
700	2.3259	2.40	0.08	161.55	3.63
710	2.3878	2.43	0.22	137.36	2.66
720	2.4606	2.34	0.06	131.75	2.07
730	2.5365	2.45	0.31	131.58	2.03
740	2.6125	2.49	0.35	131.67	2.10
760	2.7644	2.34	0.08	131.75	2.80
770	2.8403	2.47	0.25	131.58	2.60
780	2.9163	2.33	0.00	112.74	4.31
790	3.005	2.38	0.11	104.82	2.15
800	3.1004	2.29	0.21	104.71	1.94
810	3.1959	2.38	0.10	104.71	2.15

Depth (cm)	Age (ka)	d18O	d13C	Sed Rate (cm/kyr)	Coarse Fraction (%)
820	3.2914	2.62	0.30	104.82	
830	3.3868	2.44	0.09	104.71	1.32
840	3.4823	2.48	0.23	104.71	1.18
850	3.5778	2.40	0.10	90.58	1.33
860	3.6882	2.40	-0.03	80.91	1.26
870	3.8118	2.48	0.05	80.91	1.18
900	4.1826	2.42	0.05		
900	4.1826	2.63	0.35	80.84	1.19
910	4.3063	2.37	0.06	80.91	0.77
920	4.4299	2.38	0.11	70.92	1.09
930	4.5709	2.48	0.03	60.10	0.68
940	4.7373	2.51	0.03	60.10	0.92
950	4.9037	2.48	0.14	60.13	1.57
960	5.07	2.75	-0.78		0.13
960	5.07	2.37	0.15	60.10	1.19
970	5.2364	2.29	0.27	60.10	0.51
980	5.4028	2.37	0.06	60.13	0.01
990	5.5691			53.68	0.01
1000	5.7554			42.39	0.40
1010	5.9913	2.39	0.40	42.39	0.40
1020	6.2272	2.53	0.03	42.39	1.36
1030	6.4631	2.50	-0.08	42.37	0.57
1040	6.6991			42.39	0.52
1050	6.935	2.44	-0.13	42.39	2.10
1060	7.1709	2.41	0.00	39.02	2.41
1070	7.4272	2.60	0.18	27.73	0.66
1100	8.5092	2.77	0.01	27.73	0.85
1110	8.8698	2.66	0.00	27.72	2.00
1120	9.2305	2.67	-0.25	27.73	1.97
1130	9.5911	2.88	-0.11	19.93	3.12
1160	11.096	3.34	0.27	17.61	2.02
1170	11.664	3.53	0.18	17.61	4.60
1200	13.368	3.47	0.09	17.61	0.68
1210	13.936	3.36	-0.07	16.23	0.68
1220	14.552	2.93	-0.13	16.10	0.81
1230	15.173	4.50	-0.05	16.10	9.94
1240	15.794	4.59	0.01	16.13	1.70
1250	16.414	4.70	-0.02	16.10	5.08

Depth (cm)	Age (ka)	d18O	d13C	Sed Rate (cm/kyr)	Coarse Fraction (%)
1260	17.035	4.70	0.07	16.10	11.83
1270	17.656	4.46	-0.09	16.13	18.83
1280	18.276	4.46	0.00	5.56	10.36
1290	20.074	4.42	0.20	4.76	9.53
1300	22.173	4.26	0.27	4.76	9.04
1310	24.272	4.32	0.45	4.76	5.18
1320	26.371	4.36	0.61	4.76	5.35
1330	28.47	4.49	-0.20	4.76	4.46
1340	30.569	4.19	0.47	4.76	7.15
1350	32.668	3.74	0.46	4.68	6.87
1360	34.805	3.73	0.09	4.64	25.24
1370	36.96	3.80	0.21	4.64	10.51
1380	39.116			4.64	8.55
1390	41.271			4.64	2.02
1400	43.427	4.04	0.21	4.64	0.96
1410	45.582	3.86	0.59	4.64	4.81
1420	47.738	4.52	0.39	4.74	8.91
1430	49.847	4.37	0.26	4.83	5.39
1440	51.917	3.76	0.22	4.83	6.21
1450	53.988	3.83	0.18	4.83	8.36
1460	56.059	3.80	0.03	4.83	5.68
1470	58.13	4.00	0.00	4.83	7.03
1480	60.201	4.34	0.06	4.83	10.57
1490	62.271	3.93	-0.08	5.40	4.43
1500	64.124	3.75	-0.10	6.40	7.81
1510	65.687	4.17	-0.07	6.40	8.92
1520	67.249			6.40	6.79
1530	68.811			6.40	8.65
1540	70.374	3.64	0.50	6.40	0.73
1550	71.936	3.68	0.40	6.40	1.31
1560	73.499	3.86	0.58	8.31	8.37
1570	74.703	3.68	0.64	25.51	3.57
1580	75.095	3.57	0.59	25.51	1.68
1590	75.487	3.67	0.64	25.51	1.22
1600	75.879	4.01	0.64	25.45	5.45
1610	76.272	4.13	0.53	25.51	8.23
1620	76.664	4.12	0.79	25.51	2.65
1630	77.056	3.99	0.87	28.41	26.40

Depth (cm)	Age (ka)	d18O	d13C	Sed Rate (cm/kyr)	Coarse Fraction (%)
1640	77.408			58.82	1.49
1650	77.578	3.51	0.27	58.82	1.55
1660	77.748	3.40	0.31	58.82	1.12
1670	77.918	3.48	0.36	59.17	1.42
1680	78.087	3.56	0.36	58.82	0.52
1690	78.257	3.41	0.22	58.82	1.63
1700	78.427	3.31	0.24	44.64	1.37
1710	78.651	3.32	0.26	9.63	1.37
1720	79.689	3.16	0.36	9.62	0.68
1730	80.728	3.21	0.16	9.62	0.52
1740	81.767	3.51	0.10	9.62	0.56
1750	82.806	3.57	0.39	9.62	2.33
1760	83.845	3.29	0.23	9.62	0.41
1770	84.884	3.57	0.55	9.62	1.00
1780	85.923	3.86	0.52	8.55	
1790	87.093	3.83	0.57	8.49	0.95
1800	88.271	3.96	0.49	8.48	0.54
1810	89.45	4.04	0.73	8.49	0.72
1820	90.628	3.72	0.60	8.48	1.22
1830	91.807	3.78	0.61	8.49	1.67
1840	92.985	3.66	0.61	8.48	1.10
1850	94.164	3.64	0.61	21.83	0.76
1860	94.622	3.55	0.62	33.67	2.81
1870	94.919	3.46	0.20	33.67	5.72
1880	95.216	3.74	0.40	33.67	3.20
1890	95.513	3.65	-0.06	33.67	2.37
1900	95.81	3.72	0.17	33.67	0.47
1910	96.107	3.70	0.41	33.78	1.68
1920	96.403	3.73	0.07	34.60	1.18
1930	96.692	3.63	0.35	35.09	0.89
1940	96.977	3.87	0.29	34.97	0.85
1950	97.263	3.74	0.40	35.09	1.77
1960	97.548	3.82	0.25	35.09	1.18
1970	97.833	3.92	0.41	35.09	1.83
1980	98.118	3.64	0.18	34.97	1.92
1990	98.404	3.66	0.01	36.76	0.51
2000	98.676			38.17	1.03
2010	98.938	3.91	0.44	38.17	2.73

Depth (cm)	Age (ka)	d18O	d13C	Sed Rate (cm/kyr)	Coarse Fraction (%)
2020	99.2	3.58	0.31	38.17	4.48
2030	99.462	3.66	0.31	38.17	0.75
2040	99.724	3.66	0.29	38.17	0.64
2050	99.986	3.55	0.15	37.88	0.95
2060	100.25	3.57	0.25	43.48	0.82
2070	100.48	3.32	0.20	52.63	1.10
2080	100.67	3.70	0.33	50.00	1.11
2090	100.87	3.69	0.16	52.63	9.20
2100	101.06	3.79	0.22	50.00	1.71
2110	101.26	3.68	0.34	52.63	1.13
2120	101.45	3.60	0.20	50.00	1.16
2130	101.65	3.55	0.25	55.56	0.96
2140	101.83	3.68	0.24	71.43	1.03
2150	101.97	3.22	0.39	66.67	0.87
2160	102.12	3.63	0.35	71.43	4.19
2170	102.26	3.49	0.37	66.67	2.59
2180	102.41	3.60	0.35	66.67	3.02
2190	102.56	3.54	0.09	71.43	2.10
2200	102.7	3.48	0.26	62.50	5.62
2210	102.86	3.61	0.39	45.45	4.29
2220	103.08	3.60	0.47	45.45	8.29
2230	103.3	3.52	0.25	45.45	4.98
2240	103.52	3.63	0.33	45.45	5.45
2250	103.74	3.65	0.47	45.45	3.42
2260	103.96	3.41	0.29	45.45	2.19
2270	104.18			37.04	1.21
2280	104.45	3.27	0.10	11.63	1.58
2290	105.31	3.51	0.29	11.49	0.65
2300	106.18	3.77	0.53	11.63	1.73
2310	107.04	3.53	-0.04	11.63	1.25
2320	107.9	3.65	0.22	11.49	1.24
2330	108.77	3.53	-0.29	11.63	1.46
2340	109.63	3.47	-0.15	11.63	2.42
2350	110.49	3.58	0.01	14.08	2.01
2360	111.2	3.45	0.10	14.29	6.37
2370	111.9	3.51	0.10	14.29	4.13
2380	112.6	3.38	0.18	14.49	5.79
2390	113.29	2.99	0.36	14.29	3.60

Depth (cm)	Age (ka)	d18O	d13C	Sed Rate (cm/kyr)	Coarse Fraction (%)
2400	113.99	2.61	0.02	14.29	2.83
2410	114.69	2.64	-0.04	14.29	4.01
2420	115.39	2.72	0.25	37.04	1.26
2430	115.66	2.44	0.09	52.63	9.13
2440	115.85			55.56	1.06
2450	116.03	2.46	0.20	55.56	4.66
2460	116.21	2.49	0.18	52.63	10.71
2470	116.4	2.45	0.33	55.56	9.09
2480	116.58	2.65	0.30	52.63	7.05
2490	116.77	2.26	0.32	58.82	7.73
2500	116.94	2.39	0.29	62.50	9.67
2510	117.1	2.59	0.29	62.50	7.50
2520	117.26	2.50	0.27	58.82	2.36
2530	117.43	2.40	0.17	62.50	11.53
2540	117.59	2.70	0.29	62.50	4.52
2550	117.75	2.44	0.19	58.82	1.94
2560	117.92	2.54	0.30	45.45	9.36
2570	118.14	2.57	0.26	40.00	9.48
2580	118.39	2.34	-0.01	38.46	10.41
2590	118.65	2.56	0.08	38.46	8.11
2600	118.91	2.46	0.17	38.46	6.42
2610	119.17	2.61	0.32	38.46	5.88
2620	119.43	2.58	0.24	38.46	4.54
2630	119.69	2.50	0.23	32.26	3.88
2640	120	2.56	0.27	28.57	2.78
2650	120.35	2.62	0.15	27.78	1.90
2660	120.71	2.56	0.26	28.57	3.41
2670	121.06	2.45	0.12	27.78	0.72
2680	121.42	2.54	0.14	28.57	1.87
2690	121.77	2.38	-0.04	27.78	0.46
2700	122.13	2.60	-0.03	27.78	0.26
2710	122.49	2.42	-0.07	27.03	1.27
2720	122.86	2.43	-0.02	26.32	0.74
2730	123.24	2.44	0.06	27.03	0.29
2740	123.61	2.31	-0.18	26.32	0.34
2750	123.99	2.46	-0.19	27.03	0.39
2760	124.36			26.32	0.17
2770	124.74	2.49	-0.30	20.41	0.99

Depth (cm)	Age (ka)	d18O	d13C	Sed Rate (cm/kyr)	Coarse Fraction (%)
2780	125.23			11.24	0.12
2790	126.12			11.24	0.02
2800	127.01	3.40	-0.06	11.24	0.05
2810	127.9	2.85	-0.10	11.11	11.58
2820	128.8	4.09	-0.03	11.24	6.22
2830	129.69	4.64	0.03	11.24	11.29
2840	130.58	4.71	-0.02	9.35	8.40
2850	131.65	4.78	-0.04	3.77	8.69
2860	134.3	4.36	-0.22	3.77	0.34
2870	136.95	4.45	-0.28	3.77	0.26
2880	139.6	4.33	-0.18	3.77	1.29
2890	142.25	3.99	-0.33	3.77	0.59
2900	144.9	3.53	-0.33	3.77	8.32
2910	147.55	4.28	-0.22	3.77	9.79
2920	150.2	4.60	-0.22	2.26	9.38
2930	154.63	4.28	-0.24	2.24	11.06
2940	159.09	4.30	-0.12	2.24	5.09
2950	163.55	4.36	0.00	2.24	7.14
2960	168.02	3.95	-0.06	2.24	2.62
2970	172.48	4.32	-0.13	2.24	13.80
2980	176.95	4.28	-0.17	2.24	10.68
2990	181.41	4.19	-0.31	2.84	3.10
3000	184.93	4.35	-0.21	2.99	10.03
3010	188.28	4.52	0.14	2.98	9.40
3020	191.64	3.93	0.14	2.98	0.50
3030	195	3.48	0.29	2.98	0.61
3040	198.36	3.63	0.34	2.98	10.89
3050	201.72	3.52	0.37	2.98	8.69
3060	205.08	3.24	0.41	4.90	1.95
3070	207.12	3.33	0.41	6.37	0.53
3080	208.69			6.33	0.26
3090	210.27	2.90	0.22	6.37	0.57
3100	211.84	3.08	0.13	6.37	0.51
3110	213.41	2.90	0.19	6.37	0.60
3120	214.98	3.05	0.04	6.37	0.75
3130	216.55	3.07	0.28	11.24	5.14
3140	217.44	3.44	0.00	21.28	2.70
3150	217.91	3.53	0.16	21.74	1.40

Depth (cm)	Age (ka)	d18O	d13C	Sed Rate (cm/kyr)	Coarse Fraction (%)
3160	218.37			21.74	1.10
3170	218.83			21.28	1.26
3180	219.3			21.74	0.35
3190	219.76			21.74	0.65
3200	220.22	3.83	0.12	11.36	1.21
3210	221.1	3.61	0.19	7.69	11.51
3220	222.4			7.69	0.49
3230	223.7	3.72	0.02	7.69	0.93
3240	225	3.82	0.23	7.63	0.56
3250	226.31			7.69	2.17
3260	227.61	3.41	0.23	7.69	0.82
3270	228.91			8.20	0.95
3280	230.13	3.28	0.31	9.09	0.32
3290	231.23	3.42	0.13	9.17	0.49
3300	232.32	3.56	0.39	9.09	0.56
3310	233.42	3.19	0.17	9.17	0.43
3320	234.51	3.28	0.27	9.17	0.27
3330	235.6	3.61	0.39	9.09	0.61
3340	236.7	3.21	0.29	9.62	0.35
3350	237.74	2.90	0.06	11.24	0.84
3360	238.63	3.28	0.45	11.36	0.70
3370	239.51	3.26	0.46	11.24	0.58
3380	240.4	3.14	0.50	11.24	0.45
3390	241.29	3.16	0.41	11.36	0.92
3400	242.17	2.99	0.28	11.24	0.60
3410	243.06	2.91	0.11	11.11	1.36
3420	243.96	2.88	-0.02	9.90	1.52
3430	244.97	2.99	0.27	10.00	2.33
3440	245.97	3.05	0.29	9.90	0.98
3450	246.98	3.26	0.37	10.00	0.89
3460	247.98	3.12	0.40	9.90	0.70
3470	248.99	3.05	0.22	10.00	0.60
3480	249.99	3.03	0.28	9.90	2.18
3490	251	2.94	0.14	9.90	0.78
3500	252.01	3.00	0.27	11.24	1.65

6.4 Appendix 4

NPL- N. pachyderma (s) *PW- P. wuellerstorfi* *BUL- G. bulloides*

Depth(cm)	Age (ka)	d13C NPL	d18O NPL	d13C PW	d18O PW	d13C BUL	d18O BuL
0	7.25	0.52	2.52	1.4	2.85	-0.43	2.03
3	7.56	0.48	2.53	1.44	2.95	-0.65	2.02
4	7.66	0.57	2.77	1.32	3.17	-0.13	1.98
5	7.75	0.42	2.73	1.15	3.02	-0.52	2.39
6	7.84	0.51	2.93	1.18	3.3	-0.45	2.27
7	7.92	0.57	2.9	1.39	3.34	-0.53	2
8	7.99	0.51	2.83	1.26	2.94	-0.57	2.21
9	8.05	0.49	2.63	1.14	2.73	-0.63	2.41
10	8.10	0.57	2.68	0.52	2.77	-0.44	2.16
11	8.14	0.53	2.56	1.1	2.78	-0.79	2.04
12	8.18	0.51	2.63	0.66	2.96	-0.68	2.17
13	8.21	0.47	2.58	1.39	3.04	-0.63	2.25
14	8.23	0.52	2.61	1.5	2.88	-0.27	2.23
15	8.25	0.57	2.68	1.21	2.74	-0.51	2.15
16	8.28	0.49	2.69	1.27	3.02	-0.5	2
17	8.30	0.39	2.95	1.25	2.87	-0.24	2.28
18	8.32	0.27	3.34	0.63	3.31	-0.66	2.07
19	8.34	0.24	3.36	0.8	3.56	-0.58	1.83
20	8.38	0.33	3.23	0.89	3.5	-0.5	1.88
21	8.41	0.13	3.47	0.67	3.52	-0.05	2.2
22	8.45	0.34	3.24	1.06	3.34	-0.78	2.08
23	8.50	0.23	3.42	0.85	3.54	0.06	2.23
24	8.56	0.29	3.33	0.92	3.25	-0.46	2.47
25	8.63	0.32	3.26	0.97	3.31	-0.25	1.98
26	8.71	0.39	3.06	1.21	3.28	-0.39	2.43
27	8.78	0.36	3.22	1.32	3.23	-0.4	2.19
28	8.86	0.3	3.5	1.09	3.41	-0.24	1.9
29	8.94	0.37	2.92	0.93	2.94	-0.4	2.14
30	9.02	0.35	3.13	1.08	3.18	-0.36	2.1
31	9.11	0.32	3.46	1.19	3.14	-0.32	2.29
32	9.19	0.39	2.97	1.3	3.22	-0.71	2.16
33	9.28	0.4	3.4			-0.42	2.16
34	9.38	0.35	3.48	0.71	3.46	-0.23	2.29
35	9.48						
36	9.59	0.36	3.29	1.03	3.11	-0.39	2.21
37	9.71	0.37	3.43	1.29	3.2	-1.16	2.07
38	9.85	0.29	3.68	1.35	3.49	-0.42	2.2
39	10.03	0.25	3.67			-0.95	2.09
40	10.24	0.34	3.26	1.39	3.18	-0.71	1.79
41	11.96	0.35	3.2	1.42	3.25	-0.43	2.25

Depth(cm)	Age (ka)	d13C NPL	d18O NPL	d13C PW	d18O PW	d13C BUL	d18O BuL
42	11.99	0.35	2.91	0.73	3.02	-0.54	2.04
43	12.01	0.52	2.95	1.4	3.06	-0.15	2.07
44	12.04	0.36	3.33	0.7	3.21	-0.73	2.14
45	12.07	0.45	2.89				
46	12.10	0.34	3.18	0.92	3.69	-0.48	2.11
47	12.12	0.56	3.34	0.53	3.51	-0.31	2.26
48	12.15	0.29	3.7	0.73	3.76	-0.75	2.17
49	12.18	0.25	3.66	0.87	3.49		
50	12.21	0.04	3.6			-1.26	3.27
51	12.23	0.96	3.79			-0.72	2.93
52	12.26	0.26	3.74			-0.8	2.8
53	12.29	0.21	3.64	1.16	3.59	-0.88	2.66
54	12.32	0.17	3.53			-0.48	2.21
55	12.34	0.19	3.45	0.95	2.94	-0.39	2.36
56	12.37	0.19	3.45	0.72	3.73	-0.25	1.8
57	12.40	0.3	3.44	1.06	3.72	-0.34	2.16
58	12.43	0.14	3.95			-0.76	2.42
59	12.45	0.26	3.94	-0.01	3.96	-0.32	2.37
60	12.48	0.29	3.83			-0.21	2.6
61	12.51	0.32	3.92			-0.69	1.34
62	12.54	0.15	3.9				
63	12.56	0.23	3.79	1.12	3.91	-1.09	2.85
64	12.59	0.44	3.63				
65	12.62	0.72	2.95	0.87	3.73	-0.44	2
66	12.65	0.71	2.95	1.3	3.16	-0.19	2.14
67	12.68	0.74	3.35			-0.22	2.55
68	12.70	0.75	3.32			-0.34	2.61
69	12.73	0.39	3.85	1.12	3.36	-0.09	2.82
70	12.76	0.51	3.75	0.93	3.5	0.15	2.28
71	12.79	0.36	3.78	0.67	3.98		
72	12.81	0.64	3.73	0.84	3.76	-0.44	2.53
73	12.84	0.05	3.18			-0.78	3.27
74	12.87	0.09	3.35			-0.55	3.21
75	12.90	-0.13	3.36			-1.02	3.39
76	12.92	0.2	3.92			-1.09	3.25
77	12.95	0.13	3.85			-0.03	2.86
78	12.98	0.15	3.79			-0.98	3.2
79	13.01	0.12	3.67				
80	13.03	0.05	3.76	1.16	3.51	-0.45	2.82
81	13.06	-0.06	3.53			-0.44	2.34
82	13.09	0.01	3.59			-0.57	2.3
83	13.12	-0.1	3.65				
84	13.14	0.23	3.34			-0.56	2.46

Depth(cm)	Age (ka)	d13C NPL	d18O NPL	d13C PW	d18O PW	d13C BUL	d18O BuL
85	13.17	0.02	3.17				
86	13.20	0.19	3.89			-1.56	2.07
87	13.23	0.12	3.67			-1.56	2.86
88	13.25	0.07	3.77	1.18	3.58	-1.15	2.65
89	13.28	0.05	3.75	0.81	3.56	-1.04	2.61
90	13.31	0.07	3.63	0.91	3.82		
91	13.34	0.15	3.82				
92	13.36	0.07	3.67			-1.33	2.78
93	13.39	-0.37	3.22			-1.06	2.51
94	13.42	0.07	3.62			-0.85	2.38
95	13.45	-0.05	3.84	1.12	3.79	-0.89	2.54
96	13.47	0.23	3.69	0.95	3.82	-0.92	2.67
97	13.50	0.21	3.6			-0.79	2.75
98	13.53	0.06	3.63			-0.94	3.3
99	13.56	-0.02	3.4			-0.78	3.36
100	13.58	0.18	3.59			-1.07	3.65
101	13.61	0.21	3.53	1.22	3.37	-0.67	2.7
102	13.64	0.11	3.48			-1.14	3.14
103	13.67	0.16	3.5			-0.72	2.76
104	13.69	0.02	3.57				
105	13.72	-0.16	3.07	1.09	3.59	-1.45	3.21
106	13.75	0.15	3.38	1.32	3.59	-0.37	2.88
107	13.78	-0.1	3.09			-0.58	2.08
108	13.81	0.1	3.15			-0.81	2.87
109	13.83	0.23	3.6	0.9	3.49	-0.85	2.83
110	13.86	0.14	3.64			-0.72	3.16
111	13.89	0.2	3.64	0.99	3.65	-0.85	3.44
112	13.92	0.09	3.72			-0.9	2.68
113	13.94	0.07	3.69				
114	13.97	-0.12	3.44			-0.71	3.11
115	14.00	-0.17	3.36				
116	14.03	-0.05	3.69			-0.98	3.43
117	14.05	-0.12	3.44			-1.15	3.27
118	14.08	-0.39	3.12			-1.58	3.13
119	14.11	-0.21	3.31			-1.37	3.58
120	14.14	-0.08	3.6	1.09	3.63	-1.29	3.26
121	14.16	-0.11	3.39			-1.25	3.17
122	14.19	-0.1	3.38			-1	3.26
123	14.22	-0.13	3.43			-0.86	3.04
124	14.25						
125	14.27	-0.11	3.39	-0.23	3.37	0.39	4.01
126	14.28	-0.21	3.42	-0.17	3.64	-0.99	2.89

Depth(cm)	Age (ka)	d13C NPL	d18O NPL	d13C PW	d18O PW	d13C BUL	d18O BuL
128	14.30	-0.28	3.63	-0.36	4.13	-1.05	3.37
129	14.31	-0.02	3.75	0.35	3.74	-1.2	3.22
130	14.31	-0.18	3.66			-1.6	3.52
131	14.44	-0.22	3.63			-1.15	3.14
132	14.58	-0.03	3.53	0.39	4.01	-1.56	3.18
133	14.71	-0.1	3.66	-0.19	4.19	-1.15	3.34
134	14.84	-0.18	3.56	0.15	4.02	-0.89	3.55
135	14.97	-0.1	3.79	0.26	4.09	-1.11	3.49
136	15.11	-0.08	3.65	-0.06	3.51	-0.85	3.14
137	15.24	-0.1	3.63	0.1	3.7	-0.79	2.93
138	15.37	-0.21	3.3	0.97	3.35	-0.66	3.05
139	15.50	-0.11	3.67	0.08	3.88	-1.18	2.96
140	15.64	-0.17	3.38	0.24	4.16	-1.28	3.23
141	15.77	0.02	3.84	0.28	4.25	-0.99	3.22
142	15.90	-0.31	3.55	0.43	3.77	-2.42	2.58
143	16.03	-0.2	3.35	0.56	3.71	-0.73	3.1
144	16.17	-0.06	3.86	0.29	3.95	-1.17	2.8
145	16.30	0.03	4.25	0.1	4.22	-0.69	1.67
146	16.43	-0.07	3.99	0.15	4.37	-0.34	3.28
147	16.56	-0.01	4.31	-0.22	4.02	-0.38	2.67
148	16.70	0	4.71	-0.02	4.09	-0.89	2.71
149	16.83	-0.04	4.14	-0.08	4.49	-0.76	3.11
150	16.96	-0.08	4.53	-0.01	4.77	-0.41	4.03
151	17.09	-0.04	4.76			-0.68	4.62
152	17.23	-0.11	4.65	0.1	4.67	-1.49	3.69
153	17.36	-0.03	4.5	-0.1	4.8	-0.68	4.03
154	17.49	-0.15	4.52	0.16	4.66	-0.96	2.99
155	17.62	0.01	4.85				
156	17.76	0.04	4.63	0.15	4.46	-0.3	3.78
157	17.89	0.19	4.73	0.56	4.69	-0.77	3.75
158	18.51	0.14	4.73	0.8	4.72		
159	18.55			0.71	4.85	-0.8	4.39
160	18.60	0.07	4.72	0.75	4.72	-0.44	3.22
161	18.65	-0.03	4.68	0.43	4.68	-1	4.65
162	18.70	0.05	4.73	0.97	4.4	-0.28	3.71
163	18.74	-0.04	4.58				
164	18.79	-0.11	4.53			-0.73	2.76
165	18.84	-0.01	4.48	0.52	4.54	-0.96	2.22
166	18.89	-0.12	4.75	0.34	4.47	0.08	3.47
167	18.93	-0.1	4.69	0.29	4.34	-0.62	3.48
168	18.98	0.01	4.6	1.12	4.33	-0.28	4.39
169	19.03	-0.02	4.54			-0.49	4.41
170	19.07	-0.12	4.52	0.39	4.44	-0.43	4.68

Depth(cm)	Age (ka)	d13C NPL	d18O NPL	d13C PW	d18O PW	d13C BUL	d18O BuL
171	19.12	-0.02	4.65	0.32	4.51	-0.87	4.02
172	19.17	-0.39	4.27	0.27	4.45	-0.7	3.97
173	19.22	-0.03	4.692	0.21	4.401		
174	19.26	-0.025	4.595	0.515	4.483		
175	19.31	-0.053	4.591	0.232	4.552		
176	19.36	0.008	4.631	0.466	4.527	-0.39	2.707
177	19.41	0.085	4.594				
178	19.45	-0.017	4.591	0.328	4.509		
179	19.50	0.064	4.65	0.656	4.737	-0.678	2.76
180	19.55	0.038	4.832	0.581	4.636	-0.574	3.079
181	19.59	-0.362	4.788	0.566	4.796	-0.236	4.658
182	19.64	-1.669	4.706	0.58	4.669	-0.917	3.265
183	19.69	-0.595	4.76	0.587	4.612	-1.051	2.316
184	19.74	-0.939	4.534	0.266	4.142	-0.702	3.012
185	19.78	-1.411	4.53	0.573	4.568	-0.134	3.23
186	19.83	-1.266	4.614	0.546	4.667	-0.092	3.658
187	19.88	-1.533	4.58	0.04	4.287	-1.086	3.16
188	19.93	0.168	4.483	0.347	4.565	-0.838	2.353
189	19.97	0.042	4.861	0.637	4.662	-0.557	2.665
190	20.02	-0.039	4.836	0.585	4.621	-0.067	2.215
Depth(cm)	**Age (ka)**	**%CF**	**%CaCO3**				
0	7.25	62.08	26.15				
3	7.56	57.86	21.28				
4	7.66	34.22	11.41				
5	7.75	35.61	14.49				
6	7.84	32.37	8.3				
7	7.92		9.49				
8	7.99	25.19	10.06				
9	8.05	17.19	10.78				
10	8.10	18.73	10.23				
11	8.14	17.48	9.79				
12	8.18		10.59				
13	8.21	23.26	10.9				
14	8.23	21.75	11.01				
15	8.25	14.39	9.95				
16	8.28	21.98	10.09				
17	8.30	30.61	10.36				
18	8.32	31.24	12.91				
19	8.34	31.44	11.82				
20	8.38	31.36	10.12				
21	8.41	28.41	11.91				
22	8.45	41.68	11.08				

Depth(cm)	Age (ka)	%CF	%CaCO3
23	8.50	22.37	11.63
24	8.56	36.8	12.85
25	8.63	43.18	10.99
26	8.71	24.09	11.36
27	8.78	14.52	10.54
28	8.86	10.85	11
29	8.94	21.89	11.87
30	9.02	11.68	12.11
31	9.11	12.78	12.42
32	9.19	11.17	9.75
33	9.28	8.52	10.85
34	9.38	10.89	12.69
35	9.48		
36	9.59	6.59	11.02
37	9.71	6.97	10.01
38	9.85	7.67	10.12
39	10.03	8.04	10.3
40	10.24	9.85	9.65
41	11.96	9.03	9.19
42	11.99	11.4	9.74
43	12.01	9.36	10.22
44	12.04	10.15	9.06
45	12.07	14.16	9.38
46	12.10		8.61
47	12.12	8.29	8.16
48	12.15	7.51	8.5
49	12.18	6.83	9.48
50	12.21	7.97	8.96
51	12.23	8.91	9.08
52	12.26	9.4	10.22
53	12.29	6.92	8.98
54	12.32	1.77	8.94
55	12.34	10.93	9.3
56	12.37	5.9	9.01
57	12.40	6.77	8.92
58	12.43	5.77	10.21
59	12.45		10.25
60	12.48	7.49	9.29
61	12.51	8.63	10.92
62	12.54		9.43
63	12.56	9.69	8.86
64	12.59	8.41	8.76
65	12.62	7.38	9.01

Depth(cm)	Age (ka)	%CF	%CaCO3
66	12.65	7.33	8.53
67	12.68	6.72	8.31
68	12.70	4.09	7.64
69	12.73	3.95	8.93
70	12.76	4.08	8.38
71	12.79	5.04	8.46
72	12.81	4.97	7.55
73	12.84	5.37	9.81
74	12.87	5.64	9.46
75	12.90	7.07	9.09
76	12.92	6.69	10.03
77	12.95	6.33	8.43
78	12.98	5.31	9.34
79	13.01	4.68	9.11
80	13.03	4.68	9.49
81	13.06	3.77	9.17
82	13.09	3.68	9.19
83	13.12	3.13	9.15
84	13.14	3.77	9.77
85	13.17	3.28	10
86	13.20	3.2	10.45
87	13.23	3.36	9.94
88	13.25	4.48	10.33
89	13.28	3.94	10.3
90	13.31	3.63	9.91
91	13.34	4.81	9.67
92	13.36	5.64	10.42
93	13.39	7.25	9.41
94	13.42	6.16	9.67
95	13.45	6.8	9.41
96	13.47	6.23	10.6
97	13.50	4.5	9.6
98	13.53	5.97	10.81
99	13.56	4.71	9.86
100	13.58	4.42	9.88
101	13.61	4.88	9.53
102	13.64	5.77	9.23
103	13.67	7.02	9.81
104	13.69	5.08	7.91
105	13.72	4.92	8.09
106	13.75	4.48	8.47
107	13.78	4.51	9.01
108	13.81	4.12	8.65

Depth(cm)	Age (ka)	%CF	%CaCO3
109	13.83	4.14	8.95
110	13.86	4.35	9.09
111	13.89	4.38	9.51
112	13.92	4.83	10.18
113	13.94	4.89	9.68
114	13.97	4.82	8
115	14.00	6	9.29
116	14.03	6.69	8.67
117	14.05	5.67	8.82
118	14.08	6.72	8.62
119	14.11	5.84	7.96
120	14.14	5.17	8.2
121	14.16	5.58	7.86
122	14.19	4.6	8.26
123	14.22	5.53	8.22
124	14.25		8.18
125	14.27	7.07	7.76
126	14.28	6.31	8.56
127	14.29	5.66	8.81
128	14.30	5.19	8.69
129	14.31	4.23	9.23
130	14.31	4.21	9.37
131	14.44	5.08	10.08
132	14.58	4.12	9.38
133	14.71	5.53	9.37
134	14.84	7.52	9.26
135	14.97	11.61	10.05
136	15.11	13.49	10.5
137	15.24	15.42	11.02
138	15.37	17.35	11.54
139	15.50	13.59	11.81
140	15.64	16.71	11.17
141	15.77	17.05	11.58
142	15.90	18.17	12.64
143	16.03	16.02	12.39
144	16.17	13.27	12.95
145	16.30	27.82	12.58
146	16.43	27.3	11.88
147	16.56	17.17	12.11
148	16.70	12.41	11.42
149	16.83	12.78	11.14
150	16.96	15.87	10.8
151	17.09	12.7	11.51

Depth(cm)	Age (ka)	%CF	%CaCO3
152	17.23	15.82	10.97
153	17.36	6.98	12.07
154	17.49	6.19	10.46
155	17.62	6.38	10.73
156	17.76	6.29	11.32
157	17.89	7	11.24
158	18.51	7.88	10.27
159	18.55	8.24	10.46
160	18.60	8.49	10.71
161	18.65	10.68	11.24
162	18.70	9.21	10.81
163	18.74	7.69	11.18
164	18.79	8.23	11.16
165	18.84	7.22	11.05
166	18.89	6.8	10.77
167	18.93	7.15	9.63
168	18.98	7.38	9.3
169	19.03	6.66	9.25
170	19.07	6.45	10.06
171	19.12	5.4	10.32
172	19.17	5.6	10.25
173	19.22	5.39	
174	19.26	6.28	
175	19.31	5.23	
176	19.36	7.2	
177	19.41	6.31	
178	19.45	6.79	
179	19.50	6.51	
180	19.55	7.05	
181	19.59	7.6	
182	19.64	7.31	
183	19.69	9.18	
184	19.74	11.48	
185	19.78	10.14	
186	19.83	11.21	
187	19.88	8.74	
188	19.93	8.11	
189	19.97	7.82	
190	20.02	8.5	

IRD Depth (cm)	IRD Age (ka)	#IRD
2.5	7.302	3151.8
7.5	7.424	
12.5	7.564	382.86
17.5	7.723	
22.5	7.928	3317.1
27.5	8.242	
32.5	8.608	1353.8
37.5	9.079	298.59
47.5	12.007	
52.5	12.276	236.82
57.5	12.413	
62.5	12.551	355.4
67.5	12.689	
72.5	12.827	191.07
77.5	12.965	
82.5	13.102	237.62
87.5	13.240	
92.5	13.378	267.22
97.5	13.516	
102.5	13.653	154.68
107.5	13.791	
112.5	13.929	217.93
117.5	14.067	
122.5	14.205	140.45
127.5	14.342	
132.5	14.641	320
137.5	15.304	
142.5	15.966	1292.3
147.5	16.629	
152.5	17.291	231.3
157.5	17.954	
162.5	18.616	1345.2
167.5	19.279	
172.5	19.941	642.99
177.5	20.604	
186.5	21.796	587.05
189.5	22.194	
194.7	22.883	245